Research Project Number TPF-5(193) Supplement 27

EXTENDING TL-2 SHORT-RADIUS GUARDRAIL TO LARGER RADII

Submitted by

Cody S. Stolle, Ph.D., E.I.T.
Post-Doctoral Research Associate

John D. Reid, Ph.D.
Professor

Robert W. Bielenberg, M.S.M.E., E.I.T.
Research Associate Engineer

Ronald K. Faller, Ph.D., P.E.
Research Associate Professor and
MwRSF Director

Dean L. Sicking, Ph.D., P.E.
Emeritus Professor

Karla A. Lechtenberg, M.S.M.E., E.I.T.
Research Associate Engineer

MIDWEST ROADSIDE SAFETY FACILITY
Nebraska Transportation Center
University of Nebraska-Lincoln
130 Whittier Research Center
2200 Vine Street
Lincoln, Nebraska 68583-0853
(402) 472-0965

Submitted to

WISCONSIN DEPARTMENT OF TRANSPORTATION
4802 Sheboygan Avenue
Madison, Wisconsin 53707

MwRSF Research Report No. TRP-03-296-14

March 31, 2014

TECHNICAL REPORT DOCUMENTATION PAGE

1. Report No. TRP-03-296-14	2.	3. Recipient's Accession No.	
4. Title and Subtitle Extending TL-2 Short-Radius Guardrail to Larger Radii		5. Report Date March 31, 2014	
		6.	
7. Author(s) Stolle, C.S., Reid, J.D., Bielenberg, R.W., Faller, R.K., Sicking, D.L., and Lechtenberg, K.A.		8. Performing Organization Report No. TRP-03-296-14	
9. Performing Organization Name and Address Midwest Roadside Safety Facility (MwRSF) Nebraska Transportation Center University of Nebraska-Lincoln 130 Whittier Research Center 2200 Vine Street Lincoln, Nebraska 68583-0853		10. Project/Task/Work Unit No.	
		11. Contract © or Grant (G) No. TPF-5(193) Supp. 27	
12. Sponsoring Organization Name and Address Wisconsin Department of Transportation 4802 Sheboygan Avenue Madison, Wisconsin 53707		13. Type of Report and Period Covered Final Report: 2010-2014	
		14. Sponsoring Agency Code TPF-5(193) Supplement #27	
15. Supplementary Notes			

16. Abstract (Limit: 200 words)

Longitudinal barriers are commonly used to shield hazards including bridge rail ends, bridge parapets, and slopes. In some locations, a secondary roadway intersects the primary roadway within the guardrail's length-of-need (LON). Some intersections have radii as large as 72 ft (22 m) between primary and secondary roadways, which require untested modifications to existing short radius guardrail systems. No short radius systems have been tested and approved to shield hazards with these conditions.

A validated computer simulation model of the Yuma County system was modified and simulated with larger radii of 24, 48, and 72 ft (7.3, 15, and 22 m) using a 2000P vehicle in LS-DYNA. Impacts with 27-in. (686-mm) tall systems frequently resulted in vehicle vaulting when impacted at 45 mph (72 km/h), although blockouts reduced vaulting and increased system effectiveness. Maximum practical speeds to utilize 27-in. (686-mm) tall curved guardrail systems with blockouts were 19, 22, and 23 mph (31, 35, and 37 km/h) for radii of 24, 48, and 72 ft (7.3, 15, and 22 m), respectively. Maximum practical speeds without blockouts were 29, 26, and 41 mph (47, 42, and 66 km/h), respectively. Blockouts reduced vaulting by maintaining rail height, reducing tire interaction with post debris, and facilitating easier rail release via post twisting. A 29-in. (737-mm) tall system with blockouts and a 31-in. (787-mm) tall system without blockouts performed acceptably at 45 mph (72 km/h) and 25 degrees, downstream of the beginning of the Length-of-Need (LON).

17. Document Analysis/Descriptors Highway Safety, Roadside Appurtenances, Short-Radius Guardrail, Simulation, LS-DYNA, Curved Guardrail, Intersection, and NCHRP Report No. 350		18. Availability Statement No restrictions. Document available from: National Technical Information Services, Springfield, Virginia 22161	
19. Security Class (this report) Unclassified	20. Security Class (this page) Unclassified	21. No. of Pages 253	22. Price

DISCLAIMER STATEMENT

This report was completed with funding from the Wisconsin Department of Transportation. The contents of this report reflect the views and opinions of the authors who are responsible for the facts and the accuracy of the data presented herein. The contents do not necessarily reflect the official views or policies of the Wisconsin Department of Transportation nor the Federal Highway Administration, U.S. Department of Transportation. This report does not constitute a standard, specification, regulation, product endorsement, or an endorsement of manufacturers.

ACKNOWLEDGEMENTS

The authors wish to acknowledge the Wisconsin Department of Transportation for sponsoring this project.

Acknowledgement is also given to the following individuals who made a contribution to the completion of this research project.

Midwest Roadside Safety Facility

J.C. Holloway, M.S.C.E., E.I.T., Test Site Manager
S.K. Rosenbaugh, M.S.C.E., E.I.T., Research Associate Engineer
J.D. Schmidt, Ph.D., P.E., Post-Doctoral Research Assistant
A.T. Russell, B.S.B.A., Shop Manager
K.L. Krenk, B.S.M.A., Maintenance Mechanic
S.M. Tighe, Laboratory Mechanic
D.S. Charroin, Laboratory Mechanic
Undergraduate and Graduate Research Assistants

Wisconsin Department of Transportation

Jerry Zogg, P.E., Chief Roadway Standards Engineer
Erik Emerson, P.E., Standards Development Engineer

TABLE OF CONTENTS

LIST OF FIGURES

LIST OF TABLES

1 INTRODUCTION

1.1 Background

Bridge rails are commonly used to shield errant vehicles from falling into a hazard being spanned by the bridge. To shield the ends of the bridge railings and to provide guardrail runout length upstream from the bridge hazard, crashworthy guardrail systems with transitions and end terminals are frequently utilized. The minimum length of guardrail required to shield a hazard is determined using length-of-need (LON) formulas found the American Association of State Highway and Transportation Officials (AASHTO's) *Roadside Design Guide* [1]. In some instances, the location of a bridge is very close to an intersection, such that the secondary or intersecting roadway is within the guardrail LON.

Short-radius guardrail systems were designed to prevent errant vehicles from interacting with the bridge hazard, as well as to provide a stiffness transition to a stiff bridge rail. To date, no systems have yet passed the Test Level 3 (TL-3) impact criteria identified in either the National Cooperative Highway Research Program (NCHRP) Report No. 350 [2] or the American Association of Highway Transportation Officials (AASHTO) *Manual for Assessing Safety Hardware* (MASH) [3]. Most short radius systems were tested in accordance with NCHRP Report No. 230 [4]. The Yuma County short-radius system was first tested in accordance with the AASHTO *Guide Specifications for Bridge Railings* [5], and was later approved for use with NCHRP Report No. 350 TL-2 impact conditions [6].

Although short-radius guardrails have been recommended for use with radii up to 30 ft (9.1 m) in the FHWA Technical Advisory T5040.32 [7], the performance of systems with radii larger than 10 ft (3.0 m) is not well-documented. Systems with radii larger than previously tested may not be as stiff as systems with smaller radii. Increased flexibility during impact may disrupt beneficial bumper-to-rail engagement and culminate in vaulting override or underride. At very

large radii, the guardrail stiffness may initially increase as the rail tensile forces become increasingly tangential.

Wisconsin DOT commissioned a study to evaluate currently-accepted designs of short-radius guardrail systems with larger radii of curvature using computer simulation. Because crash testing was beyond the scope of this project, no federal approval of the designs will be pursued. It was believed that the research would provide guidance for safe intersection speed and radius combinations and suggest potential improvements in the design of current short-radius guardrail systems when used on large radius intersections.

1.2 Research Objectives

The research objective of this project was to evaluate modifications to the design of an approved short-radius guardrail systems with larger radii of curvature, determine the performance limits of the systems, and evaluate the limiting travel speeds on roadways for which the simulated short-radius guardrail could still perform adequately.

1.3 Project Outline

A series of tasks were conducted to complete the research objectives:

1. Evaluate existing short-radius guardrail designs which received approval from FHWA;
2. Develop and validate baseline models of short-radius guardrail systems using crash test results;
3. Modify the validated short radius design with larger radii and different rail heights;
4. Determine the maximum speeds at which the larger-radius designs were still determined to be crashworthy; and
5. Provide an approximate percentage of crashes which could be contained by various radius and hardware configurations.

2 LITERATURE REVIEW

Several short-radius systems were successfully tested according to criteria presented in NCHRP Report No. 230 [4]. The tested systems typically consisted of W-beam guardrail with radii between 8 and 10 ft (2.4 and 3.0 m) mounted on rectangular or circular Controlled Release Terminal (CRT) posts with 42-in. (1,067-mm) embedment depths and anchorages. Criteria presented in NCHRP Report 230 required a minimum of four crash tests conducted at 60 mph (97 km/h):

1) 4,500-lb (2,041-kg) sedan at 0 degrees, centerline aligned with stiff bridge rail;
2) 4,500-lb (2,041-kg) sedan at 25 degrees, at the critical impact point (CIP) near the transition;
3) 4,500-lb (2,041-kg) sedan at 25 degrees, centerline aligned with midpoint of radius; and
4) 1,900-lb (862-kg) small car at 20 degrees, centerline aligned with midpoint of radius.

The Yuma County short-radius guardrail system was tested in accordance with the AASHTO *Guide Specifications* [5] Performance Level 1 (PL-1) impact conditions. A total of six tests conducted at 45 mph (72 km/h) were required:

1) 1,984-lb (900-kg) small car at 20 degrees, at the CIP near the transition;
2) 5,401-lb (2,450-kg) pickup truck at 20 degrees, at the CIP near the transition;
3) 1,984-lb (900-kg) small car at 20 degrees, centerline aligned with midpoint of radius;
4) 5,401-lb (2,450-kg) pickup truck at 20 degrees, centerline aligned with midpoint of radius;
5) 1,984-lb (900-kg) small car at 0 degrees, centerline aligned with stiff bridge rail; and
6) 5,401-lb (2,450-kg) pickup truck at 0 degrees, centerline aligned with stiff bridge rail.

No short-radius systems have been successfully crash tested according to NCHRP Report No. 350 [2] or MASH [3] TL-3 impact conditions. Seven tests were required according to NCHRP Report No. 350 crash test conditions. NCHRP Report No. 350 impact conditions are discussed in literature [8-9].

A summary of previously-tested short-radius systems are shown in Tables 1 through 5. Bullnose systems, which share many similar features as short-radius systems, are summarized in Tables 7 through 13.

2.1 Historical W-Beam Short Radius Systems

2.1.1 Systems Tested to NCHRP Report No. 230

Two W-beam short-radius systems which were successfully tested according to NCHRP Report 230 criteria included the Washington [10] and Texas Transportation Institute (TTI) [11] designs. Each design consisted of curved W-beam guardrail mounted on wooden breakaway posts connected to a downstream anchorage and rigid or semi-rigid bridge railing.

The final design of the Washington short-radius design is shown in Figure 1. The system consisted of a curved W-beam end termination, 25 ft (7.6 m) of W-beam including a Breakaway Cable Terminal (BCT) end anchorage system with two cable anchors: one attached to each BCT post. The cables were spliced together near the ground line. The guardrail radius was 8-ft 6-in. (2,591-mm), and 25 ft (7.6 m) of W-beam guardrail was used to transition to a rigid bridge rail. The system was configured such that the barrier adjacent to the secondary roadway was installed parallel with the road, whereas the primary side of the system had a 10:1 flare upstream of the bridge rail. Posts installed at the transition were 6 in. x 8 in. x 72 in. (152 mm x 203 mm x 1,829 mm) rectangular timber posts, and posts installed on the radius and secondary side of the system were 6 in. x 8 in. x 72 in. (152 mm x 203 mm x 1,829 mm) rectangular CRT posts. One CRT post on the primary roadway side and all six transition posts utilized 6 in. x 8 in. x 14 ¼ in. (152

Table 1. Summary of Short Radius Guardrail Systems

Test No.	Reference No.	Secondary Road Anchorage	Secondary Side Rail	Radius	Primary Side Rail	Post Details A	Post Details B	Post Details C	Post Details D	Post Details E	Post Details F	Post Details G	NOTES
WA-1	10	Buffer end section (curved, flattened W-beam piece) with BCT cable anchor and 1 BCT post	12-ft 6-in. parallel to road, 12-gauge W-beam	8-ft 6-in. radius, 12.5-ft Long, 12-gauge W-beam	25 ft with 10:1 flare, 12-gauge W-beam	BCT post in concrete footer with BCT cable anchor Post No. 1 (Secondary Side)	6-in. x 8-in. x 7 ft long timber post Post No. 2, 6-ft 3-in. from Post No. 1	4-in. x 6-in. x 7-ft long timber post Post No. 3, 6-ft 3-in. from Post No. 2 (start of radius)	4-in. x 6-in. x 7-ft long timber post Post No. 4, 6-ft 3-in. from Post No. 3 (center of radius)	BCT post in concrete footer with BCT cable anchor Post No. 5, 6-ft 3-in. from Post No. 4 (end of radius)	Est. 6-in. x 8-in. x 7-ft long timber post (unk) with 6-in. x 8-in. blockouts Post Nos. 6-8, 3-ft 1.5-in. spacing, 6-ft 3-in. from Post No. 5	10-in. x 10-in. x 7-ft long timber posts with 8-in. x 8-in. x 14-in. blockouts Post Nos. 9-11, 3-ft 1.5-in. spacing, 3-ft 6-in. from Post No. 8	W-beam End Shoe Attachment to Concrete Bridge Rail 1:2 Slope at Center of Posts
WA-1M		Buffer end section (curved, flattened W-beam piece) with BCT cable anchor and 1 BCT post	Same as WA-1	Same as WA-1	Same as WA-1	BCT post in concrete footer with BCT cable anchor Post No. 1 (Secondary Side)	6-in. x 8-in. x 7 ft long timber post with pipe substituted for post-to-rail attachment Post No. 2, 6-ft 3-in. from Post No. 1	4-in. x 6-in. x 7-ft long timber breakaway post Post No. 3, 6-ft 3-in. from Post No. 2 (start of radius)	4-in. x 6-in. x 7-ft long timber breakaway post Post No. 4, 6-ft 3-in. from Post No. 3 (center of radius)	BCT post in concrete footer Post No. 5, 6-ft 3-in. from Post No. 4 (end of radius)	Same as WA-1	Same as WA-1	Same as WA-1, pipe post-to-rail attachment used at secondary side BCT anchor
WA-2M		Same as WA-1M	Same as WA-1M	Same as WA-1M	Same as WA-1M	Same as WA-1M	Same as WA-1M	4-in. x 6-in. x 7-ft long timber breakaway post Post Nos. 3-5, 6-ft 3-in. from Post No. 2 (start of radius)	4-in. x 6-in. x 7-ft long timber breakaway post Post No. 6, 6-ft 3-in. from Post No. 3 (center of radius)	BCT post in concrete footer Post No. 7, 6-ft 3-in. from Post No. 6 (end of radius)	Est. 6-in. x 8-in. x 7-ft long timber post (unk) with 6-in. x 8-in. blockouts Post Nos. 8-10, 3-ft 1.5-in. spacing, 6-ft 3-in. from Post No. 7	10-in. x 10-in. x 7-ft long timber posts with 8-in. x 8-in. x 14-in. blockouts Post Nos. 11-13, 3-ft 1.5-in. spacing, 3-ft 6-in. from Post No. 10	Added 12-ft 6-in. W-beam and two additional breakaway posts to secondary side of system
WA-3M		Buffer end section (curved, flattened W-beam piece) with 2 BCT cable anchors and 2 BCT posts	Same as WA-2M	Same as WA-2M	Same as WA-2M	Same as WA-2M	BCT post in soil foundation tube with BCT cable anchor attached to foundation tube Post No. 2, 6-ft 3-in. from Post No. 1	Same as WA-2M	Same as WA-2M	Same as WA-2M	Same as WA-2M	Same as WA-2M	Second post converted to BCT post with addl cable anchor attached to foundation tube, spliced to first cable
WA-4M		Same as WA-3M	Same as WA-3M	Same as WA-3M	Same as WA-3M	Same as WA-3M	Same as WA-3M	Same as WA-3M	Same as WA-3M with post-to-rail attachment removed	Same as WA-3M	Same as WA-3M	Same as WA-3M	Bolt removed from post no. 6; final system design shown in Figure 1
WA-5M													
1263-1	11	25-ft Long turndown anchor	25-ft parallel to road, 12-gauge W-beam	25-ft with 14-ft 3-in. radius, 25-ft long (90-deg bend)	9-ft 4.5-in. straight W-beam, 12-ft 6-in. tubular W-beam transition, 12-gauge W-beam	7-in. diameter timber posts Post nos. 1-2, 6-ft 3-in. spacing (secondary side)	7-in. diameter CRT posts Post nos. 3-4, 6-ft 3-in. spacing	BCT post with cable anchor Post no. 5 (start of radius)	7-in. diameter CRT posts Post nos. 6-7, 6-ft 3-in. spacing (along radius)	BCT post with cable anchor Post no. 8 (end of curve)	7-in. diameter timber posts Post nos. 9-10, 6-ft 3-in. from post no. 8, with 3-ft 1.5-in. spacing	7-in. diameter timber posts (attached to bridge rail) Post Nos. 11-14, 3-ft 1.5-in. from Post No. 10, 1-ft 6.75-in. Spacing	Tubular W-beam transition to stiff bridge rail (safety shape concrete barrier)
1263-2		Same as 1263-1	Same as 1263-1	Same as 1263-1	Same as 1263-1	Same as 1263-1	Same as 1263-1 except anchorage depth was increased from 38 to 44 in.	Same as 1263-1	Same as 1263-1 except anchorage depth was increased from 38 to 44 in.	7-in. diameter CRT posts Post no. 8, 6-ft 3-in. spacing (end of radius)	Same as 1263-1	Same as 1263-1	Post no. 8 converted from BCT to CRT post
1263-3		Same as 1263-2 with nested W-beam	Same as 1263-2 with nested W-beam	Same as 1263-2 with nested W-beam	Same as 1263-2 with nested W-beam	Same as 1263-2	Same as 1263-2	Same as 1263-2	Same as 1263-2	Same as 1263-2	Same as 1263-2	Same as 1263-2	Rail nested throughout
1263-4		Same as 1263-3	Same as 1263-3	Same as 1263-3, except radius increased to 16 ft	Same as 1263-3	Same as 1263-3	Same as 1263-3	Same as 1263-3	Same as 1263-3	Same as 1263-3	Same as 1263-3	Same as 1263-3	Radius increased to cause splices to occur at post locations
1263-5													
1263-6		Same as 1263-5, except that post no. 2 converted to 7-in. diameter CRT	Same as 1263-5	Same as 1263-5	Same as 1263-5	7-in. diameter timber post Post nos. 1	7-in. diameter CRT posts Post nos. 2-4, 6-ft 3-in. spacing	Same as 1263-5	Same as 1263-5	Same as 1263-5	Same as 1263-5	Same as 1263-5	Post no. 2 converted to 7-in. diameter CRT System shown in Figures 2 through 7

Table 2. Summary of Short-Radius Guardrail Systems Full-Scale Crash Testing

Test No.	Reference No.	Vehicle	Impact Conditions	Impact Location	Rail Height (in.)	Result
WA-1	10	1978 Plymouth sedan 4,520 lb	60.0 mph and 0 deg	Centerline of vehicle with center point of radius	27	Failed - vehicle vaulted system
WA-1M		1978 Honda small car 1,903 lb	60.8 mph and 23.7 deg	Angled hit into guardrail	27	Conditionally Failed - longitudinal ΔV exceeded limits
WA-2M		1977 Dodge sedan 4,789 lb	60.6 mph and 13.4 deg	Angled hit into guardrail	27	Failed - all posts on secondary side fractured
WA-3M		1978 Dodge sedan 4,640 lb	58.9 mph and 16.6 deg	Angled hit into guardrail	27	Failed - W-beam fractured during impact
WA-4M		1978 Dodge sedan 4,650 lb	58.8 mph and 14.6 deg	Angled hit into guardrail	27	Passed (despite yaw, back tires overriding system)
WA-5M		4,640 lb 1978 Plymouth sedan	59.0 mph and 1.1 deg	Centerline of vehicle aligned with center point of radius	27	Passed
1263-1	11	1987 Yugo GV small car 1,970 lb	58.4 mph and 20.5 deg	Center point of radius	~27.1	Failed - High occupant accelerations, overrode system
1263-2		1987 Yugo GV small car 1,970 lb	59.0 mph and 20.4 deg	Center point of radius	~27.1	Failed - splice rupture, car penetrated system
1263-3		1987 Yugo GV small car 1,970 lb	60.2 mph and 20.7 deg	Center point of radius	~27.1	Passed
1263-4		1982 Cadillac sedan 4,500 lb	57.1 mph and 24.7 deg	75 in. from end of concrete barrier	~27.1	Passed
1263-5		1985 Cadillac coupe sedan 4,500 lb	58.5 mph and 26.8 deg	Centerline of vehicle with center point of radius	~27.1	Failed - underride and roof crush
1263-6		1983 Cadillac coupe 4,500 lb	58.3 mph and 2.0 deg	Centerline of vehicle aligned with bridge rail	~27.1	Passed

Table 3. Summary of Short Radius Guardrail Systems (cont)

Test No.	Reference No.	Secondary Road Anchorage	Secondary Side Rail	Radius	Primary Side Rail	Post Details A	Post Details B	Post Details C	Post Details D	Post Details E	Post Details F	Post Details G	NOTES
YC-1	6	BCT end terminal with two wood posts in foundation tubes, two BCT cables	12-ft 6-in. straight W-beam (includes anchor) with 10:1 flare, 12-gauge W-beam	8-ft radius, 12-ft 6-in. long W-beam, 12-gauge, 90-degree bend	18-ft 9-in. straight W-beam with 10:1 flare, 12-gauge W-beam	BCT posts in soil foundation tubes, BCT cable attached to rail and post no. 1, BCT cable spliced to first cable, attached to post no. 2 Post nos. 1-2, 6-ft 3-in. post spacing	6-in. x 8-in. CRT posts Post nos. 3-5, 6-ft 3-in. post spacing (all on radius) Offset post nos. A&B, not attached to rail (behind radius)	6-in. x 8-in. timber posts with 6-in. x 8-in. x 14.25-in. timber blockouts Post nos. 6-7, 3-ft 1.5-in. spacing, located 3-ft 1.5-in. from post no. 5	8-in. x 8-in. timber post with timber blockout Post no. 8, located 3-ft 1.5-in. from post no. 7	10-in. x 10-in. timber posts with timber blockouts Post nos. 9-11, 1-ft 6.75-in. spacing, located 1-ft 6.75-in. from post no. 8	N/A	N/A	Two BCT cables were spliced together at upstream anchor; one attached to BCT bearing plate at post no. 1, the other was attached to the foundation tube at post no. 2
YC-2													
YC-3													
YC-4		Same as YC-1 through YC-3	25-ft straight W-beam (includes anchor) with 10:1 flare, 12-gauge W-beam	Same as YC-1 through YC-3	Same as YC-1 through YC-3	Same as YC-1 through YC-3	6-in. x 8-in. CRT posts Post nos. 3-4, 6-ft 3-in. post spacing	6-in. x 8-in. CRT posts Post nos. 5-7, 6-ft 3-in. post spacing (all on radius) Offset post nos. A&B, not attached to rail	6-in. x 8-in. timber posts with 6-in. x 8-in. x 14.25-in. timber blockouts Post nos. 8-9, 3-ft 1.5-in. spacing, located 3-ft 1.5-in. from post no. 5	8-in. x 8-in. timber post with timber blockout Post no. 10, located 3-ft 1.5-in. from post no. 7	10-in. x 10-in. timber posts with timber blockouts Post nos. 11-13, 1-ft 6.75-in. spacing, located 1-ft 6.75-in. from post no. 8	N/A	Secondary roadway side lengthened to increase anchorage capacity System shown in Figure 8
YC-5													
YC-6													
YC-7													
1442-1	8	W-beam turndown anchor	12-ft 6-in. W-beam to thrie beam transition piece, 12-ft 6-in. 10-gauge thrie beam	25-ft. thrie beam forming 16-ft radius, 10-gauge	12-ft 6-in. thrie beam and 6-ft 3-in. nested thrie beam transition, 10-gauge	7-in. diameter wood post Post no. 1 (at turndown anchor)	7-in. diameter CRT posts Post nos. 2-8, 6-ft 3-in. spacing, located 6-ft 3-in. from post no. 1	7-in. diameter timber posts Post nos. 9-10, 3-ft 1.5-in. spacing, located 6-ft 3-in. from post no. 8	7-in. diameter timber posts Post nos. 11-13, 1-ft 6.75-in. spacing, located 3-ft 1.5-in. from post no. 8	N/A	N/A	N/A	Similar to first TTI system tested, using thrie beam in lieu of nested W-beam
1442-2													
1442-3		Same as 1442-1 and 1442-2	Same as 1442-1 and 1442-2	Same as 1442-1 and 1442-2	Same as 1442-1 and 1442-2	Same as 1442-1 and 1442-2	Same as 1442-1 and 1442-2, except that post-to-rail bolts removed from several posts on radius	Same as 1442-1 and 1442-2	Same as 1442-1 and 1442-2	Same as 1442-1 and 1442-2	Same as 1442-1 and 1442-2	Same as 1442-1 and 1442-2	Post-to-rail attachments removed from posts on radius System shown in Figures 9 through 14
1442-4													
1442-5													

Table 4. Summary of Short-Radius Guardrail Systems Full-Scale Crash Testing

Test No.	Reference No.	Vehicle	Impact Conditions	Impact Location	Rail Height (in.)	Result
YC-1	6	1982 Chevrolet pickup 5,376 lb	45 mph and 1.4 deg	Centerline of vehicle with tangent line to bridge rail	27	Passed
YC-2		Volkswagen Rabbit 1,978 lb	50.3 mph and 0.7 deg	Centerline of vehicle with tangent line to bridge rail	27	Passed
YC-3		Chevrolet pickup 5,380 lb	44.8 mph and 19.7 deg	Centerline of vehicle aligned with radius	27	Failed - rail released from BCT post
YC-4		Chevrolet pickup 5,381 lb	44.9 mph and 20.1 deg	Centerline of vehicle aligned with radius	27	Passed
YC-5		Volkswagen Rabbit 1,980 lb	44.2 mph and 20 deg	Centerline of vehicle with center of 2nd freestanding CRT	27	Passed
YC-6		Volkswagen Rabbit 1,980 lb	51.1 mph and 19.4 deg	13 ft upstream of bridge end	27	Passed
YC-7		1982 Chevrolet pickup 5,424 lb	45.2 mph and 20.7 deg	12 ft upstream of bridge end	27	Passed
1442-1	8	1986 Chevrolet 2500 4,409 lb	60.9 mph and 26.0 deg	3.5 posts upstream from concrete barrier	31.625 (thrie beam)	Passed
1442-2		1985 Chevrolet pickup 4,409 lb	63.0 mph and 25.6 deg	Centerline of vehicle with center post of radius	31.625 (thrie beam)	Overrode system - rail formed ramp
1442-3		1988 Ford F250 4,409 lb	63.0 mph and 24.6 deg	Centerline of vehicle with center post of radius	31.625 (thrie beam)	Overrode system - rail formed ramp
1442-4		1988 Chevrolet Sprint 1,978 lb	60.1 mph and 19.1 deg	Centerline of vehicle with center post of radius	31.625 (thrie beam)	Marginal pass - rail crushed windshield
1442-5		1984 Lincoln Town Car 4,500 lb	60.4 mph and 24.5 deg	Centerline of vehicle with center post of radius	31.625 (thrie beam)	Limited pass - rail released from terminal

Table 5. Summary of Short Radius Guardrail Systems (cont)

Test No.	Reference No.	Secondary Road Anchorage	Secondary Side Rail	Radius	Primary Side Rail	Post Details A	Post Details B	Post Details C	Post Details D	Post Details E	Post Details F	Post Details G	NOTES
SR-1	9, 12	FLEAT end terminal (secondary road side)	25-ft straight W-beam, 6-ft 3-in. straight W-beam-to-thrie transition, 12-ft 6-in. straight thrie beam, 12-gauge	7-ft 10-in. radius, 12-ft 6-in. long, 90-degree bend slotted thrie beam, 12-gauge, reinforced with nose cable & button swages	12-ft 6-in. straight slotted, 12-gauge thrie beam, 12-ft 6-in. straight, 12-gauge thrie beam, 12-ft 6-in. thrie beam 10-gauge transition to stiff bridge rail	FLEAT end anchorage	8-in. x 6-in. CRT posts with blockouts Post nos. 1-2, 6-ft 3-in. spacing	6-in. x 8-in. thrie beam CRT post with two 6-in. x 8-in. blockouts (one tapered) Post no. 3, located 6-ft 3-in. from post no. 2	5.5-in. x 7.5-in. thrie BCT posts in 6-ft soil foundation tube Post nos. 4-5 (start and end of radius) with secondary and primary side cable anchors, located 6-ft 3-in. from post no. 3	6-in. x 8-in. thrie beam CRT posts with two 6-in. x 8-in. blockouts (one tapered) Post nos. 6-9, 3-ft 1.5-in. spacing, located 3-ft 1.5-in. from post no. 5	6-in. x 8-in. thrie beam CRT posts with one 6-in. x 8-in. blockout Post nos. 10-13, 3-ft 1.5-in. spacing, located 3-ft 1.5-in. from post no. 9	6-in. x 8-in. thrie beam CRT posts with two 6-in. x 8-in. blockouts (one tapered) Post nos. 14-17, 1-ft 6.75-in. spacing, located 3-ft 1.5-in. from post no. 5	2:1 slope break point (SBP) at center of post Shown in Figure 15
SR-2		Same as SR-1	Same as SR-1	Same as SR-1	Same as SR-1	Same as SR-1	8-in. x 6-in. CRT posts with blockouts Post nos. 1, 1.5, 2, 2.5, 3-ft 1.5-in. spacing	Same as SR-1	Same as SR-1	Same as SR-1	Same as SR-1	Same as SR-1	Slope eliminated and post spacing between post nos. 1 and 3 halved
SR-3													
SR-4		FLEAT end terminal (secondary road side)	25-ft straight W-beam, 6-ft 3-in. straight W-beam-to-thrie transition, 12-ft 6-in. straight thrie beam, 12-gauge	8-ft 11⅜-in. radius, 12-ft 6-in. long, 90-degree bend slotted thrie beam, 12-gauge, reinforced with nose cable & button swages	37-ft 6-in. slotted thrie beam in a parabolic flare, 12-gauge, and 12-ft 6-in. thrie beam, 10-gauge transition to stiff bridge rail	Non-proprietary W-beam end terminal system (5.5-in. x 7.5-in. BCT posts in soil foundation tubes with cable anchor) Post nos. 10S-11S, 6-ft 3-in. spacing	8-in. x 6-in. CRT posts with blockouts Post nos. 7S-9S, 6-ft 3-in. spacing, located 6-ft 3-in. from post no. 2	8-in. x 6-in. CRT posts with blockouts Post nos. 7S-9S, 6-ft 3-in. spacing, located 6-ft 3-in. from post no. 10S Post no. 6S, 3-ft 1.5-in. from post no. 7S	8-in. x 6-in. CRT posts with double blockouts (one tapered) Post nos. 3S-5S, 6-ft 3-in. spacing, located 6-ft 3-in. from post no. 6S	5.5-in. x 7.5-in. thrie BCT posts in soil foundation tubes Post nos. 1P, 1S-2S (start and end of radius) with secondary and primary side cable anchors, located 3-ft 1.5-in. from post no. 3S	6-in. x 8-in. thrie beam CRT posts with two 6-in. x 8-in. blockouts (one tapered) Post nos. 2P-13P, 1-ft 6.75-in. spacing, located 1-ft 6.75-in. from post no. 1P	6-in. x 8-in. thrie beam CRT posts with two 6-in. x 8-in. blockouts (one tapered) Post nos. 2P-13P, 1-ft 6.75-in. spacing, located 1-ft 6.75-in. from post no. 1P	Parabolic flare added to primary side of system
SR-5	13	Same as SR-4	Same as SR-4	Same as SR-4	Same as SR-4	Same as SR-4	Same as SR-4	Same as SR-4	Same as SR-4	Same as SR-4	Same as SR-4	Same as SR-4	In test no. SR-5: external cable anchor added to front of system; in test no. SR-6, external anchor was modified such that it was entirely within the system (no external trigger in front of system)
SR-6													
SR-7	14	Same as SR-6	Same as SR-6	Same as SR-6	Same as SR-6	Same as SR-6	Same as SR-6	Same as SR-6	Same as SR-6	5.5-in. x 7.5-in. thrie BCT post (post nos. 2S) and BSR posts (post nos. 1P and 1S) in soil foundation tubes with secondary and primary side cable anchors, located 3-ft 1.5-in. from post no. 3S	Same as SR-6	Same as SR-6	Post nos. 1S, 1P converted to BSR posts (shown in Figures 16 through 34); (2) plate washers added to post nos. 1S-2S and 1P-4P; (3) thrie beam slot tabs reduced from 2 in. wide to 1 in.
SR-8													

Table 6. Summary of Short-Radius Guardrail Systems Full-Scale Crash Testing

Test No.	Reference No.	Vehicle	Impact Conditions	Impact Location	Rail Height (in.)	Result
SR-1	9, 12	1995 Ford F-250 pickup 4,473 lb	61.5 mph and 19.0 deg	Centerline of pickup with centerpoint of radius	31.625 (thrie beam)	Failed - rollover on top of system
SR-2		1994 Chevrolet C2500 pickup 4,440 lb	64.7 mph and 16.1 deg	Centerline of pickup with centerpoint of radius	31.625 (thrie beam)	Failed - rollover on top of system
SR-3		Ford F250 pickup 4,489 lb	63.9 mph and 0.9 deg	Centerline of pickup with centerline of primary-side post no. 1	31.625 (thrie beam)	Failed - rollover on top of system
SR-4		1999 Chevrolet C2500 pickup 4,420 lb	66.0 mph and 1.8 deg	Centerline of pickup with centerline of primary-side post no. 1	33.625 (thrie beam)	Failed - tear in floorboard
SR-5	13	1997 Ford F250 pickup 4,411 lb	63.3 mph and 0.9 deg	Centerline of pickup with centerline of primary-side post no. 1	31 (thrie beam)	Passed
SR-6		1996 Geo Metro small car 1,969 lb	61.8 mph and 0.8 deg	Right front quarter point of vehicle with centerline of nose	31 (thrie beam)	Failed - windshield crushed by rail and hood
SR-7	14	2002 Dodge Ram pickup 4,989 lb	62.3 mph and 18.1 deg	Centerline of pickup with centerpoint of radius	31 (thrie beam)	Failed - rollover at end of event
SR-8		2002 Dodge Ram pickup 5,000 lb	62.8 mph and 17.9 deg	Centerline of pickup with centerpoint of radius	31 (thrie beam)	Failed - vehicle overrode rail at end of impact sequence

Table 7. Summary of Tested Bullnose Guardrail Systems

Test No.	Reference No.	Anchorages	Rail Configuration	System Dimensions	Post Details A	Post Details B	Post Details C	Post Details D	Post Details E	Post Details F	NOTES
B1	15	W-beam end anchorages with BCT cables adjacent to bridge piers, front and back sides of system	Back side: Two 12-ft 6-in., straight W-beam (to anchor) Nose: 12-ft 6-in., 5-ft radius asymmetrical nose Transition: Two 12-ft 6-in., 40-ft radius W-beam transitioning to straight guardrail Front side: 12-ft 6-in., straight W-beam (to anchor)	16 ft Wide 30-ft Long (half-length)	6-in. x 8-in. timber posts with 6-in. x 8-in. blockouts, placed in holes backfilled with lean concrete; 5 posts on back side, 7 posts on front side	N/A	N/A	N/A	N/A	N/A	Concrete fill behind posts to simulate frozen soil conditions
B2											Asymmetrical system
271	16	W-beam end anchorages with cable anchors at nose and ends of system	Nose: 12-ft 6-in., 4.3-ft radius W-beam (90-degree bend) Front and back sides: Two 12-ft 6-in., straight W-beams	8.6-ft Wide 29.3-ft Long (half-length)	6-in. x 6-in. Douglas Fir timber post in concrete footing at center of nose Post no. 1	6-in. x 6-in. Douglas Fir timber post with cable anchor Post no. 2, located 6-ft 3-in. from post no. 1	8-in. x 6-in. timber posts with 6-in. x 8-in. blockouts Post nos. 3-4, 6-ft 3-in. spacing, located 6-ft 3-in. from post no. 2	8-in. x 6-in. timber post with 6-in. x 8-in. blockout and cable anchor Post no. 5-6, 6-ft 3-in. spacing, located 6-ft 3-in. from post no. 4	N/A	N/A	Symmetrical system
275		W-beam breakaway cable anchors at nose, W-beam end anchorages with cable anchors at ends of system with swaged fittings	Nose: 12-ft 6-in., 4.6-ft radius W-beam with two rail strengthening cables Transition: 12-ft 6-in. rail with 10-degree bend Front and back sides: Two 12-ft 6-in., straight W-beams	8.6-ft Wide 42.1-ft Long (half-length)	Same as test no. 271	6-in. x 6-in. Douglas Fir timber post with breakaway cable anchor Post no. 2, located 6-ft 3-in. from post no. 1	8-in. x 6-in. timber posts with 6-in. x 8-in. blockouts Post nos. 3-6, 6-ft 3-in. spacing, located 6-ft 3-in. from post no. 2	8-in. x 6-in. timber post with 6-in. x 8-in. blockout and cable anchor Post no. 7-8, 6-ft 3-in. spacing, located 6-ft 3-in. from post no. 6	N/A	N/A	Series of design changes made after each test
277		W-beam breakaway cable anchors at nose, two-directional W-beam end anchorages with cable anchors at ends of system with swaged fittings	Same as test no. 275	Same as test no. 275	Same as test no. 275	Same as test no. 275	8-in. x 8-in. timber posts with 8-in. x 8-in. blockouts Post nos. 3-6, 6-ft 3-in. spacing, located 6-ft 3-in. from post no. 2	Same as test no. 275	N/A	N/A	Nine 3 ft diameter inertial barrels used in center of system Steel angles used to support rail at each post on the system
278		Same as test no. 277	Same as test no. 277, except that steel brackets were used to retain buttons at ends of nose strengthening cables	Same as test no. 277	6-in. x 4-in. Douglas Fir timber post in concrete footing at center of nose Post no. 1	6-in. x 6-in. Douglas Fir timber post in concrete footing with breakaway cable anchor Post no. 2, located 6-ft 3-in. from post no. 1	8-in. x 8-in. timber posts with 8-in. x 8-in. blockouts and additional breakaway hole drilled Post nos. 3-6, 6-ft 3-in. spacing, located 6-ft 3-in. from post no. 2	Same as test no. 277	N/A	N/A	Sand barrels were eliminated Concrete footings resized to 24-in. diameter
1	17	Two-cable breakaway anchor attached to one post with double blockouts on both sides of post at front of system and one breakaway cable anchor on each side at post no. 2	Nose: Buffer head attachment on first post Flattened rail: 25-ft W-beam flattened and bent at every post through post no. 5 Straight rail: 12-ft 6-in. straight rail to center of system	Approx 37.5 ft long	5.5-in. x 7.5-in. BCT post with 1-in. slit, two blockouts on each of front and back sides, and two cable anchors (one to each side) Post no. 1	5.5-in. x 7.5-in. BCT post with cable anchor (attaches to rail downstream of post no. 3) and slit Post no. 2, located 6-ft 3-in. from post no. 1	6-in. x 8-in. CRT posts with 6-in. x 8-in. blockouts placed in concrete foundations and slit Post nos. 3-4, 6-ft 3-in. spacing, located 6-ft 3-in. from post no. 2	6-in. x 8-in. timber posts Post no. 5, located 6-ft 3-in. from post no. 4	N/A	N/A	Symmetrical system Bent and flattened rail sections that came to a point at "nose"
2		One breakaway cable anchor on each side at post no. 2	Similar to test no. 1, but geometry of bends and rail flattening modified	Approx 37.5 ft long	Same as test no. 1, except cable anchors were removed	Same as test no. 1, except slit in post no. 2 was modified	Same as test no. 1, except slits in post nos. 3-4 were modified	Same as test no. 1	N/A	N/A	Minor tweaks to geometry and post reactions
2A		Same as test no. 2	Similar to test no. 2, but geometry of bends and rail flattening modified	Approx 37.5 ft long	Same as test no. 2	Same as test no. 2, except slit in post no. 2 was modified	6-in. x 8-in. CRT post with 6-in. x 8-in. blockout placed in concrete foundations and slit Post no. 3, located 6-ft 3-in. from post no. 2	6-in. x 8-in. CRT posts with 6-in. x 8-in. blockouts and slit Post no. 4, located 6-ft 3-in. from post no. 3	6-in. x 8-in. timber posts Post no. 5, located 6-ft 3-in. from post no. 4	N/A	Minor tweaks to geometry and post reactions
4		Same as test no. 2	Similar to test no. 2A, but geometry of bends and rail flattening modified	Approx 37.5 ft long	Same as test no. 1, except cable anchors were removed	Same as test no. 1, except slit in post no. 2 was modified	Same as test no. 1, except slits in post nos. 3-4 were modified	Same as test no. 1	N/A	N/A	Minor tweaks to geometry and post reactions

Table 8. Summary of Short-Radius Guardrail Systems Full-Scale Crash Testing

Test No.	Reference No.	Vehicle	Impact Conditions	Impact Location	Rail Height (in.)	Result
B1	15	1971 Chevrolet Vega small car 2,290 lb	61.5 mph and 0 deg	Centerline of vehicle with furthest extent of system	27	Passed
B2		1969 Chrysler sedan 4,500 lb	62.3 mph and 0 deg	Centerline of vehicle with furthest extent of system		Passed
271	16	1968 Dodge Polara sedan 4,780 lb	41 mph and 0 deg	Centerline of vehicle aligned with centerline of system	27	Failure - rail rupture permitted vehicle penetration
275		1970 Mercury Monterey sedan 4,960 lb	63 mph and 0 deg	Centerline of vehicle aligned with centerline of system	27	Failure - vehicle struck feature behind rail
277		1970 Mercury Monterey sedan 4,960 lb	59 mph and 0 deg	Centerline of vehicle aligned with centerline of system	27	Passed
278		1970 Mercury Monterey sedan 4,960 lb	64 mph and 10 deg	Centerline of vehicle aligned with center of posts on traffic-side flare	27	Failure - rail formed ramp and vehicle vaulted rail
1	17	Small car 2,400 lb	29.1 mph and 0 deg	Centerline of vehicle aligned with centerline of system	27	Passed
2		Sedan 4,520 lb	62.7 mph and 0 deg	Centerline of vehicle aligned with centerline of system	27	Deflection was greater than desired, but passed
2A		Sedan 4,540 lb	62.7 mph and 0 deg	Centerline of vehicle aligned with centerline of system	27	Passed
4		1976 Gran Fury sedan 4,500 lb	57.4 mph and 24 deg	At cable anchor rail connection attached to post no. 2	27	Marginal - excessive deflection

Table 9. Summary of Tested Bullnose Guardrail Systems (cont)

Test No.	Reference No.	Anchorages	Rail Configuration	System Dimensions	Post Details A	Post Details B	Post Details C	Post Details D	Post Details E	Post Details F	NOTES
BN-1	18	Anchor from post no. 1 to primary side of system (not secondary side), cable anchorages on both ends of straight rail	Nose: 12-ft 6-in., 12-gauge thrie beam with 5-ft radius Transition: 12-ft 6-in., 12-gauge thrie beam with 25-ft radius and 30-in. rail height Straight rail: 37-ft 6-in., 12-gauge thrie beams with 34-in. height at post no. 6	Approx 10 ft wide, 45 ft long	5.5-in. x 7.5-in. BCT post located at center of nose with anchor to primary side of system Post no. 1	6-in. x 8-in. CRT post Post no. 2, located 6-ft 3-in. from post no. 1	6-in. x 8-in. CRT post with 6-in. x 8-in. blockout Post no. 3, located 6-ft 3-in. from post no. 2	6-in. x 8-in. CRT post with 6-in. x 8-in. x 14-in. steel blockout Post no. 4, located 6-ft 3-in. from post no. 3	6-in. x 8-in. timber post with 6-in. x 8-in. x 14-in. steel blockouts Post nos. 5-10, spaced 6-ft 3-in. on center, located 6-ft 3-in. from post no. 4	N/A	Symmetrical except that cable anchor at post no. 1 only attached to primary (upstream, or front) end of system and not secondary (downstream, or back side) of system, ditch located in front of system
BN-2		Similar to test no. BN-1, except that the anchorage on post no. 1 was removed	Similar to test no. BN-1, except that steel plates were welded to thrie beam at post locations to force bends to occur there, and the nose was flattened at post no. 1	Same as BN-1	Similar to test no. BN-1, except cable anchor was removed	Similar to test no. BN-1, except that the rail height was lowered to 27 in.	Same as test no. BN-1	Same as test no. BN-1	Same as test no. BN-1	N/A	Rail height lowered at post no. 2, primary-side cable anchor removed from post no. 1, and brackets welded to rail near posts to force rail to bend at post locations
BN-3		Same as test no. BN-2	Similar to test no. BN-2, except that welded plates adjacent to post nos. 1 and 2 (both sides) were removed to prevent stress concentrations	Same as BN-2	Same as test no. BN-2	Same as test no. BN-2	Same as test no. BN-2	Same as test no. BN-2	Same as test no. BN-2	N/A	Welded plates removed from rail near post nos. 1 and 2 (both sides)
BN-4		Anchor from post no. 2 on primary side to rail upstream of post no. 3, cable anchorages on both ends of straight rail	Same as test no. BN-3	Same as BN-3	5.5-in. x 7.5-in. BCT post rotated and attached to the rail through the weak axis Post no. 1	5.5-in. x 7.5-in. BCT post with cable attachment to rail upstream of post no. 3 and blockout added to downstream face (primary side only) Post no. 2, located 6-ft 3-in. from post no. 1	Same as BN-3	Same as BN-3	Same as BN-3	N/A	Post no. 1 rotated such that impact would engage bending through weak axis, post no. 2 modified to fracture more quickly but anchor rail until fracture
BN-5		Anchor from post no. 2 to rail upstream of post no. 3 on both sides, cable anchorages on both ends of straight rail	Same as test no. BN-4	Same as BN-4	Same as BN-4	5.5-in. x 7.5-in. BCT post with cable attachment to rail upstream of post no. 3 and blockout added to downstream face (both sides) Post no. 2, located 6-ft 3-in. from post no. 1	Same as BN-4	Same as BN-4	Same as BN-4	N/A	Similar to test no. BN-4, except that system became completely symmetrical
BN-6		Same as test no. BN-5, except excess length of BCT threaded rod cut off to prevent punching shear rupture in rail	Similar to test no. BN-5, except that the post bolt slots at post no. 3 were eliminated	Same as BN-5	Same as BN-5	Same as BN-5	Same as BN-5	Same as BN-5	Same as BN-5	N/A	Post bolt slots at post no. 3 eliminated and ends of BCT rail attachment threaded rod cut off, due to rail ruptures
BN-7		Same as test no. BN-6	Similar to test no. BN-6, except rail height was increased to 29 in. at post no. 2 (both sides)	Same as BN-6	Same as test no. BN-6, except that steel blockouts were used to space the rail from the post	Same as test no. BN-6, except that steel blockouts were used to space the rail from the post (both sides)	Same as test no. BN-6, except that steel blockouts were used to space the rail from the post (both sides)	Same as BN-6	Same as BN-6	N/A	Rail height increased to 29 in. at post no. 2 and steel blockouts were used on post nos. 1-3 (both sides)
BN-8											
BN-9											
BN-10		Anchor cable brackets attached to rail due to cable anchor at post no. 2 eliminated	Similar to test nos. BN-7 through BN-9, except that cable clamps were substituted for the cable anchor bracket for the cable anchors attached to post no. 2 (both sides)	Same as BN-7 through BN-9	Same as BN-7 through BN-9	Same as BN-7 through BN-9	Same as BN-7 through BN-9	Same as BN-7 through BN-9	Same as BN-7 through BN-9	N/A	Anchor cable brackets attached to rail due to cable anchor at post no. 2 eliminated and substituted for cable clamps

Table 10. Summary of Short-Radius Guardrail Systems Full-Scale Crash Testing

Test No.	Reference No.	Vehicle	Impact Conditions	Impact Location	Rail Height (in.)	Result
BN-1	18	Sedan 4,635 lb	60 mph and 0 deg	Centerline of vehicle aligned with centerline of system (NCHRP Report 230 test 41/50)	30 (post 2) 34 (post 6)	Failed - vehicle underrode barrier
BN-2		Sedan 4,333 lb	59.1 mph and 4.7 deg	Centerline of vehicle aligned with centerline of system (NCHRP Report 230 test 41/50)	27 (post 2) 34 (post 6)	Passed
BN-3		Small car 1,940 lb	56.9 mph and 0 deg	Centerline of vehicle aligned with centerline of system (NCHRP Report 230 test 52/45)	27 (post 2) 34 (post 6)	Failed - excessive decelerations
BN-4		Small car 1,990 lb	61.0 mph and -4.0 deg	Centerline of vehicle aligned with centerline of system (NCHRP Report 230 test 52/45)	27 (post 2) 34 (post 6)	Marginal - excessive decelerations
BN-5		Sedan 4,675 lb	58.47 mph and -0.5 deg	Centerline of vehicle aligned with centerline of system (NCHRP Report 230 test 41/50)	27 (post 2) 34 (post 6)	Passed
BN-6		Sedan 4,870 lb	59.5 mph and 18.7 deg	Critical impact point (NCHRP Report 230 test 54)	27 (post 2) 34 (post 6)	Marginal - vehicle came to rest on top of system
BN-7		Sedan 4,665 lb	59.9 mph and 0.5 deg	Centerline of vehicle aligned with centerline of system (NCHRP Report 230 test 41/50)	29 (post 2) 34 (post 6)	Passed
BN-8		Sedan 4,695 lb	61.4 mph and 19.0 deg	Critical impact point (NCHRP Report 230 test 54)	29 (post 2) 34 (post 6)	Passed
BN-9		Sedan 4,680 lb	59.9 mph and 15.5 deg	Critical impact point (NCHRP Report 230 test 54)	29 (post 2) 34 (post 6)	Failed - rail ruptured
BN-10		Sedan 4,640 lb	59.9 mph and 15.0 deg	Critical impact point (NCHRP Report 230 test 54)	29 (post 2) 34 (post 6)	Passed

Table 11. Summary of Tested Bullnose Guardrail Systems (cont)

Test No.	Reference No.	Anchorages	Rail Configuration	System Dimensions	Post Details A	Post Details B	Post Details C	Post Details D	Post Details E	Post Details F	NOTES
BN-11	17	Post nos. 9-10 were removed and replaced with rigid concrete backup to simulate bridge pier (both sides)	Same as test no. BN-10	Same as test no. BN-10	Same as test no. BN-10	Same as test no. BN-10	Same as test no. BN-10	Same as test no. BN-10	6-in. x 8-in. timber post with 6-in. x 8-in. x 14-in. steel blockouts Post nos. 5-8, spaced 6-ft 3-in. on center, located 6-ft 3-in. from post no. 4	Rigid concrete backup structure Substituted for post nos. 9-10, 6-ft 3-in. attachment spacing, located 6-ft 3-in. from post no. 8	Rigid concrete backup structure added to simulate real-world bridge pier attachments
BN-12											
BN-13											
BN-14		Same as test nos. BN11 through BN13	Same as test nos. BN-11 through BN-13, except rectangular washers were added to post nos. 2 and 3 to retain posts with rail (both sides)	Same as test nos. BN-11 through BN-13	Same as test nos. BN-11 through BN-13	Same as test nos. BN-11 through BN-13	Same as test nos. BN-11 through BN-13	Same as test nos. BN-11 through BN-13	Same as test nos. BN-11 through BN-13	Same as test nos. BN-11 through BN-13	Rectangular washers added to post nos. 2 and 3 to retain posts on rail and reduce launching
BN-15		Same as test no. BN-14	Same as test no. BN-14	Same as test no. BN-14	Same as test no. BN-14, except blockout removed	Same as test no. BN-14, except blockout removed (both sides)	Same as test no. BN-14	Same as test no. BN-14	Same as test no. BN-14	Same as test no. BN-14	Blockouts removed from post nos. 1 and 2 (both sides)
BN-16		Same as test no. BN-15	Similar to test no. BN-15, except nose piece thickened to 10-gauge and slotted to catch small car bumper	Same as test no. BN-15	Same as test no. BN-15	Same as test no. BN-15	Same as test no. BN-15	Same as test no. BN-15	Same as test no. BN-15	Same as test no. BN-15	Final symmetrical system

Table 12. Summary of Short-Radius Guardrail Systems Full-Scale Crash Testing

Test No.	Reference No.	Vehicle	Impact Conditions	Impact Location	Rail Height (in.)	Result
BN-11	17	Sedan 4,305 lb	59.9 mph and 16.2 deg	Critical impact point (NCHRP Report 230 test 54)	29 (post 2) 34 (post 6)	Vehicle came to rest on top of rail - passed
BN-12		Pickup truck 5,400 lb	55 mph and 0.1 deg	Centerline of vehicle aligned with centerline of system (NCHRP Report 230 test 41/50)	29 (post 2) 34 (post 6)	Passed
BN-13		Small car 1,820 lb	59.4 mph and	Centerline of vehicle aligned with centerline of system (NCHRP Report 230 test 52/45)	29 (post 2) 34 (post 6)	Failed - excessive decelerations
BN-14		Small car 1,800 lb	58.7 mph and 2.7 deg	Centerline of vehicle aligned with centerline of system (NCHRP Report 230 test 52/45)	29 (post 2) 34 (post 6)	Failed - underride caused rail to crush windshield (due to vehicle bouncing in approach ditch)
BN-15		Small car 1,935 lb	58.7 mph and	Centerline of vehicle aligned with centerline of system (NCHRP Report 230 test 52/45)	29 (post 2) 34 (post 6)	Failed - underride caused rail to crush windshield
BN-16		Small car 1,935 lb	60.2 mph and	Centerline of vehicle aligned with centerline of system (NCHRP Report 230 test 52/45)	29 (post 2) 34 (post 6)	Despite windshield crush, passed

Table 13. Summary of Tested Bullnose Guardrail Systems (cont)

Test No.	Reference No.	Anchorages	Rail Configuration	System Dimensions	Post Details A	Post Details B	Post Details C	Post Details D	Post Details E	Post Details F	NOTES
MBN-1	19	Cable anchorage used at post no. 2 and cable end anchor used at end of system (symmetrical, both sides)	Nose: 12-ft 6-in. long, 62 3/16-in. radius, slotted thrie beam Transition: 12-ft 6-in. long, 34-ft 1.5-in. radius slotted thrie beam Straight Rail: 37-ft 6-in. thrie beam	14-ft 10-in. wide, 53-ft long	5.5-in. x 7.5-in. BCT post at end of radius Post no. 1	5.5-in. x 7.5-in. BCT post with cable anchor and angled ground strut to post no. 1 Post no. 2, located 6-ft 3-in. from post no. 1	6-in. x 8-in. timber posts with rectangular blockouts Post nos. 3-9, 6-ft 3-in. spacing, located 6-ft 3-in. from post no. 3	BCT end anchorage with ground strut Post nos. 10-11, located 6-ft 3-in. from post no. 9	N/A	N/A	Similar to BN-14 system, except ditch in front of system eliminated, post no. 1 shifted away from center of nose, and symmetrical construction
MBN-2		Same as test no. MBN-1	Similar to test no. MBN-1, except slot tabs in transition thrie beam were reduced, and slots were added to first of straight rail segments	Same as test no. MBN-1	Same as test no. MBN-1	Same as test no. MBN-1	5.5-in. x 7.5-in. BCT post with thrie beam blockout Post no. 3, located 6-ft 3-in. from post no. 2	6-in. x 8-in. CRT post with thrie beam blockout Post no. 4, located 6-ft 3-in. from post no. 3	6-in. x 8-in. timber posts with rectangular thrie beam blockouts Post nos. 5-9, 6-ft 3-in. spacing, located 6-ft 3-in. from post no. 4	BCT end anchorage with ground strut Post nos. 10-11, located 6-ft 3-in. from post no. 9	Post nos. 3 and 4 were converted to breakaway posts (both sides)
MBN-3	20	Same as test no. MBN-2	Same as test no. MBN-2	Same as test no. MBN-2	Same as test no. MBN-2	Similar to test no. MBN-2, except blockouts were reduced to 14.25-in. long	Similar to test no. MBN-2, except blockouts were reduced to 14.25-in. long	6-in. x 8-in. CRT posts with 14.25-in. tall blockouts Post nos. 4-5, 6-ft 3-in. spacing, located 6-ft 3-in. from post no. 3	6-in. x 8-in. timber posts with 14.25-in. tall blockouts Post nos. 6-9, 6-ft 3-in. spacing, located 6-ft 3-in. from post no. 5	Same as MBN-2	Blockout sizes reduced for post nos. 2-9, and post no. 5 converted to CRT
MBN-4		Same as test no. MBN-3	Same as test no. MBN-3, except that steel cables were added to middle and top corrugations of thrie beam at nose	Same as test no. MBN-3	Same as test no. MBN-3	Same as test no. MBN-3	Same as test no. MBN-3	Same as test no. MBN-3	Same as test no. MBN-3	Same as test no. MBN-3	Steel cables added to nose to reduce rail rupture potential
MBN-5	21	Same as test no. MBN-4	Same as test no. MBN-4	Same as test no. MBN-4	Same as test no. MBN-4	Same as test no. MBN-4	Same as test no. MBN-4	Same as test no. MBN-4	Same as test no. MBN-4	Same as test no. MBN-4	Same design, but new series of tests & new report
MBN-6											
MBN-7		Same as test no. MBN-5 and MBN-6	Same as test no. MBN-5 and MBN-6	Same as test no. MBN-5 and MBN-6	Same as test no. MBN-5 and MBN-6, except standard BCT foundation tubes used	6-in. x 8-in. CRT post with cable anchor and angled ground strut to post no. 1 Post no. 2, located 6-ft 3-in. from post no. 1	6-in. x 8-in. CRT posts with 14.25-in. tall blockouts Post nos. 3 through 6, 3-ft 1.5-in. spacing, located 3-ft 1.5-in. from post no. 2	6-in. x 8-in. CRT post with 14.25-in. tall blockout Post no. 7, located 6-ft 3-in. from post no. 6	6-in. x 8-in. timber posts with 14.25-in. tall blockouts Post nos. 8-11, 6-ft 3-in. spacing, located 6-ft 3-in. from post no. 7	BCT end anchorage with ground strut Post nos. 12-13, located 6-ft 3-in. from post no. 11	Two additional CRT posts added to give additional strength
MBN-8		Similar to test no. MBN-7, except that the groundline strut between post nos. 1 and 2 was eliminated (both sides)	Same as test no. MBN-7	Same as test no. MBN-7	Same as test no. MBN-7	5.5-in. x 7.5-in. BCT post with cable anchor Post no. 2, located 3-ft 1.5-in. from post no. 1	6-in. x 8-in. CRT posts with 14.25-in. tall blockouts (one straight, one tapered) Post nos. 3 through 7, 3-ft 1.5-in. spacing, located 3-	6-in. x 8-in. CRT post with 14.25-in. tall blockouts (one straight, one tapered) Post no. 8, located 6-ft 3-in. from post no. 7	6-in. x 8-in. timber posts with 14.25-in. tall blockouts Post nos. 9-12, 6-ft 3-in. spacing, located 6-ft 3-in. from post no. 8	BCT end anchorage with ground strut Post nos. 13-14, located 6-ft 3-in. from post no. 12	Final system details, approved according to NCHRP Report No. 350 criteria
MBN-9											
USPBN-1	22,23	Cable anchorage used at post no. 2 and cable end anchor used at end of system (symmetrical, both sides)	Nose: 12-ft 6-in. long, 62 3/16-in. radius, slotted thrie beam with reinforcing cables and swaged cable buttons Transition: 12-ft 6-in. long, 34-ft 1.5-in. radius slotted thrie beam Straight Rail: 37-ft 6-in. thrie beam	14-ft 10-in. wide, 53-ft long	5.5-in. x 7.5-in. BCT post in 90-in. deep foundation tube at end of radius Post no. 1	5.5-in. x 7.5-in. BCT post in 70-in. soil foundation tube with cable anchor Post no. 2, located 3-ft 1.5-in. from post no. 1	Universal Breakaway Steel Posts with 14.25-in. tall blockouts (one straight, one tapered) Post nos. 3 through 7, 3-ft 1.5-in. spacing, located 3-ft 1.5-in. from post no. 2	Universal Breakaway Steel Post with 14.25-in. tall blockouts (one straight, one tapered) Post no. 8, located 6-ft 3-in. from post no. 7	W6x9 posts with 6-in. x 8-in. x 14.25-in. straight blockouts Post nos. 9-12, spaced 6-ft 3-in., located 6-ft 3-in. from post no. 8	BCT end anchorage with ground strut Post nos. 13-14, located 6-ft 3-in. from post no. 12	Similar to MBN-9 using Universal Breakaway Steel Posts developed at MwRSF
USPBN-2	24	Same as USPBN-1	Same as USPBN-1	Same as USPBN-1	Same as USPBN-1	Same as USPBN-1	Similar to USPBN-1, except MwRSF's modified Universal Breakaway Steel Post substituted for the original	Similar to USPBN-1, except MwRSF's modified Universal Breakaway Steel Post substituted for the original	Same as USPBN-1	Same as USPBN-1	Similar to USPBN-2 using modified Universal Breakaway Steel Posts developed at MwRSF Approved according to NCHRP Report No. 350

Table 14. Summary of Short-Radius Guardrail Systems Full-Scale Crash Testing

Test No.	Reference No.	Vehicle	Impact Conditions	Impact Location	Rail Height (in.)	Result
MBN-1	19	1989 Ford F250 pickup 4,404 lb	63.0 mph and 0.1 deg	Centerline of vehicle aligned with centerline of system	31.625 (thrie beam)	Failure - rail rupture permitted vehicle penetration
MBN-2		1988 Ford Festiva small car 1,953 lb	64.2 mph and -3.4 deg	1/4-point offset of vehicle with centerline of system	31.625 (thrie beam)	Passed
MBN-3	20	1990 Chevrolet C2500 pickup 4,384 lb	62.2 mph and -1.1 deg	Centerline of vehicle aligned with centerline of system	31.625 (thrie beam)	Failure - rail rupture permitted vehicle penetration
MBN-4		1991 Chevrolet C2500 pickup 4,431 lb	64.3 mph and 0.58 deg	Centerline of vehicle aligned with centerline of system	31.625 (thrie beam)	Passed
MBN-5	21	1993 Chevrolet C2500 pickup 4,493 lb	64.0 mph and 13.4 deg	Centerline of vehicle aligned with center point of nose	31.625 (thrie beam)	Passed
MBN-6		1991 Chevrolet C2500 pickup 4,477 lb	63.1 mph and 20.4 deg	CIP along length of thrie beam	31.625 (thrie beam)	Failure - rail formed ramp, vehicle vaulted
MBN-7		1992 Chevrolet C2500 pickup 4,488 lb	62.1 mph and 24.9 deg	CIP along length of thrie beam	31.625 (thrie beam)	Failure - rail formed ramp, vehicle vaulted
MBN-8		1992 GMC 2500 pickup 4,482 lb	62.0 mph and 21.5 deg	CIP along length of thrie beam	31.625 (thrie beam)	Passed
MBN-9		1990 Ford Festiva small car 1,993 lb	65.2 mph and 15.7 deg	Centerline of vehicle aligned with center point of nose	31.625 (thrie beam)	Passed
USPBN-1	22,23	2000 GMC 2500 pickup 4,474 lb	63.2 mph and 22.6 deg	Centerline of truck aligned with center of post no. 3	31.625 (thrie beam)	Failure - rail formed ramp, vehicle vaulted
USPBN-2	24	GMC 2500 pickup 4,564 lb	62.9 mph and 21.7 deg	Centerline of truck aligned with center of post no. 3	31.625 (thrie beam)	Passed

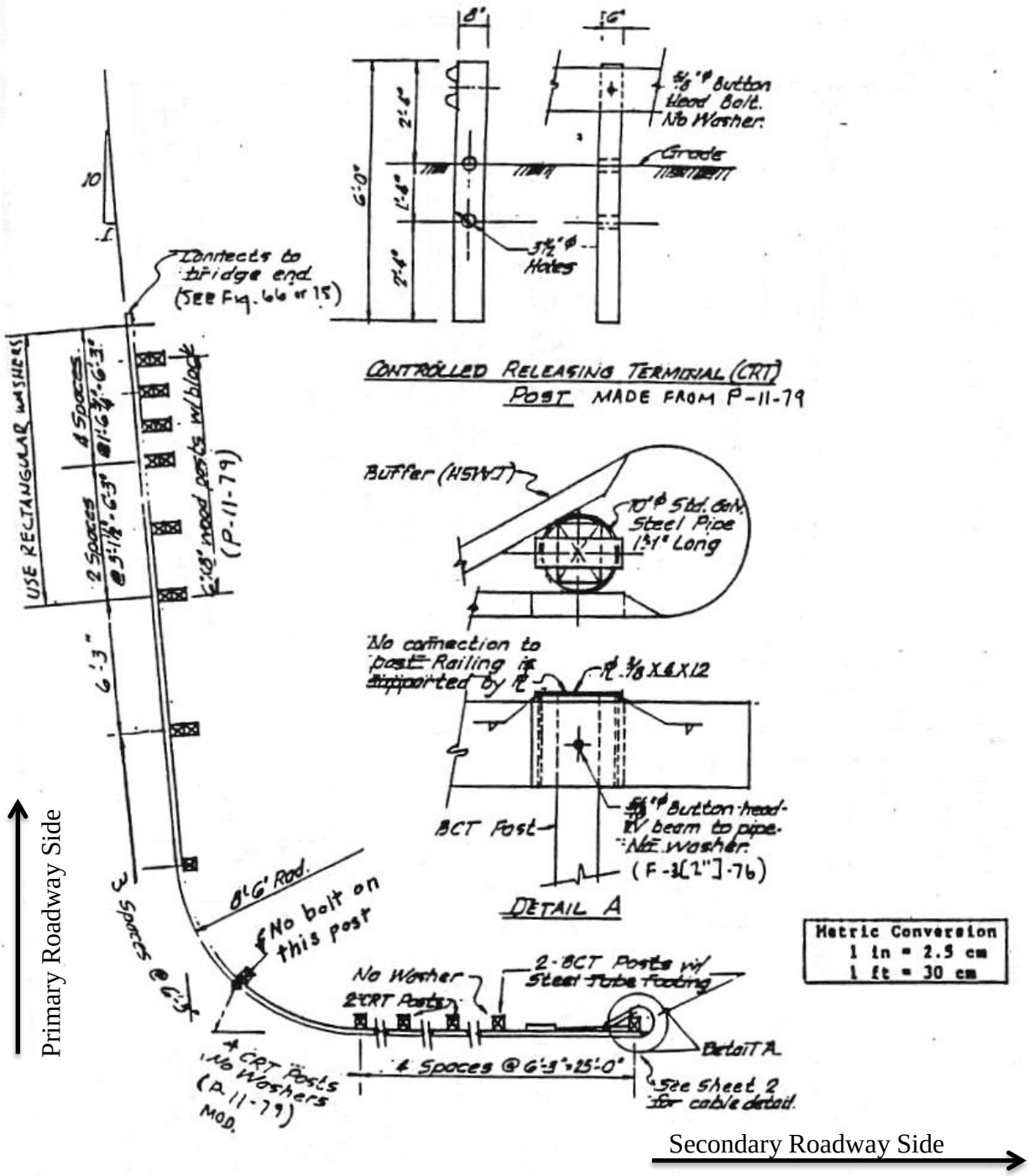

Figure 1. Washington W-Beam Short Radius Design [10]

mm x 203 mm x 362 mm) timber blockouts. The final design was determined to pass all crash test criteria according to NCHRP Report No. 230.

The TTI W-beam short radius system utilized round timber posts instead of rectangular posts, and anchored the W-beam on the secondary roadway with a W-beam turndown anchor [11]. The TTI system is shown in Figures 2 through 7. The W-beam guardrail was nested throughout the radius section. The transition utilized tubular, nested rail with an additional rail mounted backwards against the post. A cable anchor was attached to the rail downstream of the radius to develop tension in the transition region.

The TTI W-beam system was tested and evaluated according to NCHRP Report 230 evaluation criteria. The system performed acceptably during each crash test, with one exception. After the 4,500-lb (2,041-kg) sedan impacted the curved rail at 15 degrees and 90% of the vehicle's energy was dissipated, the rail disengaged from the bumper and rose up the vehicle's front end, crushing the windshield. Although this performance was determined to be unacceptable, researchers postulated that since this impact type was both infrequent and relatively severe, the system would perform acceptably in the majority of impacts. Thus, the system was recommended for use in locations with intersecting roadways.

2.1.2 System Tested to AASHTO *Guidance Specifications*

The Yuma County system [6] was designed specifically for one oblique intersection, with a 5.5-degree system flare. The successfully-tested final system details are shown in Figure 8. Researchers identified five different critical impact locations with associated impact angles to assess system performance. Light truck impacts were used to assess structural adequacy and pocketing near the transition and when impacted tangentially to the bridge rail, in addition to an angled impact on the nose. Small car impacts were used to evaluate the tendency to underride when impacting tangentially to the bridge rail and at an angle to the nose.

The preliminary design of the Yuma County system performed acceptably according to AASHTO PL-1 criteria in all but one test, in which both of the secondary-side anchorage BCT

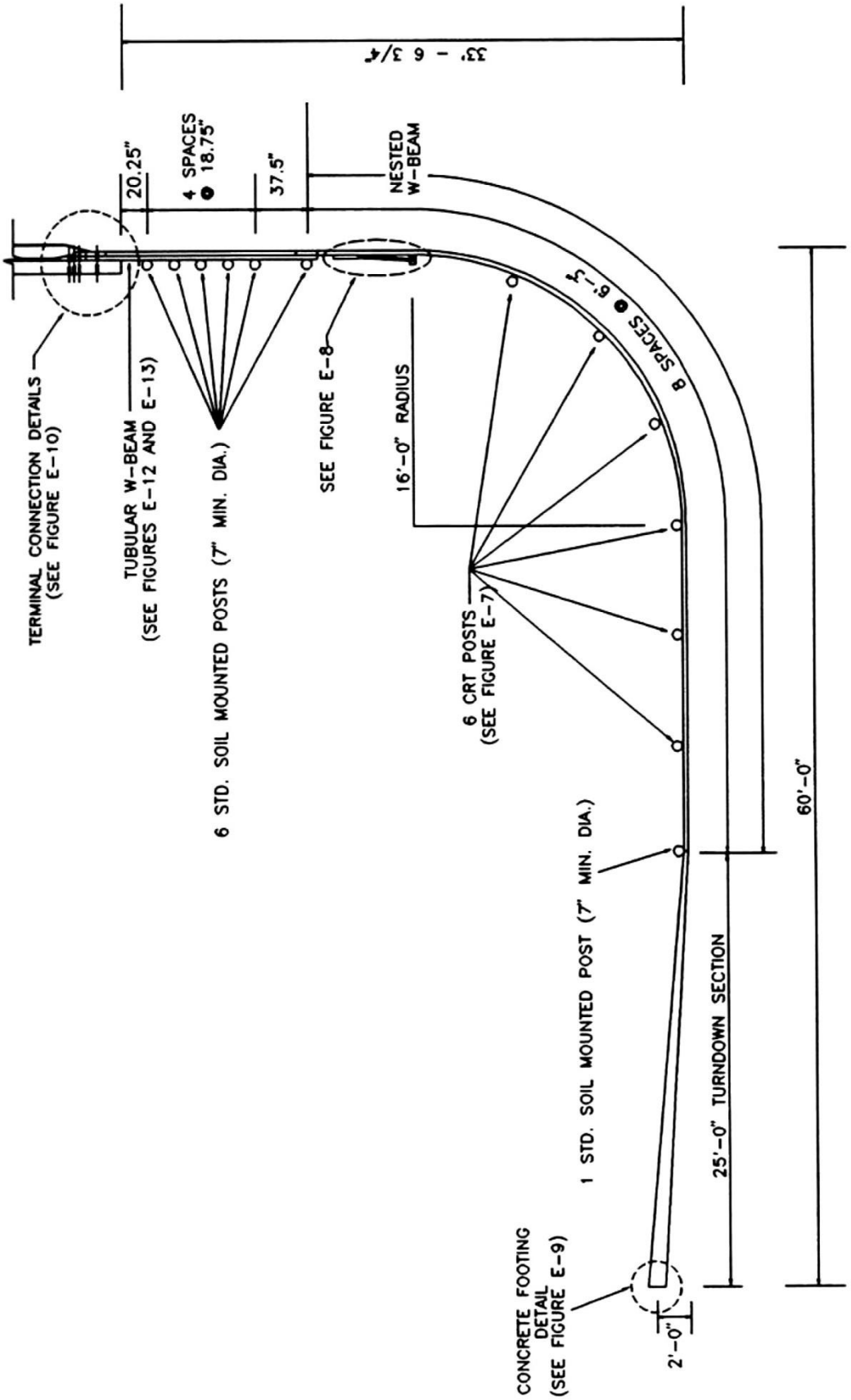

Figure 2. TTI W-Beam Short Radius Design [11]

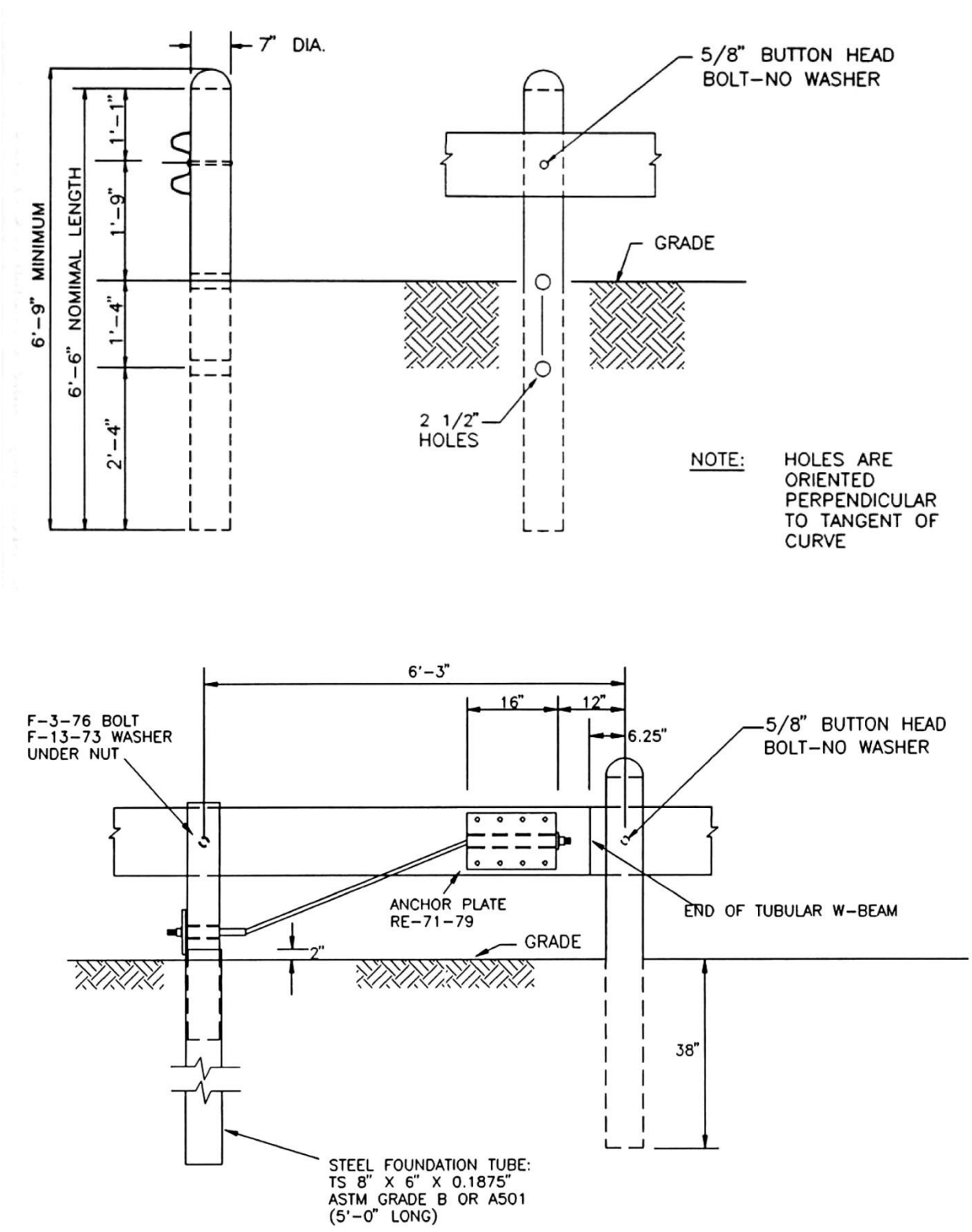

Figure 3. CRT Post and Cable Anchor Details, TTI W-Beam Short Radius System [11]

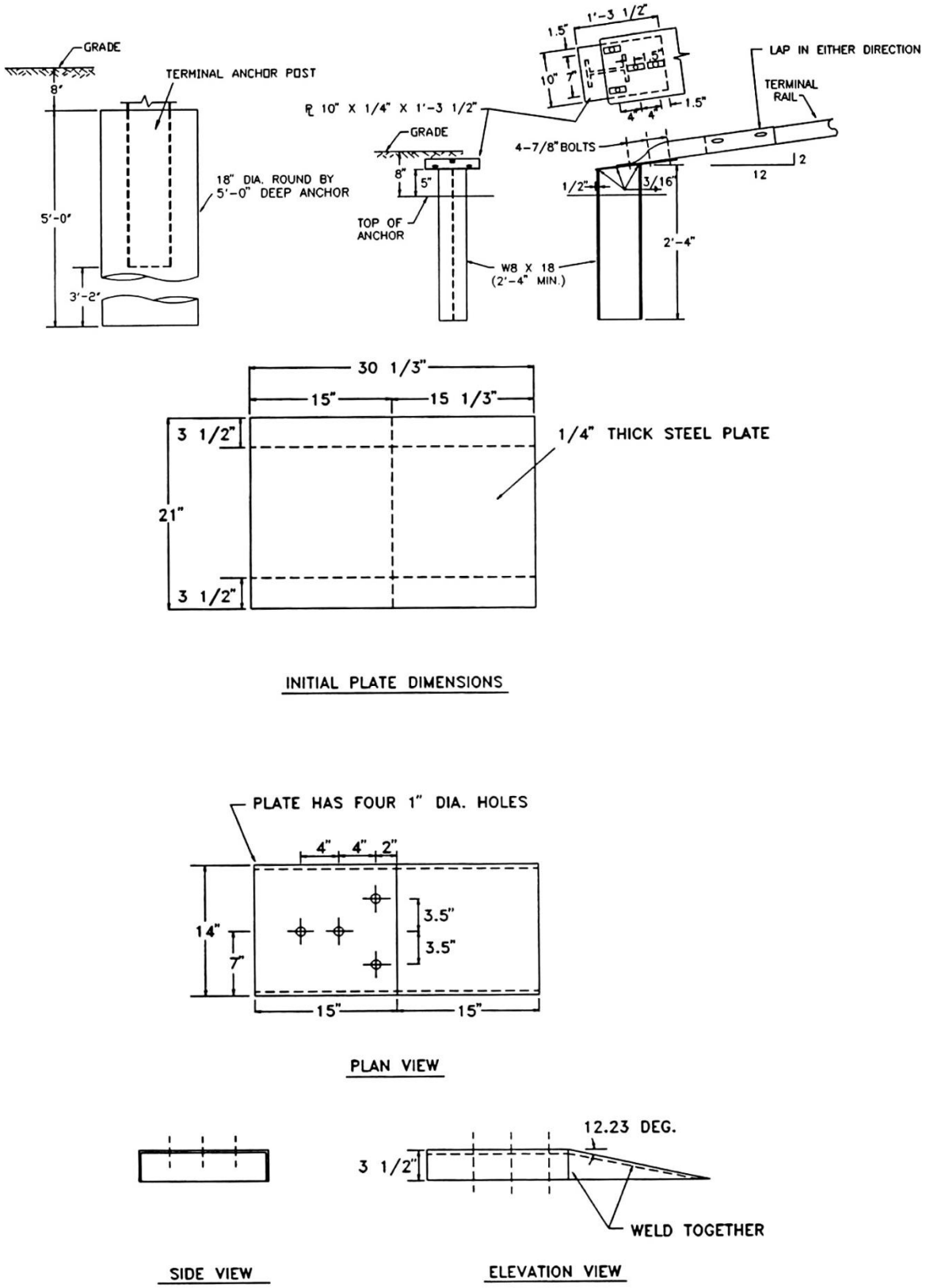

Figure 4. Turndown Rail Details, TTI W-Beam Short Radius System [11]

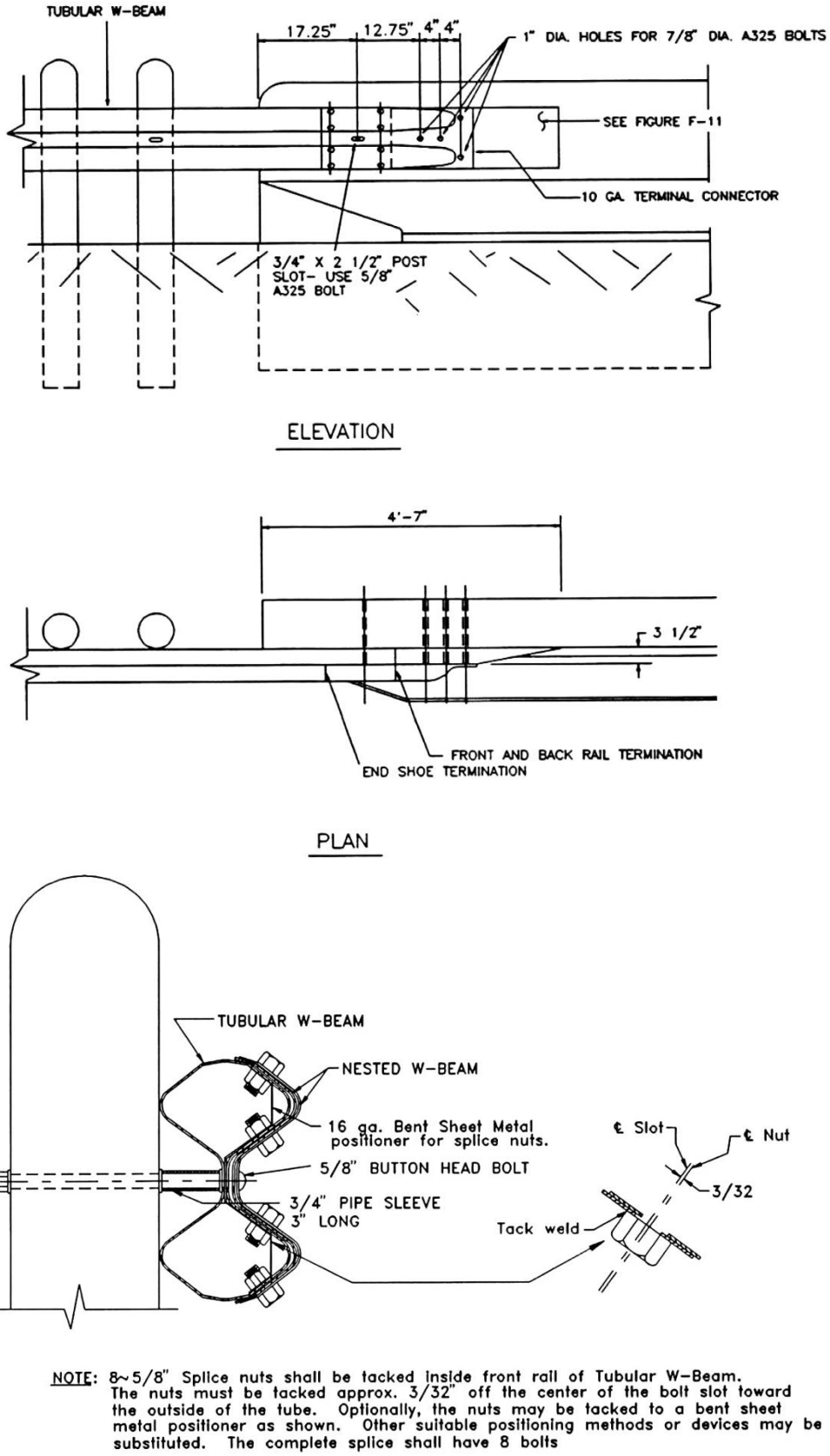

Figure 5. Transition Details, TTI W-Beam Short Radius System [11]

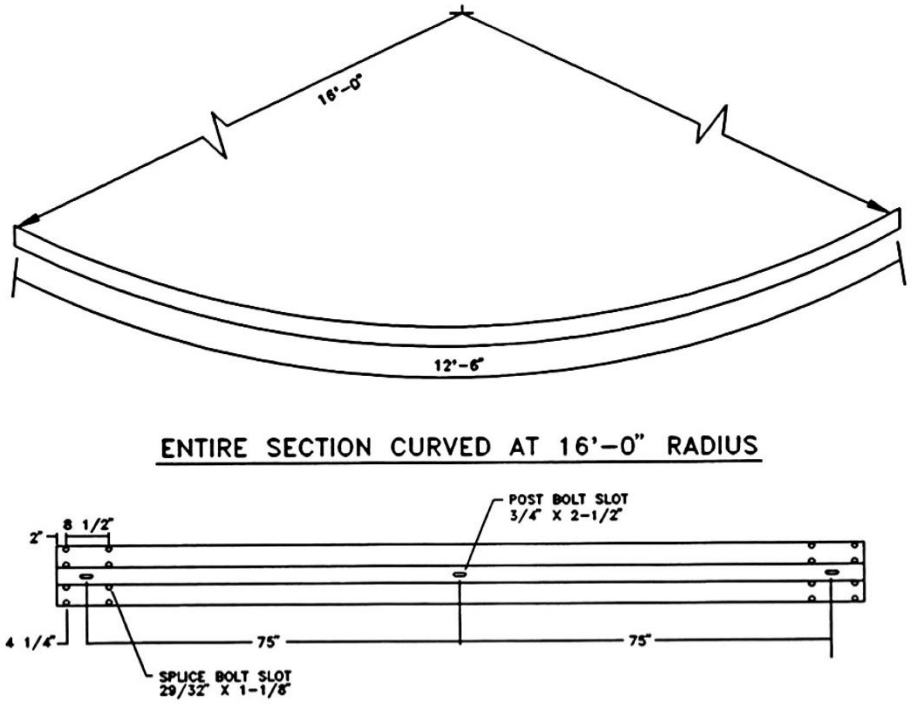

Figure 6. Curved Rail Bend Details, TTI W-Beam Short Radius System [11]

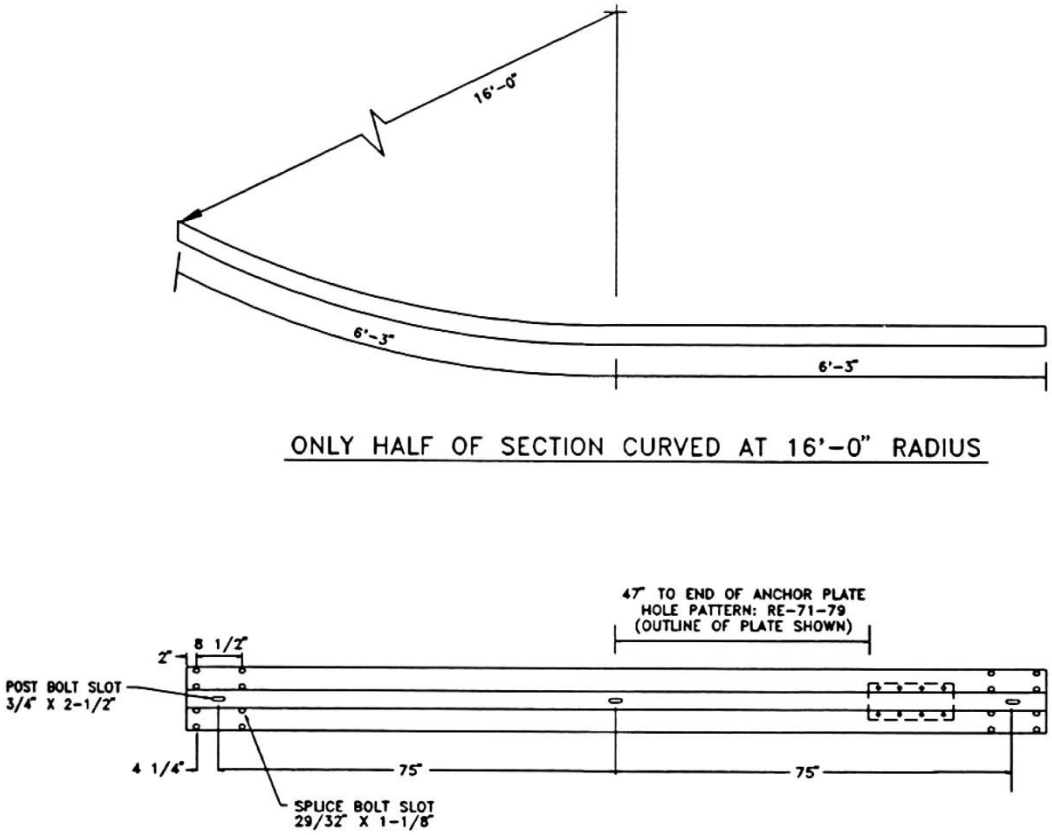

Figure 7. Downstream Curved Rail Bend Details, TTI W-Beam Short Radius System [11]

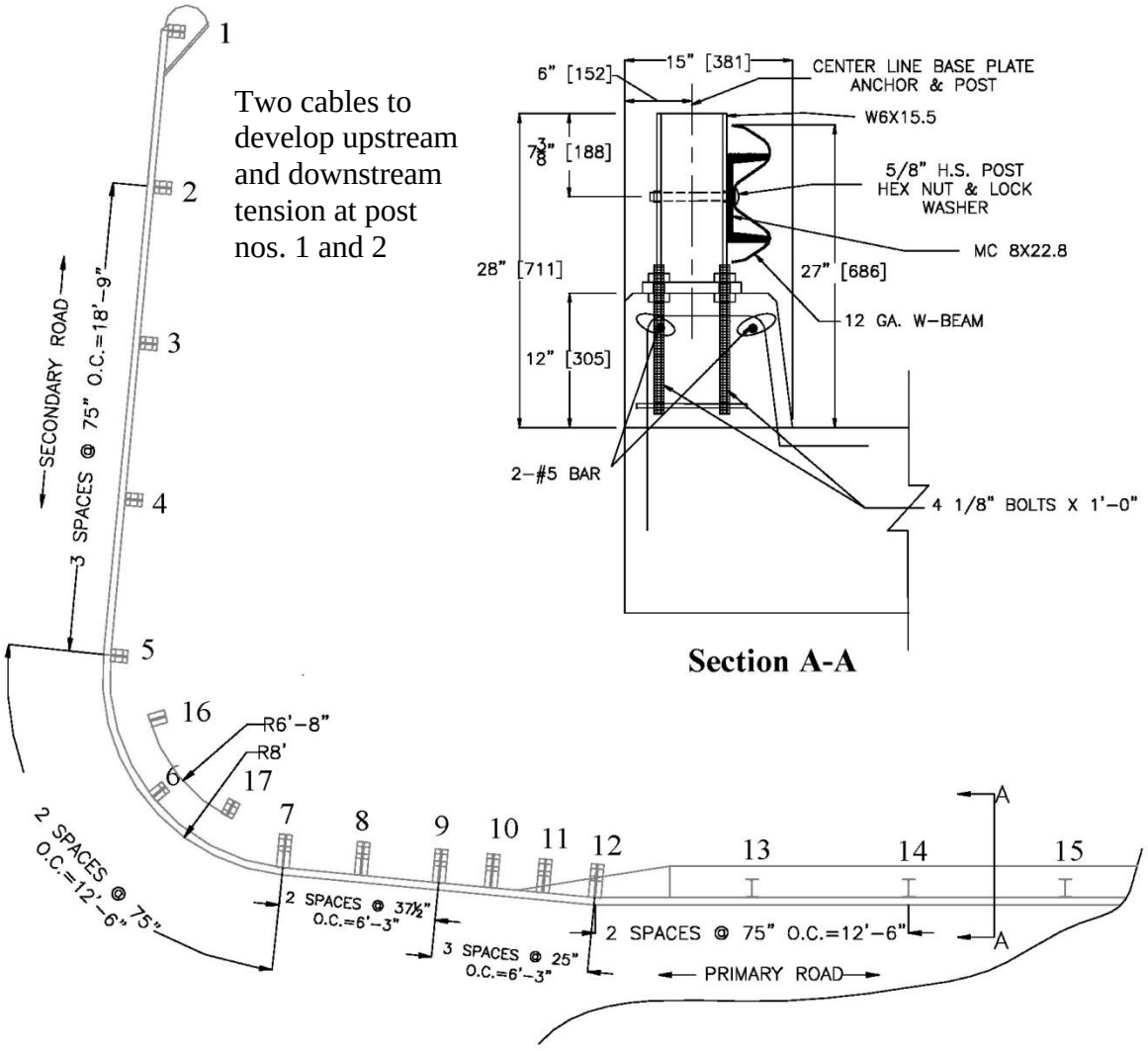

Figure 8. Yuma County Short-Radius Guardrail System Final Design Details [6, 27]

posts fractured and the spliced two-cable BCT anchor released, allowing the vehicle to encroach behind the barrier system. Researchers lengthened the secondary side of the system to increase anchoring capacity, and the system was determined to be successful.

2.2 Short Radius Systems Tested to NCHRP Report No. 350 and MASH

No short radius systems have yet been approved according to the TL-3 crash test conditions required in NCHRP Report No. 350 or MASH. The majority of NCHRP Report No. 350 and MASH-compliant tests on short-radius system were conducted at either TTI or the Midwest Roadside Safety Facility (MwRSF).

2.2.1 TTI Short-Radius Project

Researchers at TTI designed a thrie beam alternative to the TTI W-beam short-radius system successfully tested according to NCHRP Report No. 230 [8]. Final design details are shown in Figures 9 through 14. Researchers observed that the bending section of a nested 12-gauge (2.6-mm) W-beam section was approximately equivalent to the bending strength of a 10-gauge (3.3-mm) thrie beam section. Due to the broader capture area of the thrie beam, the higher top mounting height and lower bottom corrugation height, and ease of construction relative to the nested W-beam guardrails particularly at splice locations, researchers postulated that the thrie beam should perform approximately as well as the W-beam system.

Initially, the design was tested according to the TL-3 impact conditions criteria presented in NCHRP Report No. 350. The first crash test, consisting of a 2000P vehicle impacting the system at 60.9 mph (98.0 km/h) and 26 degrees near the transition, was determined to be successful. The remaining two tests conducted with a 2000P vehicle into the curved nose of the system were both determined to be failures, due to override and vaulting. Researchers concluded that the system would require extensive modification to be considered crashworthy according NCHRP Report No. 350.

Testing commenced with the 1,800-lb (816-kg) small car and 4,500-lb (2,041-kg) sedan with angled hits into the center of the curved radius in compliance with NCHRP Report No. 230. The two tests passed with marginal performance due to the release of the rail from the upstream turned-down anchor in the sedan test and underride of the small car. The marginal performance of the system was unexpected, because the increased top mounting height of 31 in. (787 mm) also resulted in a lower bottom mounting height of 13 in. (330 mm), so underride was not expected.

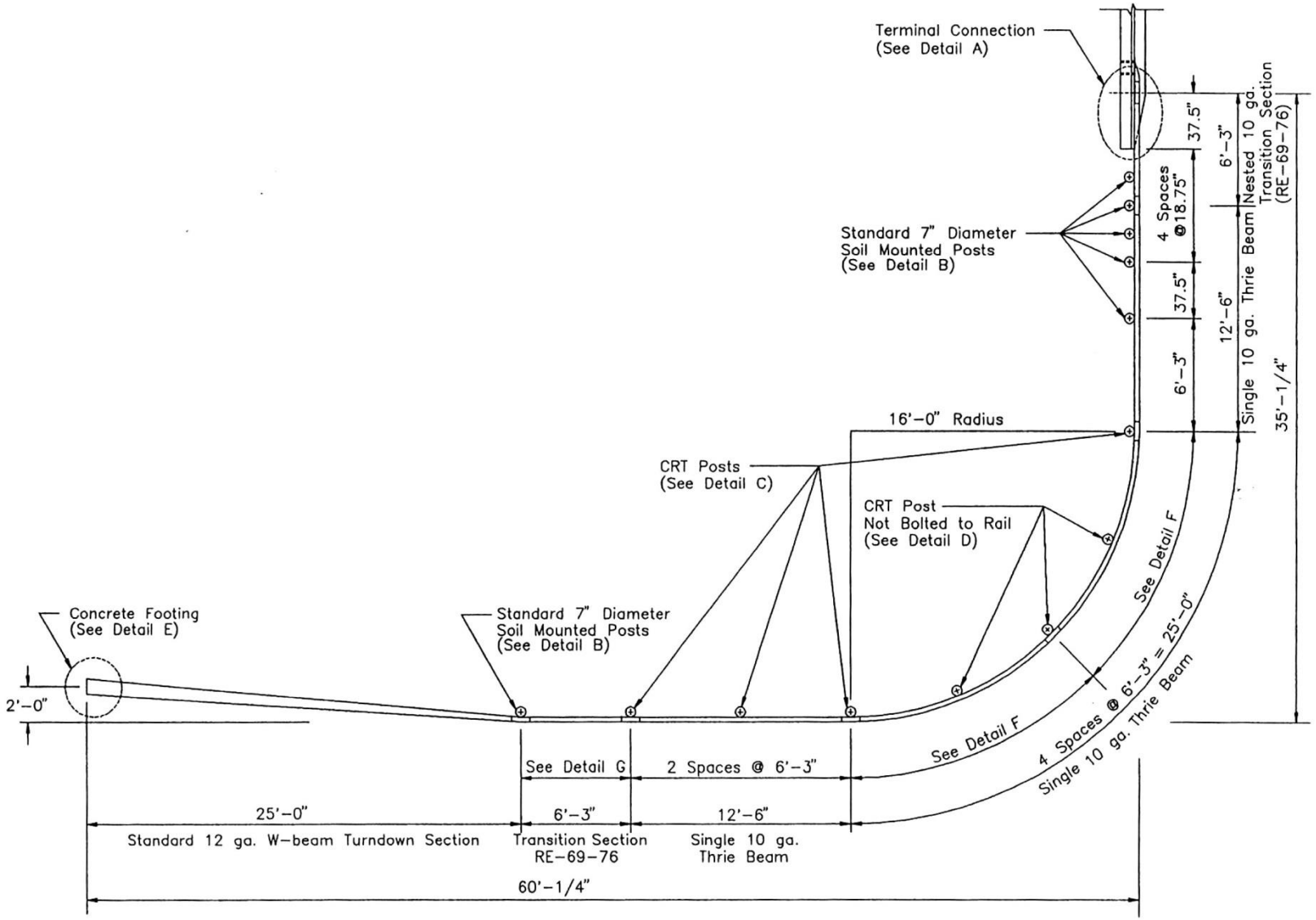

Figure 9. Final Thrie Beam Short Radius Design, TTI Thrie Beam Short Radius System [8]

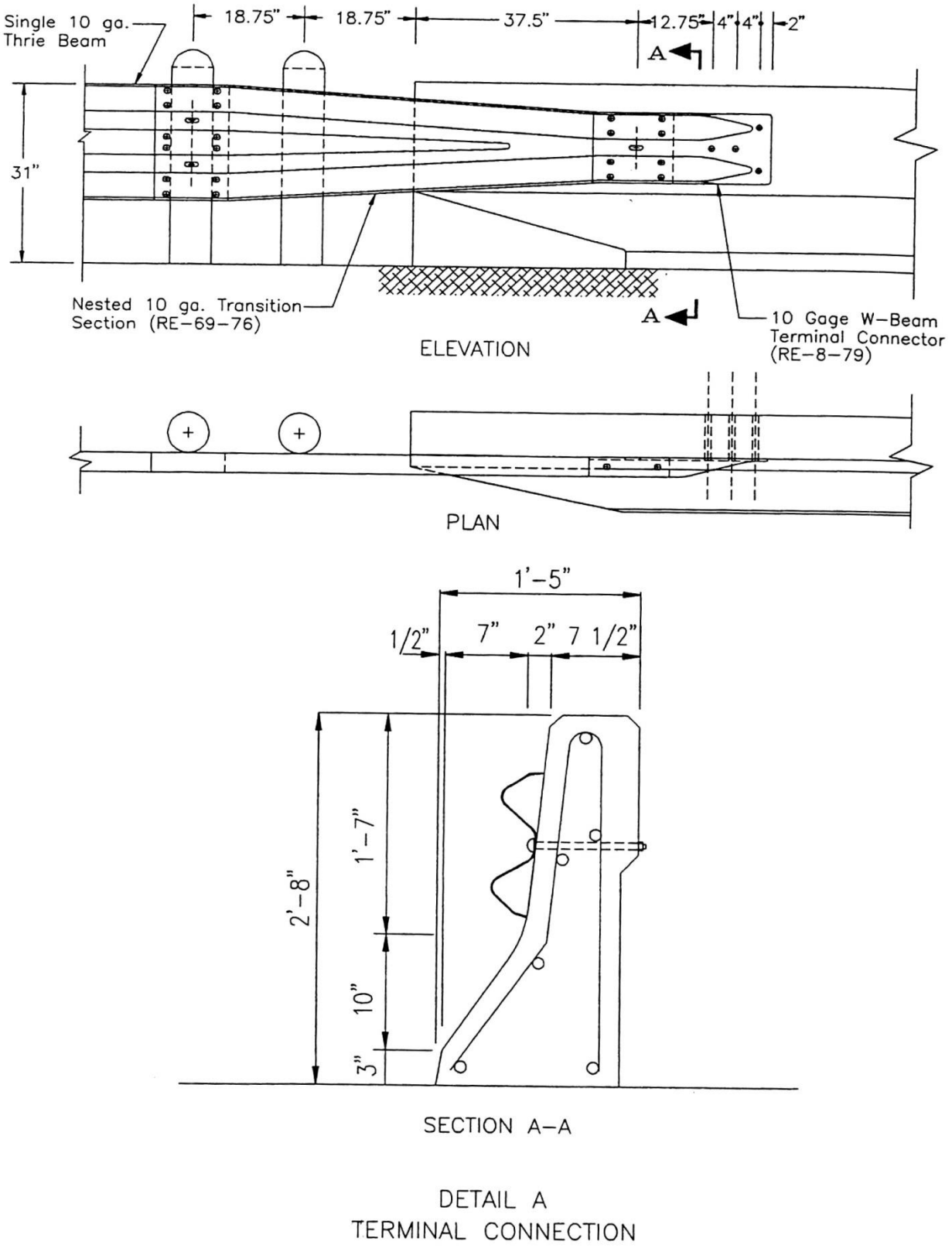

Figure 10. Transition to Rigid Bridge Rail Details, TTI Thrie Beam Short Radius System [8]

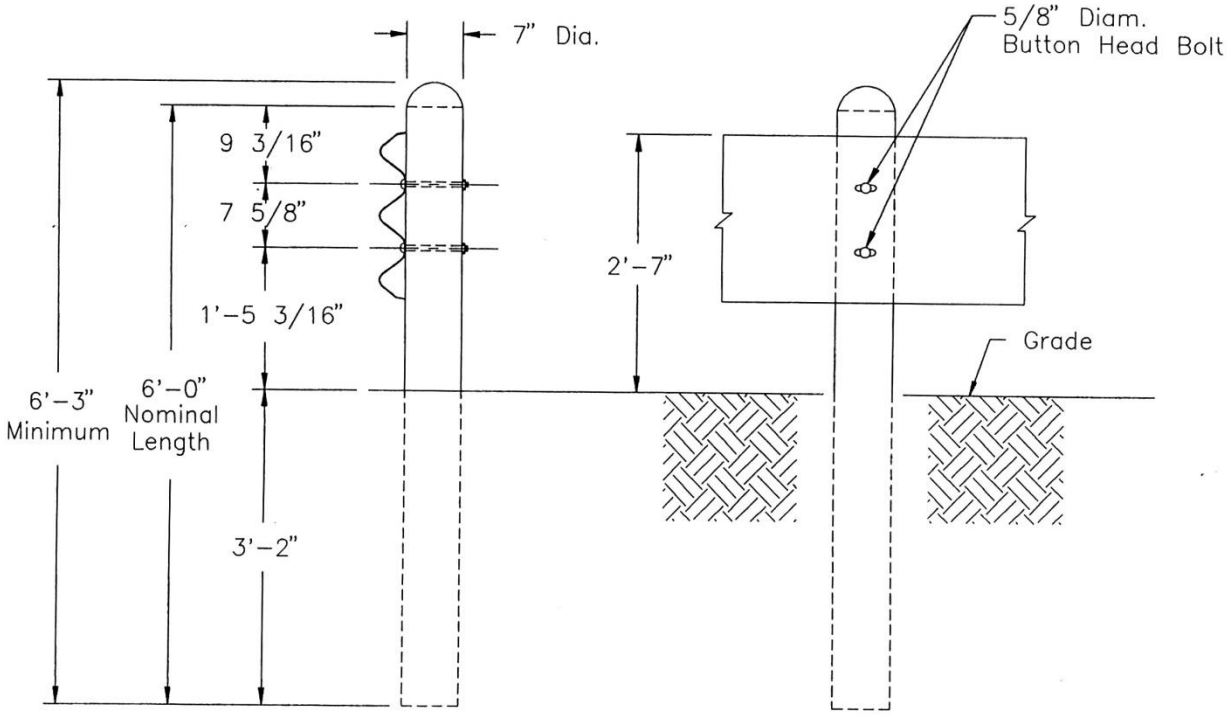

DETAIL B
STANDARD POST

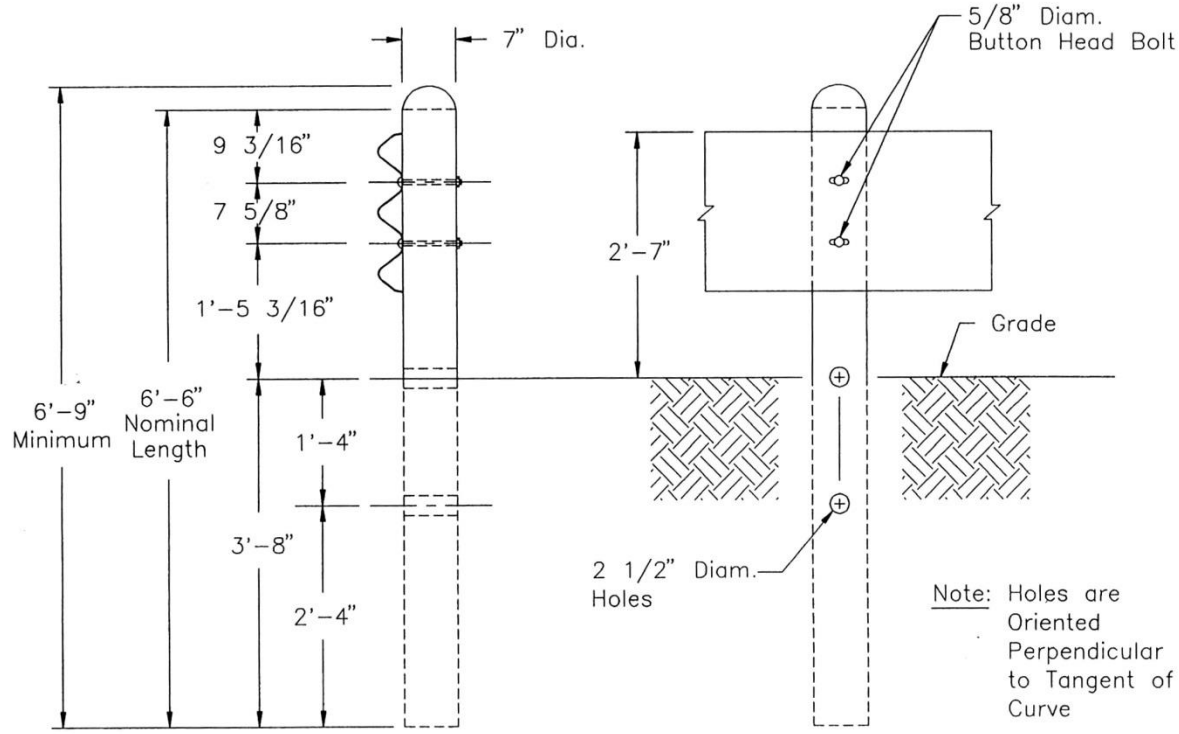

DETAIL C
CRT POST

Figure 11. Standard and CRT Post Details, TTI Thrie Beam Short Radius System [8]

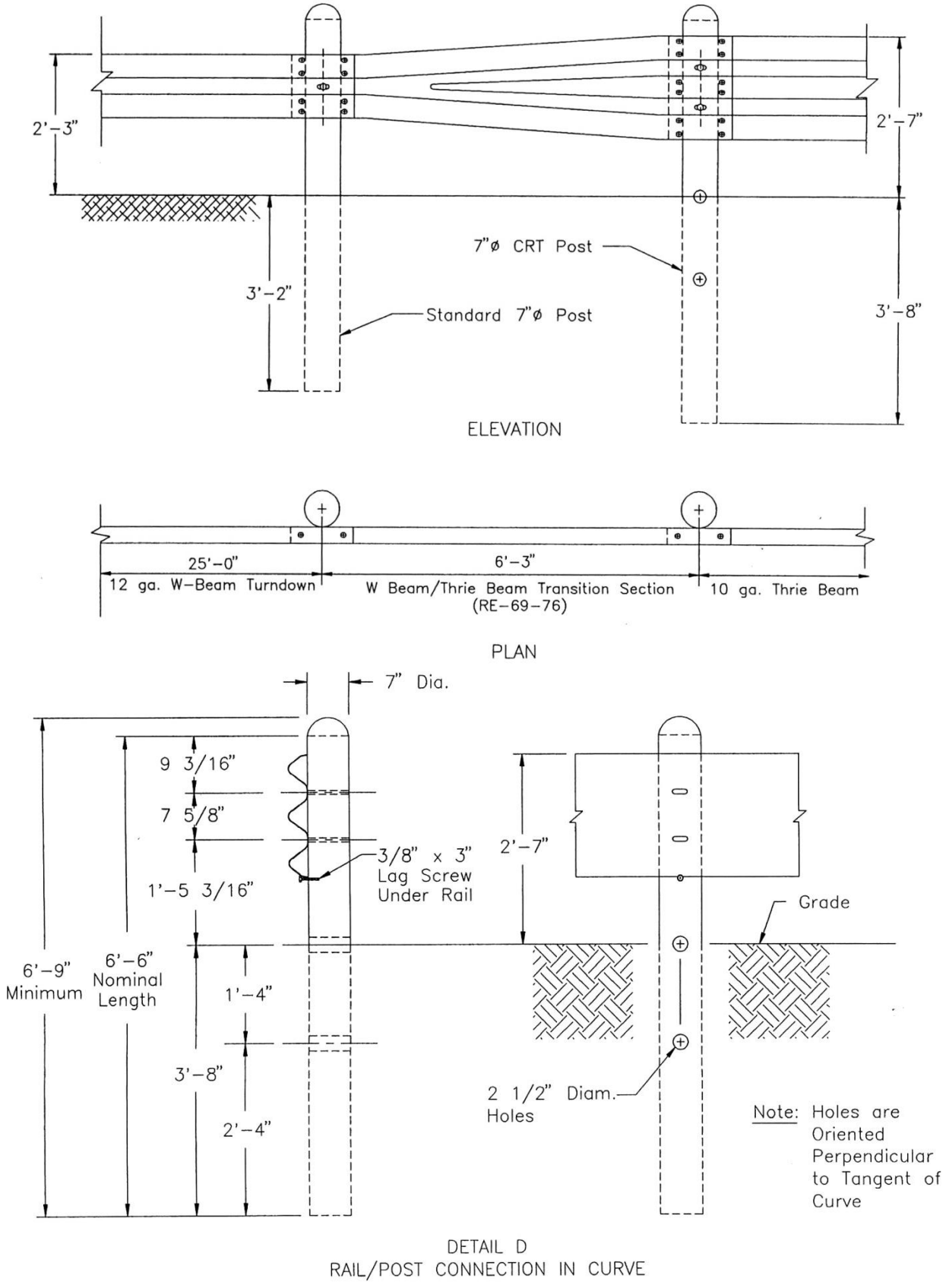

Figure 12. Rail-to-Post Connection Details, TTI Thrie Beam Short Radius System [8]

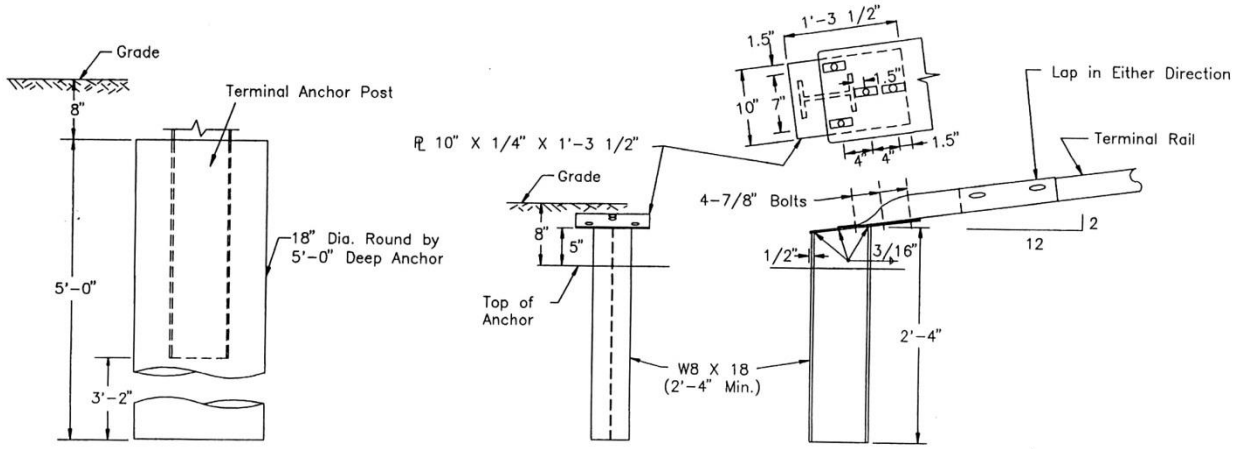

Figure 13. Turned-Down Anchor Details, TTI Thrie Beam Short Radius System [8]

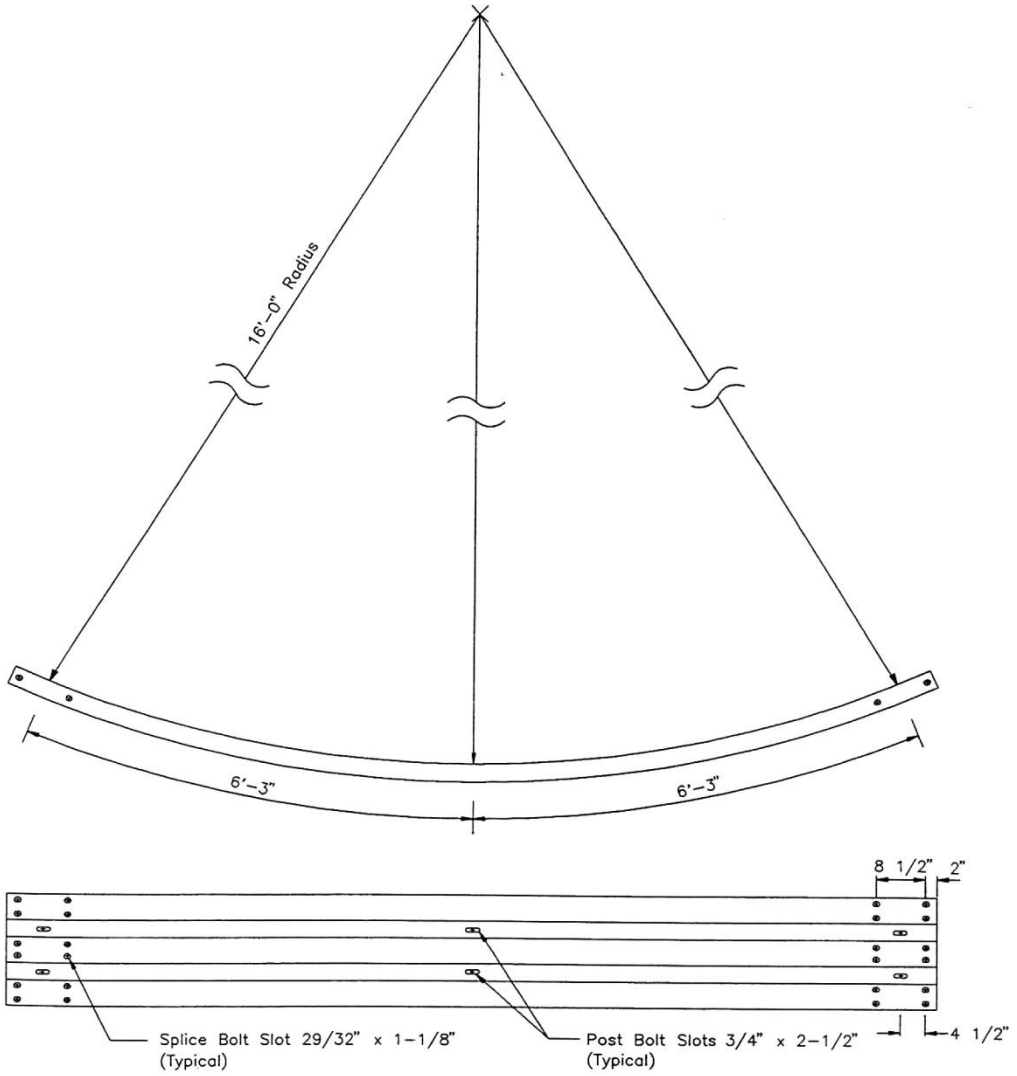

Figure 14. Curved Nose Thrie Beam Section, TTI Thrie Beam Short Radius System [8]

2.2.2 MwRSF Short-Radius Project

The Midwest Roadside Safety Facility (MwRSF) also attempted to develop a crashworthy system according to the TL-3 test criteria presented in NCHRP Report No. 350 [9, 12-13], as shown in Figure 15, and subsequently tested the system to the criteria presented in MASH [14]. The final design tested in compliance with MASH is shown in Figures 16 through 34. The short radius system was based on previous research on the NCHRP Report No. 350 tested thrie beam bullnose system and was constructed using curved thrie beam. Rectangular CRT posts were used to support the rail on both the primary and secondary sides of the roadway.

The curved nose piece initially had a 7 ft – 9¾ in. (2,381 mm) radius, which was later changed to 8 ft – 11⅜ in. (2,727 mm) when a parabolic flare was added to the system. Early tests utilized sloped terrain behind the system to replicate real-world conditions with roadside slopes, but the slopes were removed due to the increased risk of vaulting and artificial increase in instability due to interaction with the back side of the sloped cutout during testing.

A total of six tests were conducted in compliance with NCHRP Report No. 350 TL-3 test criteria [9, 12-13], and two tests were conducted in compliance with MASH TL-3 test criteria [14]. Impact conditions for each test are described in Tables 11 and 13. Only one test was determined to be successful, which consisted of a 2000P pickup truck impacting the system with the centerline of the truck aligned with a tangent line to the bridge rail. The remaining tests, primarily consisting of angled impacts with 2000P, 820C, and 2270P vehicles into the center of the nose, failed due to vaulting, rollover, or underride.

Researchers concluded that while the system performed very well overall despite the failure to comply with the evaluation criteria, it would likely be acceptable according to TL-2 impact conditions. However, the system was excessively large on the primary and secondary road sides and undesirable for a lower performance level, and no further testing was conducted.

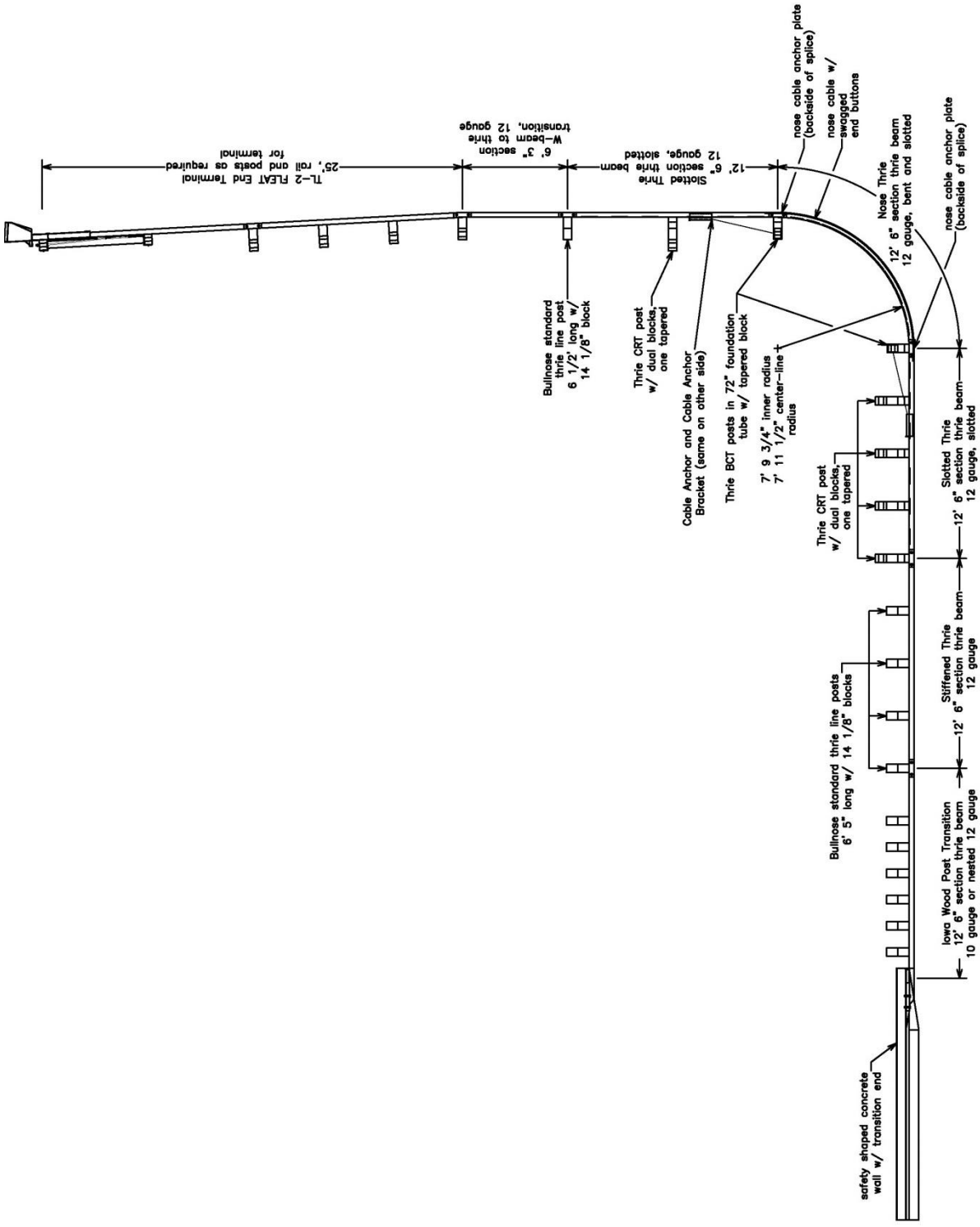

Figure 15. Preliminary Thrie Beam Short Radius Design, MwRSF Short Radius System [12, 9]

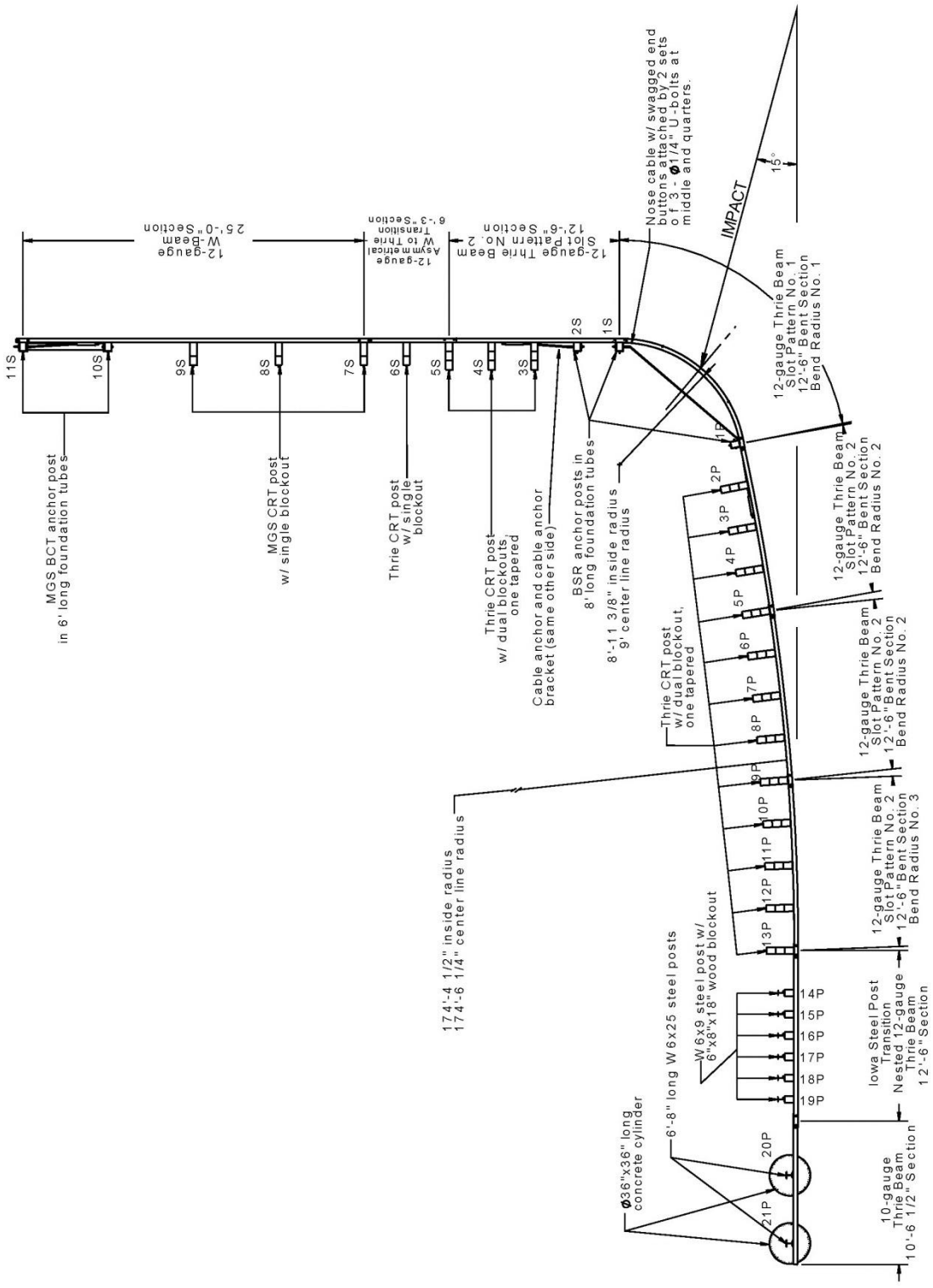

NOTE: Short radius post bolt washers located on post nos. 1P-4P and 1S-2S

Figure 16. Final Thrie Beam Short Radius Design, MwRSF Short Radius Design [14]

Post No.	Front Face D.S. Edge		Front Face U.S. Edge	
	X	Y	X	Y
1P	36'-11 1/16"	3'-11 5/8"	37'-4 5/8"	4'-0 5/8"
2P	33'-7 7/8"	4'-7 5/8"	34'-1 3/4"	4'-8 13/16"
3P	30'-7 5/16"	4'-0 3/4"	31'-1 1/4"	4'-1 13/16"
4P	27'-6 9/16"	3'-6 1/2"	28'-0 1/2"	3'-7 7/16"
5P	24'-5 1/2"	3'-0 13/16"	24'-11 7/16"	3'-1 3/4"
6P	21'-4 15/16"	2'-7 15/16"	21'-10 7/8"	2'-8 11/16"
7P	18'-3 11/16"	2'-3 5/8"	18'-9 5/8"	2'-4 3/8"
8P	15'-2 7/8"	2'-0 1/16"	15'-8 7/8"	2'-0 5/8"
9P	12'-1 11/16"	1'-9 1/8"	12'-7 11/16"	1'-9 9/16"
10P	9'-0 9/16"	1'-6 13/16"	9'-6 9/16"	1'-7 3/16"
11P	5'-11 1/2"	1'-5 1/4"	6'-5 1/2"	1'-5 7/16"
12P	2'-10 1/4"	1'-4 1/4"	3'-4 1/4"	1'-4 3/8"
13P	-0'-3"	1'-4"	0'-3"	1'-4"

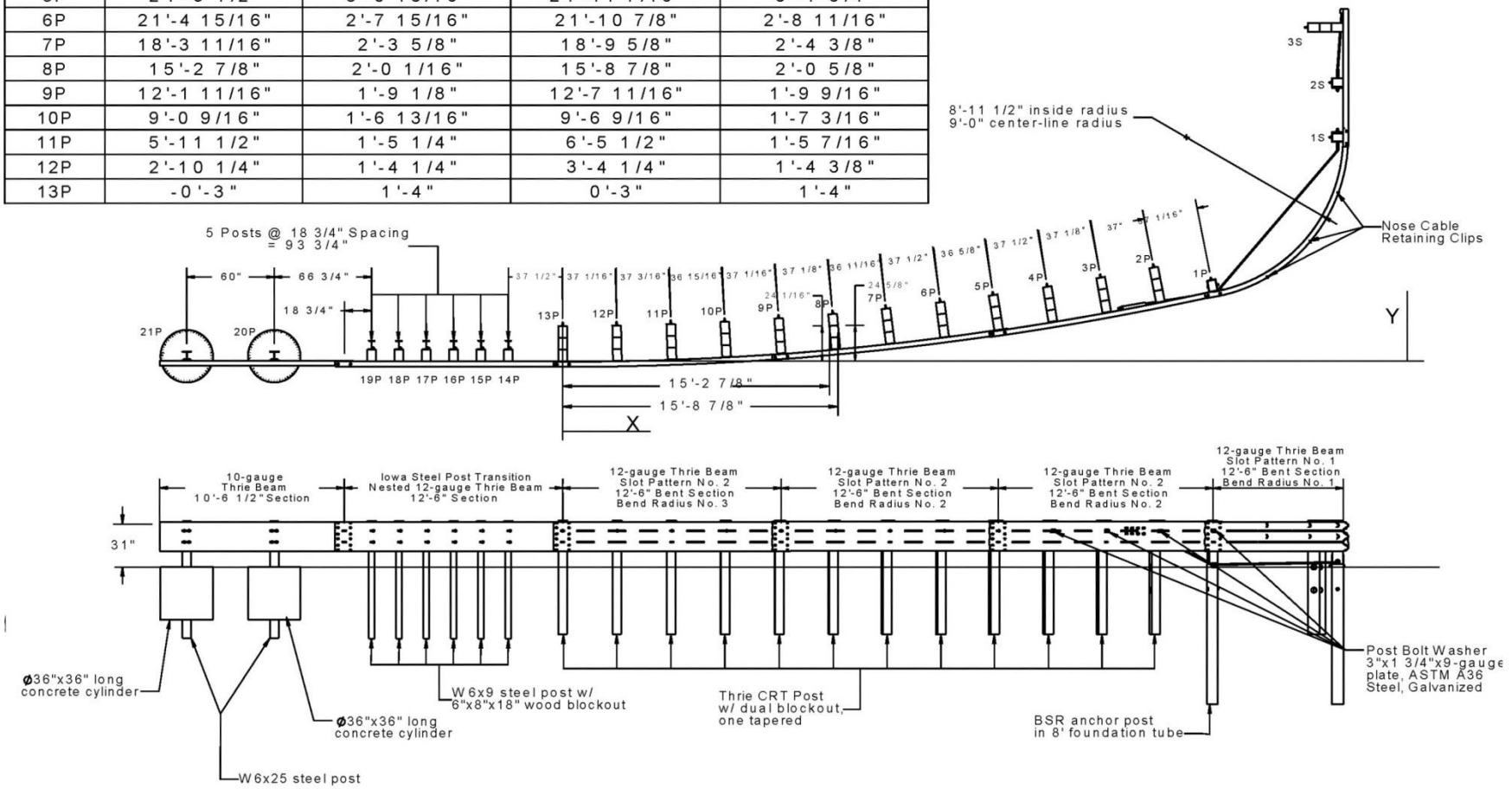

Figure 17. Primary Side Post Layout, MwRSF Short Radius Design [14]

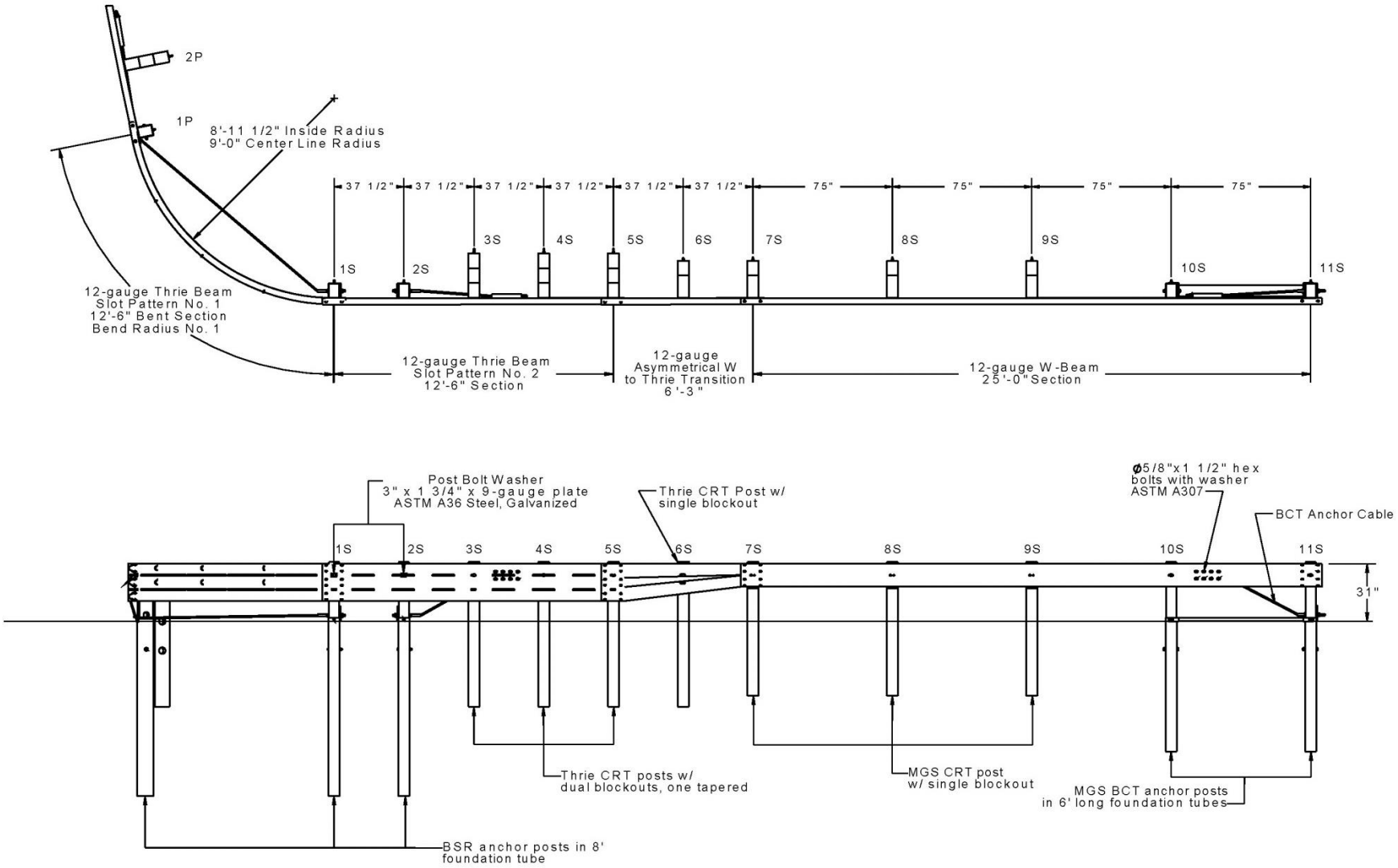

Figure 18. Secondary Side Post Layout, MwRSF Short Radius Design [14]

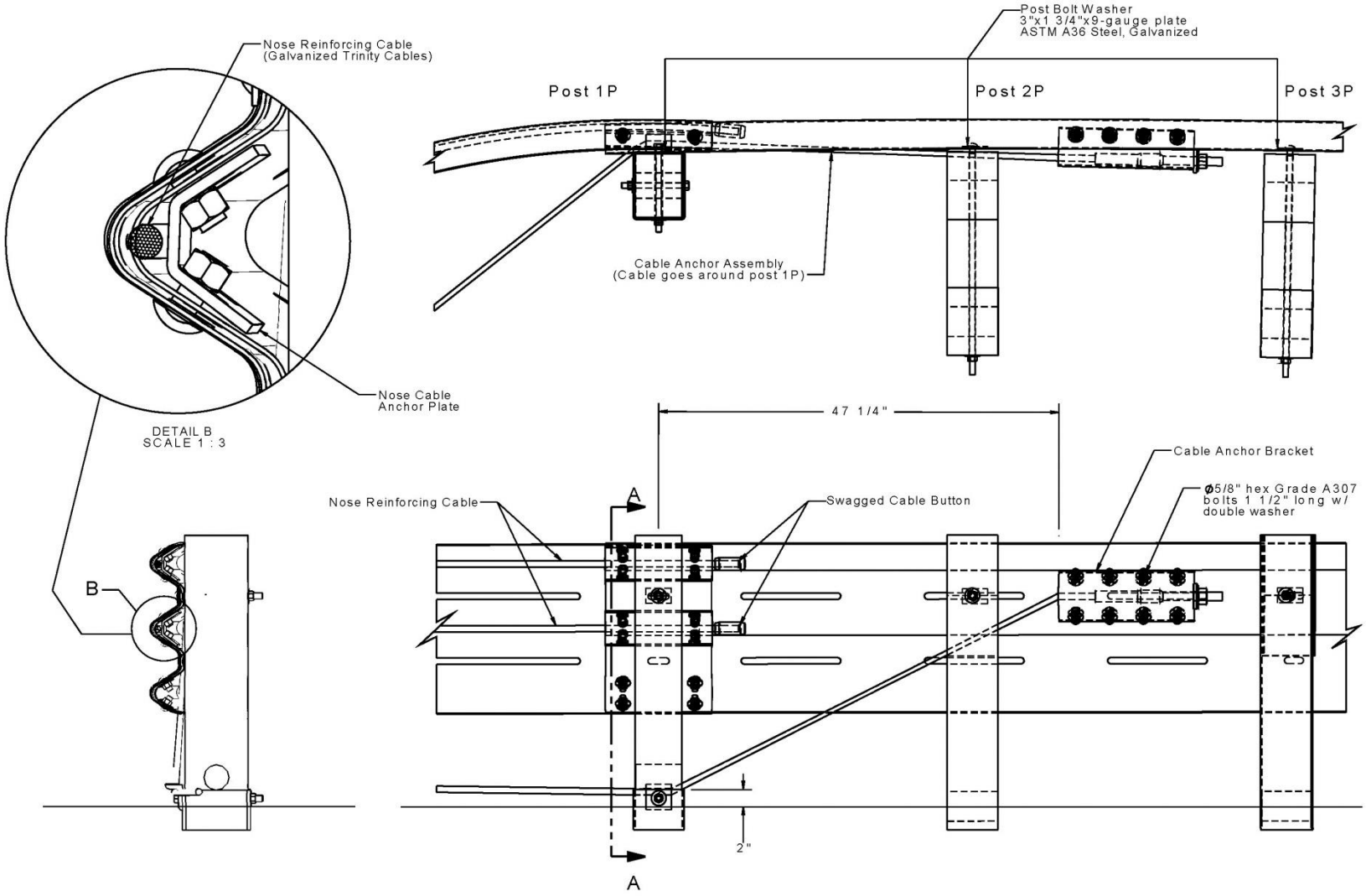

Figure 19. Primary Side Cable Anchorage Details, MwRSF Short Radius Design [14]

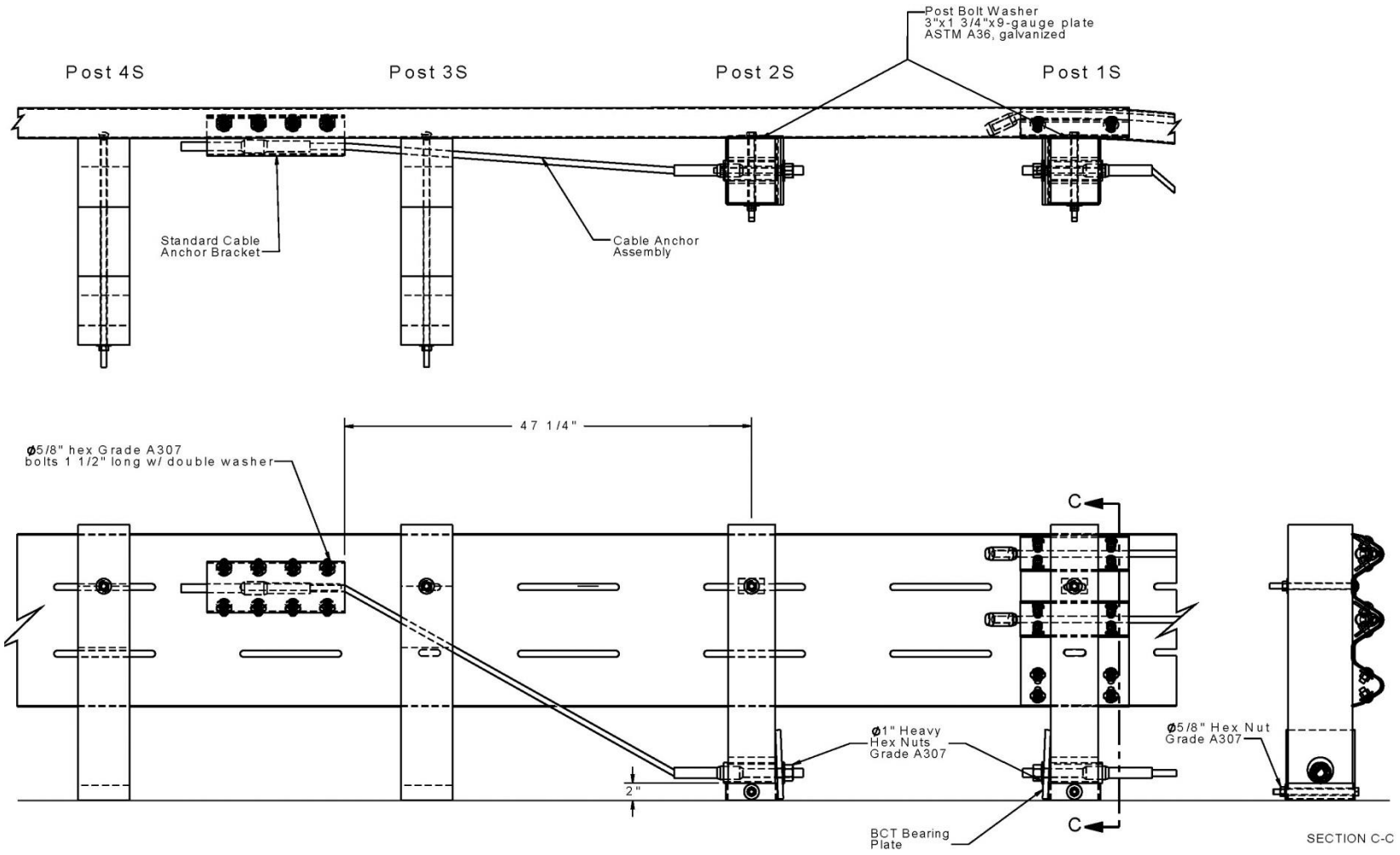

Figure 20. Secondary Side Cable Anchorage Details, MwRSF Short Radius Design [14]

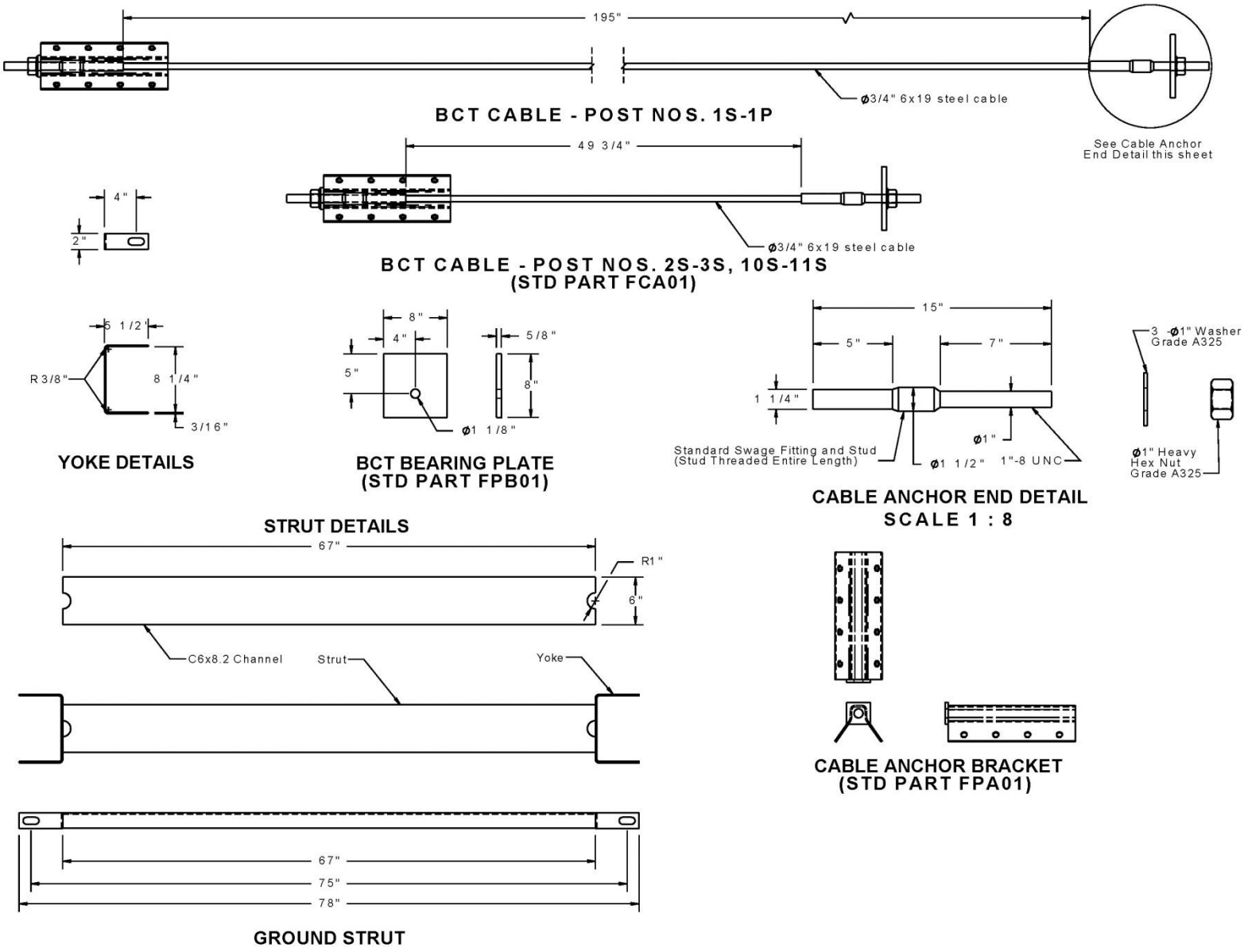

Figure 21. Cable Anchorage Component Details, MwRSF Short Radius Design [14]

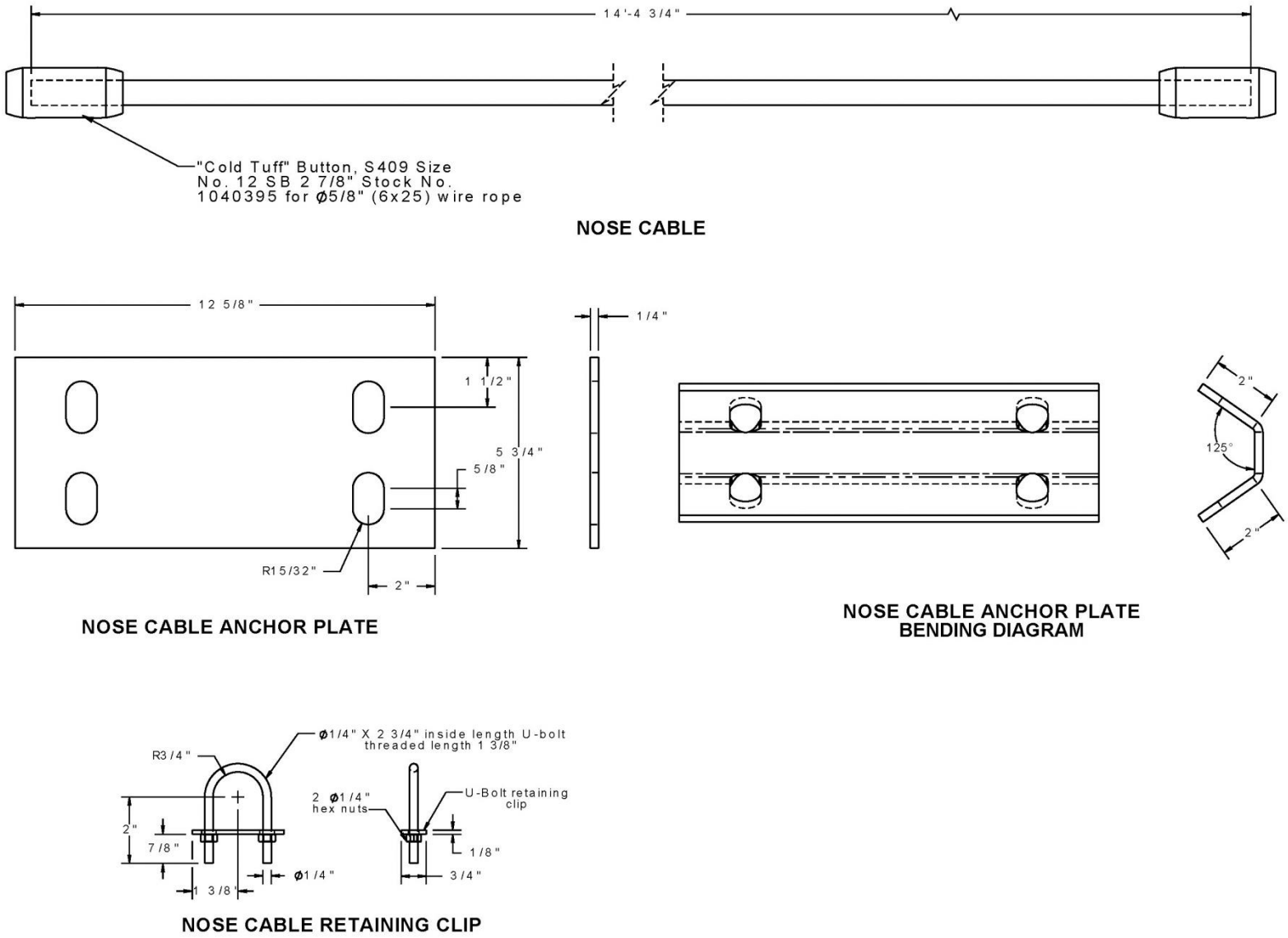

Figure 22. Tension Cable and Anchor Plate Used in Curved Nose Piece, MwRSF Short Radius Design [14]

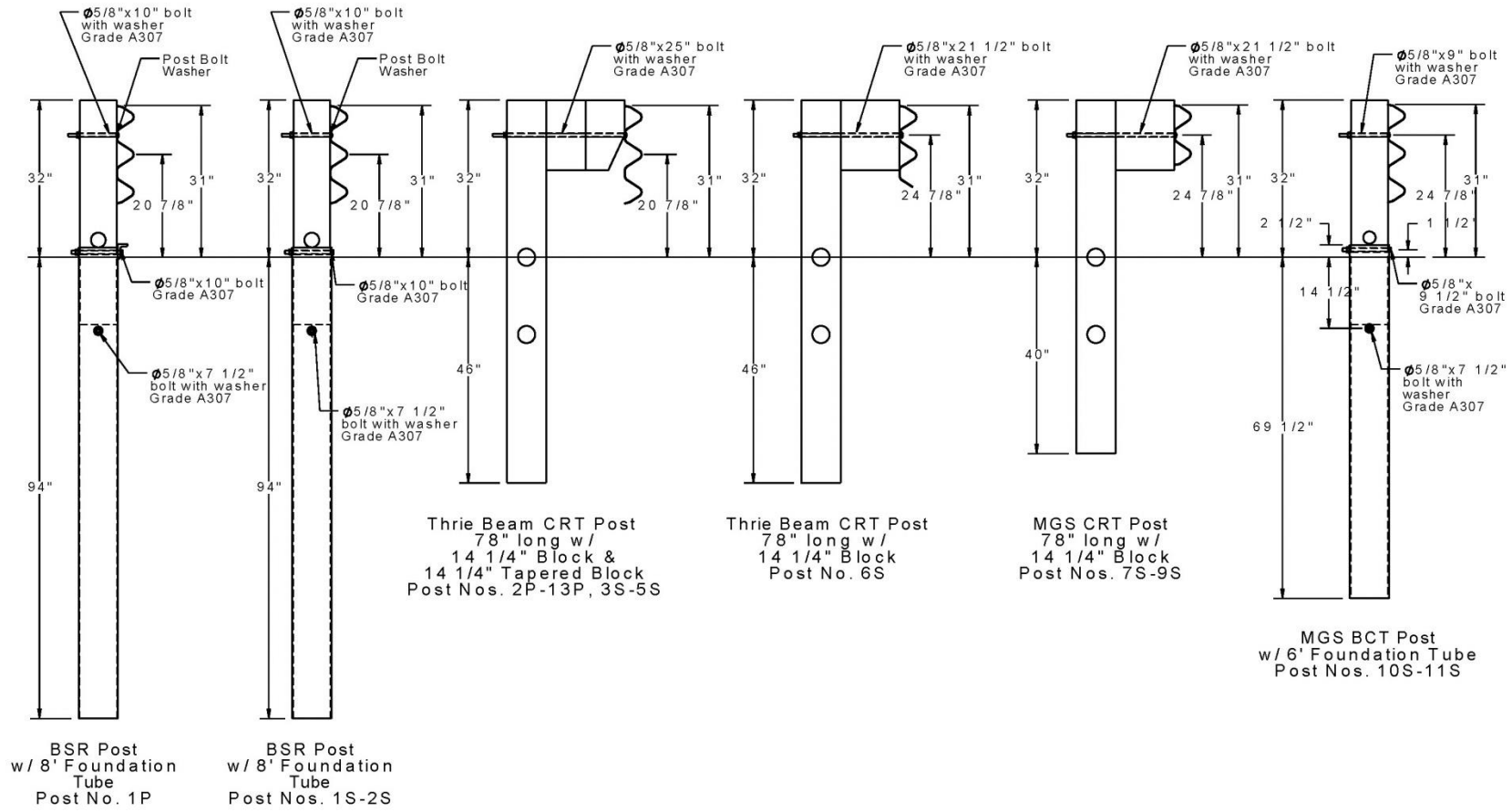

Figure 23. Post Naming Conventions and Rail Heights, MwRSF Short Radius Design [14]

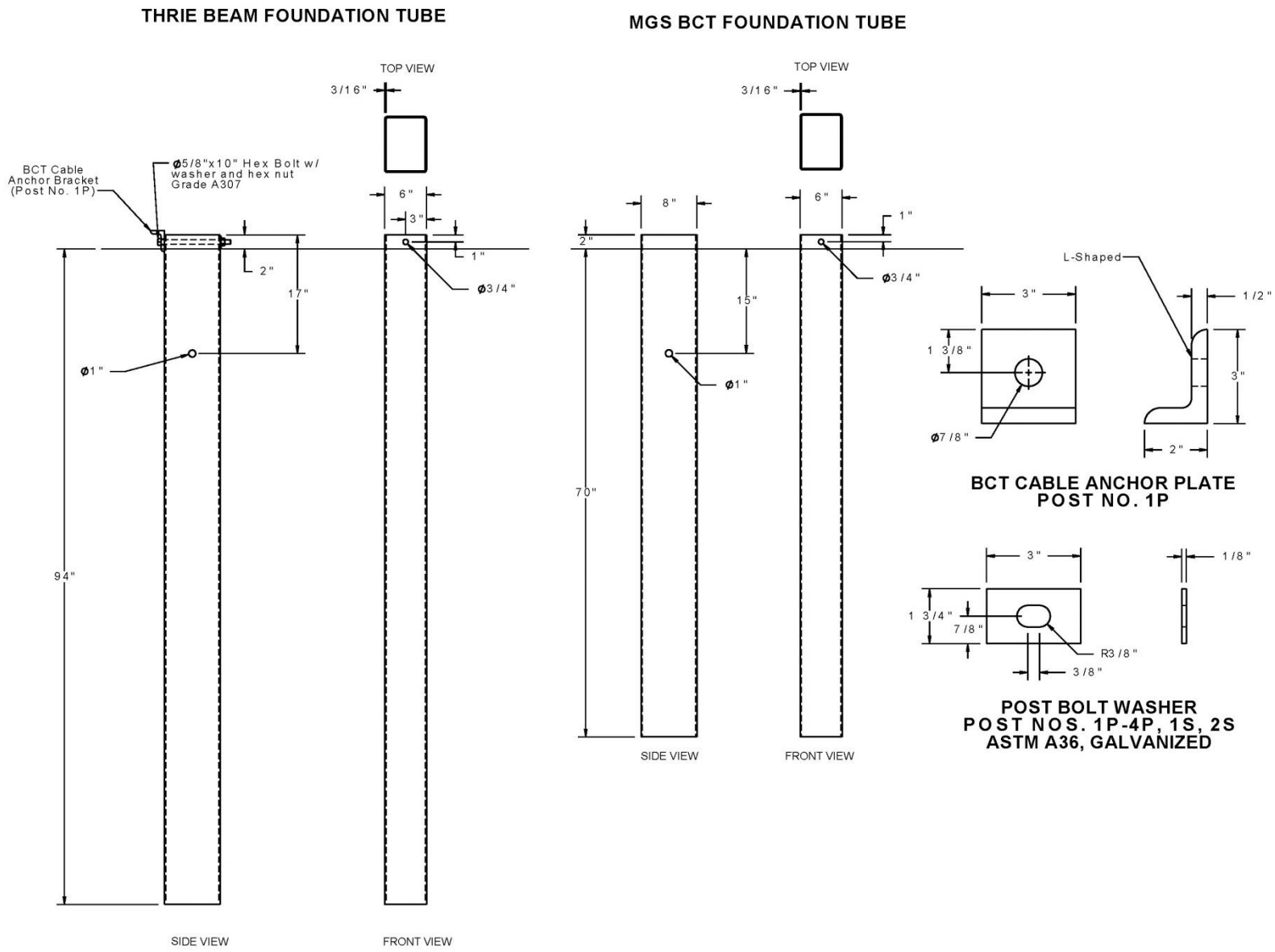

Figure 24. Foundation Tube Details, MwRSF Short Radius Design [14]

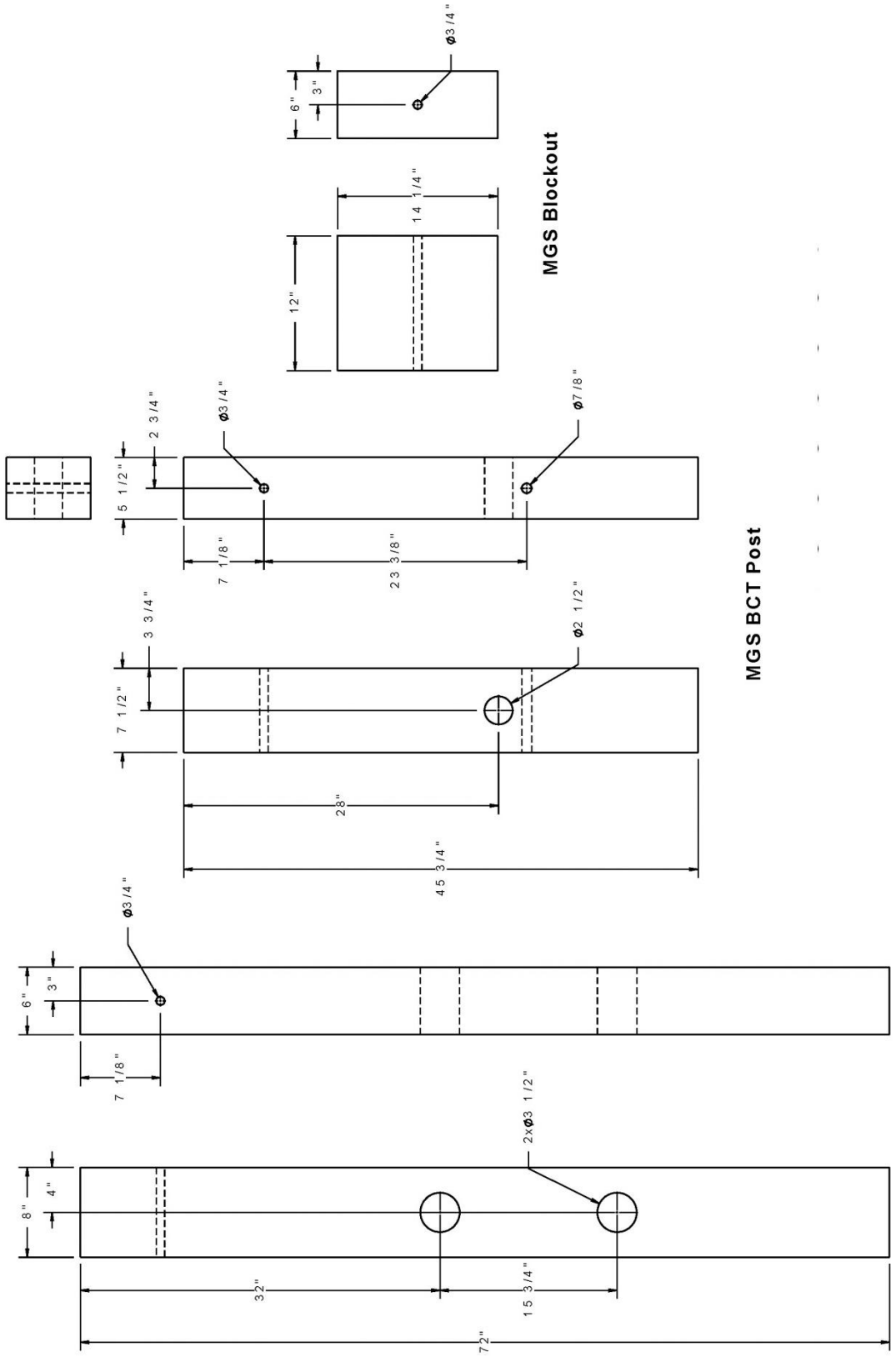

Figure 25. MGS BCT and MGS CRT Post Details, MwRSF Short Radius Design [14]

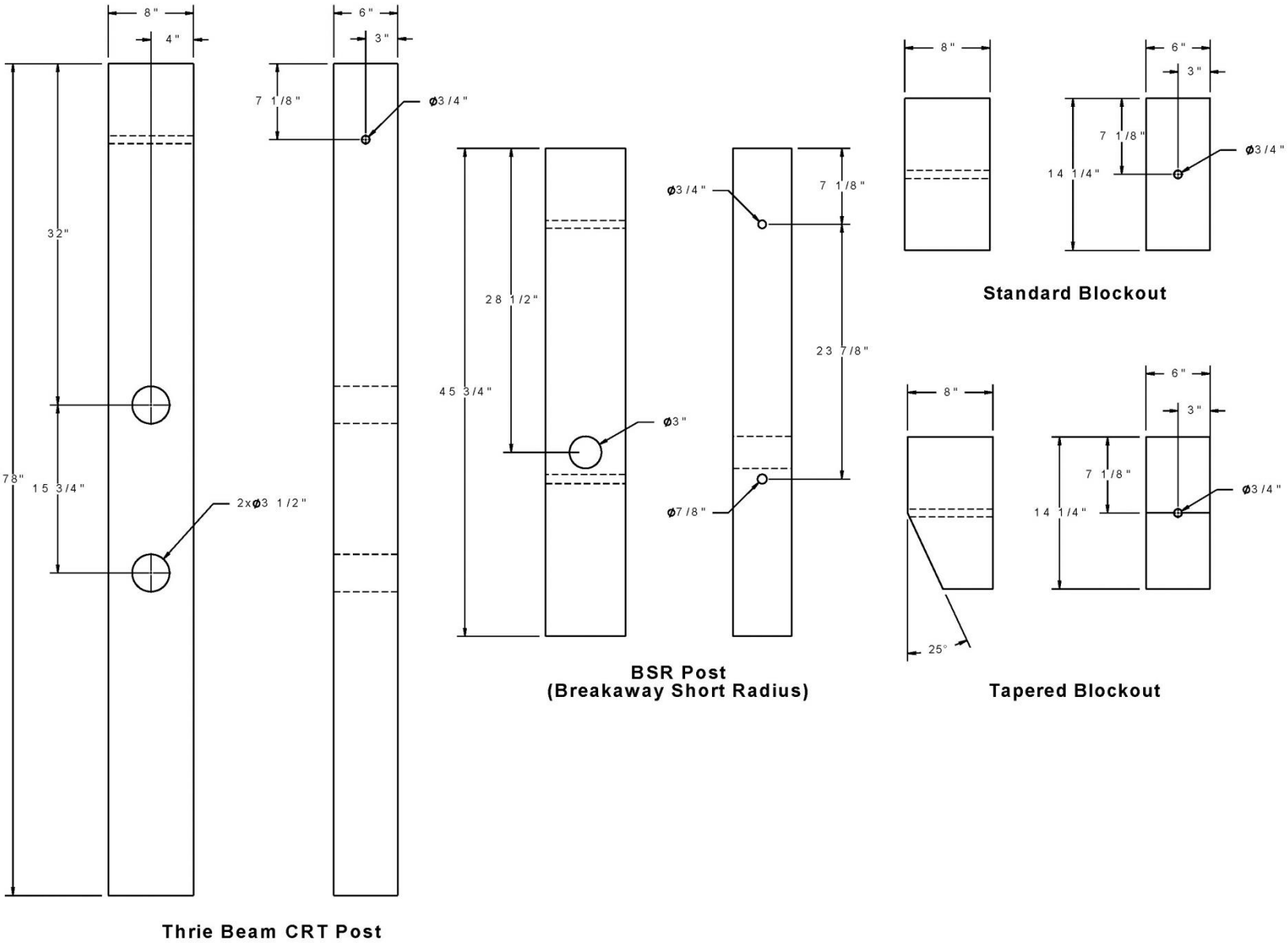

Figure 26. BSR and Thrie Beam Post Details, MwRSF Short Radius Design [14]

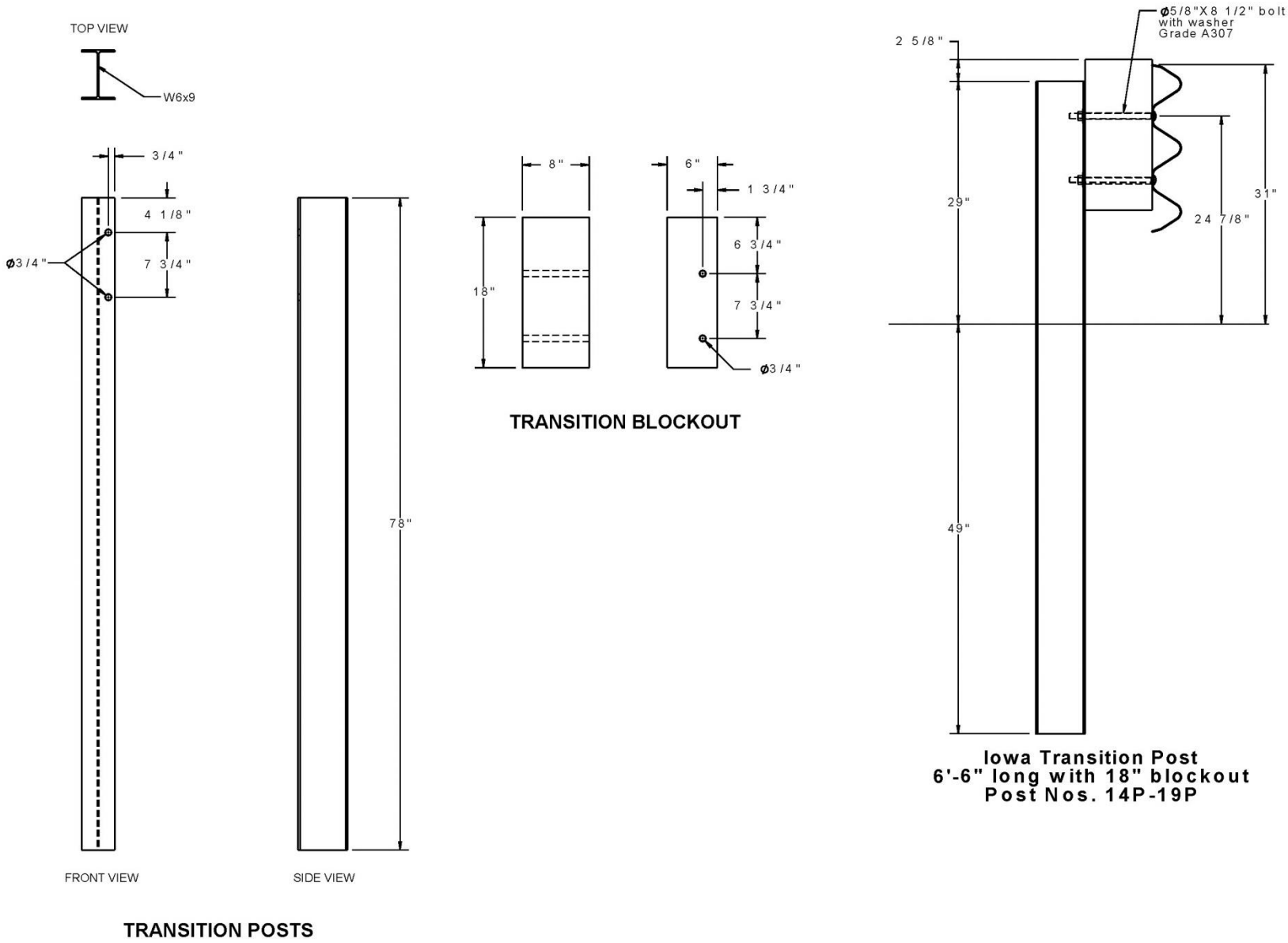

Figure 27. Post Details, MwRSF Short Radius Design [14]

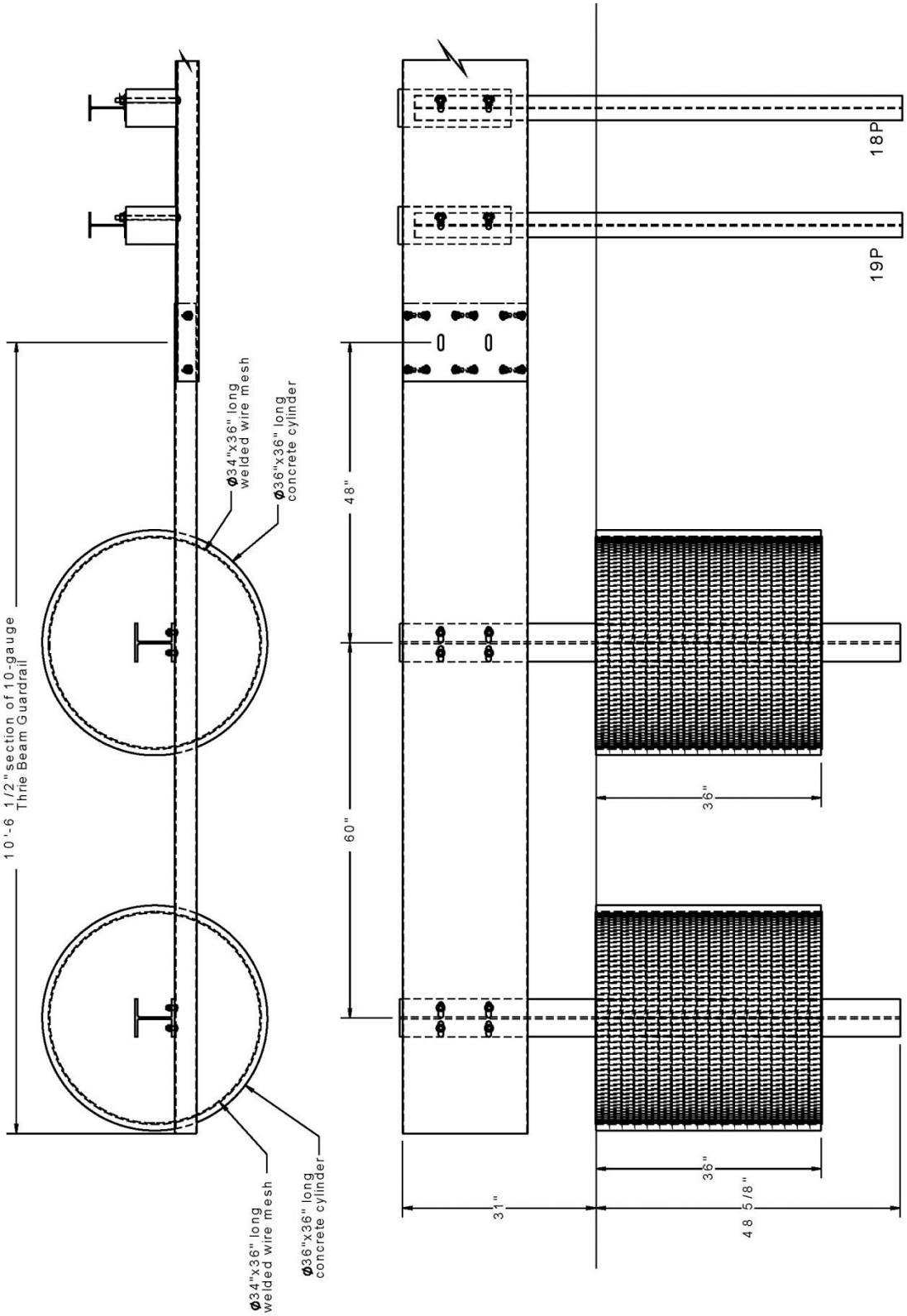

Figure 28. Stiff Bridge Rail Details, MwRSF Short Radius Design [14]

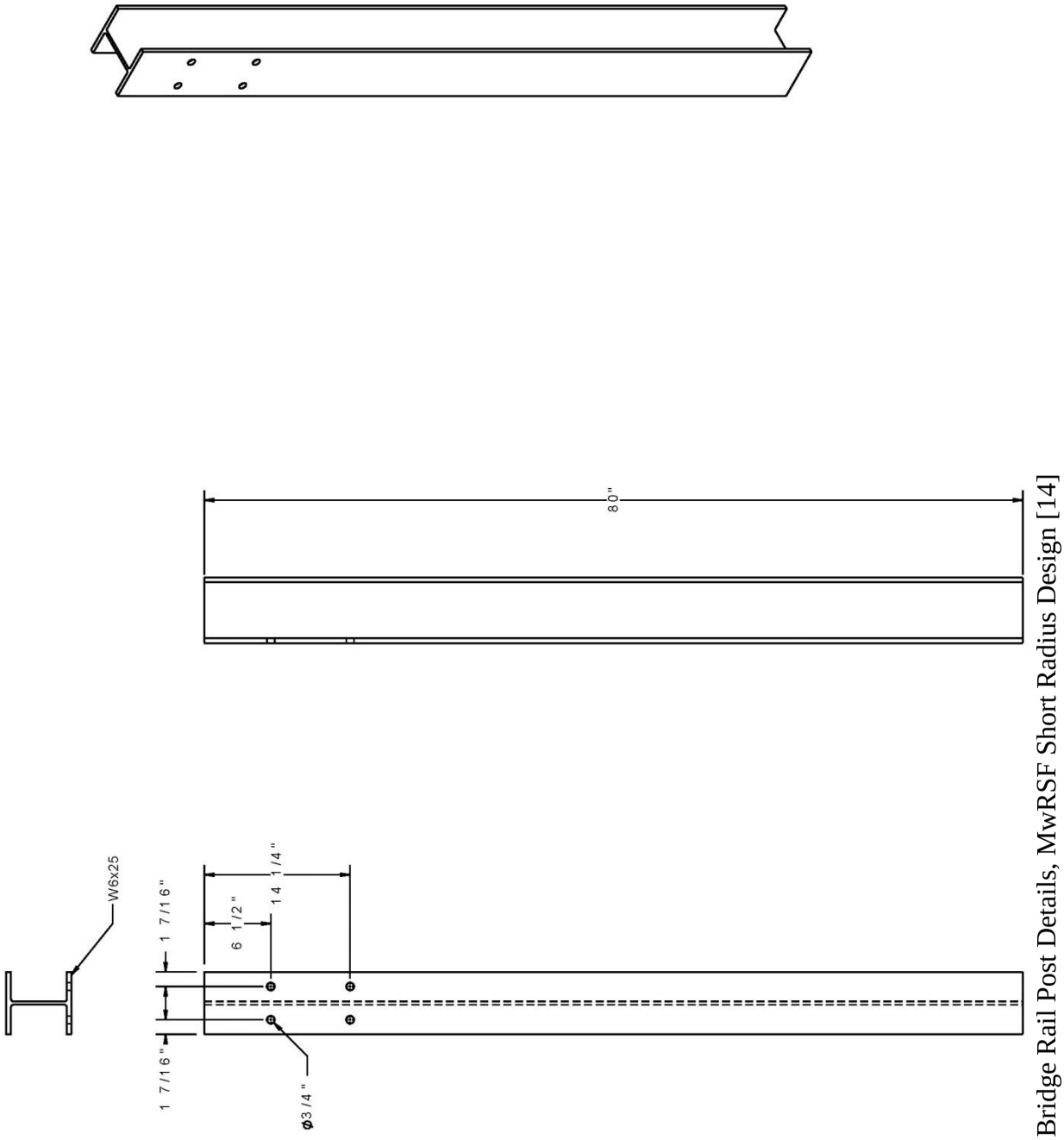

Figure 29. Stiff Bridge Rail Post Details, MwRSF Short Radius Design [14]

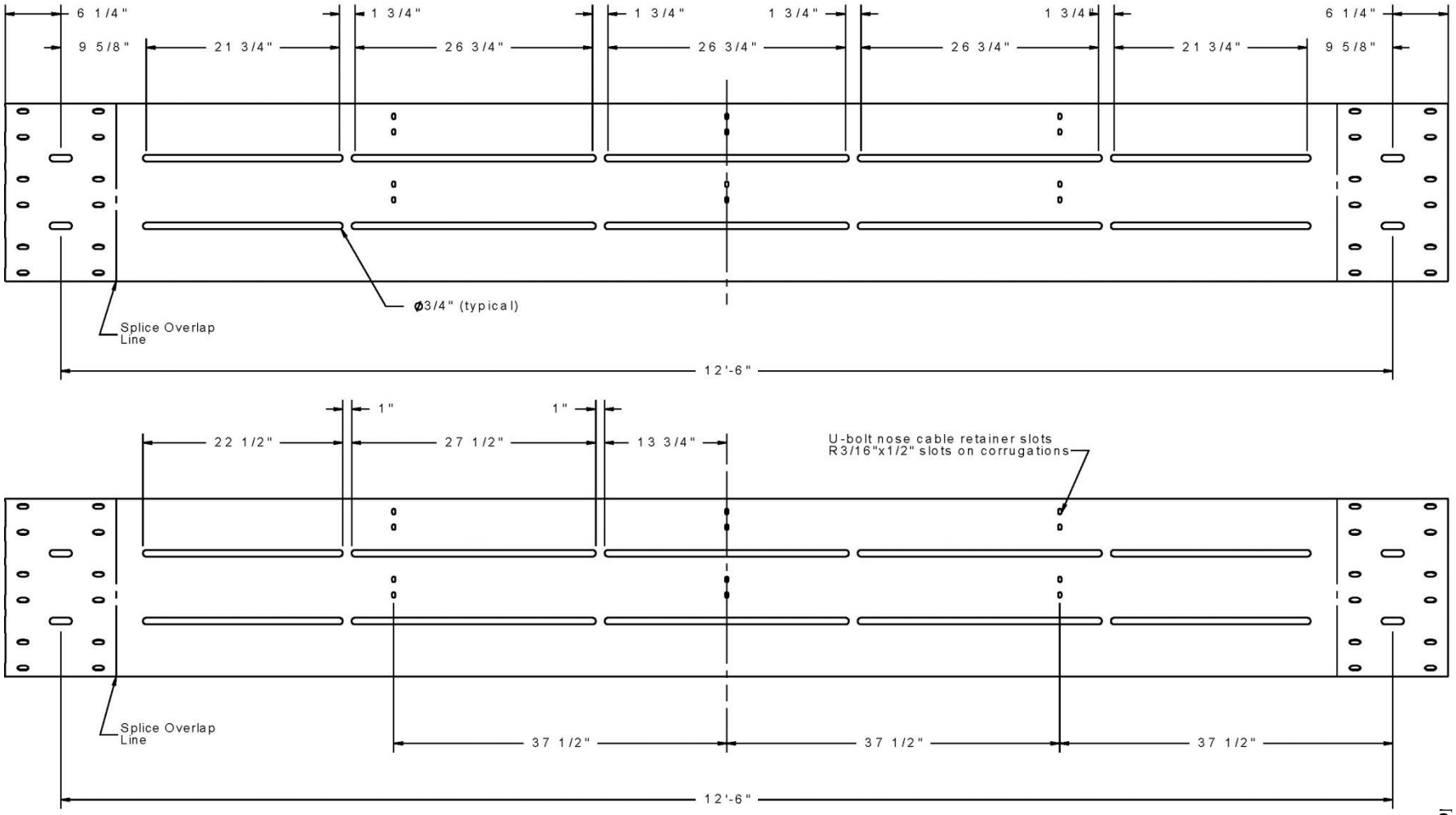

Figure 30. Rail Slot Details, MwRSF Short Radius Design [14]

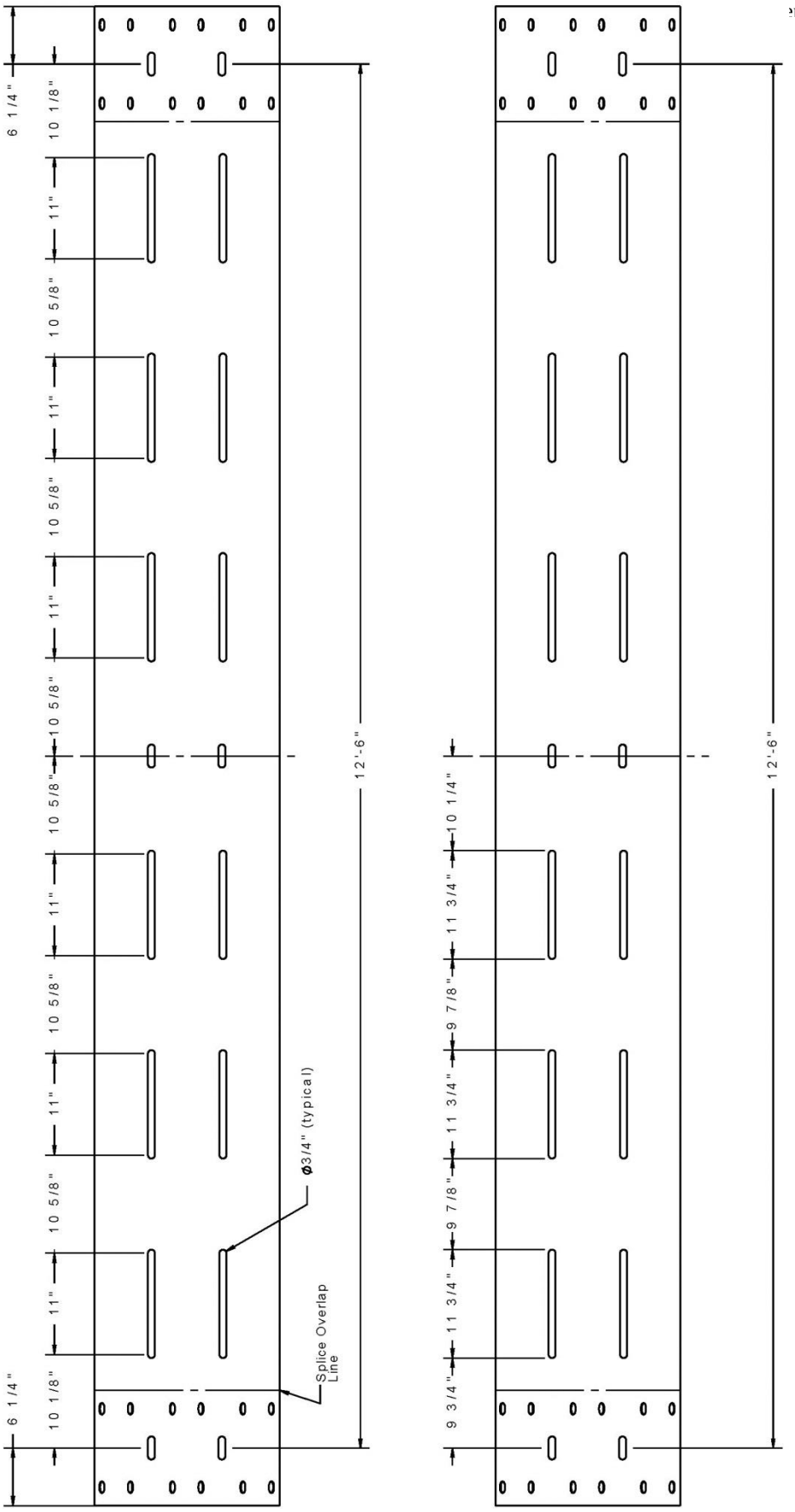

Figure 31. Rail Slot Details, MwRSF Short Radius Design [14]

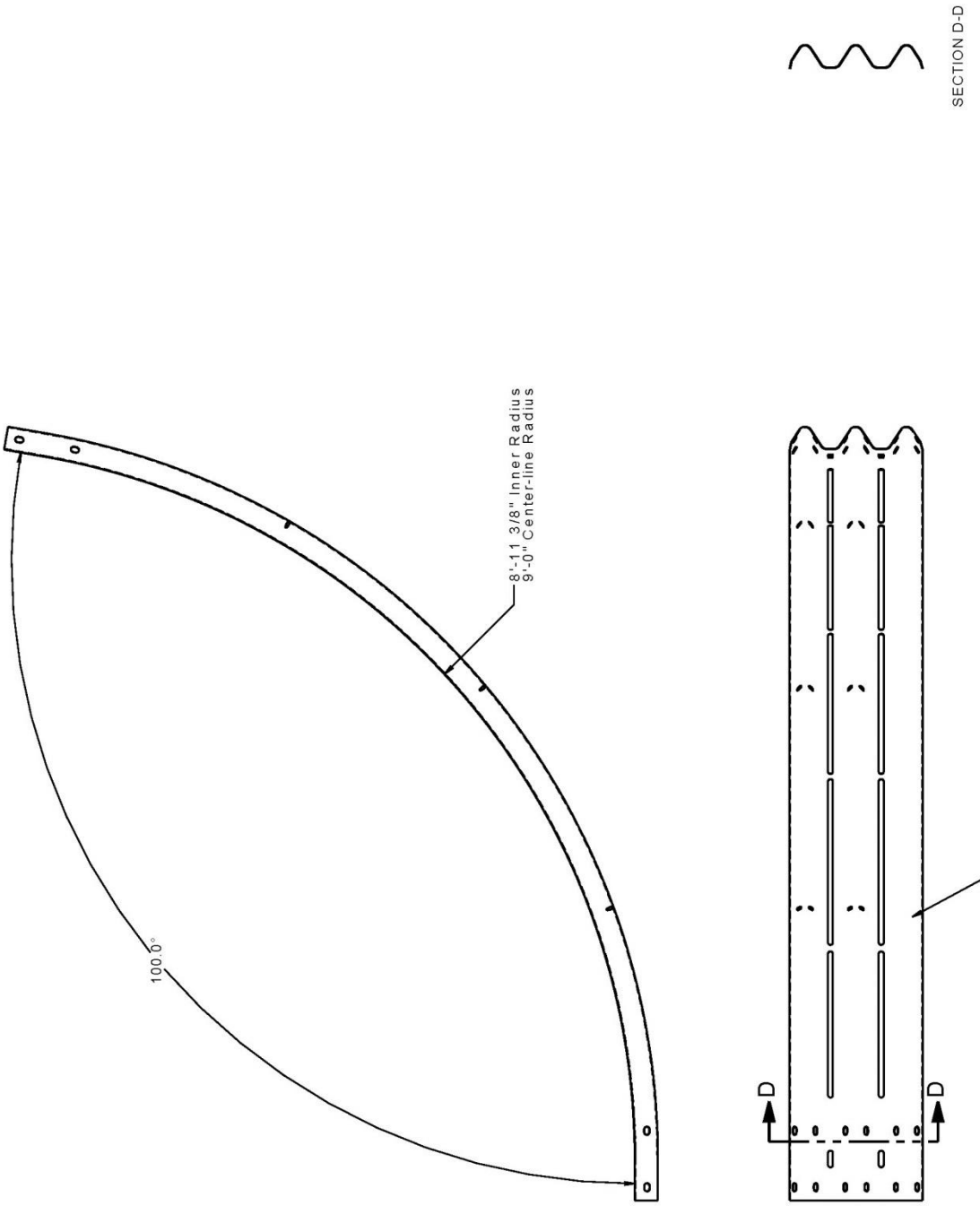

Figure 32. Thrie Beam Bend Details, MwRSF Short Radius Design [14]

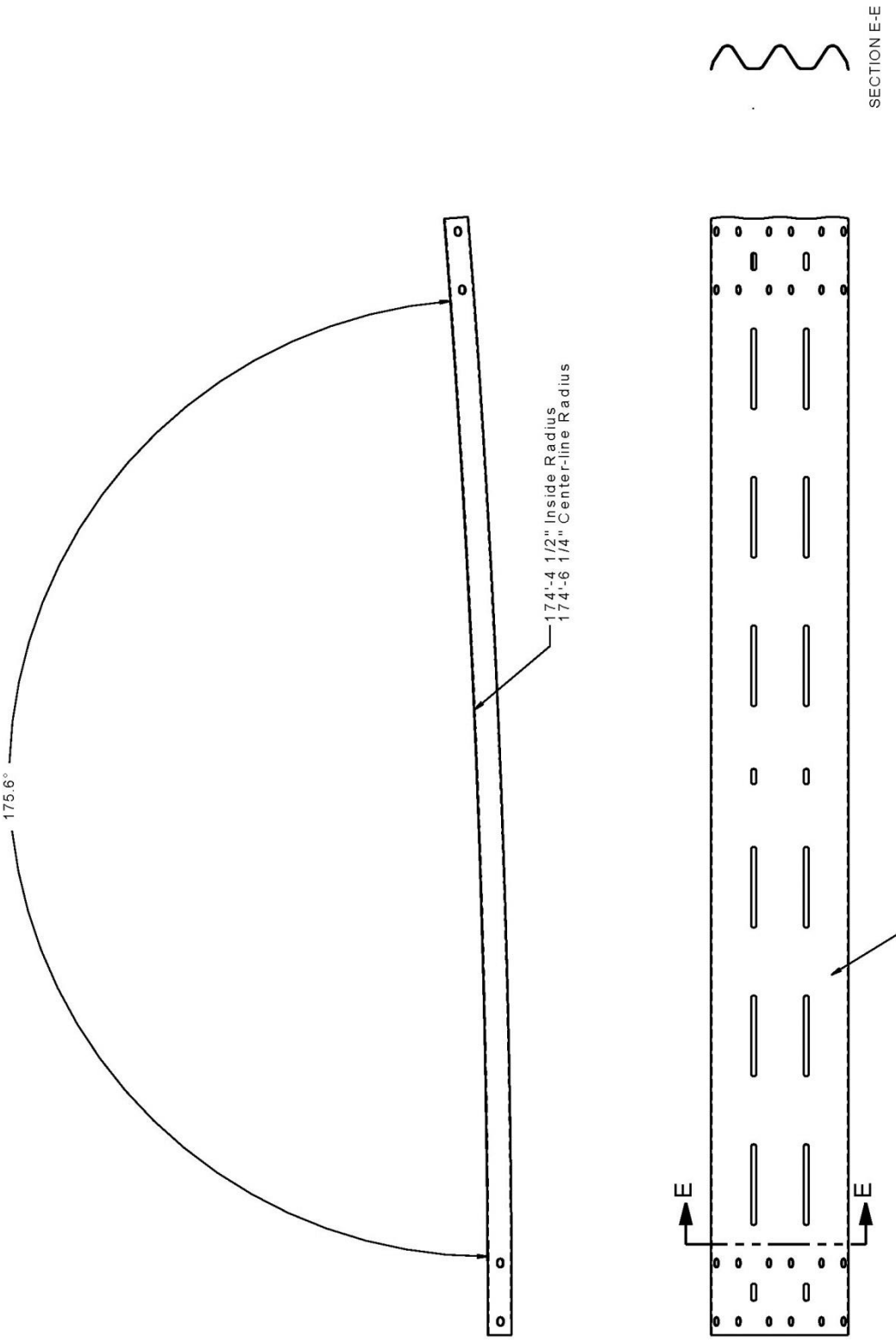

Figure 33. Thrie Beam Bend Details, MwRSF Short Radius Design [14]

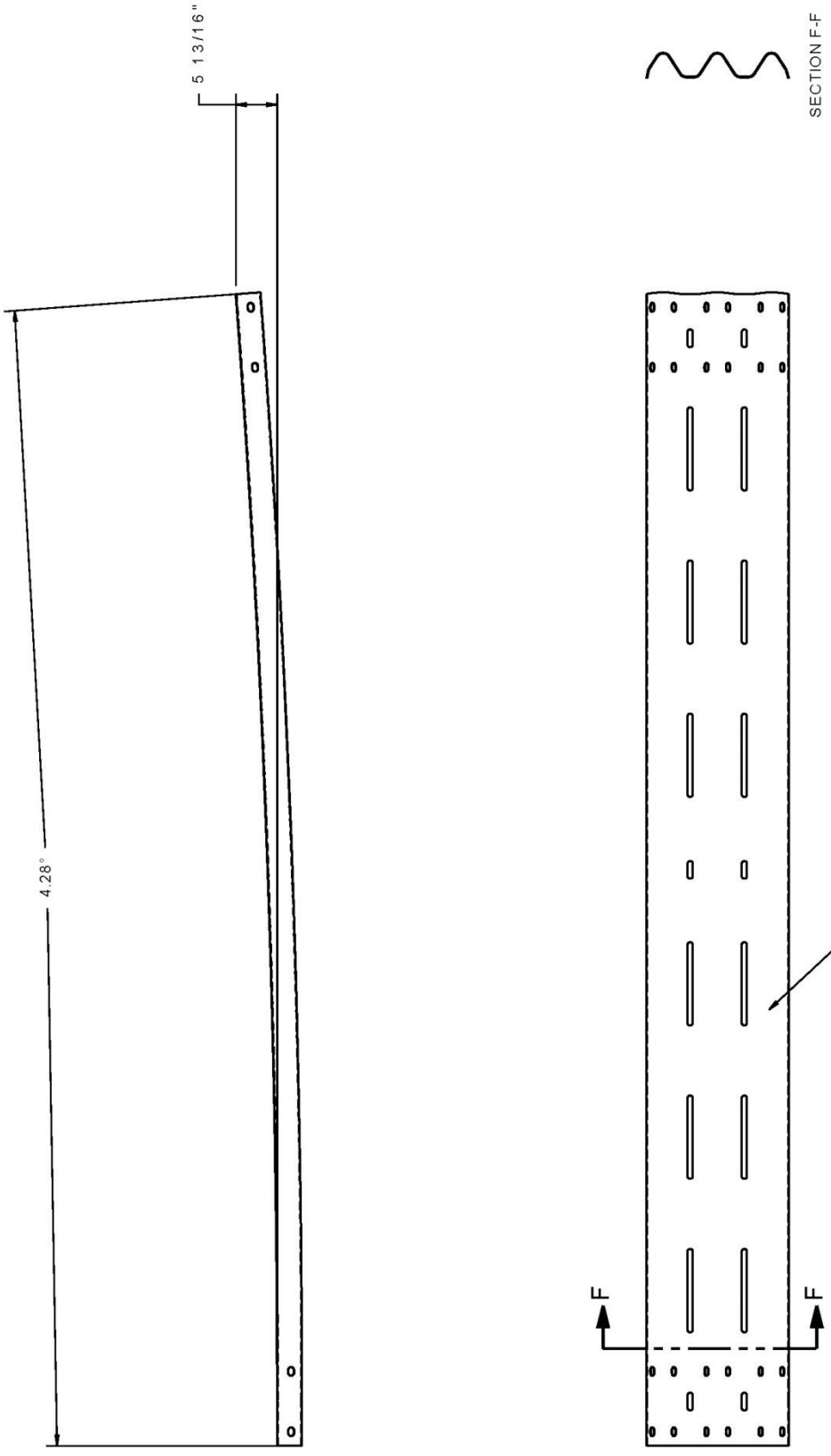

Figure 34. Thrie Beam Bend Details, MwRSF Short Radius Design [14]

2.3 Bullnose Systems Tested Prior to NCHRP Report No. 230

Bullnose system designs vary widely, but all utilized W-beam or thrie beam as the primary rail element. One of the oldest crash-tested bullnose designs was the asymmetrical Minnesota W-beam bullnose [15]. The system resembled a parabolically-flared W-beam guardrail system located upstream of a median hazard that was connected to an identical, parabolically-flared system shielding the hazard from the opposite direction of travel. Flares were transitioned over approximately 2⅓ sections of 12-ft 6-in. (3,810-mm) W-beam. A single curved W-beam rail section connected the flared rail on one side of the system to the straight rail on the other side. The system was tested in the early 1970s before NCHRP Report 230 was published. Tests consisted of a 4,500-lb (2,041-kg) sedan and a 2,290-lb (1,039-kg) small car both impacting at approximately 60 mph (97 km/h) and 0 degrees relative to the nose of the system, with the centerline of the vehicle aligned with the center point of the radius. Both tests were determined to be satisfactory.

All of the remaining bullnose systems tested to NCHRP Report No. 230 test criteria were symmetrical. One system design utilized a W-beam guardrail with a 4 ft – 6 in. (1,372 mm) radius and a 10-degree flare from the nose, and was successfully tested by the California Department of Transportation (Caltrans) after extensive revisions to the initial design [16].

A novel crumpling bullnose system with very sharp front-end profile was evaluated by TTI for the Colorado Department of Transportation [17]. The crumpling bullnose system consisted of W-beam rail flattened at the first four post locations, with staggered post locations to control W-beam buckling. A flattened, curved, buffer nose piece was attached at the front of the system to act as the impact head, eliminating the need for any curved W-beam rail segments. Four successful end-on crash tests were conducted into variations of the flattened-rail system, although one crash result was marginal due to occupant compartment deformation.

A third W-beam bullnose system design was tested and modified by the Southwest Research Institute (SwRI), incorporating a curved frontal W-beam nose section, a curved W-beam transition section, and straight sections of W-beam downstream from the nose [18]. Cable anchors, ground struts, foundation tubes, post sizes, spacings, and orientations, and rail slots were extensively modified during the development of the W-beam bullnose system. The system was successfully tested according to NCHRP Report No. 230 with 4,500-lb (2,041-kg) sedans and 1,800-lb (816-kg) small cars. A total of 16 tests were conducted on design modifications before the system was determined to be crashworthy according to NCHRP Report No. 230 performance criteria.

2.4 Bullnose Systems Tested to NCHRP Report No. 350

MwRSF conducted a series of tests on a bullnose system according to NCHRP Report No. 350 between 1997 and 2010 [19-24]. The crash test matrix required to successfully test the bullnose system was similar to the required short-radius crash tests, as shown in Figure 35. The initial concept design of the bullnose system was similar to the design tested and evaluated by SwRI according to NCHRP Report No. 230 test criteria. The system was comprised of a 12 ft – 6 in. (3,810 mm) curved and slotted thrie beam section which formed the nose, a 12 ft – 6 in. (3,810 mm) curved and slotted transition thrie beam section, and two 12 ft – 6 in. (3,810 mm) straight thrie beam sections parallel to the roadways on the respective sides.

Initially, the 2000P pickup truck test vehicle vaulted the system when the system was struck at a 0-degree angle, and the slot tabs were shortened. In subsequent tests the 2000P vehicle ruptured through the rail. The design was modified to include cables in the nose section of thrie beam to facilitate capture after the rail tore through the slot tabs.

Further tests with the 2000P vehicle into the critical impact point (NCHRP Report No. 350 test no. 3-35) resulted in vehicular launching. Researchers determined that the groundline

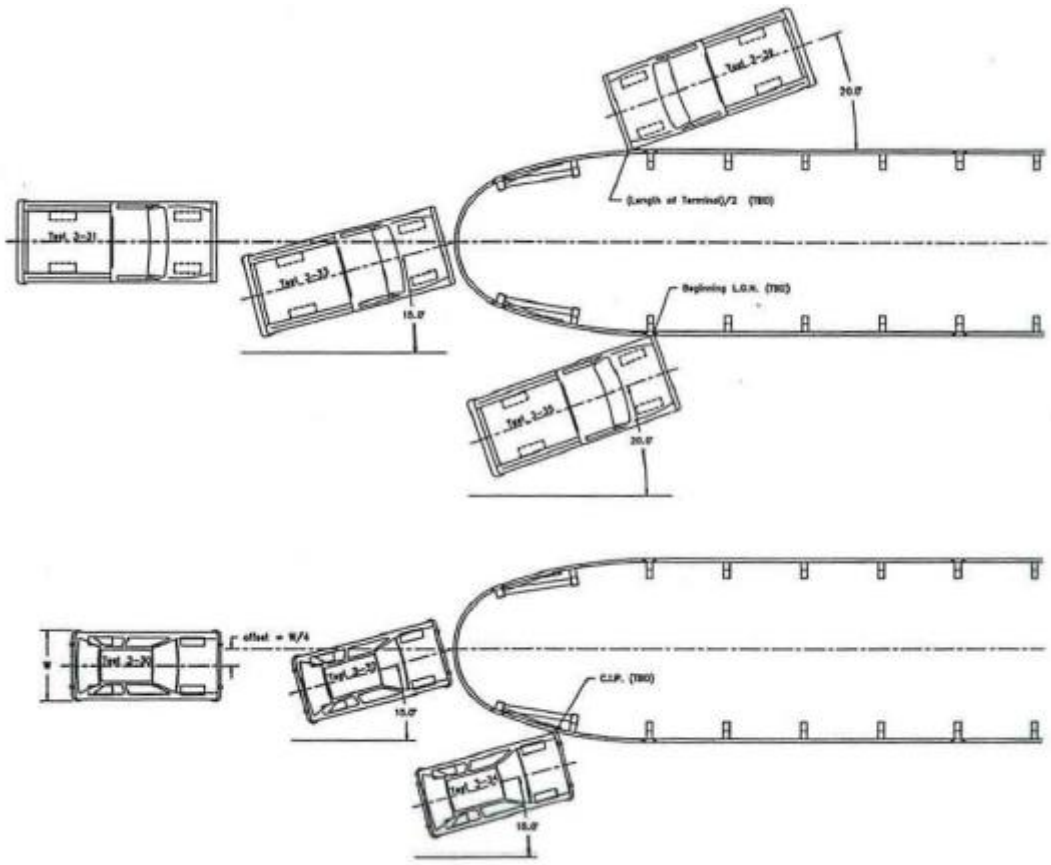

Figure 35. Required Bullnose Crash Tests According to NCHRP Report No. 350

strut connecting the first and second posts along each side of the system facilitated vehicle launching by lifting the vehicle and allowing the rail to pass beneath the vehicle's tire on the impacting corner. After further modifying the system, including eliminating the ground line strut, modifying several soil tubes, and reducing post spacing, the system successfully passed test NCHRP Report No. 350 TL-3 test no. 3-35 impact conditions consisting of a 2000P vehicle impacting at 20 degrees and 62.1 mph (100.0 km/h) at the critical impact point (CIP) of the system. Subsequently, the system was tested in accordance with to TL-3 test no. 3-30 impact conditions, consisting of an 820C small car impacting the center of the nose of the system with a ¼-point offset at 62.1 mph (100 km/h) and 100 degrees, was also successful.

2.5 Relationship Between Bullnose and Short Radius Guardrail Systems

Historical short radius systems tested according to criteria established before NCHRP Report 350 experienced fewer test failures than later systems did. Bullnose systems, due to the relevance and frequency of need, received significant attention and development. Short-radius guardrail systems are critical, but the size and scope of the problem and funds required to develop a successful system has hampered successful system development.

Rail radii used in these bullnose systems were similar to the radii used in short radius systems. Key system features such as breakaway posts, rail flares, and intermediate and end terminal cable anchors were used for both short-radius and bullnose barriers. The major differences between bullnose and short radius guardrail systems are that bullnose systems were typically symmetrical and encompassed a 180-degree bend, compared to short radius systems which more commonly encompassed approximately 90 degrees. In addition, many bullnose barriers are used in divided medians of roadways with similar traffic volumes and speeds for both directions of travel. Thus the entire bullnose system was tested to one set of performance criteria. Short-radius systems utilize a primary, higher-speed and higher-traffic volume side, and a secondary, lower-speed and lower-traffic volume side, which may not encompass the same levels of protection.

Both bullnose and short radius systems evolved from W-beam to thrie beam guardrail. Typical end anchorages, such as BCT or MGS end anchorages [25], were modified by eliminating bearing struts and using different foundation tube sizes. Traditional CRT posts, which were sufficient for vehicle redirection for the historical systems according to criteria presented in NCHRP Report 230 crash test criteria or earlier reports, were sometimes modified to include additional or larger transverse holes, varied embedments, and different lengths.

Furthermore, rail slots were added to thrie beam bullnose and short radius systems tested at MwRSF to reduce rail bending strength and improve vehicle capture.

2.6 Short Radius Systems with Larger Radii

Currently, there have been no reported full-scale crash tests to NCHRP Report Nos. 230 or 350 or MASH of short-radius systems with radii larger than 16 ft (4,877 mm). A summary of the radii of tested systems, the test result, and reference test criteria is shown in Table 15.

Although no systems have been crash-tested with a radius larger than 16 ft (4,877 mm), the FHWA Technical Advisory permitted the installation of short radius systems with radii as large as 35 ft (10.7 m) [7], as shown in Figure 36. Limited guidance is available to assess real-world impact performance of these large-radius systems. Several states have drafted standards for larger radii installations based on the recommendations provided by FHWA, many times in response to a need to accommodate large vehicles turning from secondary roadways onto primary roadways. Washington and Wisconsin DOT standards for larger-radius systems are shown in Figure 37 and Figures 37 through 39, respectively. Examples of locations in which guardrail systems with radii larger than 16 ft (4.9 m) are needed are shown in Figure 40.

Table 15. Summary of Short Radius and Bullnose Documented Testing by Radius

Reference Number	System Type	Radius of Nose Piece ft (m)	Evaluation Criteria	Pass/ Fail
10	Short Radius	8.5 (2.6)	NCHRP Report No. 230	P
6	Short Radius	8 (2.4)	NCHRP Report No. 230	P
11	Short Radius	16 (5)	NCHRP Report No. 230	P
8	Short Radius	16 (5)	NCHRP Report No. 230	P
9, 12-13	Short Radius	9 (2.7)	NCHRP Report No. 350	F
14	Short Radius	9 (2.7)	MASH	F
15	Bullnose	5 (1.5)	Historical/Unknown	P
16	Bullnose	4.6 (1.4)	NCHRP Report No. 230	P
17	Bullnose	0*	NCHRP Report No. 230	P
18	Bullnose	5 (1.5)	NCHRP Report No. 230	P
19-24	Bullnose	5.18 (1.58)	NCHRP Report No. 350	P

* Curved plate formed impact head. Rail was perpendicular to vehicle at impact.

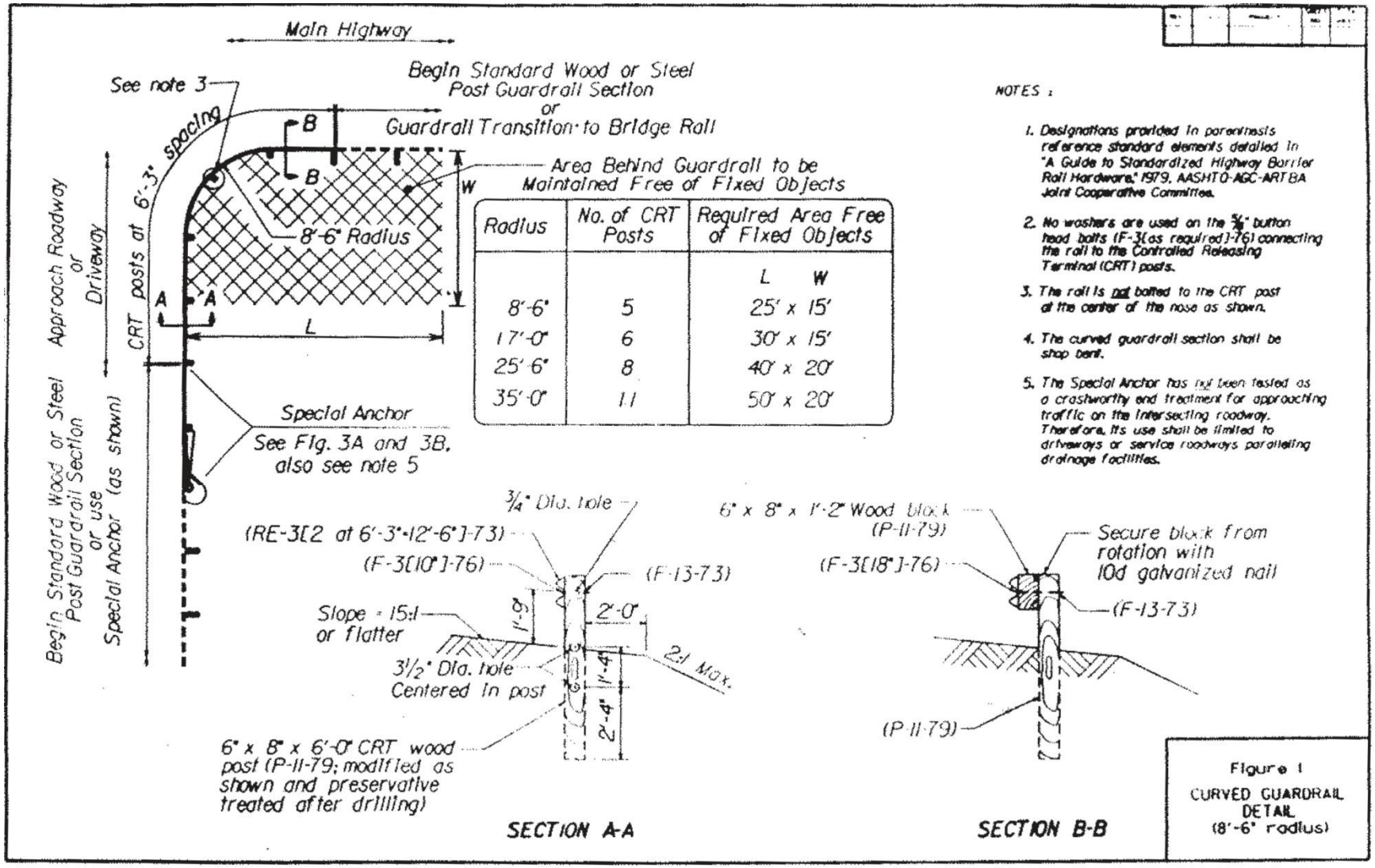

Figure 36. Acceptable Short Radius Guardrail System Designs, FHWA Technical Memorandum [7]

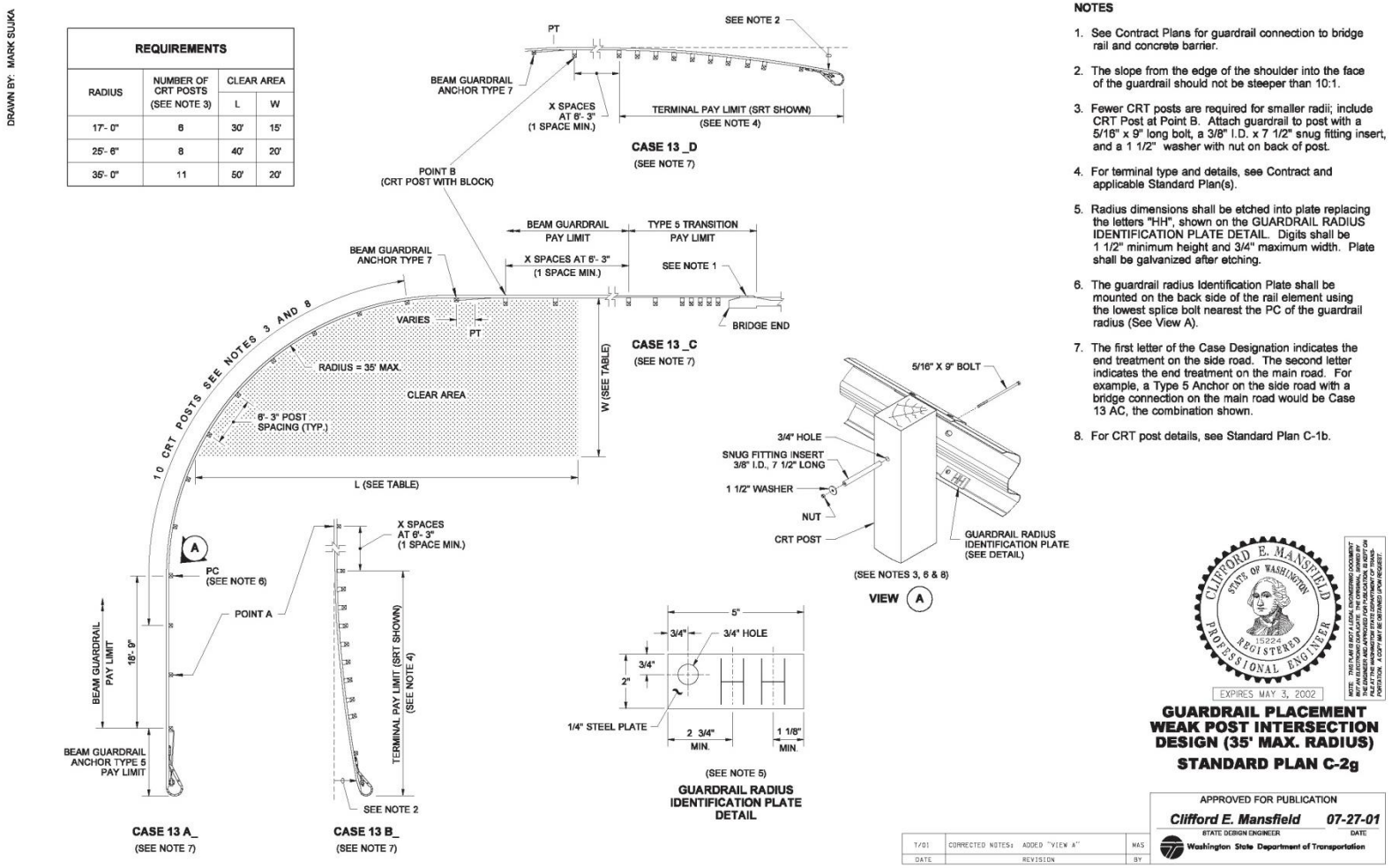

Figure 37. Washington State Standards for Short Radius Guardrail at Intersecting Roadways [26]

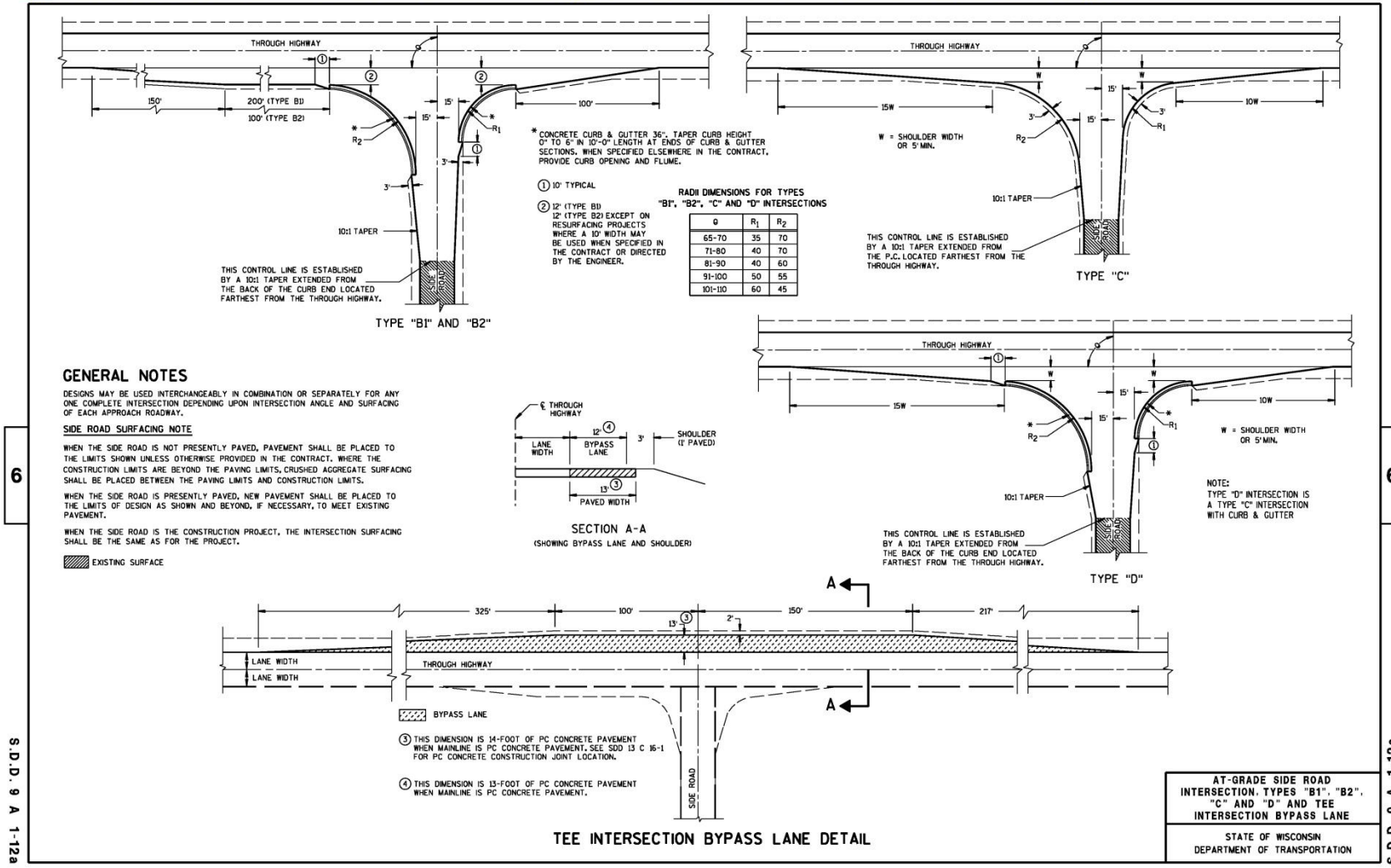

Figure 38. Wisconsin State Standards for Short Radius Guardrail at Intersecting Roadways

9A1 sheet b: At-Grade Side Road Intersection, Type 'A1' & 'A2'

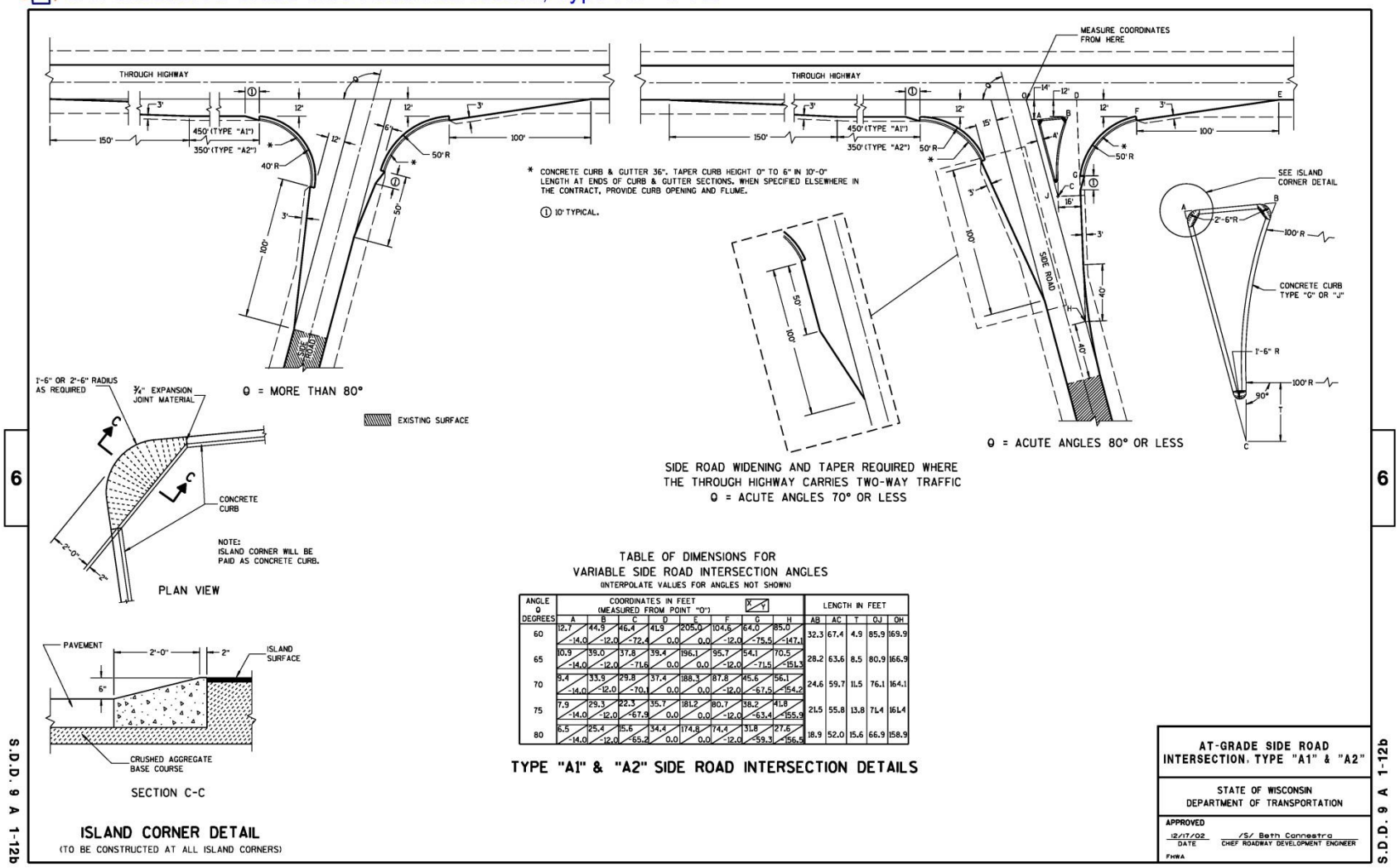

ANGLE Θ DEGREES	COORDINATES IN FEET (MEASURED FROM POINT "O") A	B	C	D	E	F	G	H	LENGTH IN FEET AB	AC	T	OJ	OH
60	12.7	44.9	46.4	41.9	205.0	104.6	64.0	85.0	32.3	67.4	4.9	85.9	169.9
	-14.0	-12.0	-72.4	0.0	0.0	-12.0	-75.5	-147.1					
65	10.9	39.0	37.8	39.4	196.1	95.7	54.1	70.5	28.2	63.6	8.5	80.9	166.9
	-14.0	-12.0	-71.6	0.0	0.0	-12.0	-71.5	-151.3					
70	9.4	33.8	29.8	37.4	188.3	87.8	45.6	56.1	24.6	59.7	11.5	76.1	164.1
	-14.0	-12.0	-70.1	0.0	0.0	-12.0	-67.5	-154.2					
75	7.9	29.3	22.3	35.7	181.2	80.7	38.2	41.8	21.5	55.8	13.8	71.4	161.4
	-14.0	-12.0	-67.9	0.0	0.0	-12.0	-63.4	-155.9					
80	6.5	25.4	15.6	34.4	174.8	74.4	31.8	27.6	18.9	52.0	15.6	66.9	158.9
	-14.0	-12.0	-65.2	0.0	0.0	-12.0	-59.3	-156.8					

Figure 39. Wisconsin State Standards for Short Radius Guardrail at Intersecting Roadways

Figure 40. Example Applications for Systems with Radii Larger than 16 ft (4.9 m)

3 SELECTION OF SHORT RADIUS GUARDRAIL SYSTEM

No TL-3 short-radius systems have been approved to either MASH or NCHRP Report No. 350. Therefore, the researchers evaluated systems successfully tested according to NCHRP Report No. 230 which could be capable of capturing errant vehicles with radii of approximately 70 ft (21.3 m). Researchers evaluated three candidate W-beam short radius systems which showed satisfactory crashworthiness performance [10-11]: TTI nested W-beam; Washington; and Yuma County short-radius systems.

The TTI W-beam short radius design was rejected because the configuration was both difficult to construct and utilized hardware which was non-standard for Wisconsin DOT. In addition, a substitute anchor would be required in lieu of the turndown anchor used in the tested system, which has been shown to be hazardous to impacting vehicles. Furthermore, the tubular rail approach transition to stiff bridge rail was undesirable, and other bridge approach transition designs would be preferred. Researchers determined that the modifications to the system which would be required to make the TTI design more practical for Wisconsin DOT were beyond the scope of this study effort.

The remaining Washington and Yuma County W-beam short radius guardrail systems were compared to determine which system was more likely to perform acceptably and would be a better candidate for larger radii. Both systems had a top mounting height of 27 in. (686 mm), and both systems had an approximately 10:1 flare along the primary side of the system. The guardrail to stiff bridge transition was tested and determined to be satisfactory for both systems, and both utilized an upstream two-cable anchoring system on the secondary roadway side.

However, the Washington W-beam short radius system was only tested with sedan and small car vehicles, whereas the Yuma County short radius guardrail system was tested with a 5,400-lb (2,449-kg) pickup truck. The pickup truck impact is more comparable with TL-2 test

conditions presented in NCHRP Report No. 350 than the NCHRP Report No. 230 sedan impact. Because crash testing was not within the scope of this research project, and because simulated impacts were planned using a pickup truck computer simulation model, the Yuma County system was better-suited for validation of a baseline system and system modifications, and would likely lead to better prediction of system performance with radii as large as 70 ft (21 m).

Furthermore, TTI conducted a study evaluating the performance of the Yuma County system, and researchers determined that the system would likely have passed NCHRP Report No. 350 TL-2 impact conditions [27]. Without a system approved at TL-3 impact conditions to either NCHRP Report No. 350 or MASH, researchers determined that the Yuma County short radius system that was approved under TL-2 impact conditions was the most desirable. Therefore, the Yuma County short radius guardrail system was selected for further consideration and modeling with LS-DYNA [28]. The drawings provided in the original Yuma County short radius guardrail analysis report are shown in Figures 41 through 43. System photographs are shown in Figure 44. An excellent drawing set with some modifications to the original PL-1 Yuma County system can be found in Appendix A.

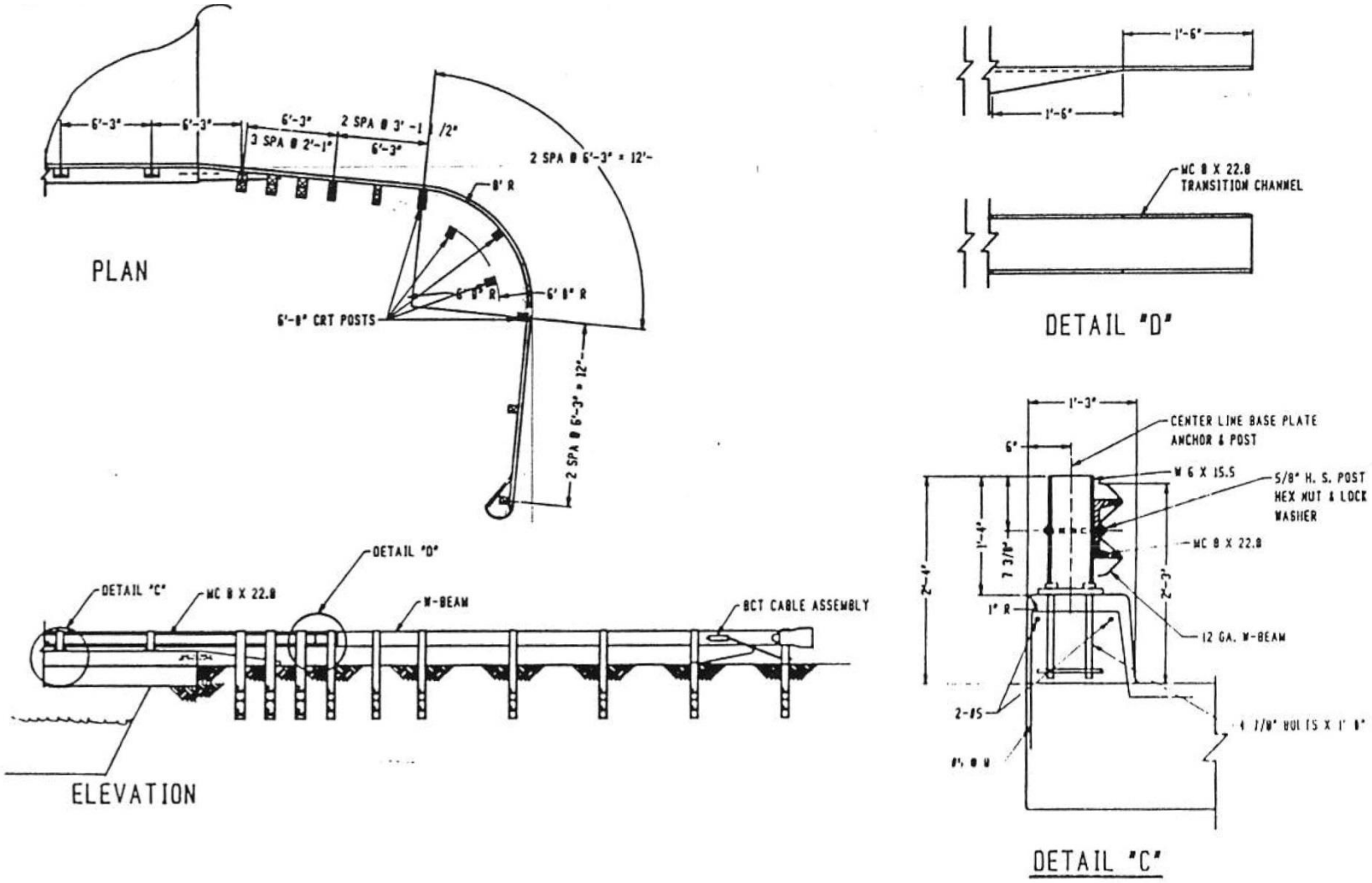

Figure 41. Construction Drawings, Yuma County Short Radius Guardrail System [6]

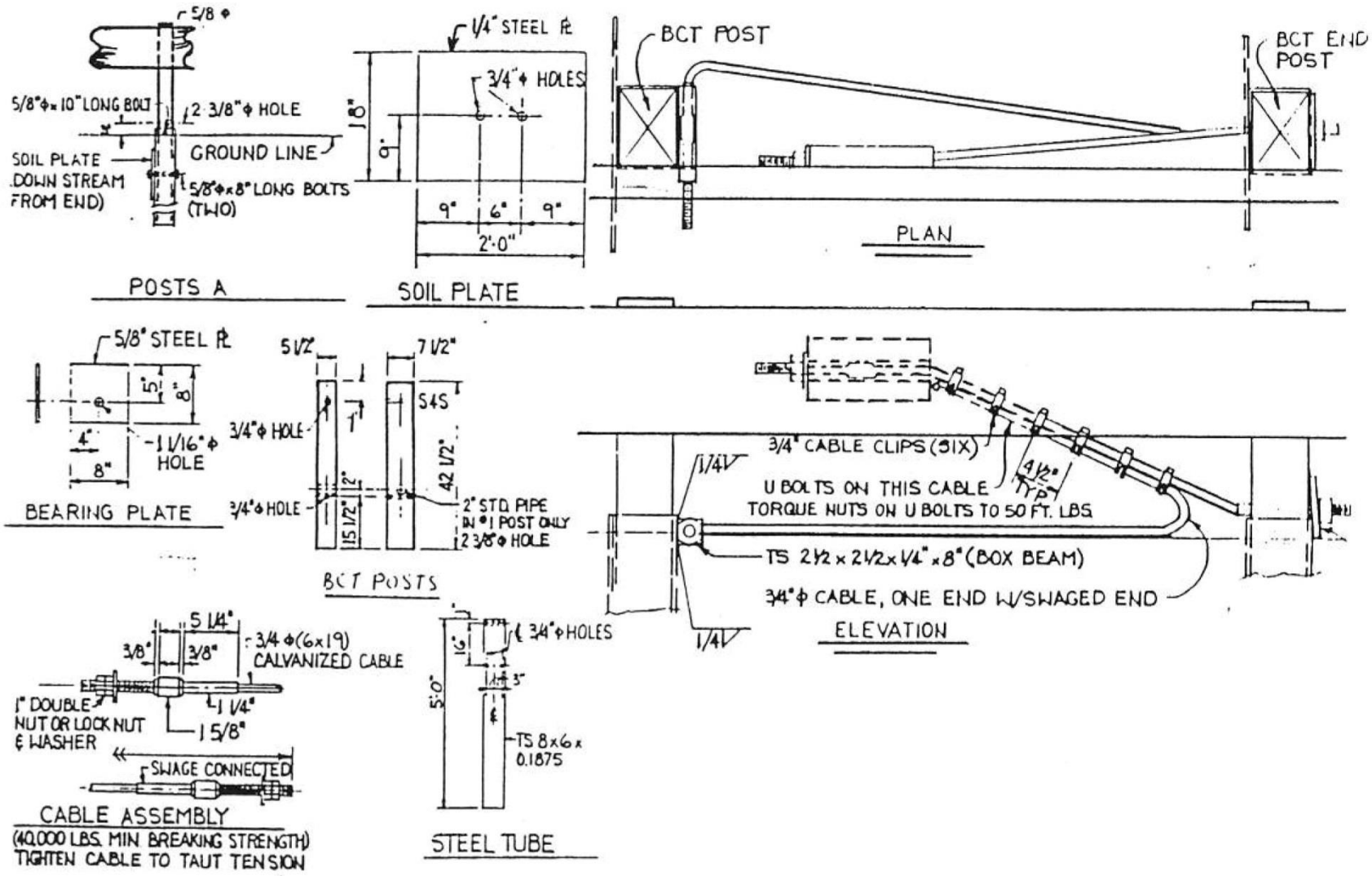

Figure 42. Cable Anchor and Foundation Details, Yuma County Short Radius Guardrail System [6]

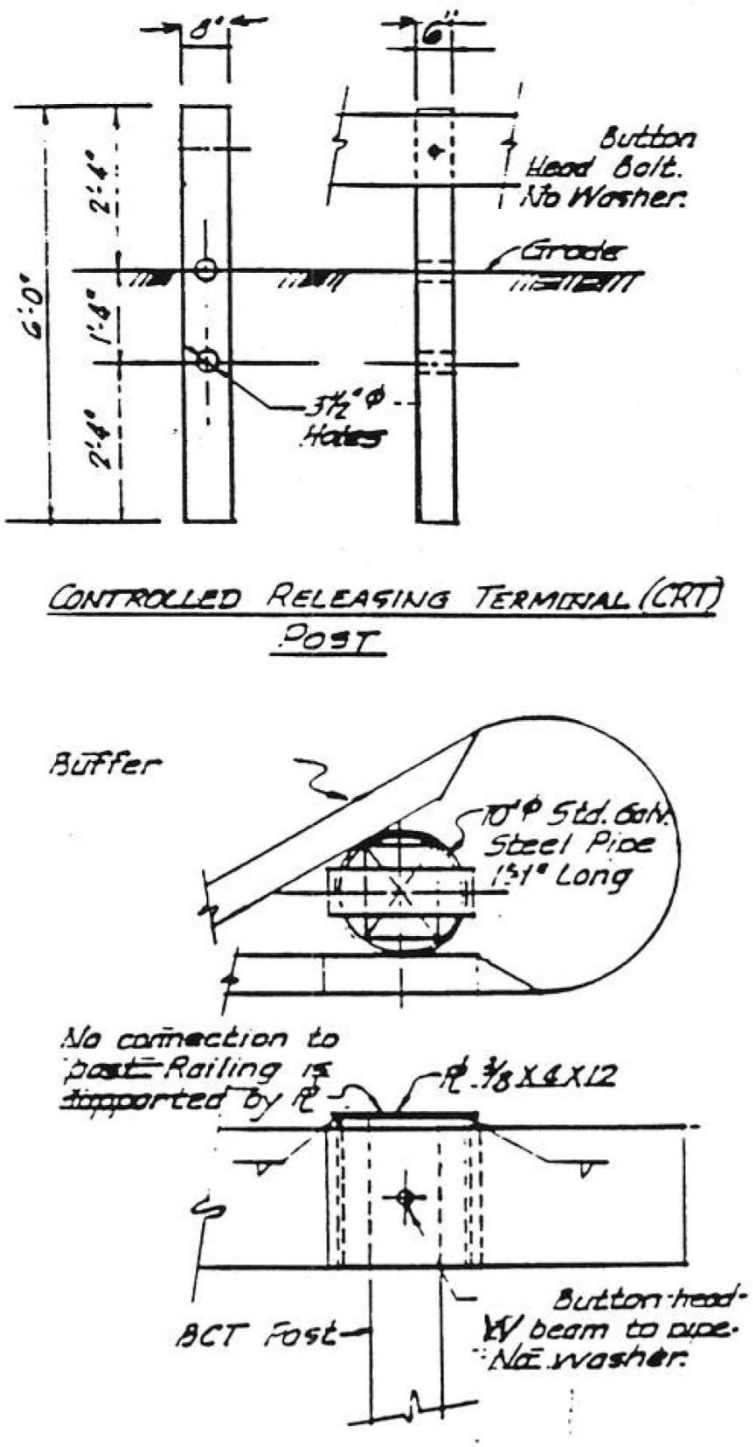

Figure 43. End Terminal Details, Yuma County Short Radius Guardrail System [6]

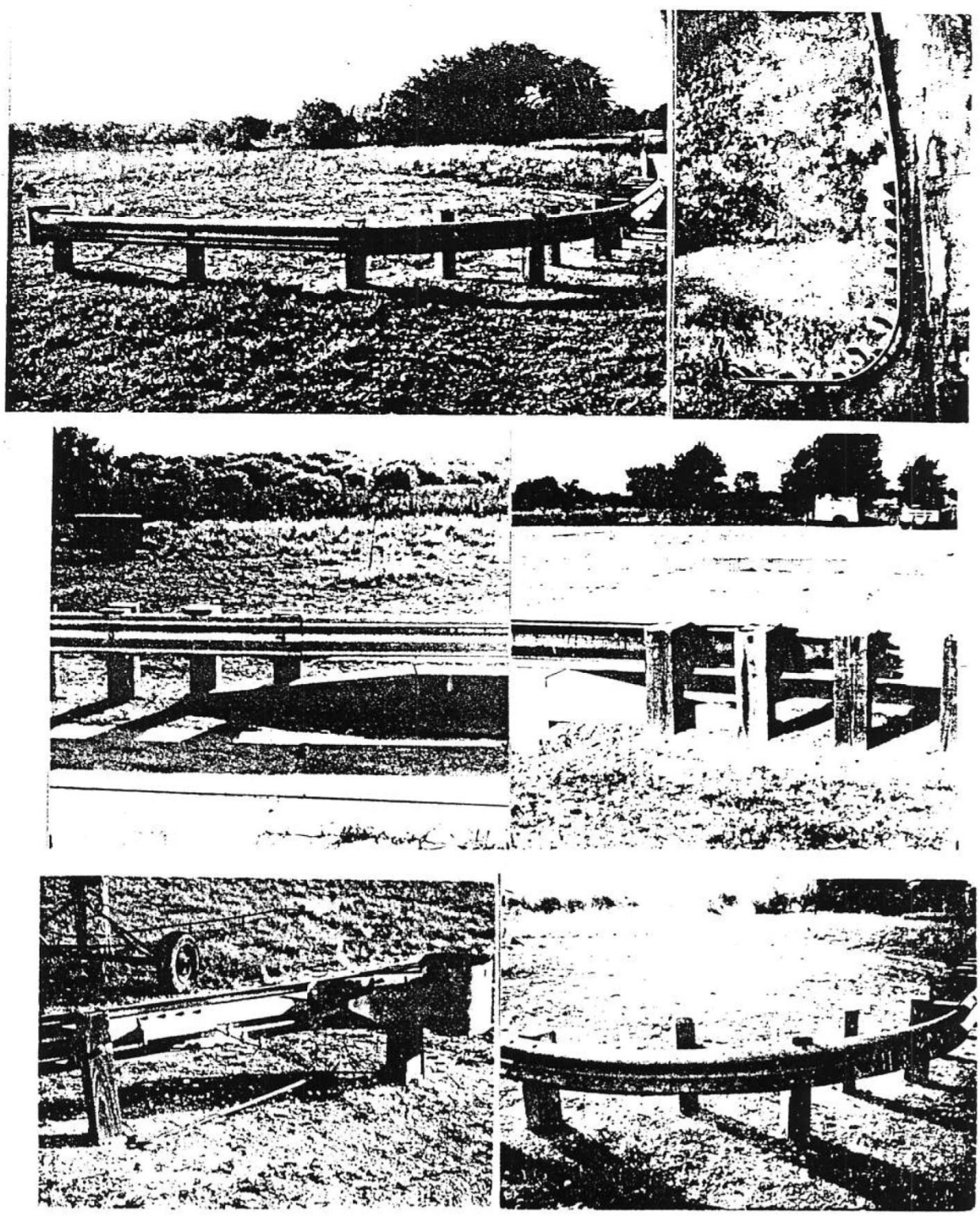

Figure 44. Developmental System Photographs, Test Nos. YC-1 through YC-3 [6]

4 BASELINE SIMULATIONS MODEL COMPOSITION

Baseline models of the Yuma County short-radius system were modeled using LS-DYNA. Based on the literature review, angled impacts into the midpoint of the radius were historically the most strenuous impact conditions. Two angled impacts into the midpoint of the radius using pickup trucks were modeled: test nos. YC-3 and YC-4. The baseline models were used to create validated initial models, which could be extended to larger-radius systems.

4.1 Summary of System Components and Computer Simulation Models

The Yuma County short radius guardrail system that was crash tested in test no. YC-3 consisted of three sub-systems:

(1) Upstream Anchor: one upstream-end terminal system consisting of one 12-ft 6-in. (3,810-mm) section of W-beam guardrail, one cable anchor assembly including two spliced anchor cables, two BCT posts and soil foundation tubes with two ⅝-in. (16-mm) diameter post bolts, nuts, and washers, and one end buffer piece to attenuate the severity of secondary-side head-on crashes.

(2) Radius: one 12 ft – 6 in. (3,810 mm) section of W-beam rail with a radius of 8 ft (2.4 m), and four 6 in. x 8 in. x 72 in. (152 mm x 203 mm x 1,829 mm) CRT posts with two ⅝-in. (16-mm) diameter post bolts, nuts, and washers. Two CRT posts were installed behind the radius and were freestanding.

(3) Downstream Transition to Stiff Bridge Rail: 18 ft – 9 in. (5,715 mm) of straight W-beam guardrail, consisting of 6-ft 3-in. (1,905-mm) and 12-ft 6-in. (3,810-mm) sections of W-beam guardrail. Two 6-in. x 8-in. x 72 in. (152 mm x 203 mm x 1,829-mm) timber posts with 6 in. x 8 in. x 14¼ in. (152 mm x 203 mm x 362 mm) blockouts, one 8 in. x 8 in. x 72 in. (203 mm x 203 mm x 1,829 mm) intermediate transition post with a 6 in. x 8 in. x 14¼ in. (152 mm x 203 mm x 362 mm) blockout and two 10 in. x 10 in.

x 78 in. (254 mm x 254 mm x 1,981 mm) transition posts with 6 in. x 8 in. x 14¼ in. (152 mm x 203 mm x 362 mm) blockouts supported the rail. An MC8x22.8 by 10 ft 5 in. long (MC203x33.9 by 3,175 mm long) C-channel rail stiffener was used to conjoin the downstream 3 posts in the system, and the rail was attached to the posts with ⅝-in. (16-mm) diameter post bolts, nuts, and washers.

4.2 Modifications for Additional Simulations

The additional baseline model of test no. YC-4 was similar to the simulation of test no. YC-3, except for the addition of one straight 12-ft 6-in. (3,810-mm) section of W-beam guardrail between the end anchorage and upstream end of the radius. This additional section of W-beam was supported by 6 in. x 8 in. (152 mm x 203 mm) CRT posts.

An additional simulation of a modified system similar to the system in test no. YC-4 was also conducted. The W-beam guardrail was raised to a top mounting height of 31 in. (787 mm) and an MGS end anchorage with groundline strut was substituted for the two-cable, spliced end anchorage. This system was not tested, and was used as a control example to determine what effect that raising guardrail height would have on system performance.

4.3 Previously Validated Models of System Components

Models of several Yuma County short-radius system components were used from previous research efforts involving simulations of guardrail systems, including soil and foundation tubes, the guardrail, splices, and post bolts, nuts, and washers [e.g., 25]. In addition, an anchor cable model suitable for use in MGS and BCT cable anchors had been developed previously and were considered validated [25, 29].

BCT posts at the end anchorages utilized 6 in. x 8 in. x 72 in. (152 mm x 203 mm x 1,829 mm) soil foundation tubes. The soil tubes were modeled with shell elements with 0.70-in. (18-mm) long diagonals, and 0.059-in. (1.5-mm) thickness. The BCT bearing plate was modeled

with rigid brick elements. Post-to-rail attachment bolts were modeled using shell elements for the round head, to improve post-to-rail contacts, and solid elements for the shanks, washers, and nuts. The components of the bolts were rigid and tied together. The use of a rigid material model was justified by examining previous testing conducted at MwRSF, which indicated that very little, if any, damage occurred to the bolts during impacts. Additionally, when blockouts were used, blockouts did not separate from the posts and either fractured or rotated around the bolt shanks, as shown in Figure 45.

Figure 45. Fractured CRT Posts without Bolt Damage [14]

W-beam guardrail was modeled with 12-gauge (2.6-mm thick) shell elements. Most of rail was modeled with 0.82-in. (21-mm) diagonal, rectangular shell elements. A finer mesh with 0.24-in. (6.0-mm) element diagonals was used around the post-to-rail attachment slots to improve attachment contacts and local rail deformation.

Rail splices have been modeled as overlapping sections of W-beam guardrail using elements with merged nodes [e.g., 9, 25]. By overlapping elements, the splices had an approximately two-times increase in both tensile strength and bending stiffness. Crack propagation and rail slippage at splices were not modeled in these simulations.

4.4 Components Validated for Use in Model

4.4.1 Wood CRT Posts

4.4.1.1 Baseline Models

Computer simulation models of 6 in. x 8 in. x 72 in. (152 mm x 203 mm x 1,829 mm) CRT posts used in the study were generated and compared to physical test data. Two material models were selected to represent the CRT post, based on previous testing and modeling of wood posts [25]. These post models were compared to 90-degree (strong-axis), 45-degree, and 0-degree (weak-axis) impacts of CRT posts in rigid foundation tubes from previous research [23].

Post models were simulated using LS-DYNA. The two material models consisted of an isotropic plastic-kinematic model (MAT_13), and a piecewise linear plasticity model (MAT_24). Material parameters in metric units are summarized in Table 16. Impact conditions of the CRT post simulations are shown in Figure 46, and time-sequential images of 0-degree (strong-axis) and 90-degree (weak-axis), MAT_13 simulations and tests in metric units are shown in Figures 53 and 54, respectively. Acceleration data was filtered using a CFC60 filter and analyzed to estimate post impact forces for both simulations and physical tests, in accordance with the Society of Automotive Engineers (SAE) J211 [31]. Force and energy versus displacement plots are shown in Figures 47 through 52. A comparison of the peak forces and energies at 8 in. (203 mm) of deflection for the simulations and bogie tests is shown in Table 17.

Table 16. Summary of Material Parameters Used in CRT Posts

Material	Young's Modulus (GPa)	Density (kg/mm^3)	Poison's Ratio	Yield Stress (MPa)	Tangent Modulus (GPa)	Effective Plastic Strain at Failure
Isotropic Elastic Failure (MAT_13)	10.2	$6.120(10^{-7})$	0.35	17.5	0.240	0.0625
Piecewise Linear Plasticity (MAT_24)	11.0	$6.274(10^{-7})$	0.30	6.0	0.250	0.0800

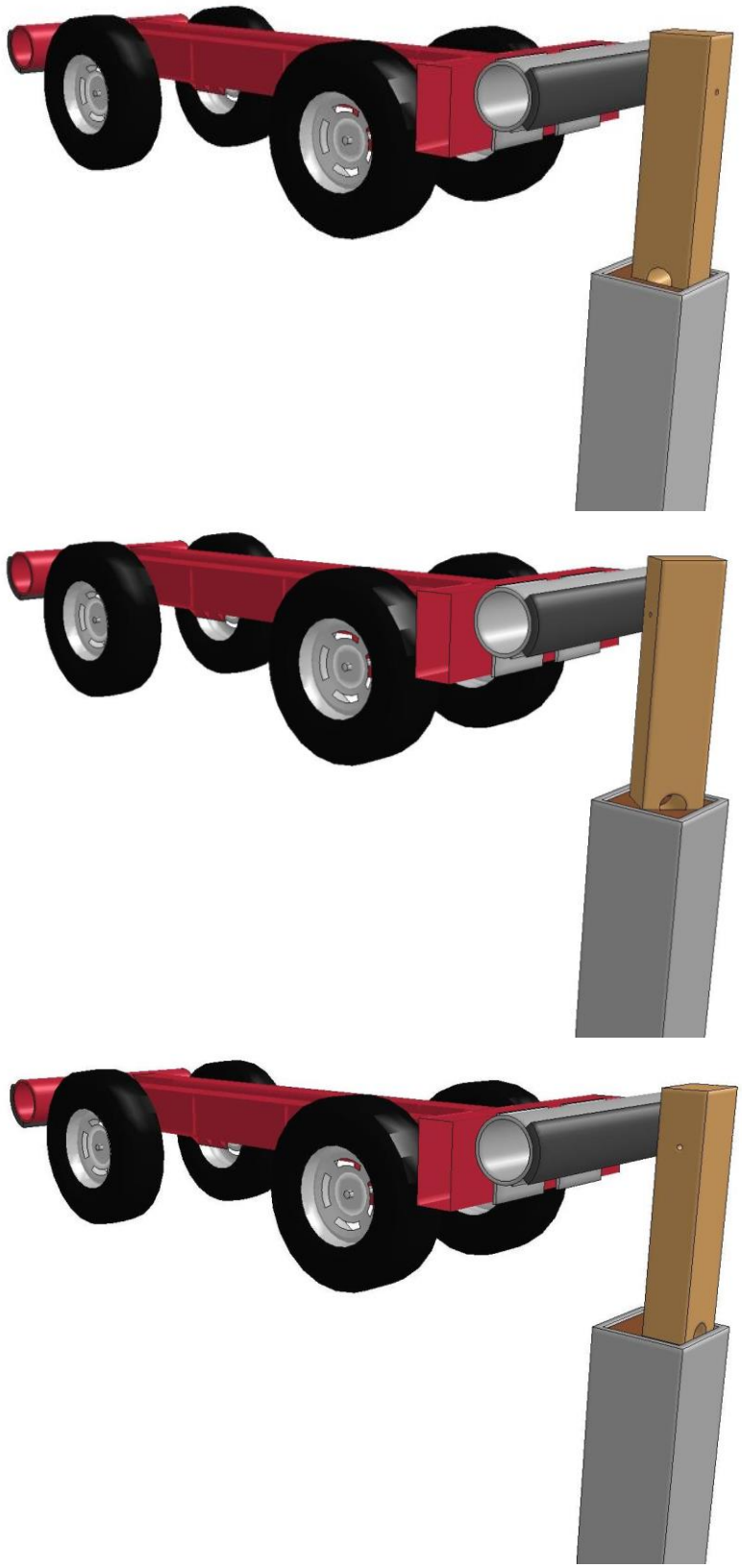

Figure 46. LS-DYNA Models of CRT Posts in Rigid Sleeves, 90, 45, and 0-Degree Orientations

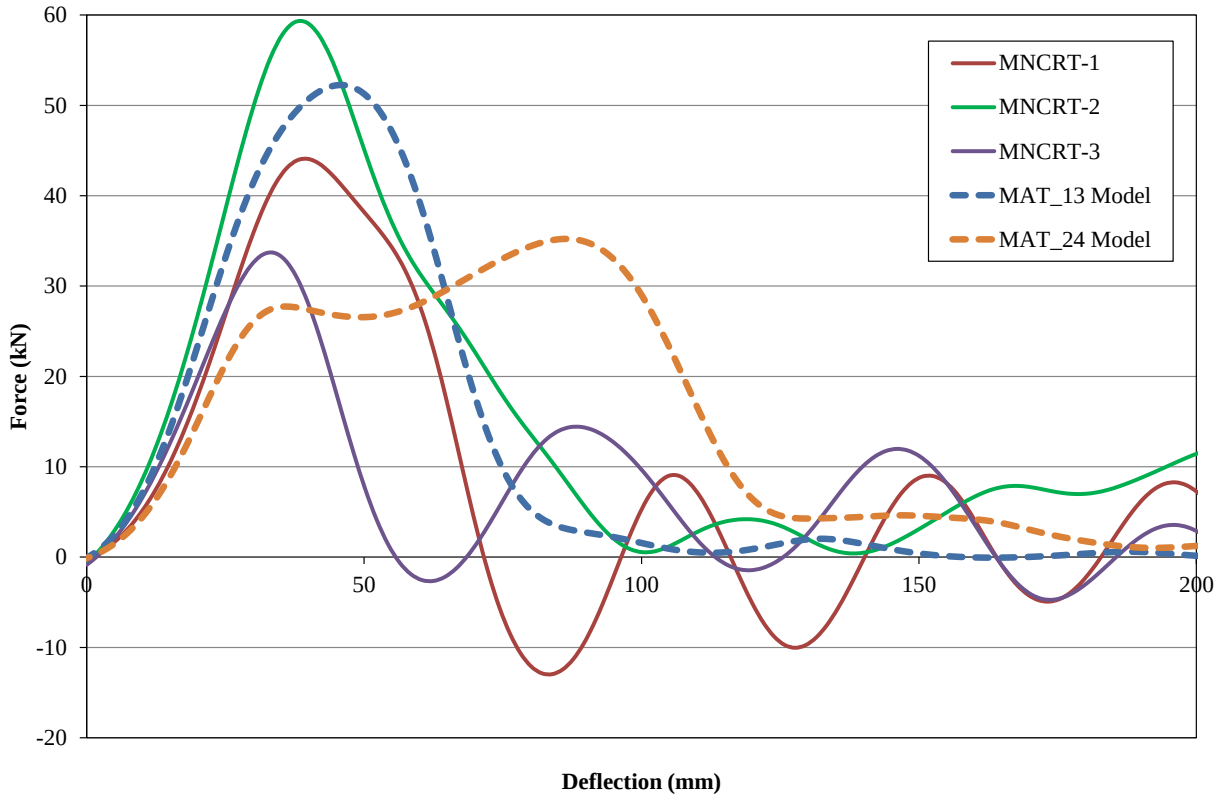

Figure 47. Force vs. Deflection, CRT Post at 90 deg in Rigid Sleeve, Models and Bogie Tests

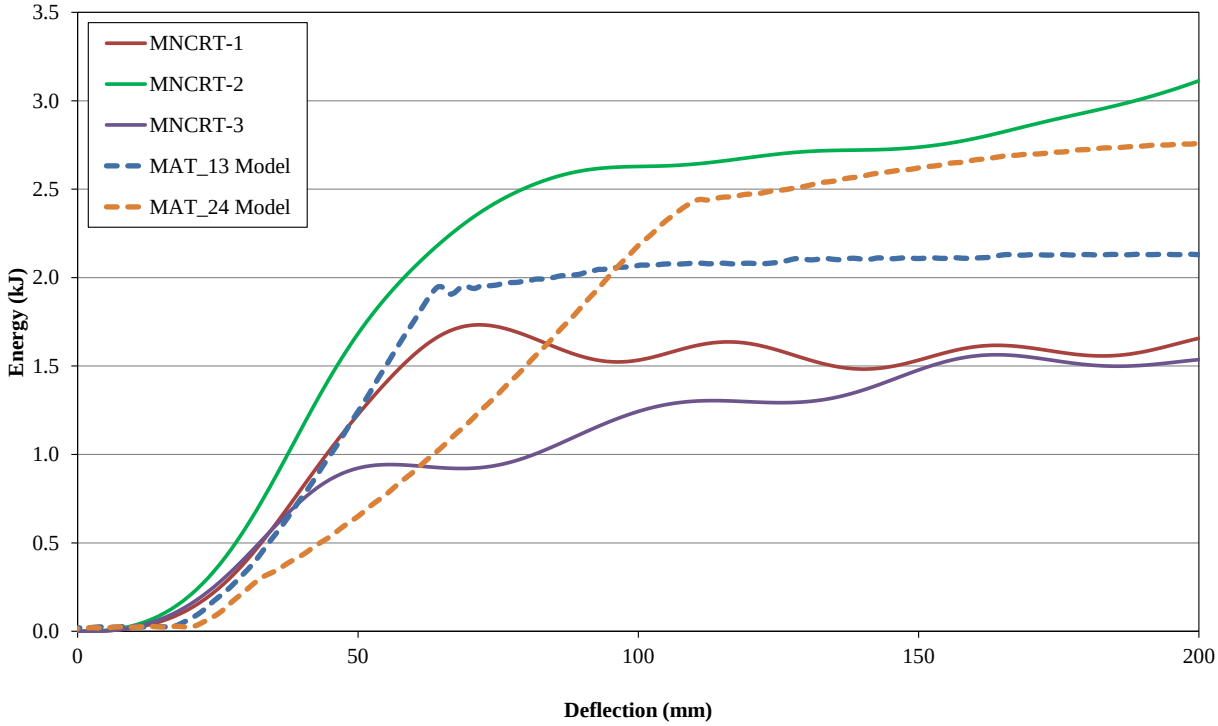

Figure 48. Energy vs. Deflection, CRT Post at 90 deg in Rigid Sleeve, Models and Bogie Tests

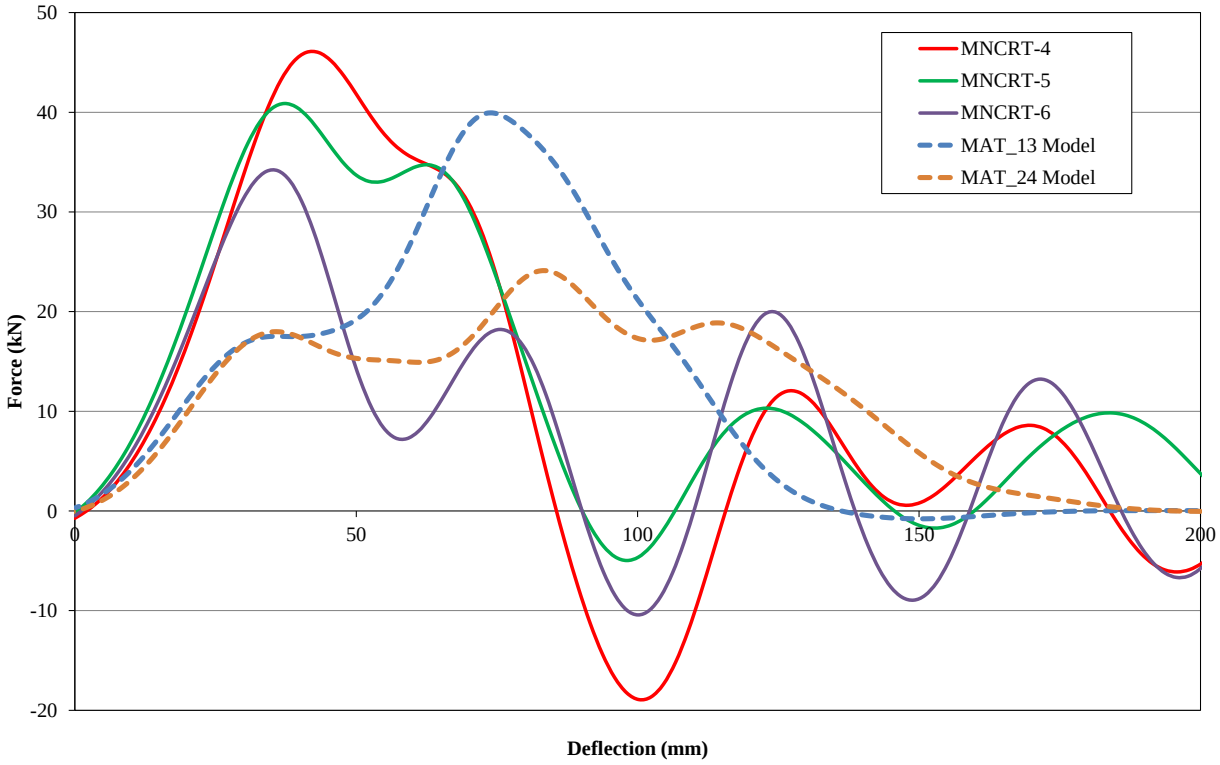

Figure 49. , Force vs. Deflection, CRT Post at 45 deg in Rigid Sleeve, Models and Bogie Tests

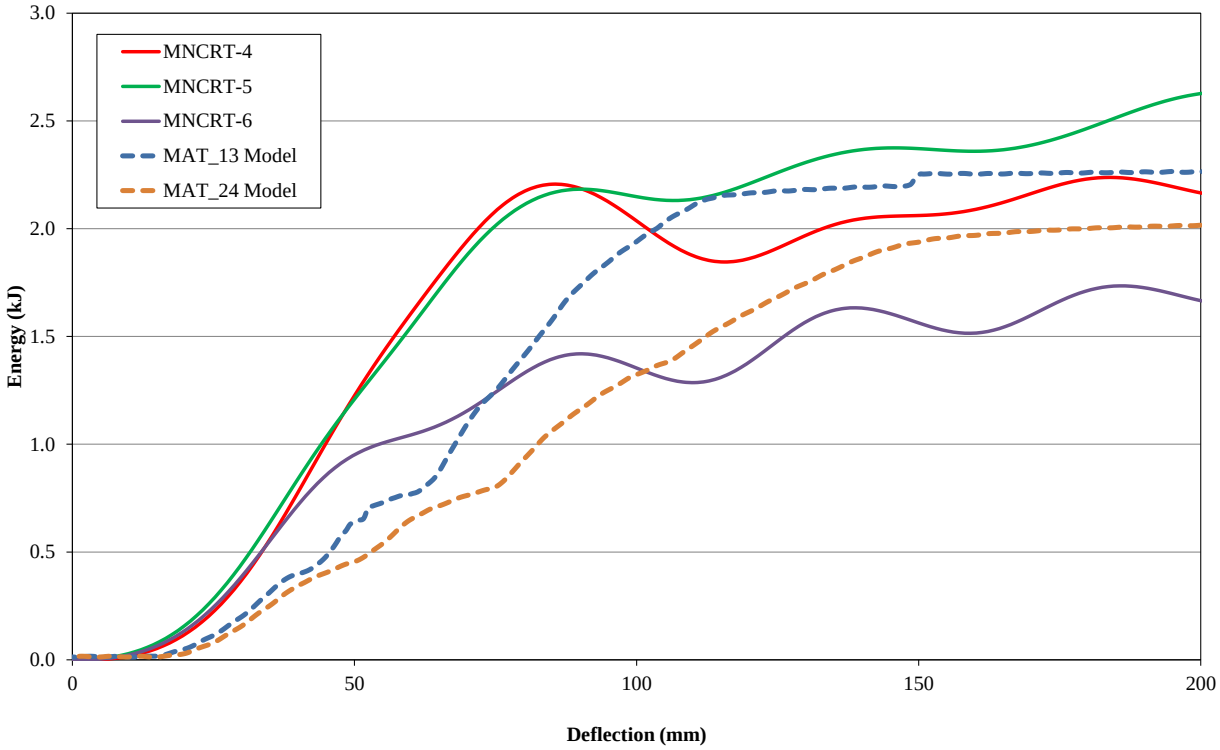

Figure 50. Energy vs. Deflection, CRT Post at 45 deg in Rigid Sleeve, Models and Bogie Tests

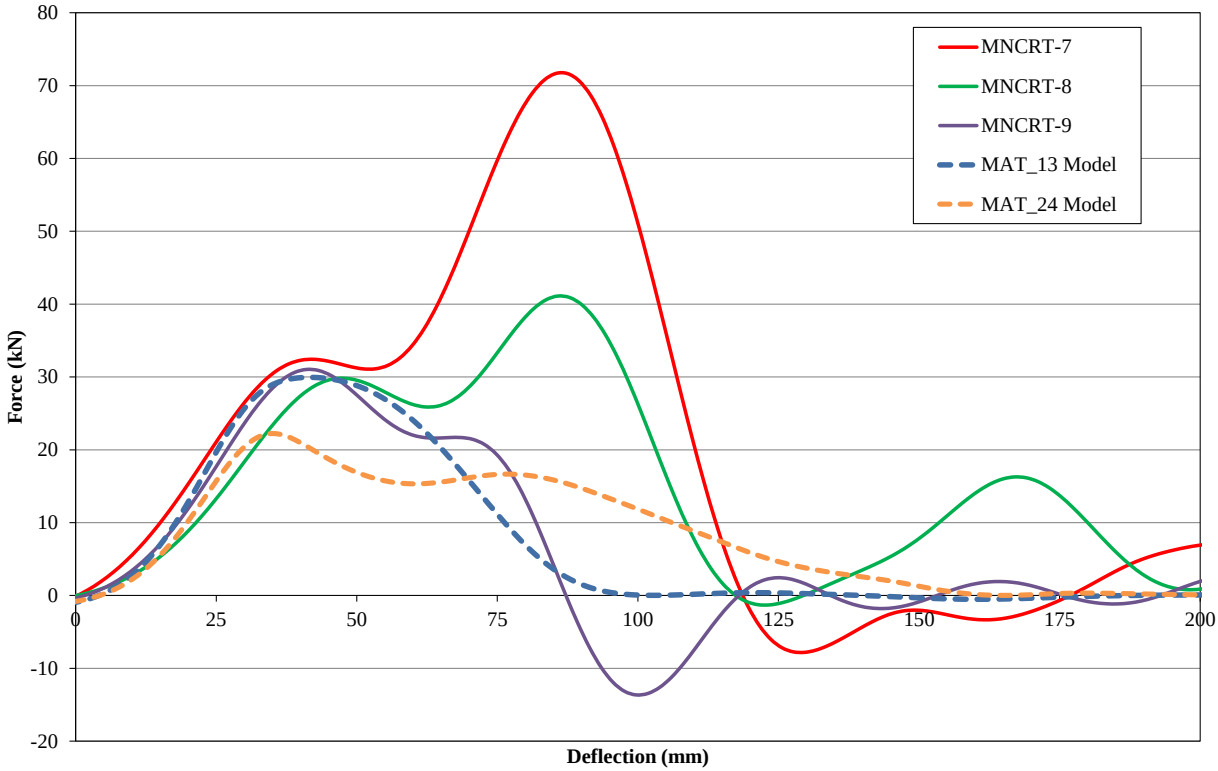

Figure 51. Force vs. Deflection, CRT Post at 0 deg in Rigid Sleeve, Models and Bogie Tests

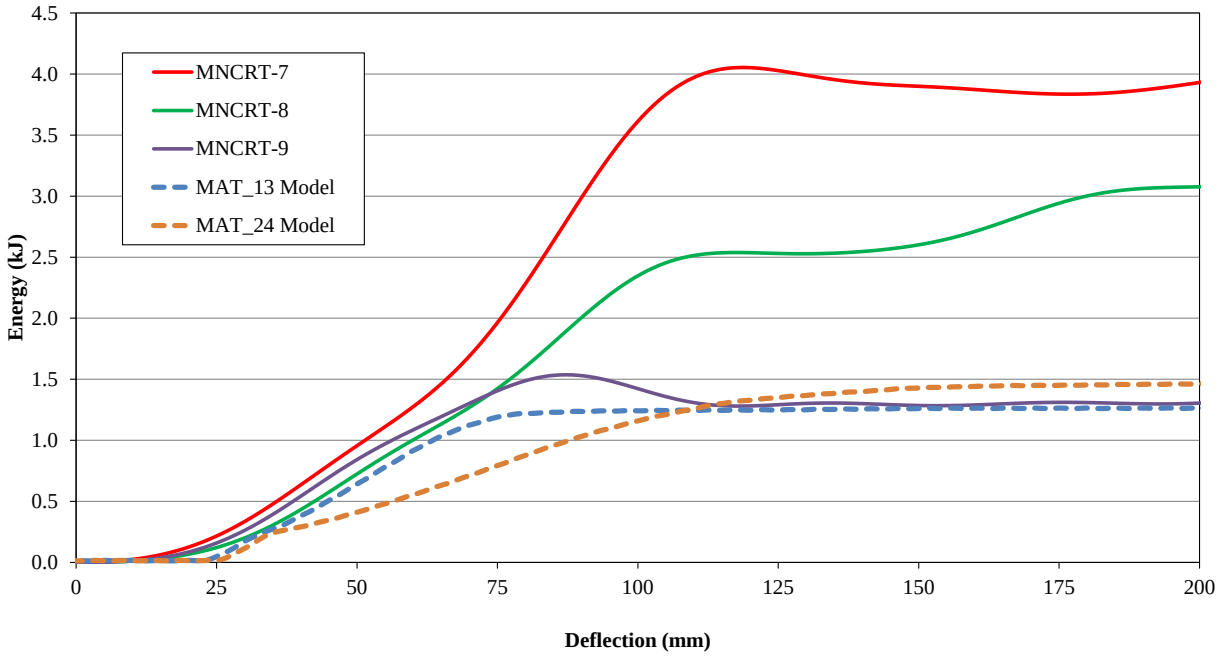

Figure 52. Energy vs. Deflection, CRT Post at 0 deg in Rigid Sleeve, Models and Bogie Tests

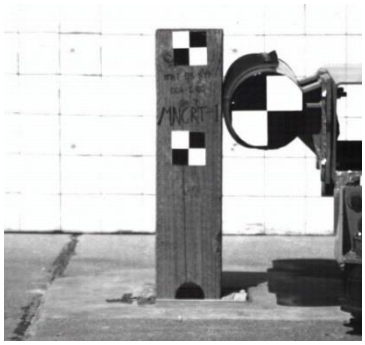

0.000 sec

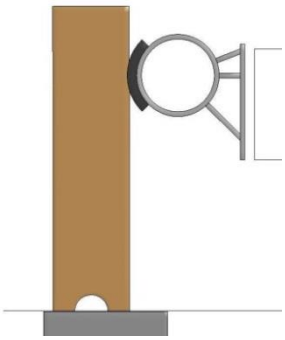

0.000 sec

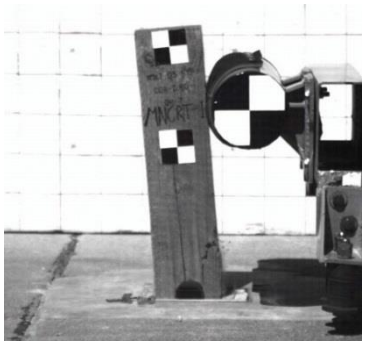

0.008 sec
Crack initiated (front side)

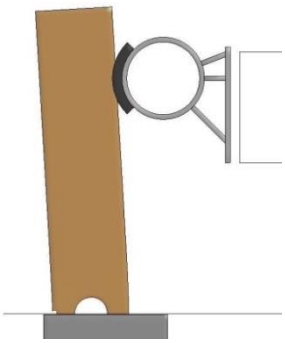

0.008 sec
Crack initiated (back side)

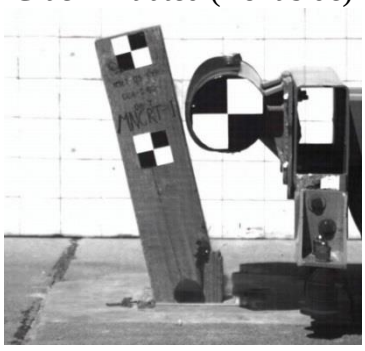

0.018 sec
Tension side of CRT hole ruptured

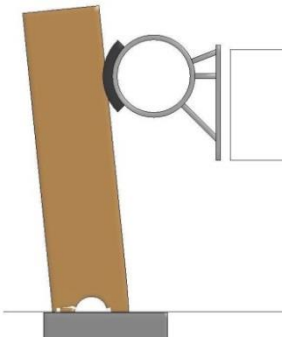

0.012 sec
Crack initiated (front side)

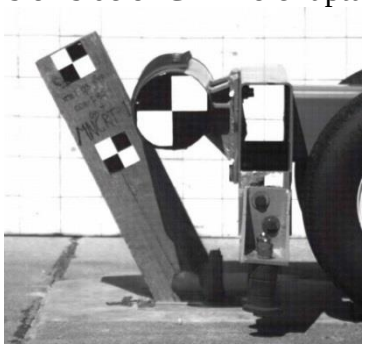

0.044 sec
Complete rupture

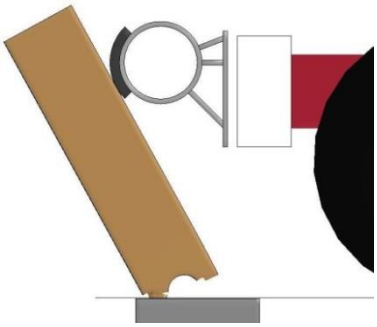

0.048 sec
Complete rupture

Figure 53. Time-Sequential Images, Simulation and Test No. MNCRT-2

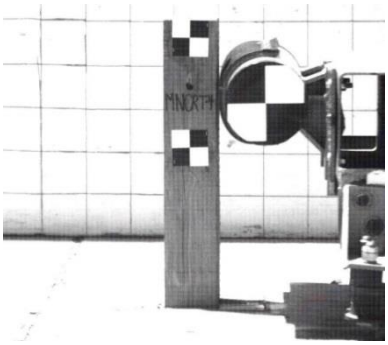

0.000 sec

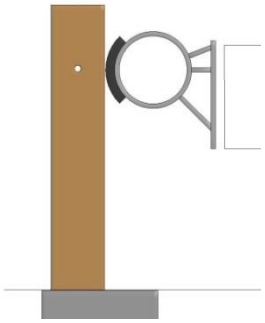

0.000 sec

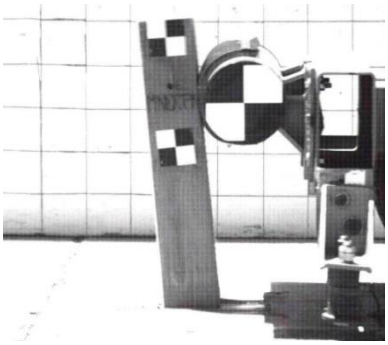

0.008 sec
Crack initiated (front side)

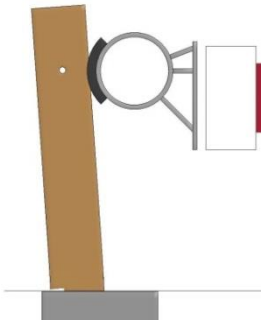

0.008 sec
Crack initiated (back side)

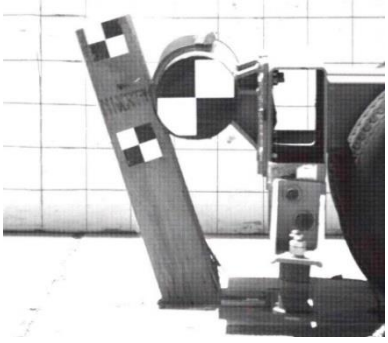

0.026 sec
Widespread delamination, splitting, cracking

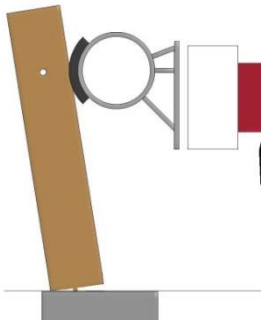

0.018 sec
Complete rupture

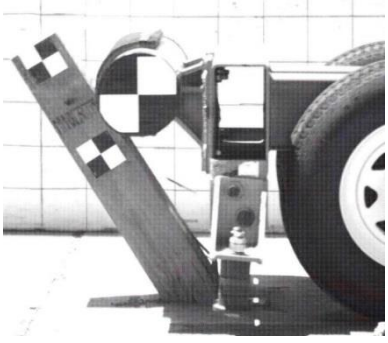

0.048 sec
Near-complete rupture

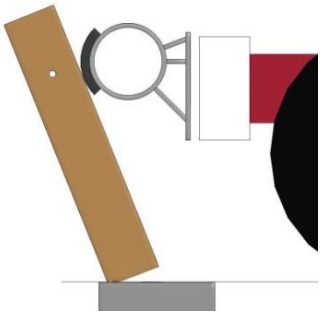

0.036 sec
Post rebounds off of impact head

Figure 54. Time-Sequential Images, Simulation and Test No. MNCRT-4

Table 17. Comparison of Results, Tests and Simulations

Observation	90-Degree				45-Degree				0-Degree			
	Average Peak Force		Energy through 8 in. (203 mm) of Deflection		Average Peak Force		Energy through 8 in. (203 mm) of Deflection		Average Peak Force		Energy through 8 in. (203 mm) of Deflection	
	kip	kN	kip-in.	kJ	kip	kN	kip-in.	kJ	kip	kN	kip-in.	kJ
Physical Tests	10.3	45.65	1.56	2.12	8.9	39.38	2.03	2.76	9.1	40.34	1.59	2.15
MAT_13	11.7	52.25	1.57	2.13	9.0	39.94	1.67	2.26	6.7	29.94	0.93	1.26
MAT_24	7.9	35.22	2.05	2.77	5.4	24.11	1.49	2.02	5.0	22.22	1.08	1.46

The strong-axis force versus deflection and energy-absorption versus deflection curves for the simulated CRT posts were comparable to the physical tests. The physical test data demonstrated a wide scatter in wood strengths, and average maximum peak forces calculated from bogie acceleration data in 90-degree, 45-degree, and 0-degree post orientations were 10.3 kip, 8.9 kip, and 9.1 kip (45.7, 39.4, and 40.3 kN), respectively.

In general, the modeled posts were weaker when impacted perpendicular to the weak axis than the wood posts in the physical tests. Simulated posts dissipated less energy through 8 in. (203 mm) of deflection, and had lower peak forces than posts in the physical tests. Simulated posts also generally fractured before posts in the physical test in weak-axis impacts. However, when impacted in 90-degree or 45-degree impacts, peak forces, average forces, and energy levels through 8 in. (203 mm) deflection closely matched test data averages. Most posts which deflected and fractured during short-radius impact simulations were loaded with angles between 90 and 0 degrees. The MAT_13 material model was determined to be better-suited for estimating both peak loads and energy than the MAT_24 model, and was selected for further investigation.

An automatic general contact type was utilized for post-to-impact head contacts. Additional simulations using an automatic single surface contact type provided identical results. However, after the post fractured and elements near the CRT holes eroded, the upper piece of the

post rotated backwards and dropped downward, causing elements on the back sides of the upper and lower posts to overlap without developing contact forces.

An eroding single surface contact type was substituted for the single-surface and general contact types previously used, to allow contact forces to develop between the upper and lower faces of the fractured posts. The force versus deflection curve for one of the orientations is shown in Figure 55. The contact force curves for the two contact types were nearly indistinguishable for all impact orientations, despite visual differences in the post fracture, as shown in Figure 56. In addition, the eroding single surface contact type increased complexity and processing time by approximately 15%. Simulations of the full-scale crash test using the eroding single surface contact definition terminated due to numerical errors associated with the eroding single surface contact. Thus, researchers utilized automatic single surface contacts for the remaining full-scale impact simulations.

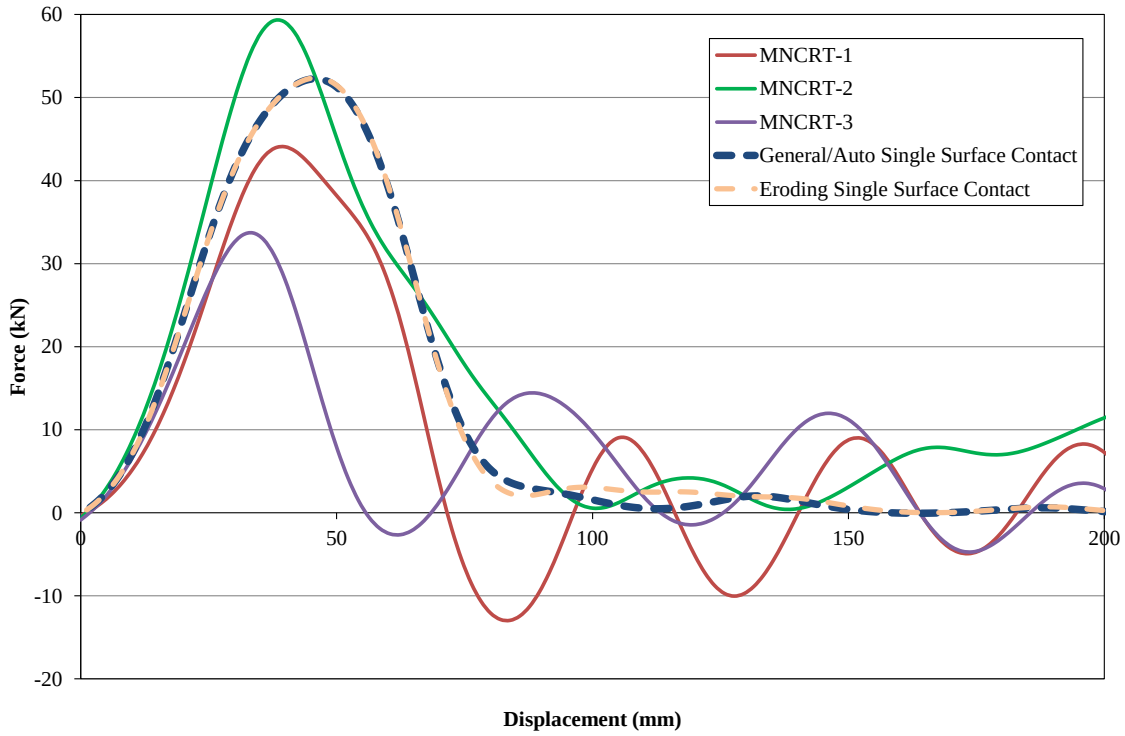

Figure 55. Comparison of Force vs. Deflection of CRT Post in 90-Degree Orientation, General/Automatic Single Surface and Eroding Single Surface Contact Types

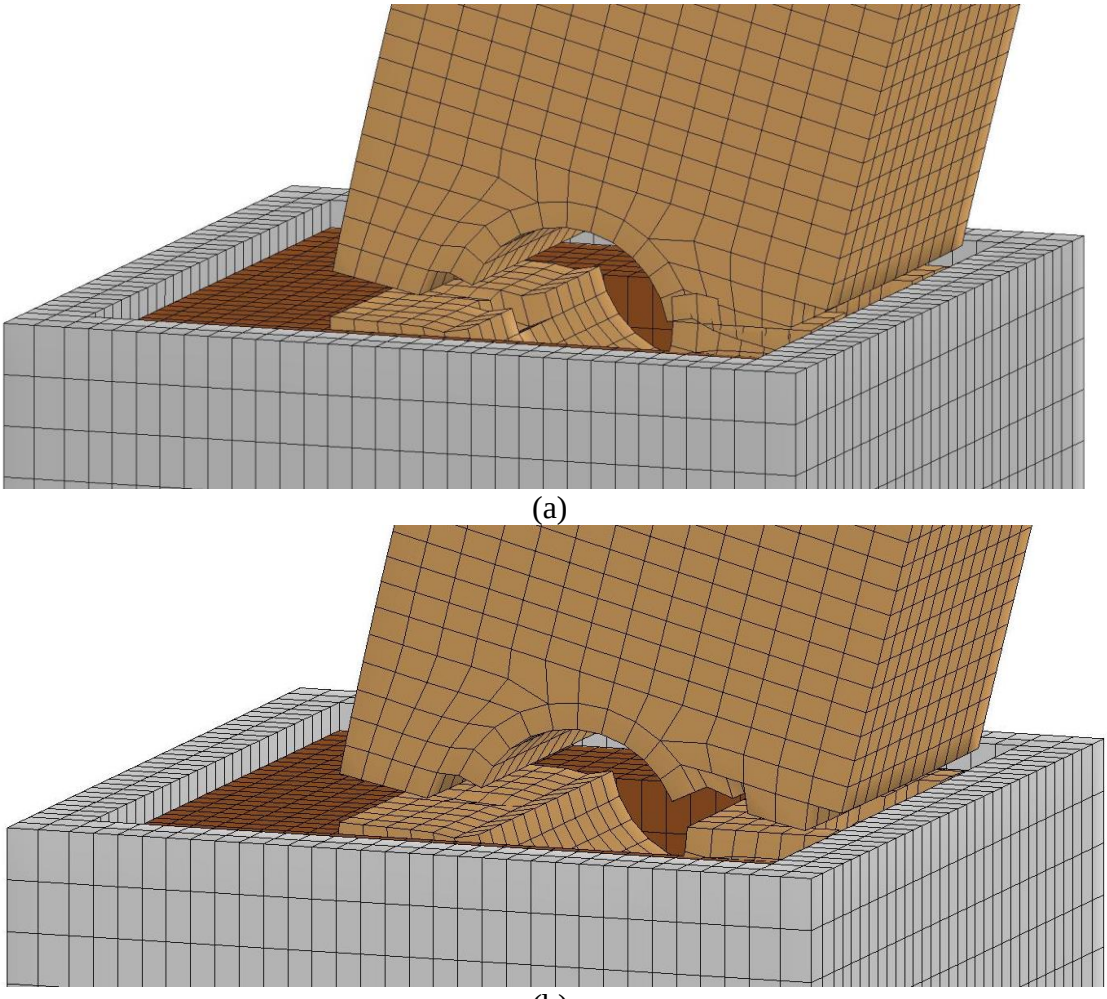

(a)

(b)

Figure 56. Comparison between (a) General/Automatic Single Surface and (b) Eroding Single Surface Contact Types at Same Instant in Time

4.4.1.2 Mesh Sensitivity

A fine mesh was initially used to model the CRT post. Brick elements had typical edge lengths of 0.50-in. (12.7 mm). A more feasible mesh size of the posts utilized brick elements with 1.00-in. (25.4-mm) edge lengths. The posts were modeled with both mesh sizes and the results were compared. The post with a coarser mesh was determined to be 2% stronger than the finer mesh during strong-axis impacts and 7% weaker during weak-axis impacts. However, the coarse mesh post dissipated more energy during strong and weak-axis impacts than the fine mesh post.

4.4.1.3 Post Calibration through Dimensional Variation

Maximum impact loads during weak-axis impacts were lower than the average peak force and energy dissipation calculated from physical testing. Researchers proposed an idea to evaluate the performance of the posts using a surrogate post size to significantly increase the weak-axis impact strength without adversely affecting the strong-axis post strength by linearly scaling the width of the post. Weak axis dimensions were increased by 10%, 20%, 30%, and 40%, with resulting widths of 6.6 in., 7.2 in., 7.8 in., and 8.4 in. (168 mm, 183 mm, 198 mm, and 213 mm). The surrogate post models were simulated and compared to the results of both the 0.5-in. and 1-in. (13-mm and 25-mm) post meshes. Models of the meshes are shown in Figure 57. Results of the simulations are shown in Figures 58 through 63.

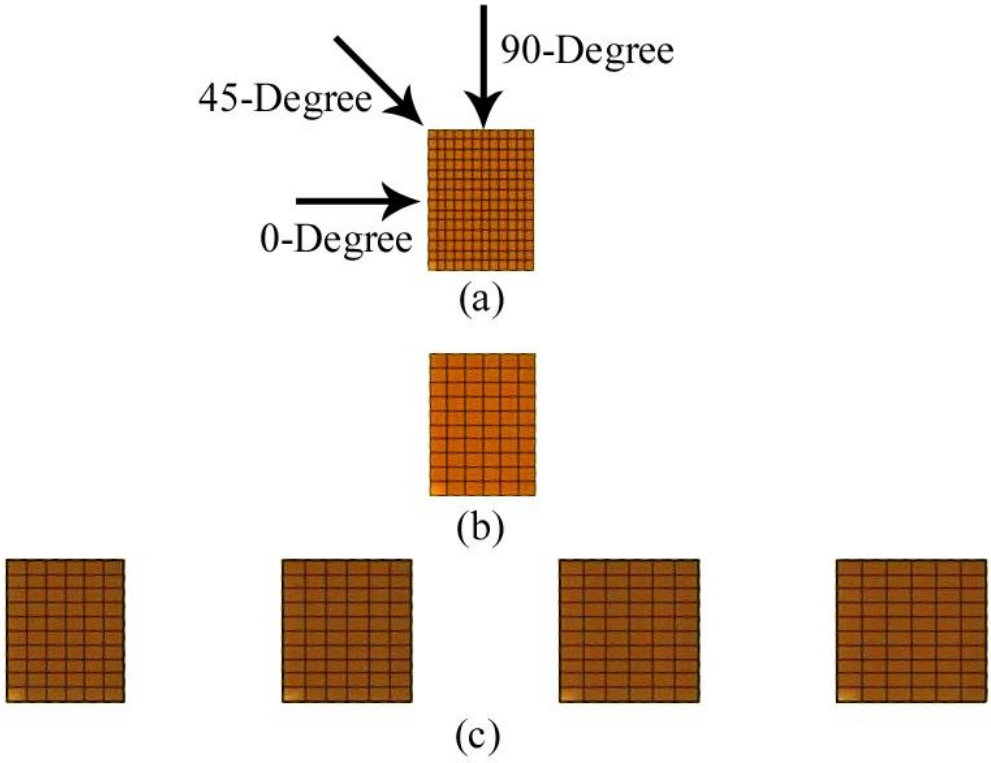

Figure 57. Post Size Comparison, (a) Fine, (b) Coarse, and (c) Surrogate Meshes

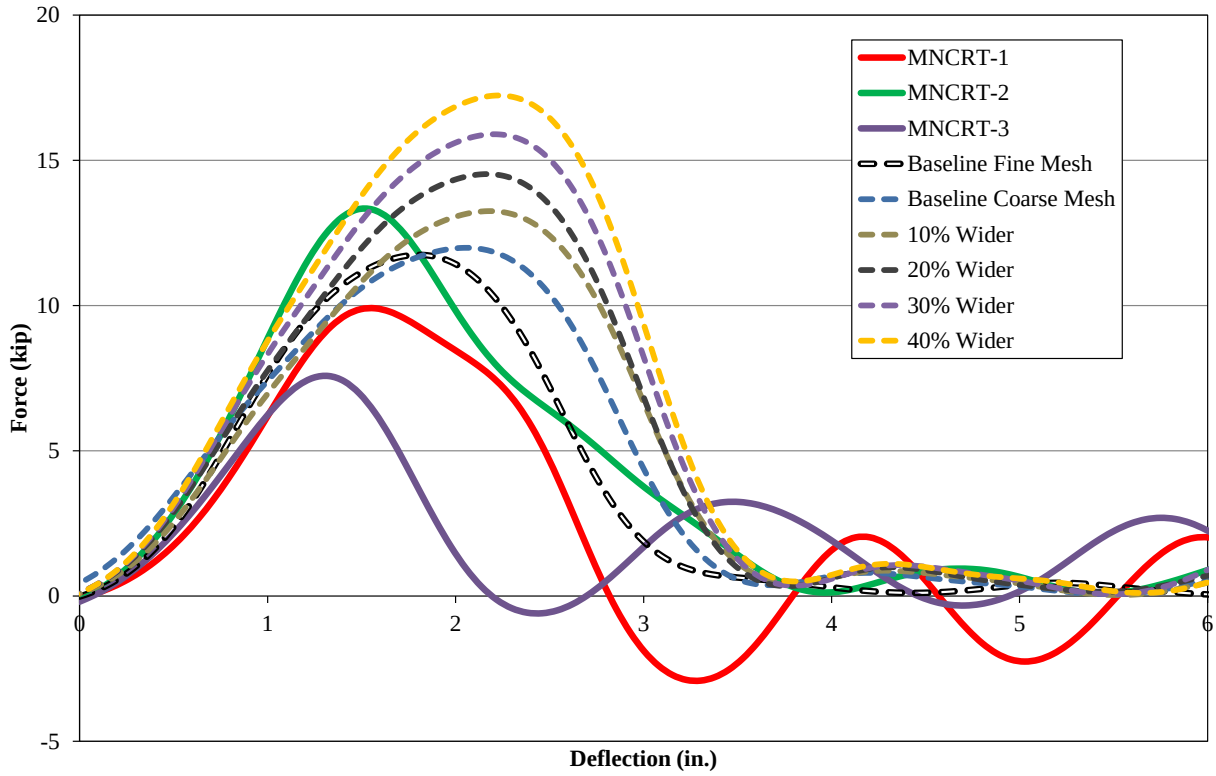

Figure 58. Force vs. Deflection, 90-Degree Impact, Tests and Surrogate Models

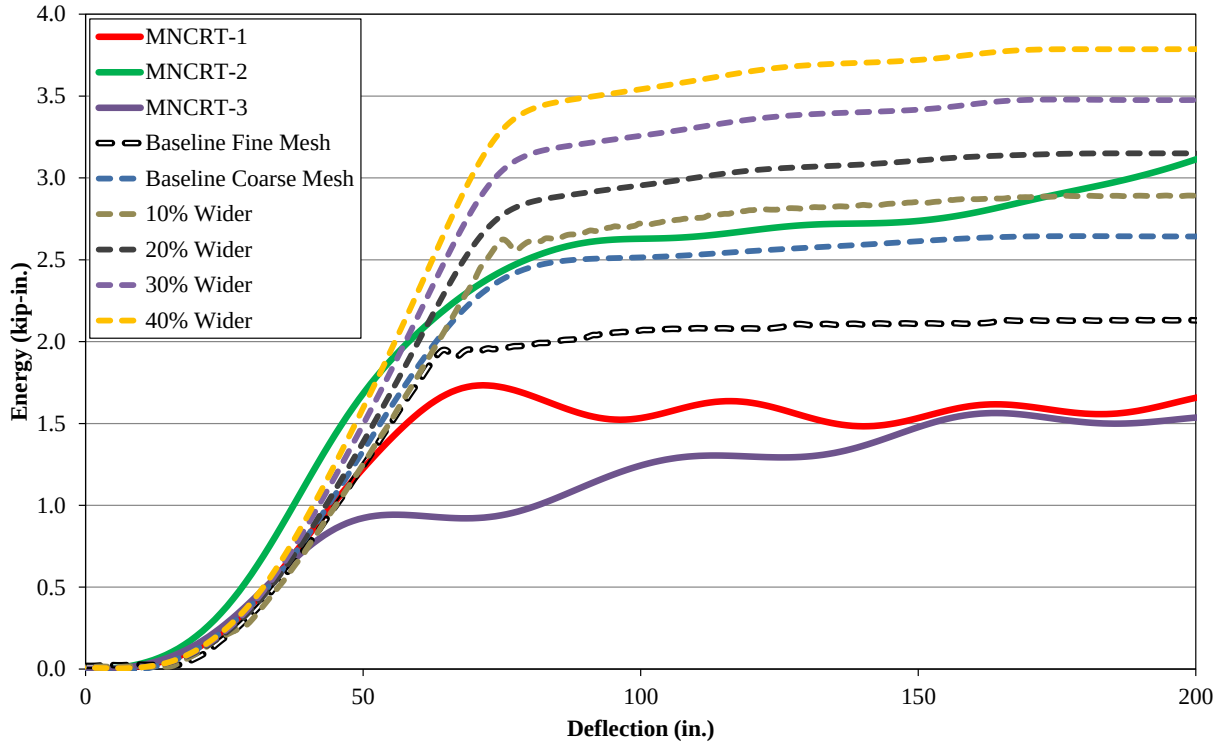

Figure 59. Energy vs. Deflection, 90-Degree Impact, Tests and Surrogate Models

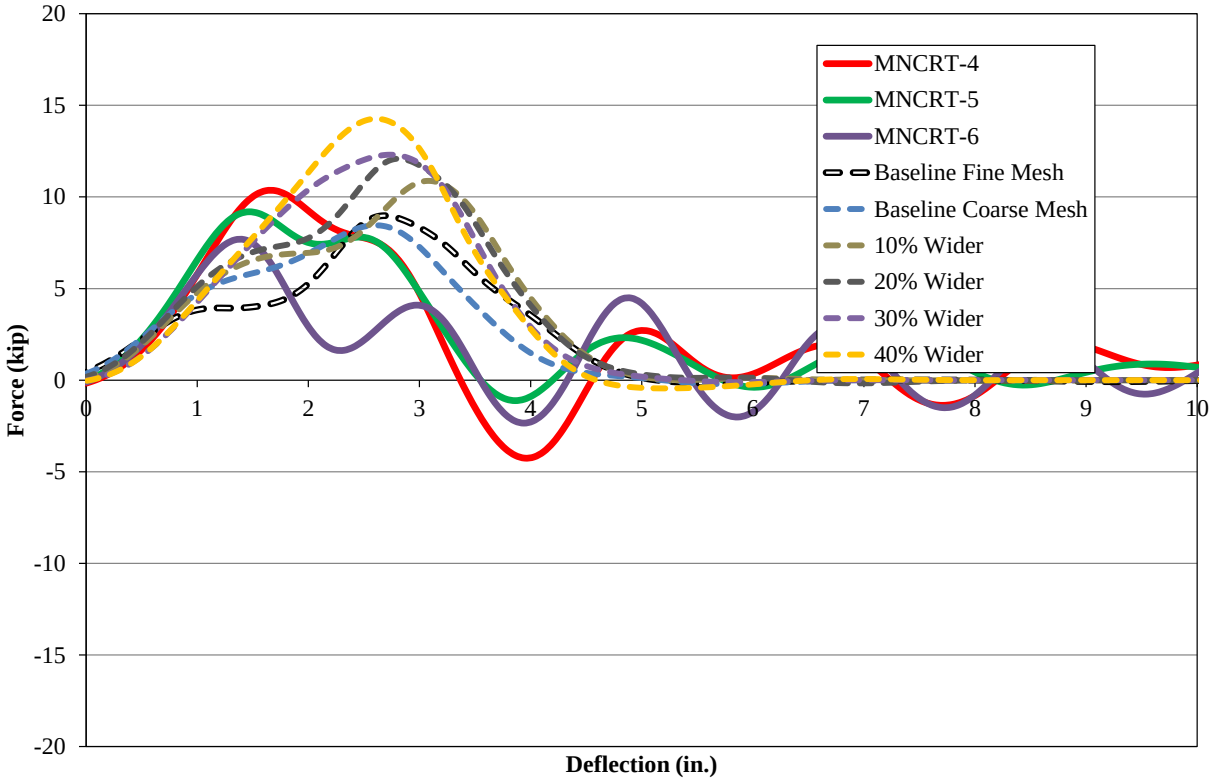

Figure 60. Force vs. Deflection, 45-Degree Impact, Tests and Surrogate Models

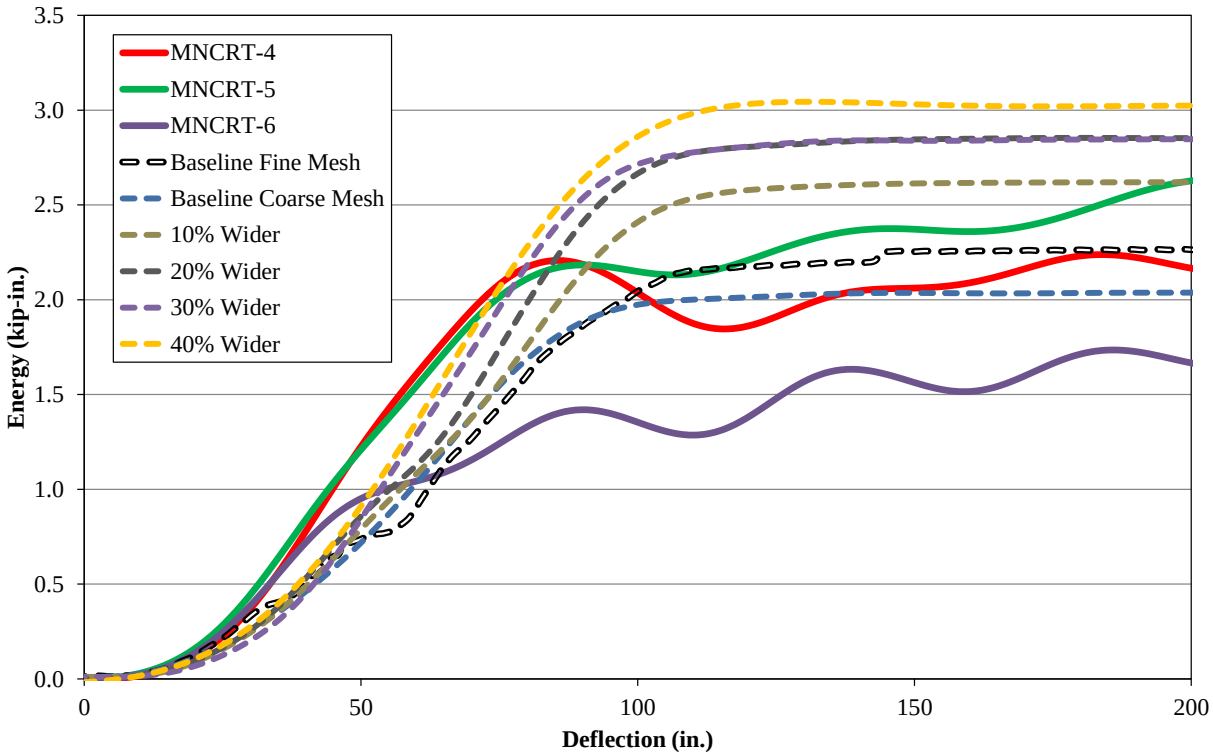

Figure 61. Energy vs. Deflection, 45-Degree Impact, Tests and Surrogate Models

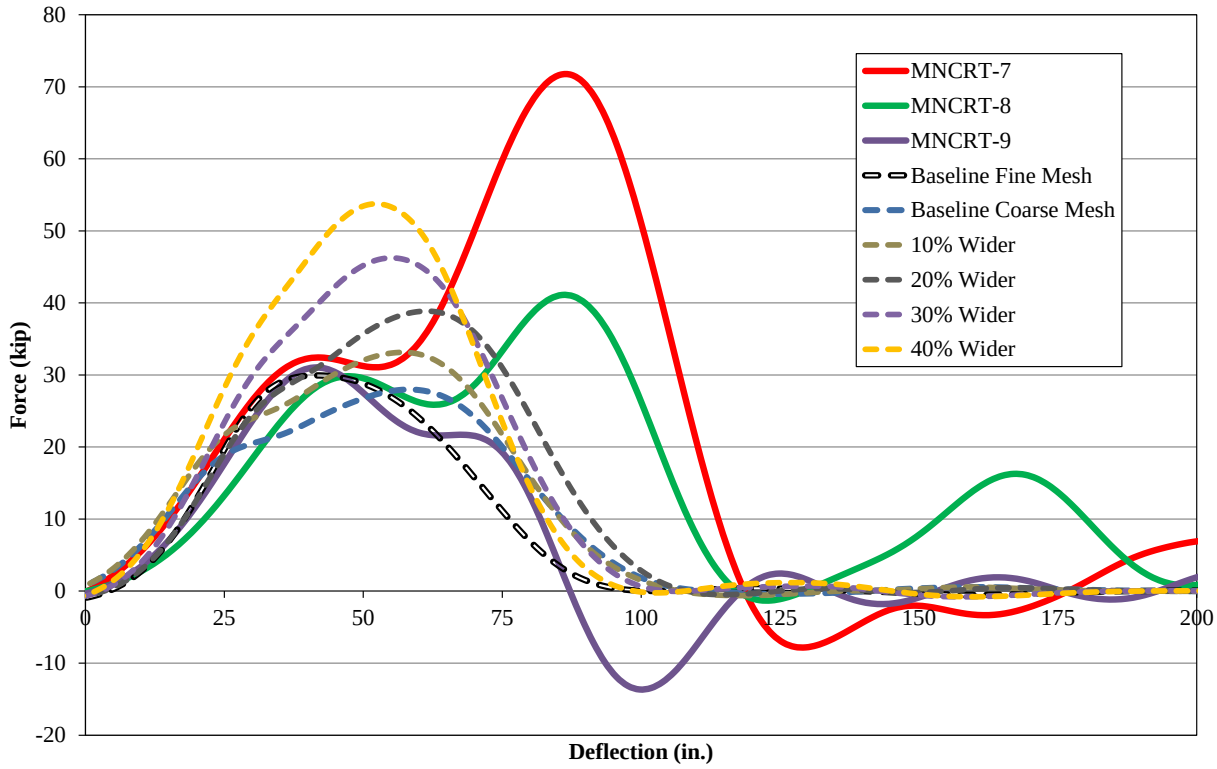

Figure 62. Force vs. Deflection, 0-Degree Impact, Tests and Surrogate Models

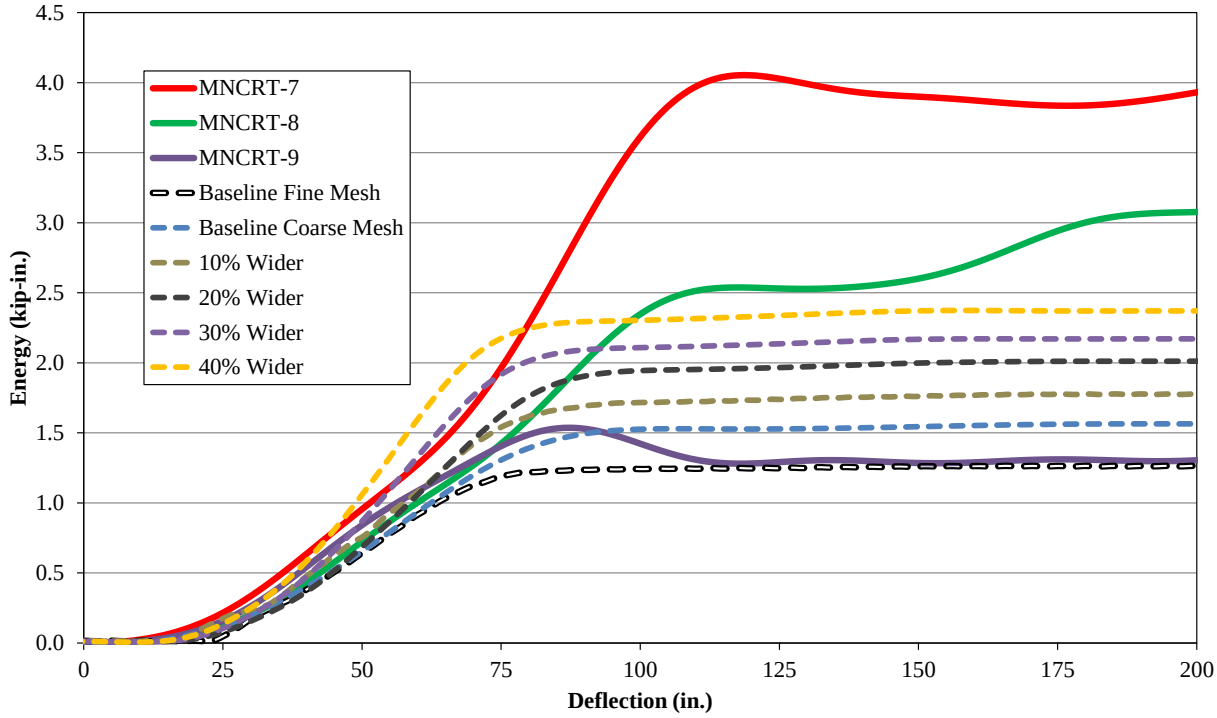

Figure 63. Energy vs. Deflection, 0-Degree Impact, Tests and Surrogate Models

Based on the results of the surrogate model evaluation, it was determined that the optimal post shape utilized a 15% increase in weak-axis width. This selection was estimated to represent the upper bound of post strengths in the strong-axis direction, above-average strength in a 45-degree direction, and below average strength in the weak-axis direction. Although the post model was overly-strong in strong-axis impacts when placed in a rigid soil foundation tube, a subsequent evaluation evaluating the post interaction with the soil was determined to be representative of test data, as discussed in Section 4.4.2.

A separate orthotropic material model, MAT_22, was also selected for evaluation. Unfortunately, the model was unstable and failed to run to completion in any impact direction simulation. After the simulated vehicle struck the post with the orthotropic material, the post vibrated rapidly and experienced significant hourglassing. The primary purpose of the research project was to evaluate short radius modifications and not to develop a new post material model, so researchers abandoned the orthotropic material model and MAT_13 was used for the remainder of the project.

4.4.2 Post-and-Soil Interaction Modeling

Post-and-soil interactions have frequently been modeled using rigid soil rotation tubes and non-linear translational spring elements in the lateral and longitudinal directions at MwRSF. Although a more representative modeled interaction is desirable, this practice has been used extensively and has been validated in previous studies [25].

Recent component tests consisting of 6-in. x 8-in. x 72-in. (152-mm x 203-mm x 1,829-mm) CRT posts embedded in coarse crushed limestone soil were conducted at the University of Nebraska-Lincoln [23]. A similar CRT study using posts also installed in highly compacted, coarse crushed limestone to simulate stronger soil conditions was conducted to compare soil strength test results [24]. Results of the two test series were compared to the simulation results

using the surrogate CRT mode with 15% wider section, and are shown in Figures 64 through 67. Note that the simulated post did not fracture during the strong-axis impact.

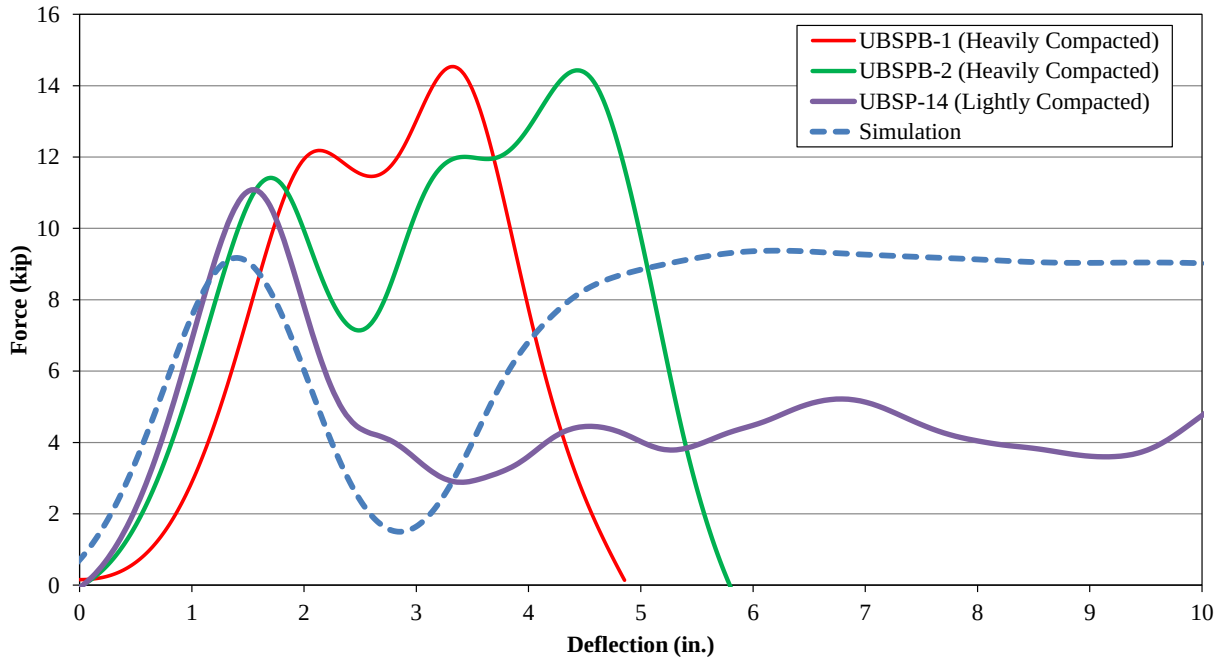

Figure 64. Strong-Axis Impact Bogie Acceleration Force vs. Displacement, Tests and Simulation

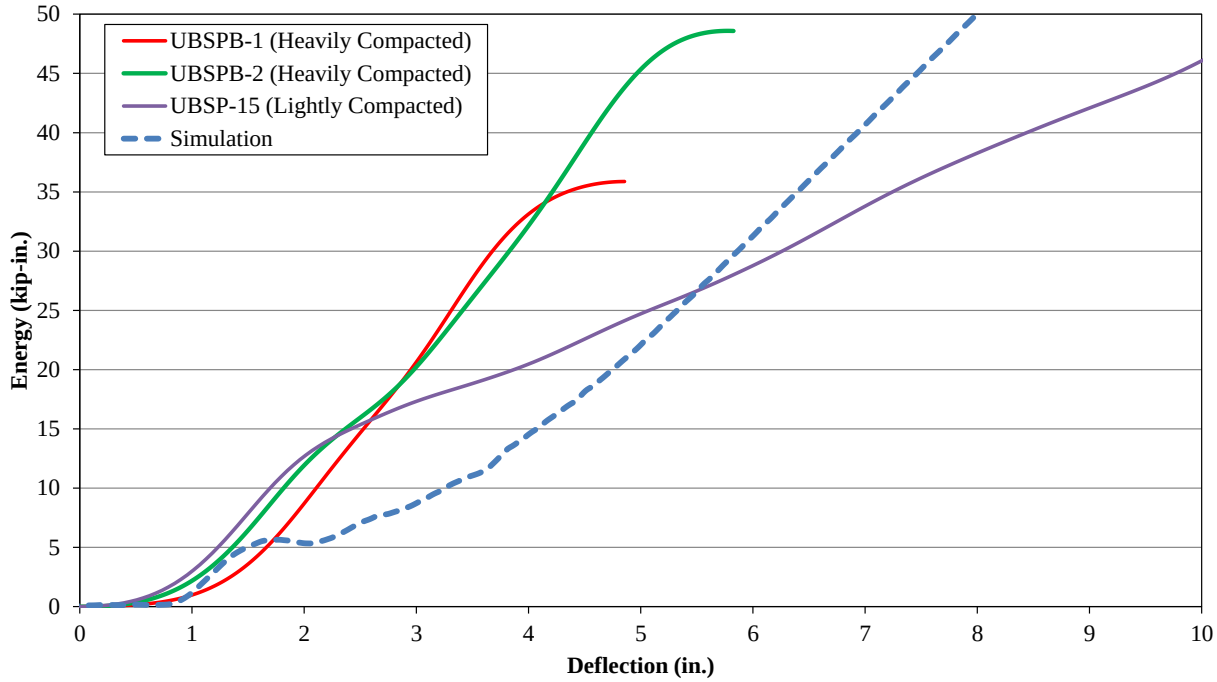

Figure 65. Strong-Axis Impact Bogie Energy vs. Displacement, Test and Simulation

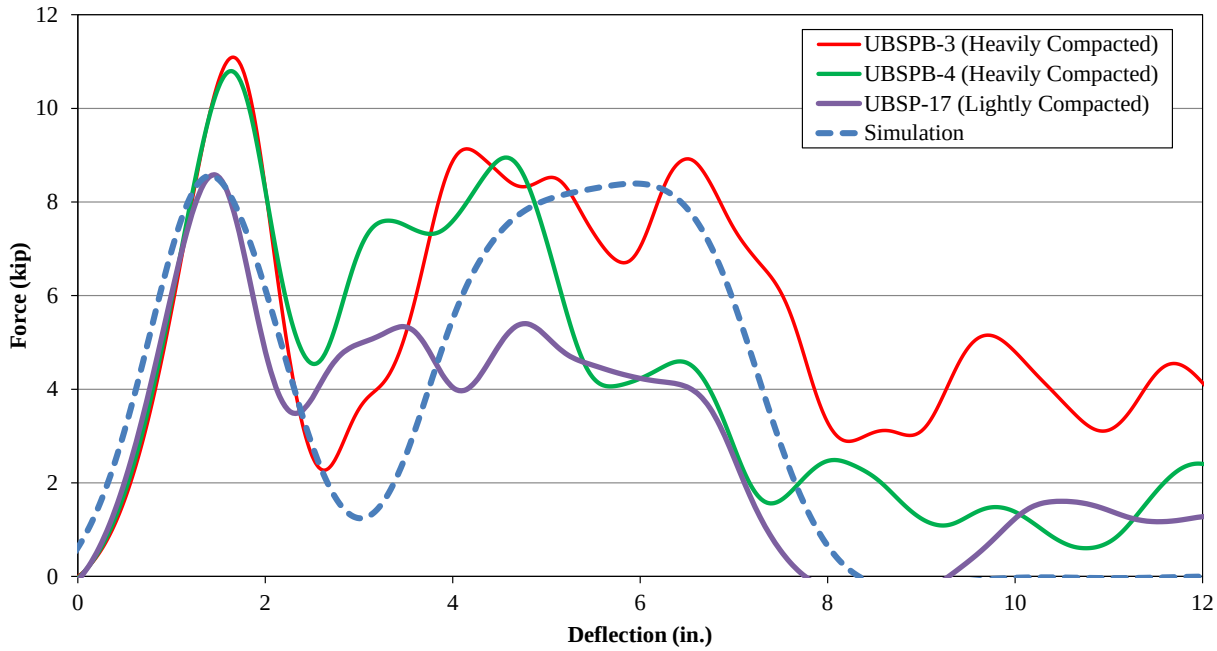

Figure 66. Weak-Axis Impact Bogie Acceleration Force vs. Displacement, Tests and Simulation

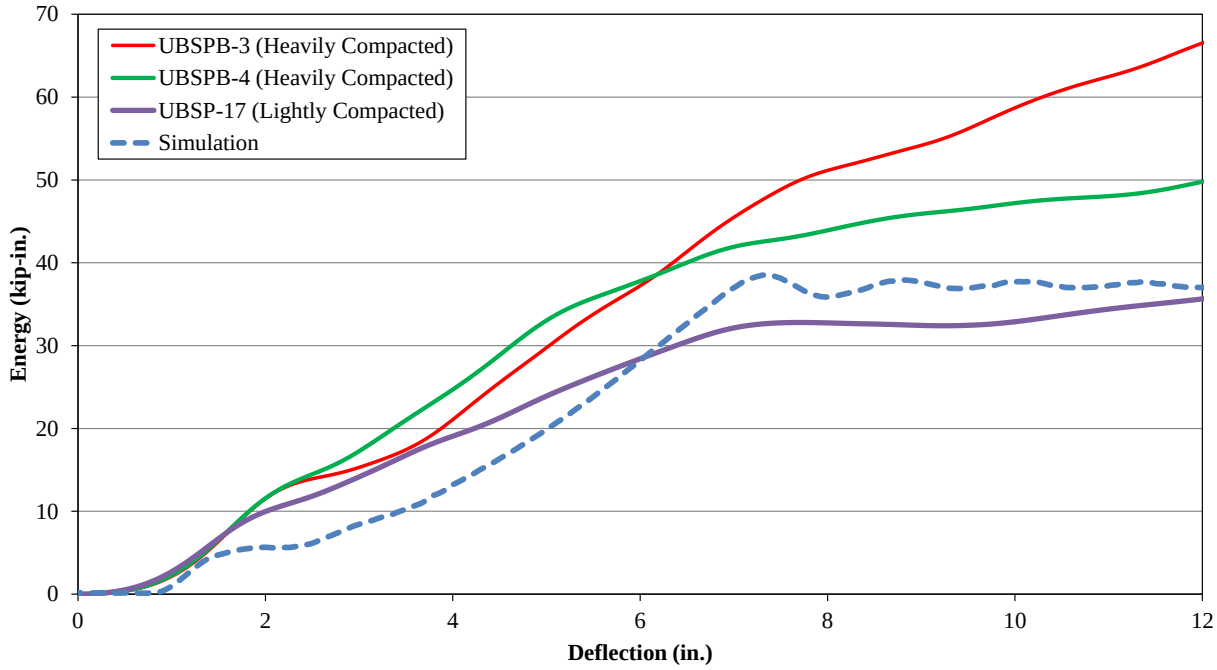

Figure 67. Weak-Axis Impact Bogie Acceleration Force vs. Displacement, Tests and Simulation

The simulated CRT post in soil model had below-average inertial peak force, but the sustained soil rotation was representative of an average between strongly- and weakly-compacted soil strengths for deflections greater than 6 in. (152 mm). Despite the wide force

range exhibited by the posts in soil, the simulated force sustained during rotation through the soil was within the range of soil strengths observable from the physical tests. Therefore, the model of 15% wider posts in soil was determined to be an acceptable approximation for use in a short-radius guardrail simulation.

4.5 Components Without Validation

Some components did not have comparable physical test data with which to compare the simulation models. Examples of these components included the 8 in. x 8 in. x 72 in. (203 mm x 203 mm x 1,829 mm) solid timber post and the 10 in. x 10 in. x 78 in. (254 mm x 254 mm x 1,981 mm) solid timber posts. There may be differences in physical test fracture forces, deflections, and energies that are not represented using the current wood post material model. Since there were no additional data to calibrate these pot models, the MAT_013 timber material model and nominal post dimensions were not modified. The fracture zone of the timber posts was identical to that used for the CRT posts.

Other components without physical test data with which to compare simulation results to include the MC8x22.8 (MC203x33.9) rail stiffener. The stiffener was a standard section with flange and web, so the section was plotted using computer-aided drafting (CAD) and the midsurface of the structural section was extracted. That midsection was meshed with shell elements and the material applied to the section was consistent with ASTM A36 steel.

Lastly, a short section of concrete bridge parapet was used to anchor the approach guardrail transition in the full-scale crash test. However, the vehicle never struck the bridge rail, and the furthest-downstream 10 in. x 10 in. (254 mm x 254 mm) transition post did not deflect in test nos. YC-3 or YC-4. As a result, the effect of the bridge rail in these tests was solely to maintain tension at the end of the W-beam rail. Therefore, the end of the W-beam transition to bridge rail was rigidly fixed.

The buffer section on the upstream end of the rail was utilized in the test, but did not contribute to the structural rigidity or deflection of the system. Thus, the buffer section was neglected in all short-radius guardrail models.

4.6 Details and Construction of Full-Scale Crash Models

Three models of the Yuma County short radius guardrail system were created. One model of the system was intended to replicate the system design and impact conditions of test no. YC-3, as shown in Figures 68 and 69. The second model was used to simulate test no. YC-4; for this model, an additional 12 ft – 6 in. (3,810 mm) section of W-beam guardrail with two non-blocked CRT posts was included between the end anchor and the start of the radius, and is discussed in Section 4.6.2.

The third model raised the guardrail mounting height used in the simulation of test no. YC-4 to 31 in. (787 mm). The system utilized MGS CRT post models in lieu of standard CRT post models, and substituted a standard ground-line strut-and-yoke assembly in place of the spliced, two-cable end anchor model utilized in simulations of test nos. YC-3 and YC-4.

4.6.1 Test No. YC-3

The model of test no. YC-3 is shown in Figures 68 and 69. Based on available drawings of the approximate impact point of the vehicle in test no. YC-3, the left side of the vehicle was aligned with the center point of post no. 3, as shown in Figure 68. To be consistent with the system construction, the model was comprised of three distinct sub models: (1) the anchorage system; (2) the radius; and (3) the transition. The three sections are discussed in greater detail in following sections.

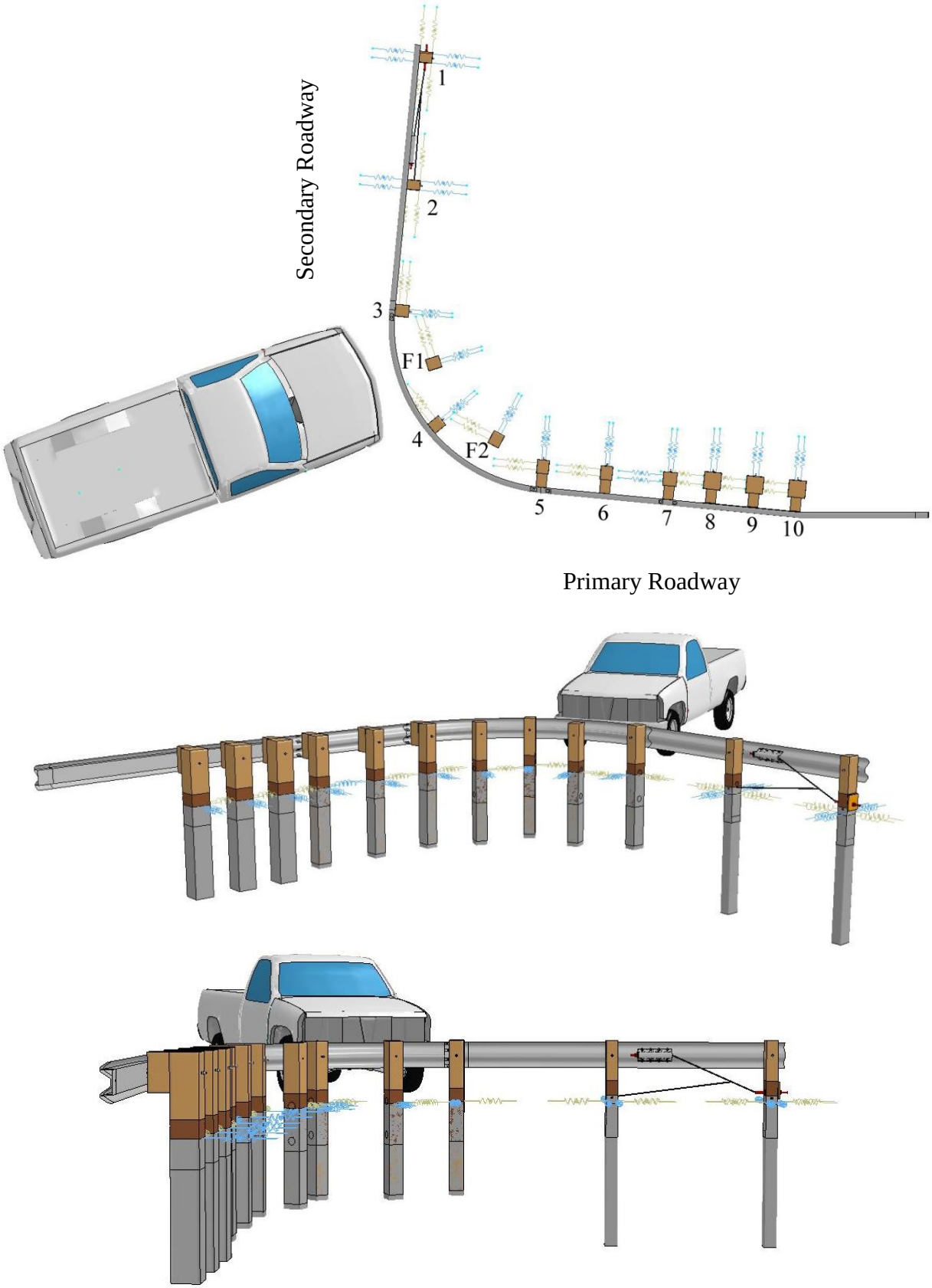

Figure 68. Model of Crash Test No. YC-3 with Post Numbers Shown

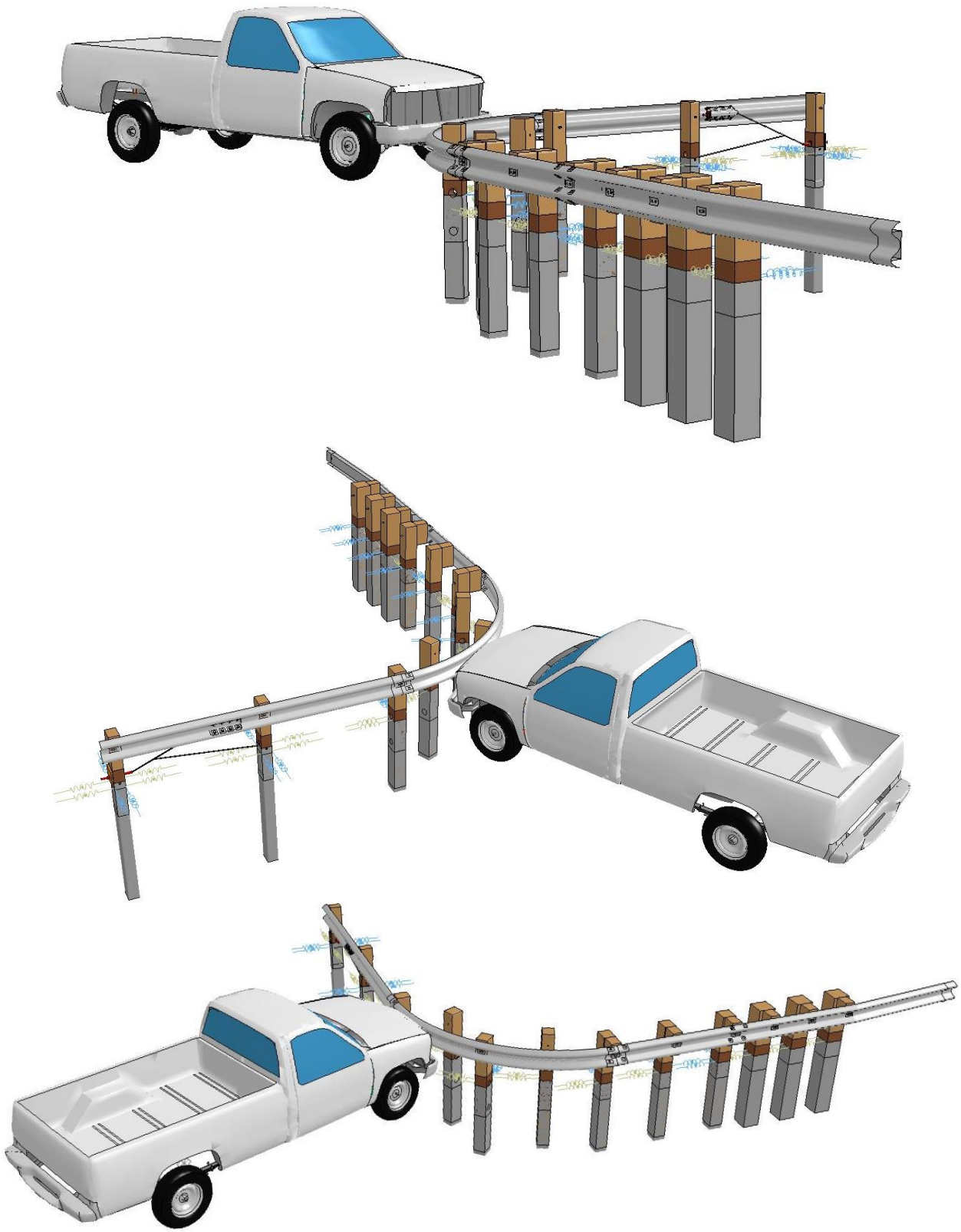

Figure 69. Model of Crash Test No. YC-3

4.6.1.1 End Anchorage

The end anchorage model used in the simulation of test no. YC-3 is shown in Figure 70. The end anchorage system was comprised of two BCT posts with 28-in. (711-mm) top mounting heights set in rigid foundation tubes, similar to the MGS BCT posts described in Reference 25. Pairs of soil springs were attached at the top of the soil tube in each of the front, back, left, and right directions to simulate the soil forces and moments to improve estimates of small permanent deflections. Post bolts attaching the rail to the posts were not tensioned, and were modeled using three parts: a rigid, solid-element shank and nut; a rigid, solid-element washer; and a rigid, shell-element bolt head. Shell elements were used on the bolt head to improve contact with the rail.

The W-beam was modeled with shell elements with a 12-gauge (2.6-mm) thickness, and used a relatively coarse mesh for the majority of the rail, and a fine mesh around slots and bolt holes as previously described. The cable anchor bracket which was attached to the W-beam, both swaged cable end terminations, and the nuts and associated washers attached to those swaged end fittings were comprised of rigid, solid elements. The spliced BCT cables were comprised of beam elements, as previously described, with an approximated splice location 6 in. (152 mm) above ground level. The spliced section of the cable was modeled with duplicate beam elements.

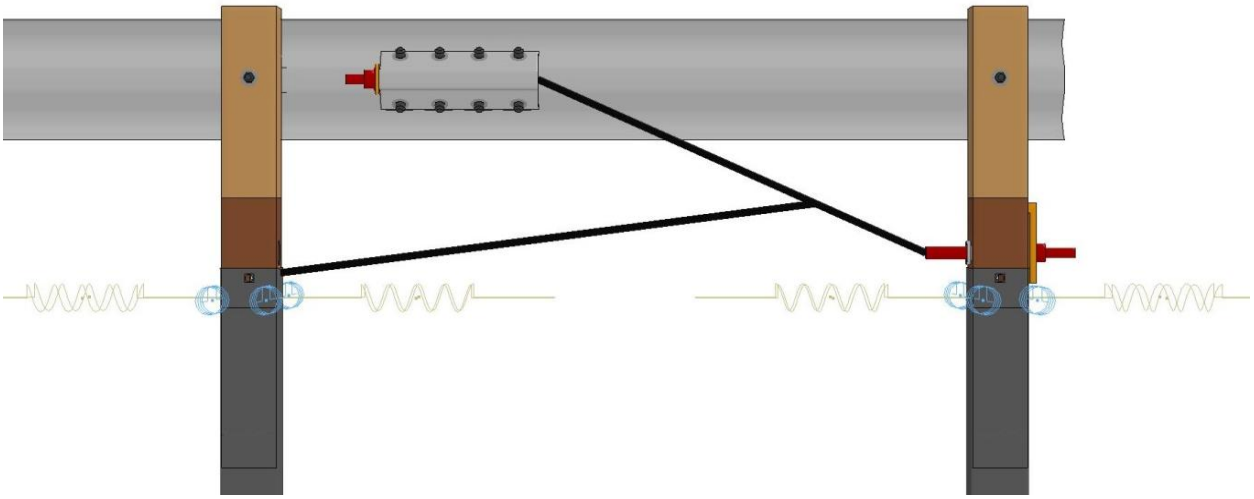

Figure 70. Model of Modified BCT End Anchorage, Model of Test No. YC-3

4.6.1.2 Radius

The model of the radius section is shown in Figure 71. The radius was comprised of four CRT posts, two of which were attached to the rail, and two of which were freestanding behind the system. Posts were placed in soil tubes using the soil spring approximation method. Each CRT post was partitioned into three sections: a non-fracturing portion of the post located below ground; the fracture region, extending from 5.25 in. (133 mm) above ground to 20.5 in. (520 mm) below ground; and a non-fracturing portion above ground that connected to the rail. All three sections utilized the *MAT_13 material previously validated. Only the fracture region utilized failure criteria, which permitted fracture via element erosion. Post-to-rail connections were identical to those used in the anchorage system.

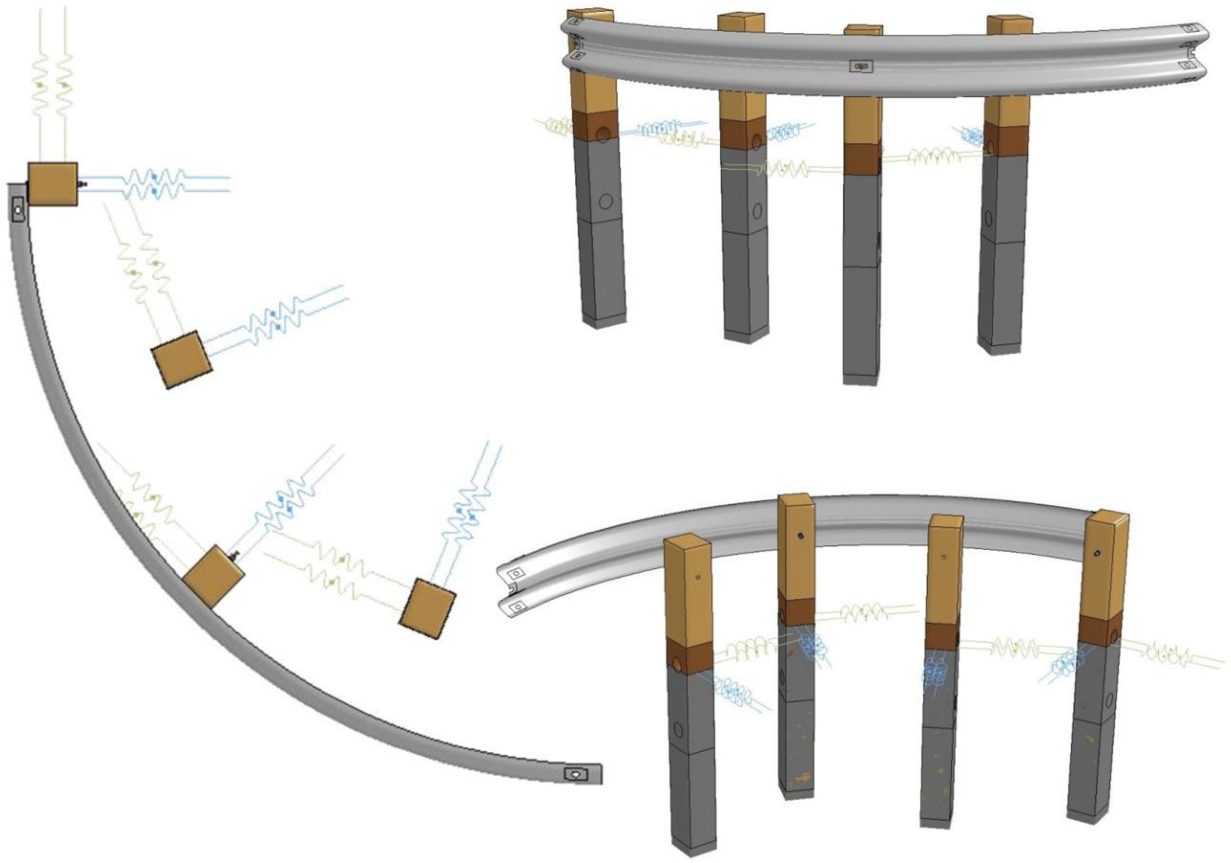

Figure 71. Model of Radius, Model of Test No. YC-3 (Fracture Region Highlighted)

4.6.1.3 Transition to Stiff Bridge Rail

The modeled transition to stiff bridge rail is shown in Figure 72. The transition to stiff bridge rail was modeled with two 6 in. x 8 in. x 72 in. (152 mm x 203 mm x 1,829 mm) solid element posts, one 8 in. x 8 in. x 72 in. (203 mm x 203 mm x 1,829 mm) solid element post, and three 10 in. x 10 in. x 78 in. (254 mm x 254 mm x 1,981 mm) solid element posts. Each of the transition section posts was modeled with a solid element, 6 in. x 8 in. x 14¼ in. (152 mm x 203 mm x 362 mm), blockout. It was estimated that the fracture region of these posts was similar to the fracture region of the CRT posts. Elements above and below the fracture region were not defined with element erosion criteria for two reasons: typically, these regions sustain little to no damage; and compressive stresses beyond plastic strain limits in LS-DYNA can cause element erosion which is non-physical.

Each solid element post was placed in a soil foundation tube and attached to soil approximation springs. Since neither the 8-in. x 8-in. (203-mm x 203-mm) or 10-in. x 10-in. (254-mm x 254-mm) posts had "strong" or "weak" axes, soil springs were prescribed with the same force-deflection curve in all directions. The soil spring force curves for the 8-in. (203-mm) square post were identical to the weak-axis CRT force curve, and the 10-in. (254-mm) square post used a modified CRT weak-axis force curve scaled using two equations:

$$Cross-Section\ Scale\ Factor = \frac{Width\ of\ New\ Post}{Width\ of\ Reference\ Post} = \frac{10\ in.}{8\ in.} = 1.25$$

$$Embedment\ Depth\ Scale\ Factor = \left(\frac{New\ Embedment\ Depth}{Reference\ Embedment\ Depth}\right)^2 = \left(\frac{50\ in.}{44\ in.}\right)^2 = 1.29$$

Post-to-rail attachments were similar to the end anchorage and CRT posts, but were lengthened to accommodate the blockouts. A 10:1 was applied to the rail downstream of the last timber post. An MC8x22.8 (MC203x33.9) stiffening channel was modeled between the rail and blockouts extending between the end of the W-beam guardrail to the midspan between the 10-in.

(254-mm) and 8-in. (203-mm) square posts. Flange and web thickness were 0.50 in. (12.7 mm) and 0.425 in. (10.80 mm), respectively.

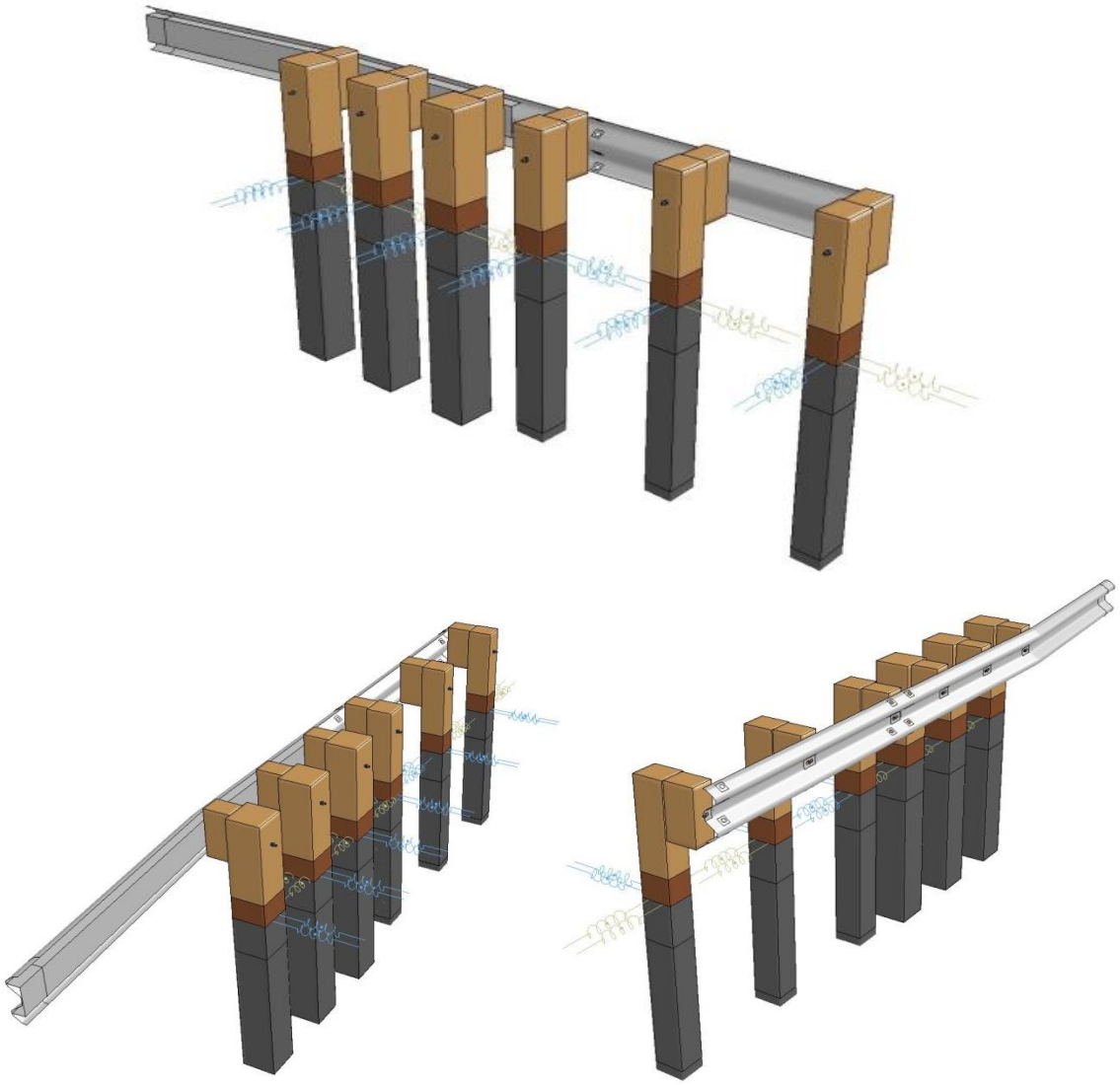

Figure 72. Transition Section, Model of Test No. YC-3

4.6.1.4 Model Assembly

The models of the end anchor, radius, and transition to stiff bridge rail were fastened together by merging nodes of the ends of each rail section. Splices were modeled by duplicating elements near the splice locations and merging the nodes of those duplicated elements. In this way, the stiffness of the rail was approximately increased by a factor of 2, rather than a factor of 4 that would occur if the thickness of the splice was doubled. The tensile stiffness of the rail

would also be approximated using this method. Because there were no observations of W-beam tearing in the Yuma County short-radius guardrail test report [6], no element erosion criteria were applied to the models of the rail.

4.6.2 Modifications for Simulation of Test No. YC-4

The system in test no. YC-4 was nearly identical to the system in test no. YC-3. The only change to the system was the lengthening of the system upstream of the radius by adding an additional 12 ft – 6 in. (3,810 mm) long section of W-beam and two additional 6 in. x 8 in. x 72 in. (152 mm x 203 mm x 1,829 mm) CRT posts adjacent to the upstream modified BCT end anchorage. The posts, rail, rail slots and splice holes, soil tubes, soil springs, and post bolts were modeled similarly to the components of the radius, except that the rail was straight instead of curved. The model of the system tested in test no. YC-4 is shown in Figure 73. The model of the truck in the simulation of test no. YC-4 was identical to the model in the simulation of test no. YC-3.

4.6.3 Modifications for Simulation of 31-in. (787-mm) Tall System

In order to gauge the effectiveness of a 31-in. (787-mm) tall guardrail installation on the performance of the Yuma County short radius guardrail system, the height of the Yuma County system was raised 4 in. (102 mm) to a top guardrail mounting height of 31 in. (787 mm), as shown in Figure 74. To accommodate the increased rail height and decreased post embedment depth, 4 in. (102 mm) was removed from the bottom of the CRT, BCT, and transition posts, and added to the upper portions of the posts. The holes were therefore shifted downward on the posts by 4 in. (102 mm) to become MGS CRT and MGS BCT posts. Transition post nos. 7 through 9 were lengthened from 72 in. (1,829 mm) to 76 in. (1,930 mm), and post nos. 10 through 12 were lengthened from 78 in. (1,981 mm) to 82 in. (2,083 mm) such that the embedment depth of the transition posts was not changed with increased rail height. In addition to modifying the posts, an

MGS BCT end anchorage [25] was included on the upstream end of the system in lieu of the two-cable modified BCT end anchorage.

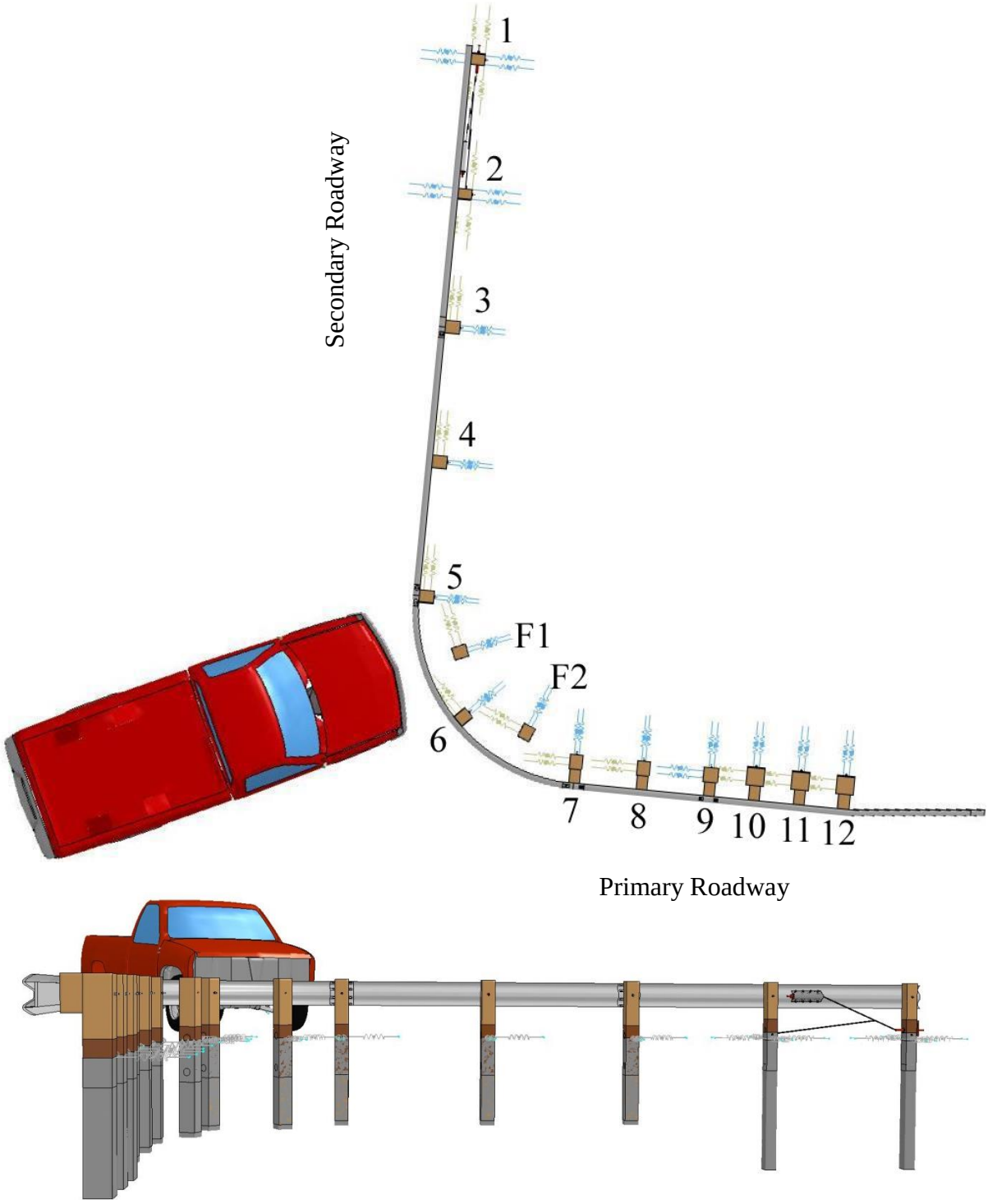

Figure 73. Model of System in Test No. YC-4 with Post Numbers Shown

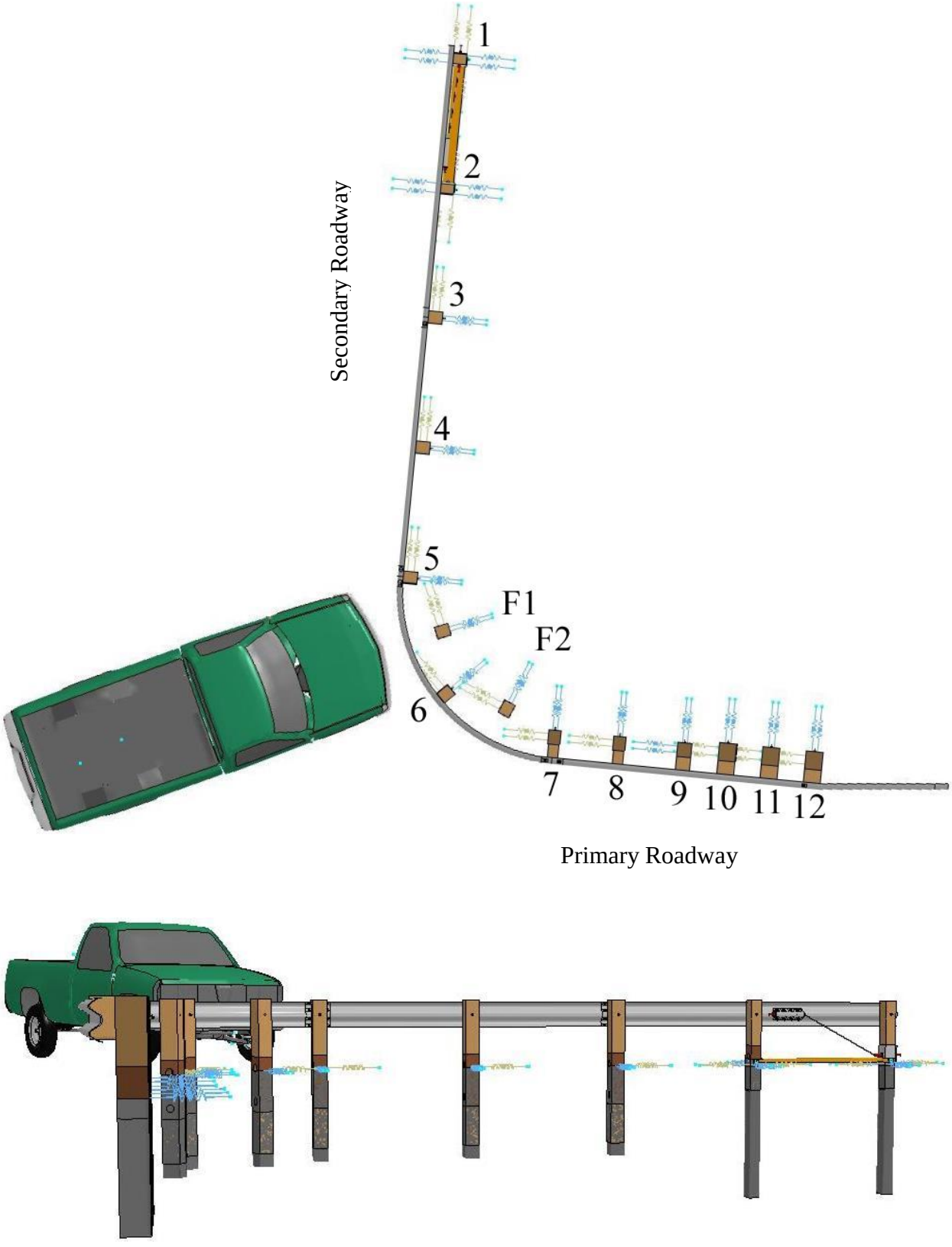

Figure 74. Model of 31-in. (787-mm) Tall, Modified System Derived from Details of Test No. YC-4 with Post Numbers Shown

4.7 Vehicle Models

The vehicles used in test nos. YC-3 and YC-4 were 1984 Ford pickup trucks weighing approximately 5,380 lb (2,440 kg). A Chevrolet C2500 vehicle model [30] was modified for use simulating test nos. YC-3 and YC-4, as well as the 31-in. (787-mm) tall, modified YC-4 system. Modifications included refining the mesh of almost all major components and replacing the suspension system, including tires, with a more detailed model. A total of 991 lb (450 kg) was added to the vehicle, distributed between components including the frame, engine, engine supports, and suspension, and a node at the center-of-gravity (CG). The modified vehicle model weighed approximately 5,401 lb (2,450 kg). The 21-lb (9.5-kg) difference in truck mass only differed from the actual mass by 0.4%. The additional mass and energy was not believed to have a significant effect on initial system deflection or performance. The modified vehicle and a 1984 Ford Pickup truck similar to the test vehicle are shown in Figure 75.

4.8 Modeling Difficulties

As full-scale models of the Yuma county system tests were simulated, a number of numerical problems were observed which warranted further consideration. Frequently, the shell element edge boundaries of the W-beam penetrated between the nodes of the solid element blockouts and posts, as well as the guardrail post bolts. Examples of these penetrations are shown in Figures 76 and 77.

The mesh penetrations led to both model instabilities and unrealistic results. When the shell elements of the mesh penetrated through the mesh of the guardrail post bolts, the exterior nodes of the bolts which were in contact definitions with the rail subsequently snag on the rail. As a result, the rail could not release from the post bolt after penetration, forcing the post to track the trajectory of the rail after impact, and weighing down on the deformed rail. Likewise, when the rail penetrated into the solid element faces of the post, the rail snagged on the outer nodes of

Figure 75. Ballasted 2500 Model and Example 1984 Ford Pickup Similar to Test Vehicle [32]

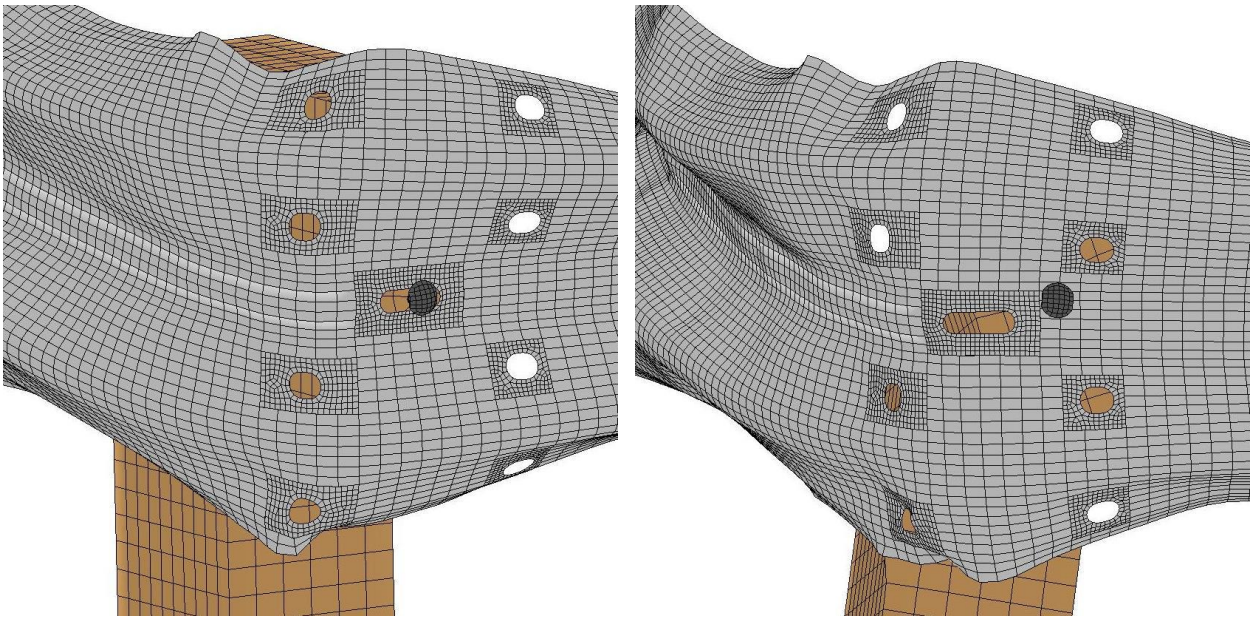

Figure 76. Shell Element Edge Penetration Behind Bolt Head

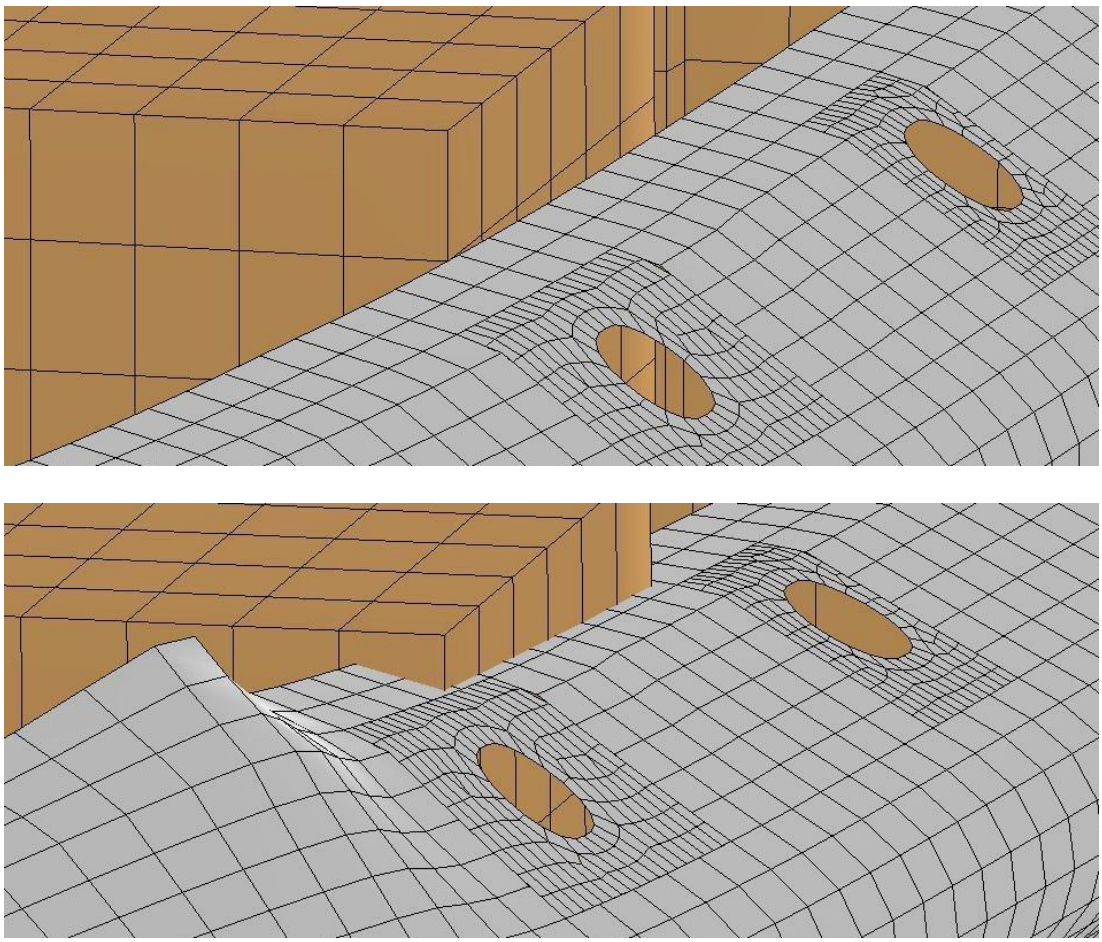

Figure 77. Shell Edge Penetration between Solid Elements of Posts

the blockouts and posts, which were not prescribed with element erosion criteria. The snagging applied forces to the interior of the post mesh and restricted post release from the rail.

Two approaches were used to solve these problems. The solid and shell elements of the post bolts and post bolt heads, respectively, were lined with beam elements along the axis of the bolt. A null material was prescribed to the beam elements, with a contact thickness of 0.0079 in. (0.2 mm), to prevent both excess mass and a larger contact surface from altering the results. Because shell elements typically have better contact interaction with beam elements than with solids, this interaction prevented edge of the rail from penetrating into the bolts. The beam element wrap method is shown in Figure 78.

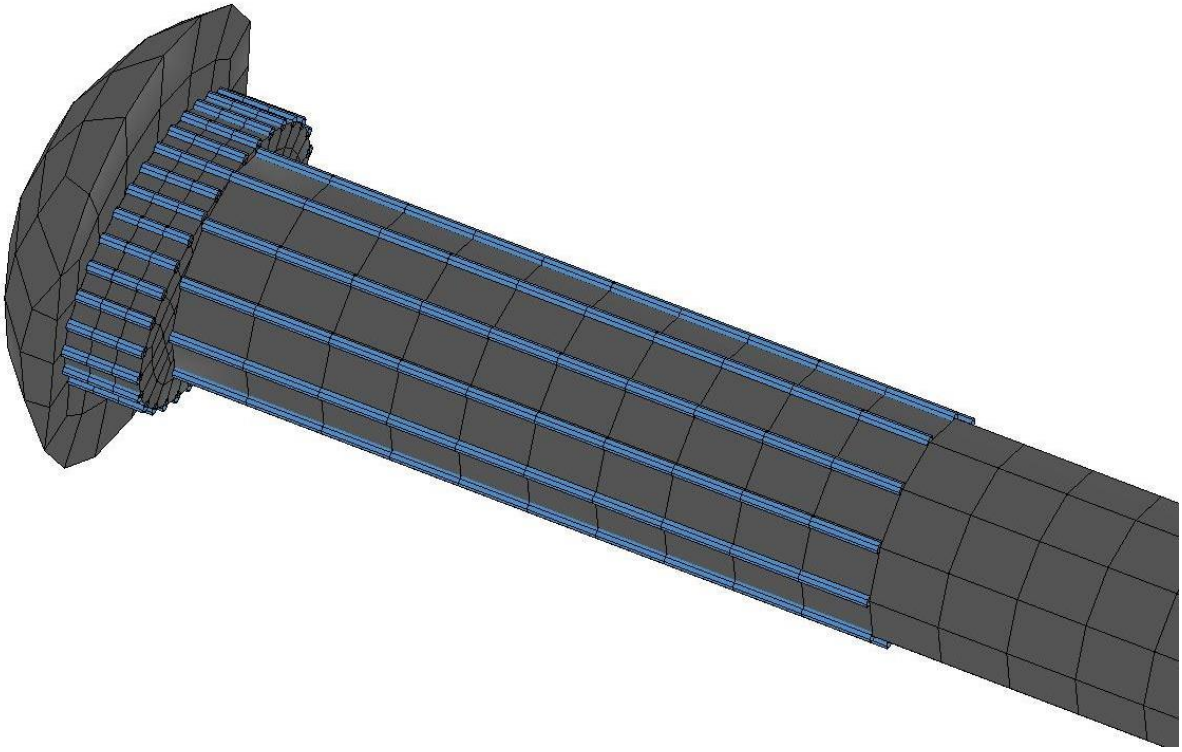

Figure 78. Beam Element Wrap around Bolt Head and Shank

To prevent the W-beam rail from penetrating into the solid element posts and blockouts, contact tolerances and contact penalty forces were increased, and the top and bottom rail edges

were shifted to a node-to-surface contact type with the posts and blockouts. As a result, the rail penetration into the solid elements was mostly eliminated.

The length of the stiffening C-channel was observed to strongly affect simulation outcome during the simulation of test no. YC-4. Based on system construction drawings, it was unclear where the end of the stiffening C-channel was located, with respect to the stiffness transition. Two simulations were conducted to investigate what effect, if any, the location of the end of the stiffening channel had on vehicle capture or redirection: at the midspan between post nos. 9 and 10, or at post no. 10. When the C-channel extended to the midspan between post nos. 9 and 10, the vehicle was captured. But when the C-channel was terminated at post no. 10, the rail twisted after post no. 9 fractured and allowed the truck to vault over the rail. Therefore it was believed, based on C-channel length and simulation results, that the stiffening C-channel used in test nos. YC-3 and YC-4 extended to the midspan between post nos. 9 and 10. A time-sequential comparison of the vaulting and capture events is shown in Figure 79.

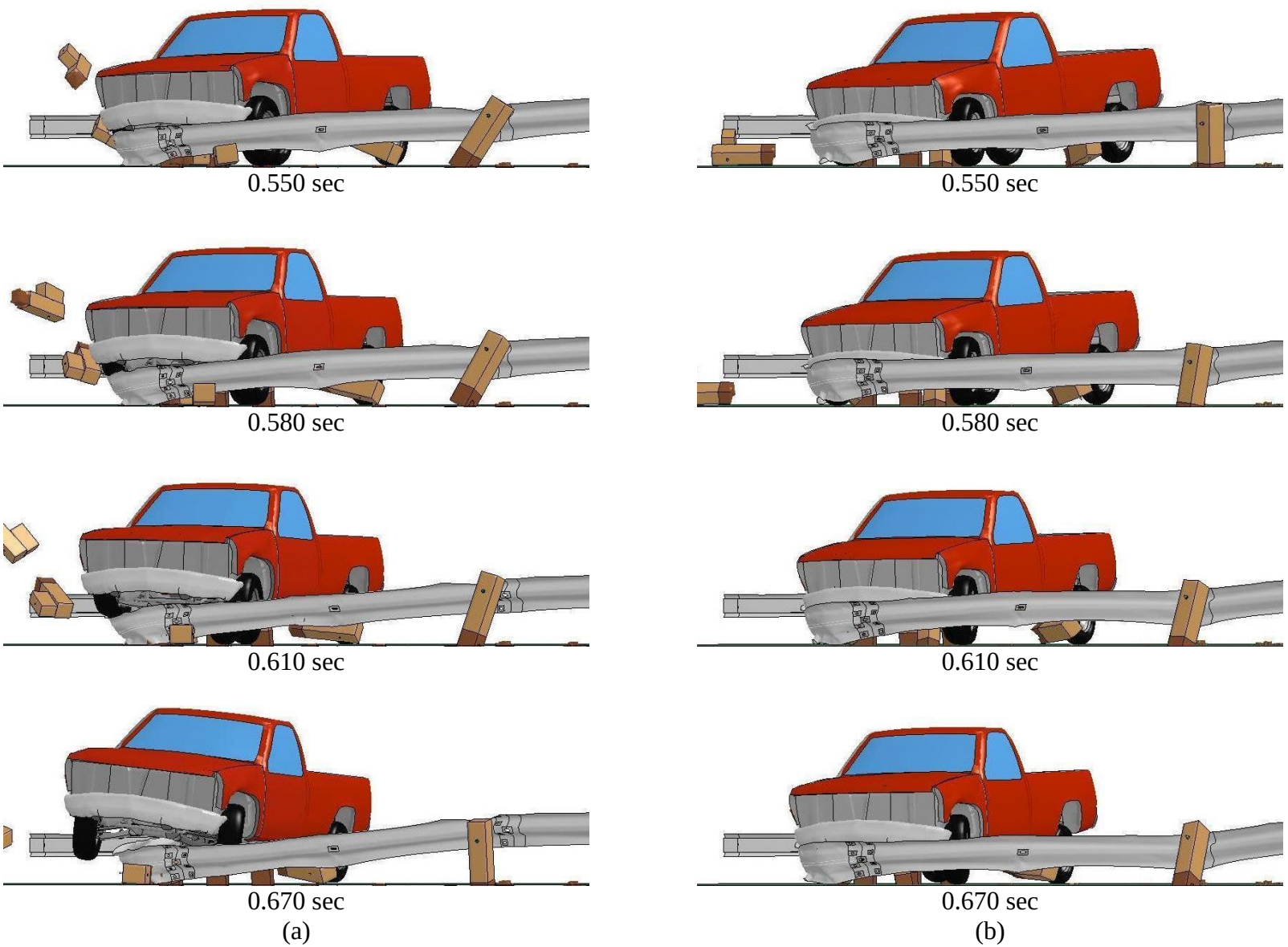

Figure 79. Effect of Stiffening C-Channel Length (a) Channel Terminates at Post (b) Channel Terminates at Midspan

March 31, 2014
MwRSF Report No. TRP-03-296-14

5 SIMULATION OF YUMA COUNTY SHORT RADIUS GUARDARIL SYSTEM

5.1 Test No. YC-3 Simulation and Full-Scale Test

The simulated truck impacted the model of the system in test no. YC-3 at 45 mph (72 km/h) and with an orientation of 20 degrees relative to the roadway, and 25.5 degrees relative to the flared guardrail system. Time-sequential images of the impact are shown in Figures 80 through 83. A comparison summary of the test and simulation post fracture times, corresponding encompassing the onset of cracking, crack propagation, and complete fracture, is shown in Table 18. Because post fracture times were not known from test sequentials, and the original crash test videos were not available, the fracture window for posts in the crash test had very low precision.

It was uncertain based on the results of the test report [6] and subsequent examination by TTI [27] how the spliced anchor cable released from post no. 2 in test no. YC-3. In the test, the load transmitted from the rail through the BCT cable caused the end post (post no. 1) to fracture due to an eccentric twisting load. However, this phenomenon was not easily modeled in LS-DYNA. BCT model instabilities contributed to models terminating prematurely. In other models, the truck vaulted the system when post no. 1 did not fracture and the W-beam remained attached to both end posts. Subsequent modifications including weakening the cable connection to post no. 2 did not prevent these problems, because the tensile load in the secondary BCT cable was very low. Instead of fracturing the end BCT post, the truck was brought to a controlled stop in contact with the system. Since test no. YC-3 was only used to assist in the validation of the system for larger radii, and the simulation and full-scale test were similar until loads were transmitted to the unusual spliced-cable anchor, further improvements to the model were not pursued.

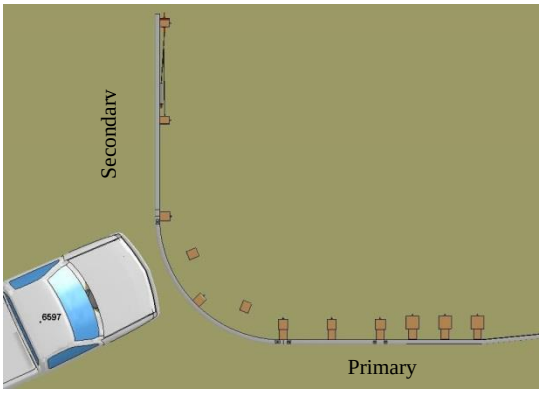

Pre-Impact

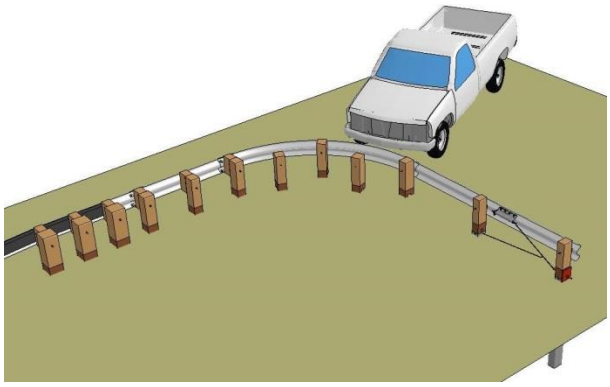

Pre-Impact

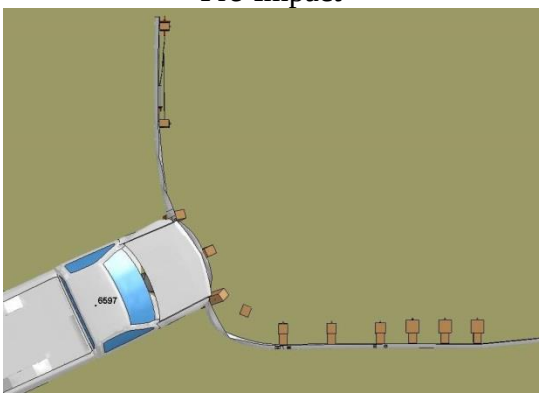

45 ms

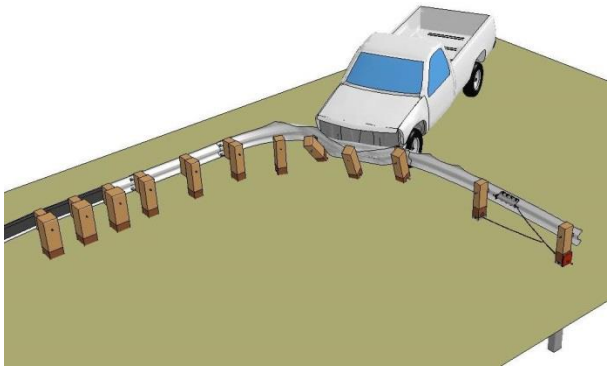

45 ms

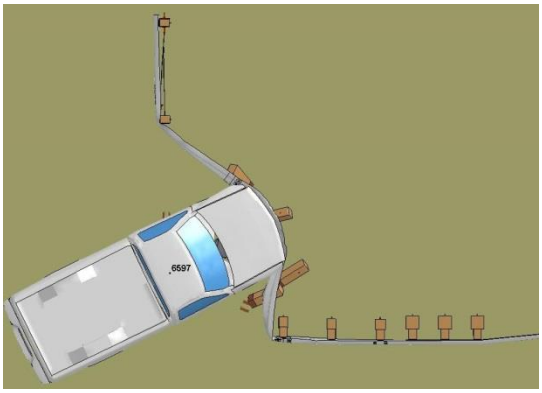

135 ms

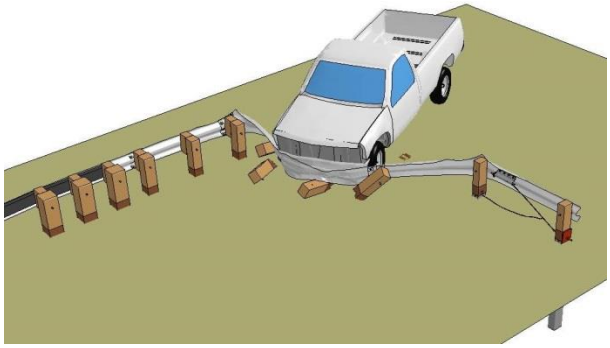

135 ms

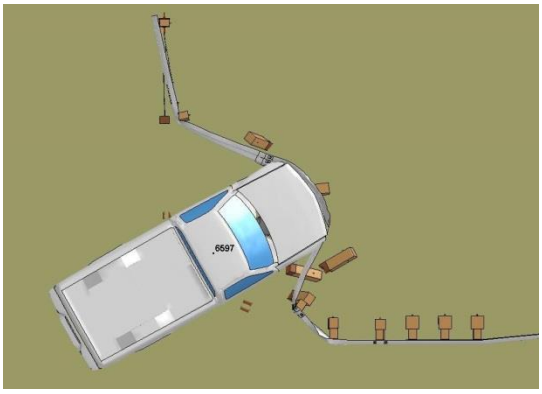

195 ms

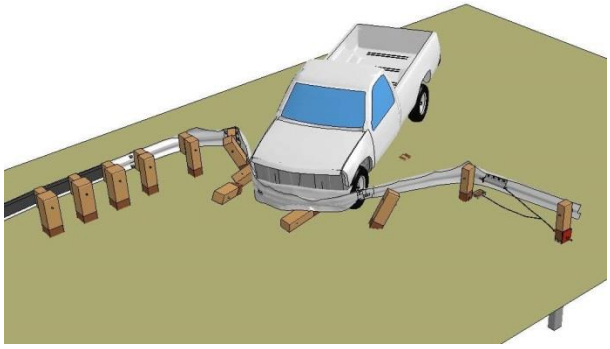

195 ms

Figure 80. Time-Sequential Photographs, Simulation of Test No. YC-3

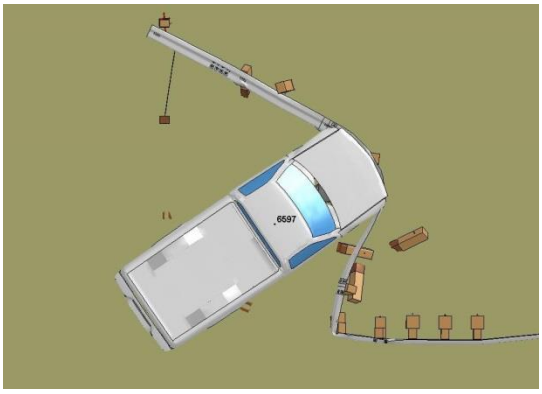

280 ms

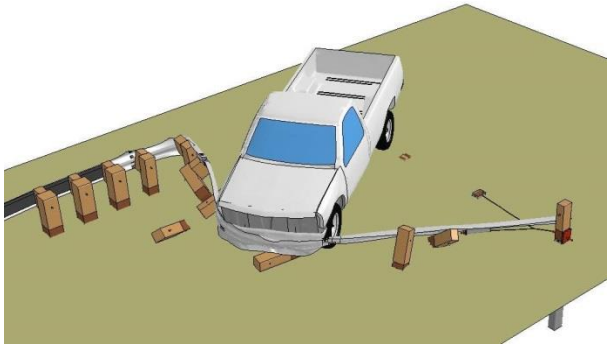

280 ms

400 ms

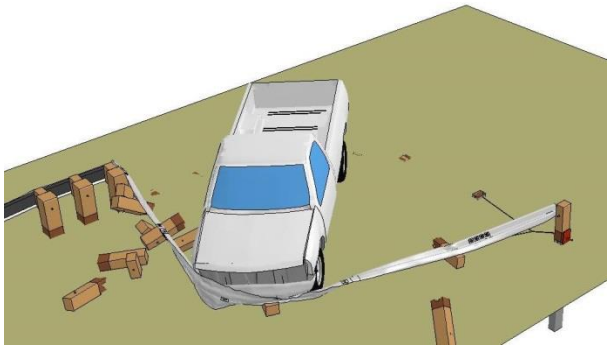

400 ms

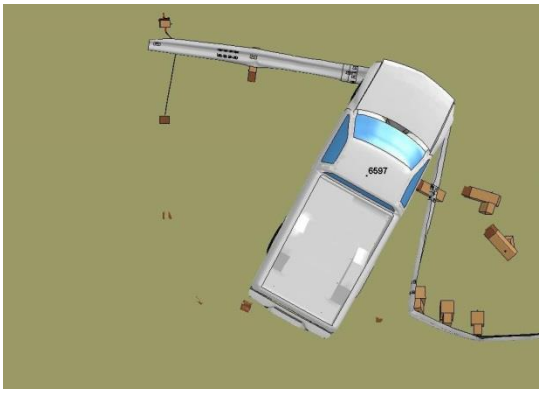

525 ms

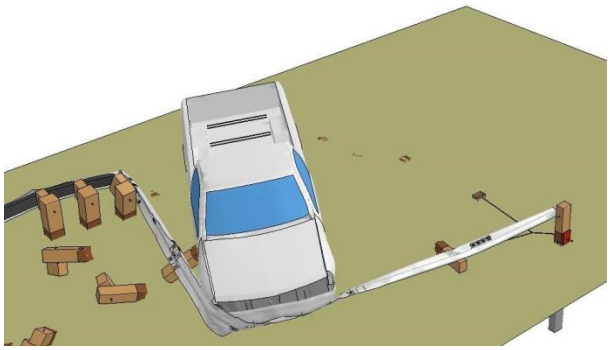

525 ms

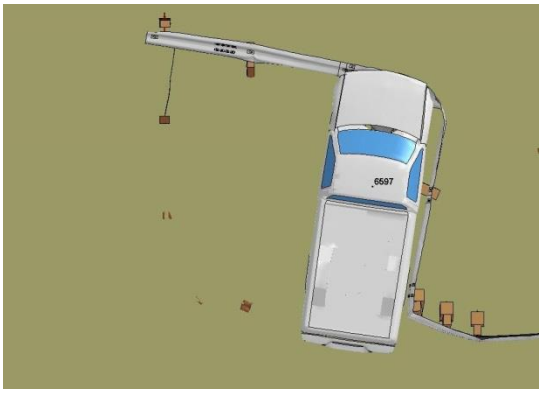

675 ms

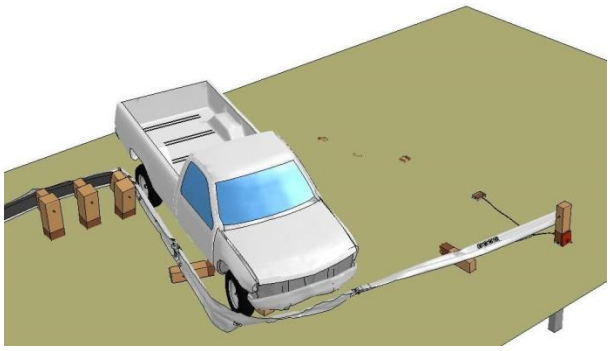

675 ms

Figure 81. Time-Sequential Photographs, Simulation of Test No. YC-3

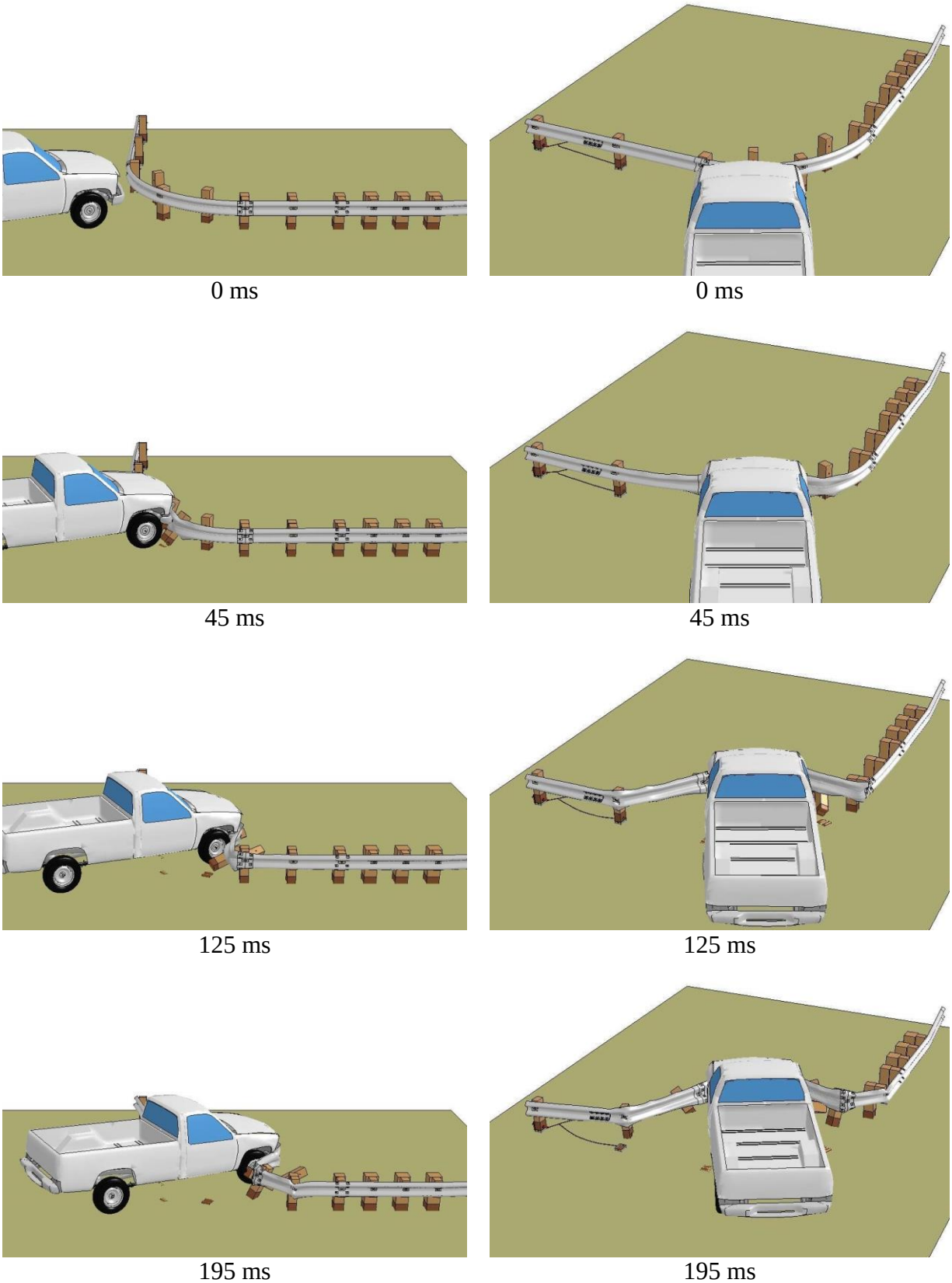

Figure 82. Time-Sequential Photographs, Simulation of Test No. YC-3

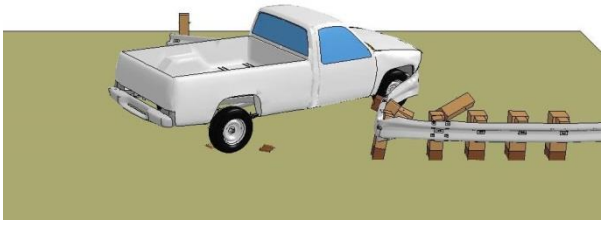
280 ms

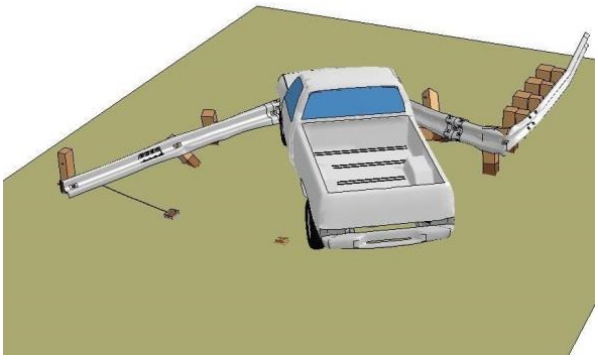
280 ms

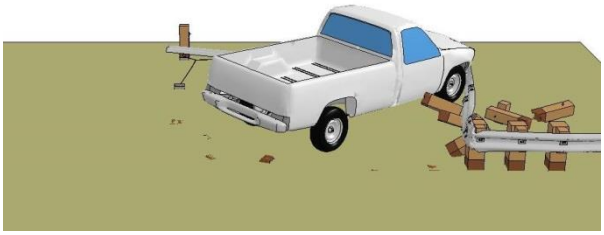
400 ms


400 ms

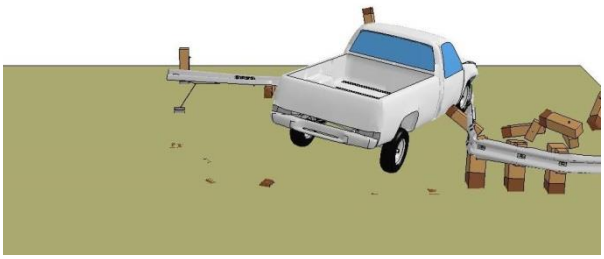
525 ms

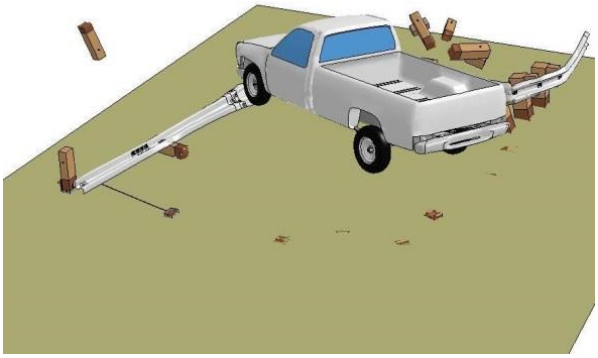
525 ms

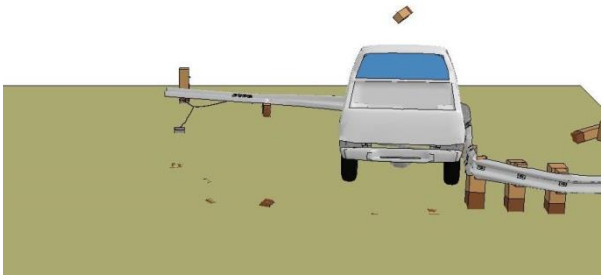
675 ms

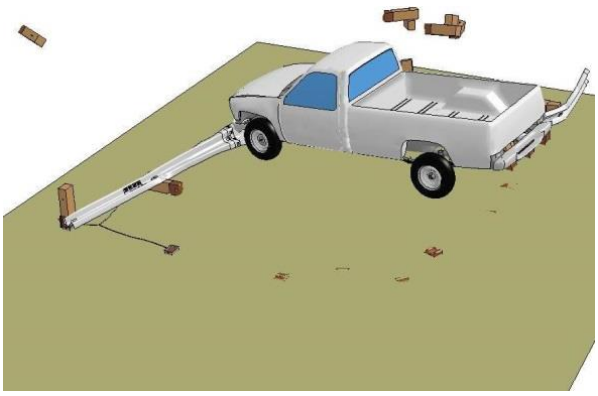
675 ms

Figure 83. Time-Sequential Photographs, Simulation of Test No. YC-3

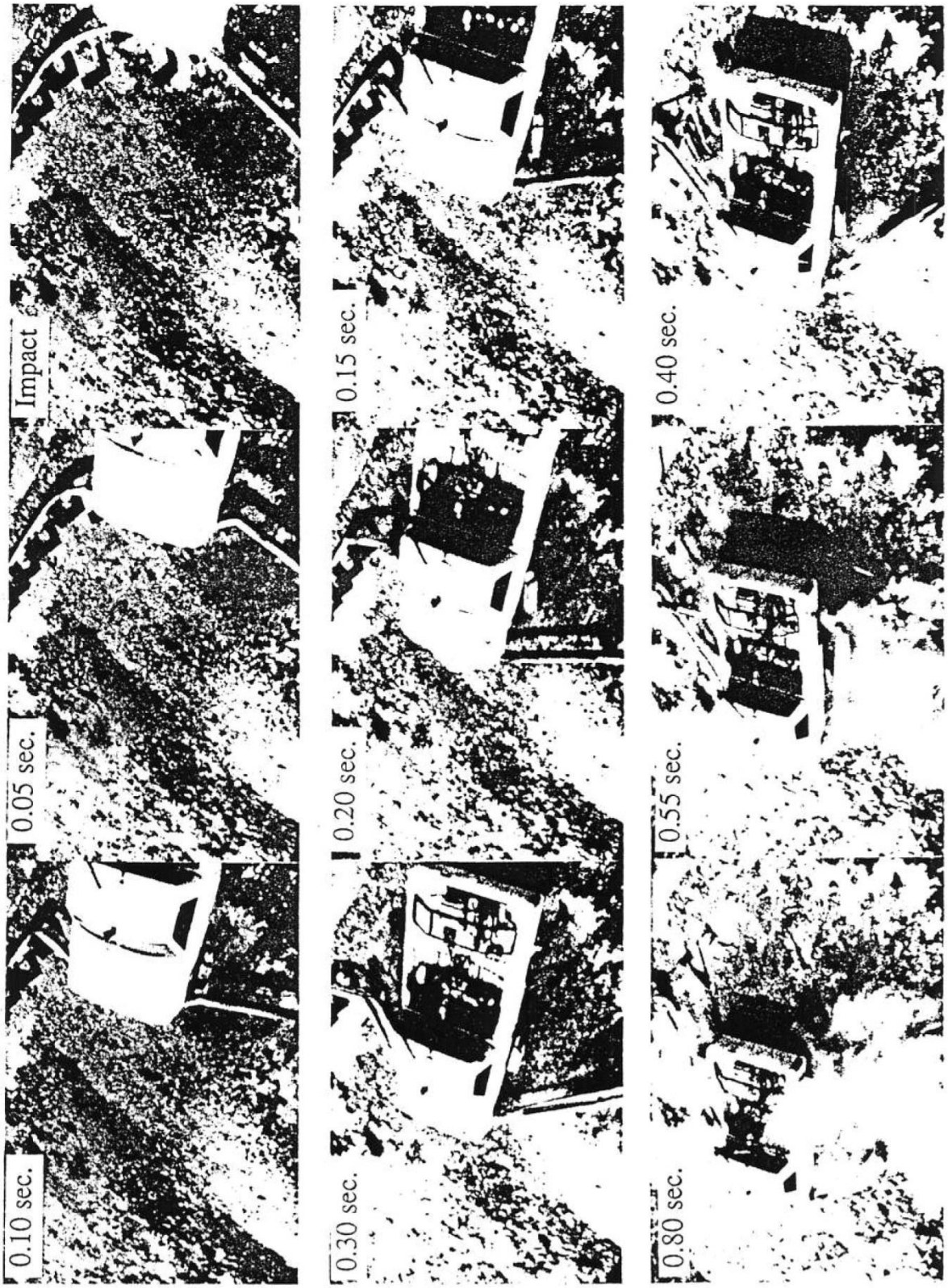

Figure 84. Time-Sequential Photographs of Test No. YC-3 [6]

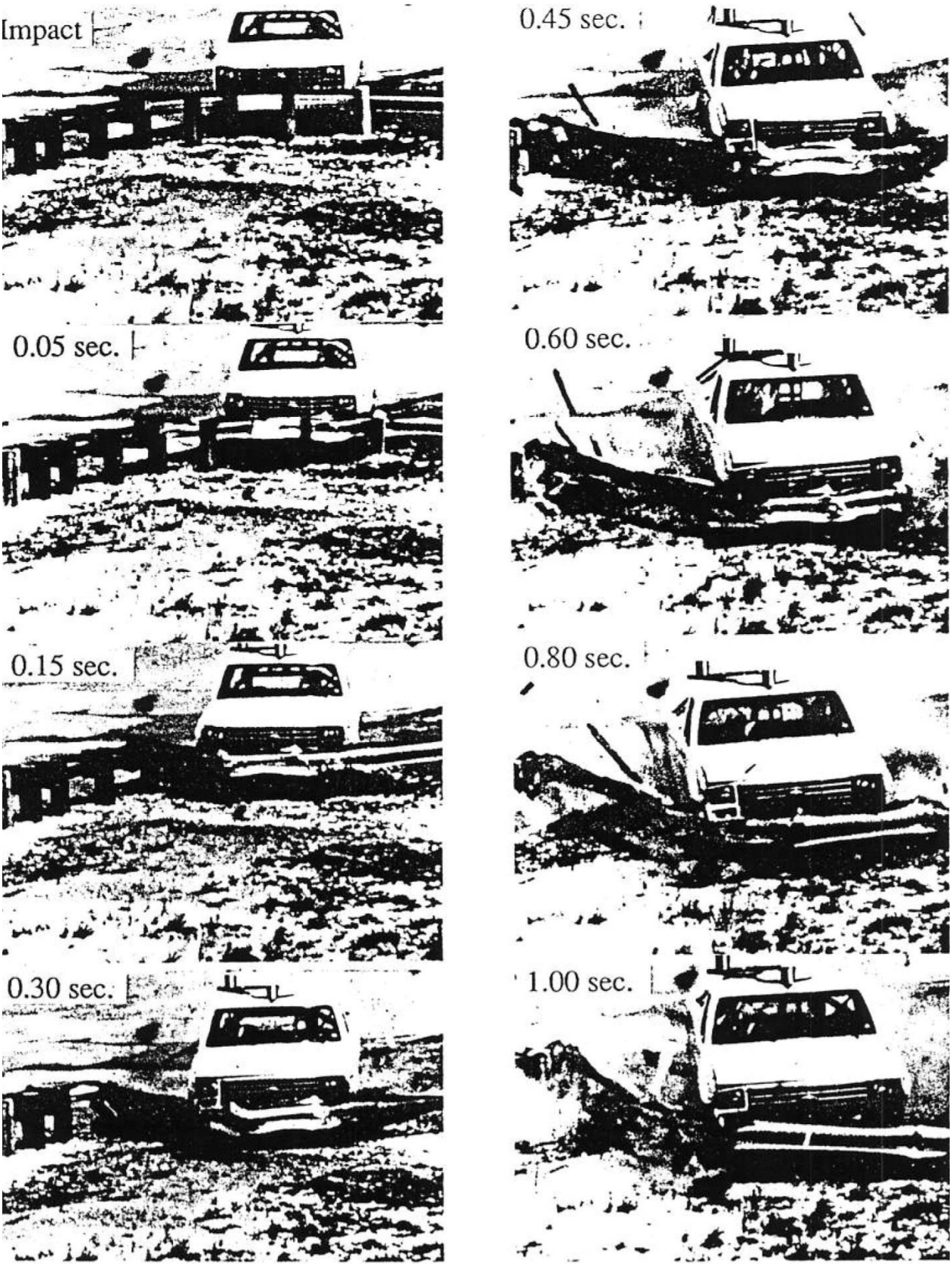

Figure 85. Time-Sequential Photographs of Test No. YC-3 [6]

Table 18. Comparison of Post Fracture Times, Simulation and Test No. YC-3

Post No.	Fracture Time Range (ms)	
	Test	Simulation
1	Unknown	Did Not Fracture
2	150-200*	160-190
3	0-50	20-45
4	0-50	20-45
5	150-200	165-175
6	200-300	280-310
7	300-400	295-310
8	400-550	Did Not Fracture
F1	0-50	20-40
F2	100-200	105-120

* post out of view; fracture time estimated

After the simulated pickup truck impacted the system, the top corrugation of the rail initially crushed and flattened around the front bumper. At approximately 10 ms after impact, the truck impacted post no. 4, deflecting it backward slightly at ground level and fracturing the post. The simulated vehicle continued forward and yawed counter-clockwise. Post no. 2 cracked at approximately 165 ms, and the post remained attached to the rail after it completely fractured at 175 ms. A plastic hinge formed in the rail at the end of the stiffening channel at post no. 8 at approximately 420 ms. However, because post no. 1 did not fracture the vehicle yawed with the front end toward the upstream anchor, and subsequent impact between the right-rear tires and the stiffness transition brought the vehicle to a complete stop. The flattened top corrugation remained engaged the top of the bumper throughout impact as the rail crushed the bumper upward and inward.

Despite the low precision of the post fracture times in the test, nearly every simulated post fractured within the indicated range identified corresponding to post fracture in the test. Overall correlation of the fracture times was acceptable, which suggested that post no. 1 fractured relatively late in the impact event, probably between 0.450 and 0.600 sec. However, in

the simulation, post no. 8 did not fracture, although fracture occurred in the test. This may be due to a combination of factors, including a slight variation in the vehicle's impact location in the simulation compared to the test, the simplified cable connection to the BCT soil foundation tube at post no. 2, below-average wood quality for the 10 in. x 10 in. (254 mm x 254 mm) post, or differences in the test vehicle such as pitch, roll, and yaw moments of inertia, which could have promoted increased loading downstream of the transition to stiff bridge rail sufficient to induce fracture of post no. 8. Nonetheless, the model appeared to perform acceptably through 310 ms, and was considered conditionally validated based on similar post fracture times, comparison of truck trajectories, and rail deformations in sequential photographs.

5.2 Test No. YC-4 Simulation and Full-Scale Test

The model of test no. YC-4 was nearly identical to the model of test no. YC-3, except that an additional 12 ft – 6 in. (3,810-mm) long section of W-beam and two additional 6 in. x 8 in. x 72 in. (152 mm x 203 mm x 1,829-mm) CRT were included upstream of the curved radius section. The impacting vehicle and impact location were the same as those used in the model of test no. YC-3. Time-sequential photographs of the crash are shown in Figures 86 through 89. A summary table of approximate post fracture times identified in the test and simulation is shown in Table 19.

System and vehicle damage results were judged similar for the test and simulation. Post nos. 1, 2, and 10 did not fracture in either the simulation or the physical test, and most post crack initiations and complete fractures in the model were within the correct time intervals identified in the full-scale test from sequential photographs. As with test no. YC-3, film and photography from the test was limited, which reduced the precision of post fracture timing.

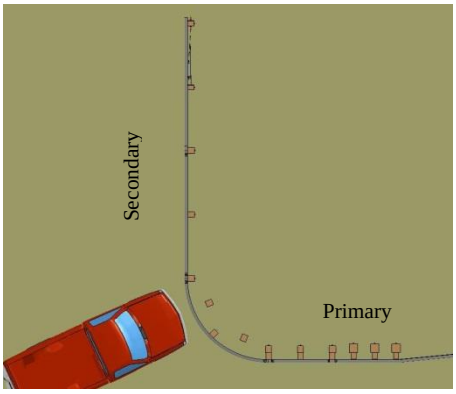

0 ms

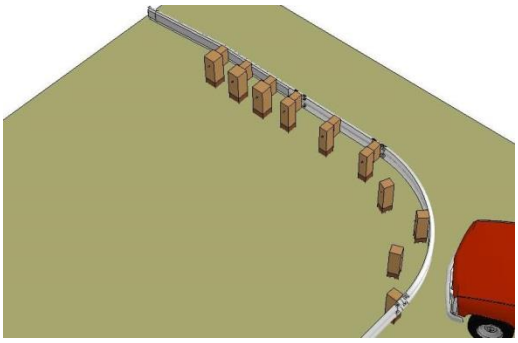

0 ms

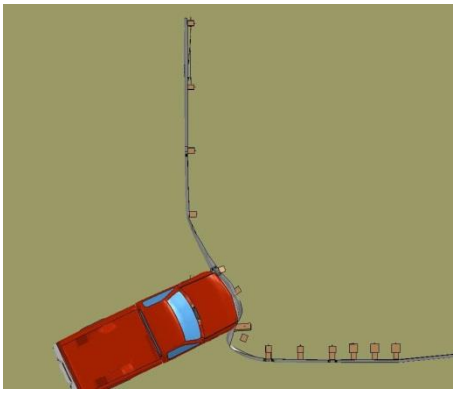

70 ms

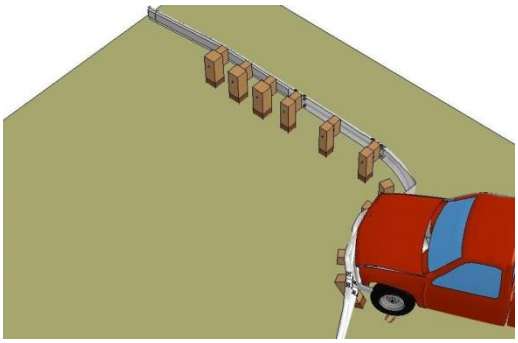

70 ms

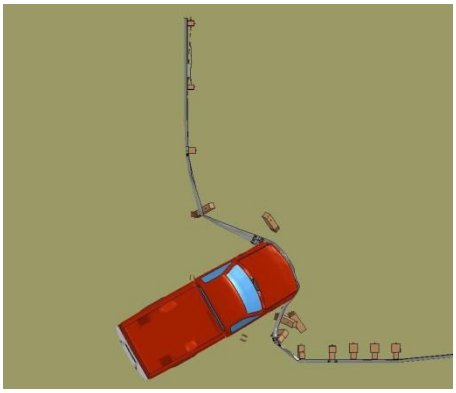

190 ms

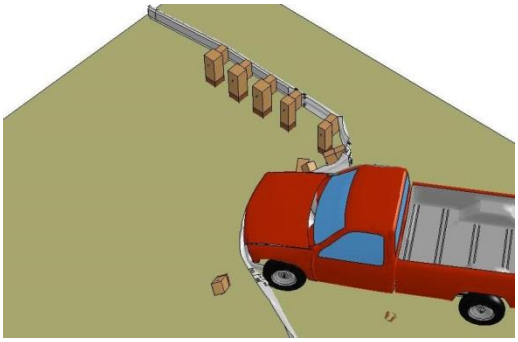

190 ms

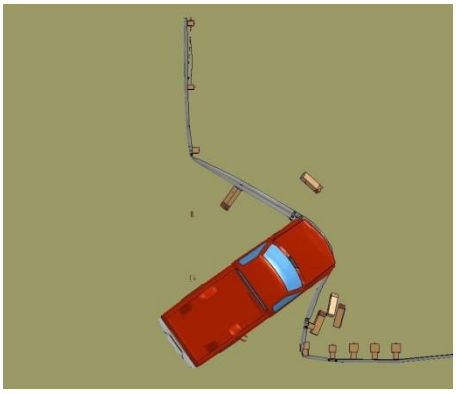

280 ms

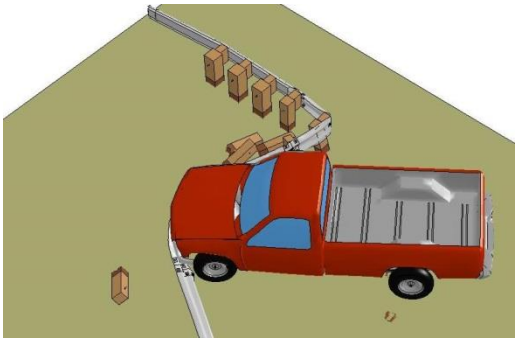

280 ms

Figure 86. Time-Sequential Images, Simulation of Test No. YC-4

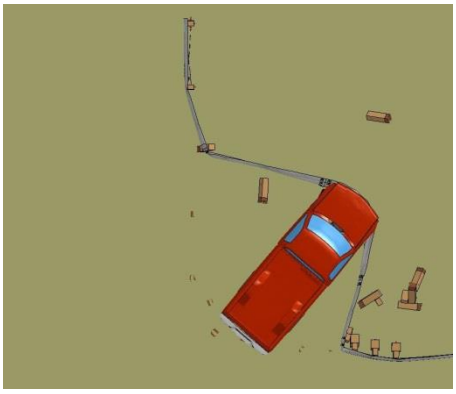
430 ms

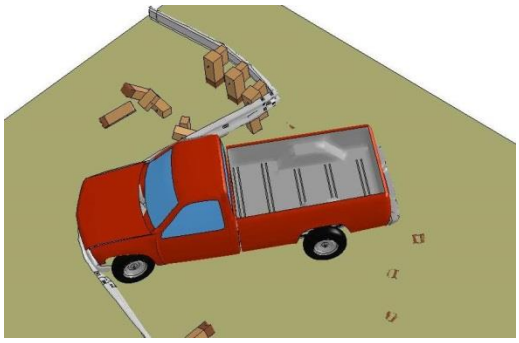
430 ms

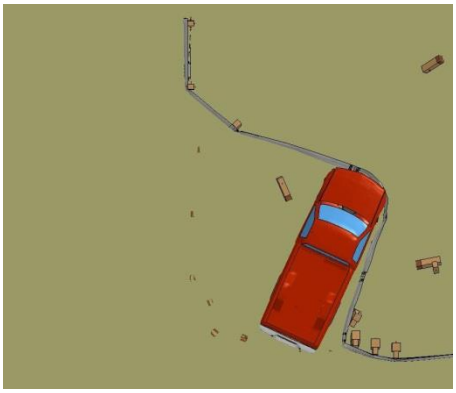
550 ms

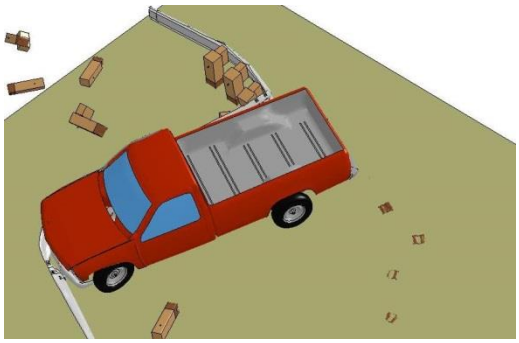
550 ms

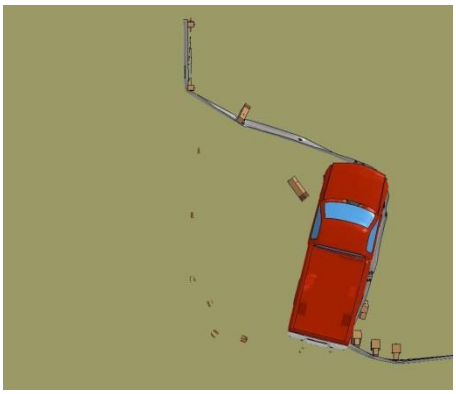
640 ms

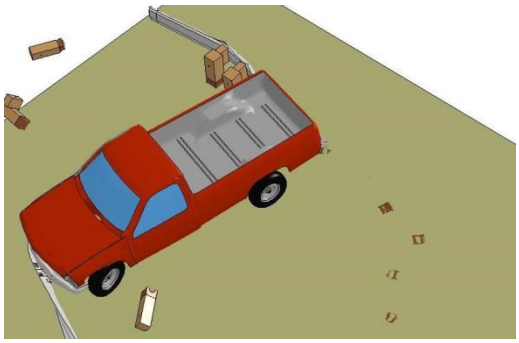
640 ms

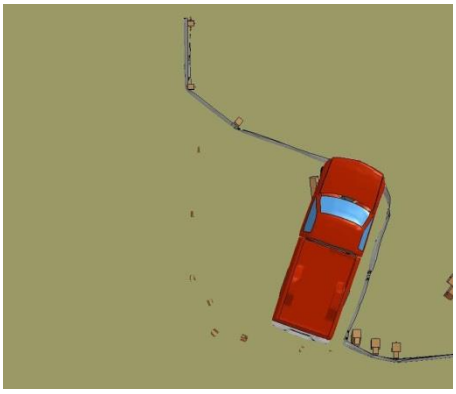
950 ms

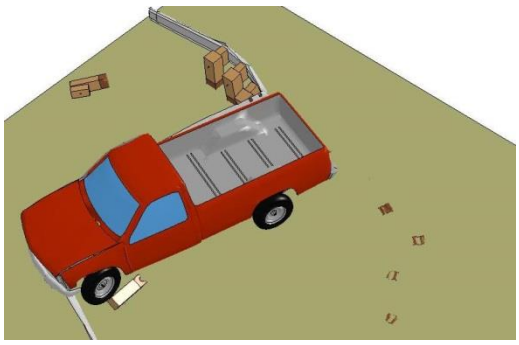
950 ms

Figure 87. Time-Sequential Images, Simulation of Test No. YC-4

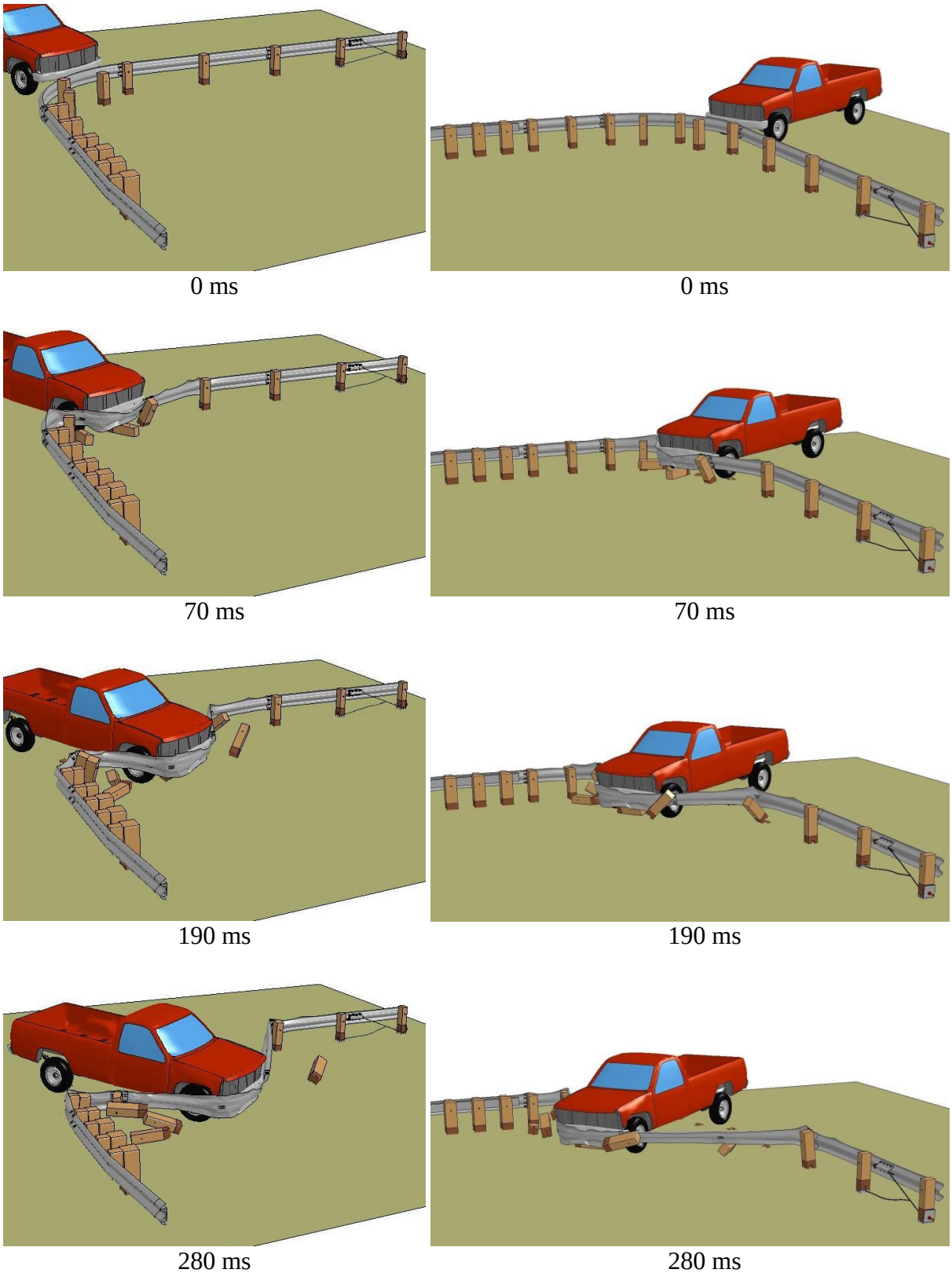

Figure 88. Time-Sequential Images, Simulation of Test No. YC-4

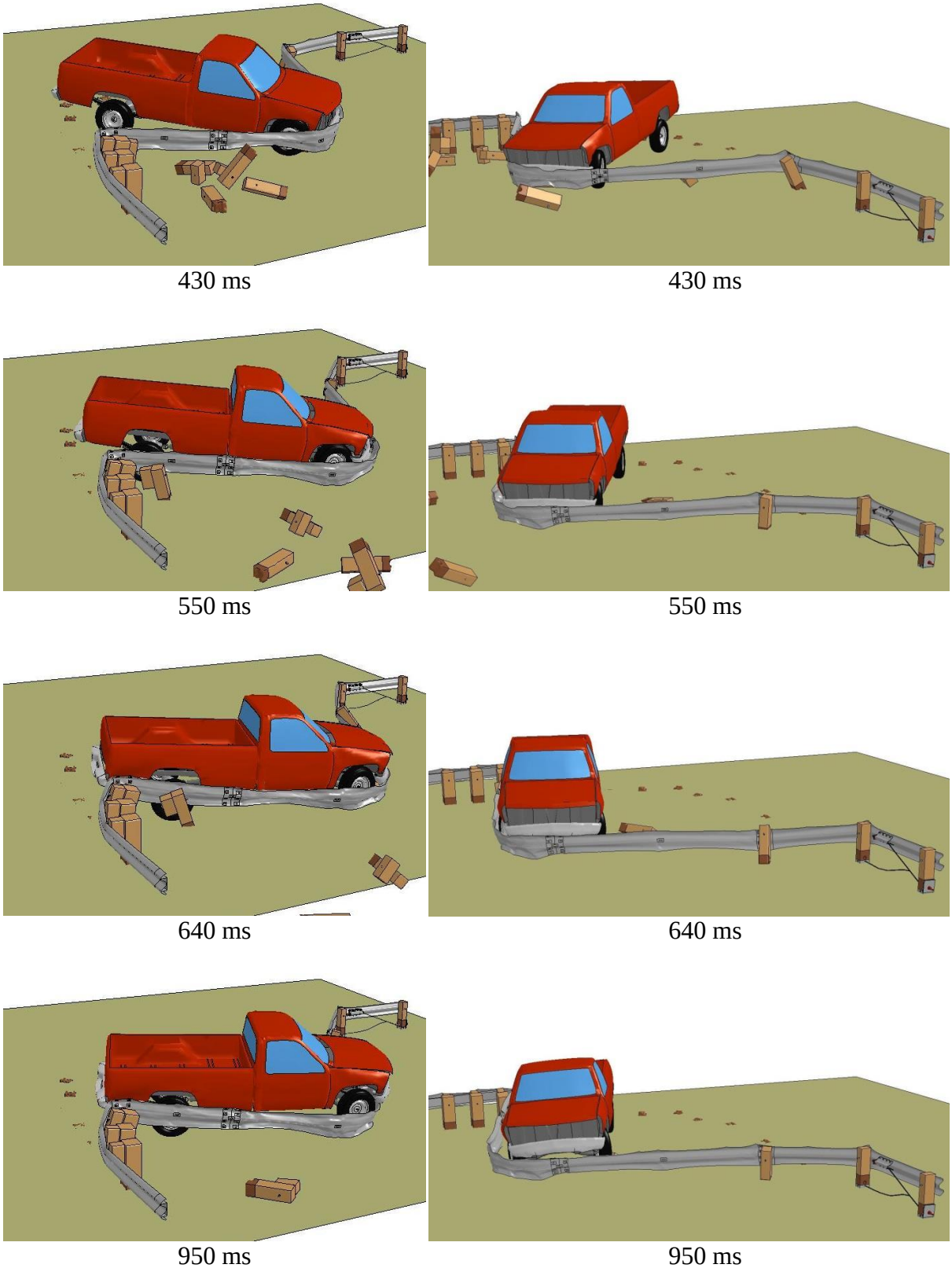

Figure 89. Time-Sequential Images, Simulation of Test No. YC-4

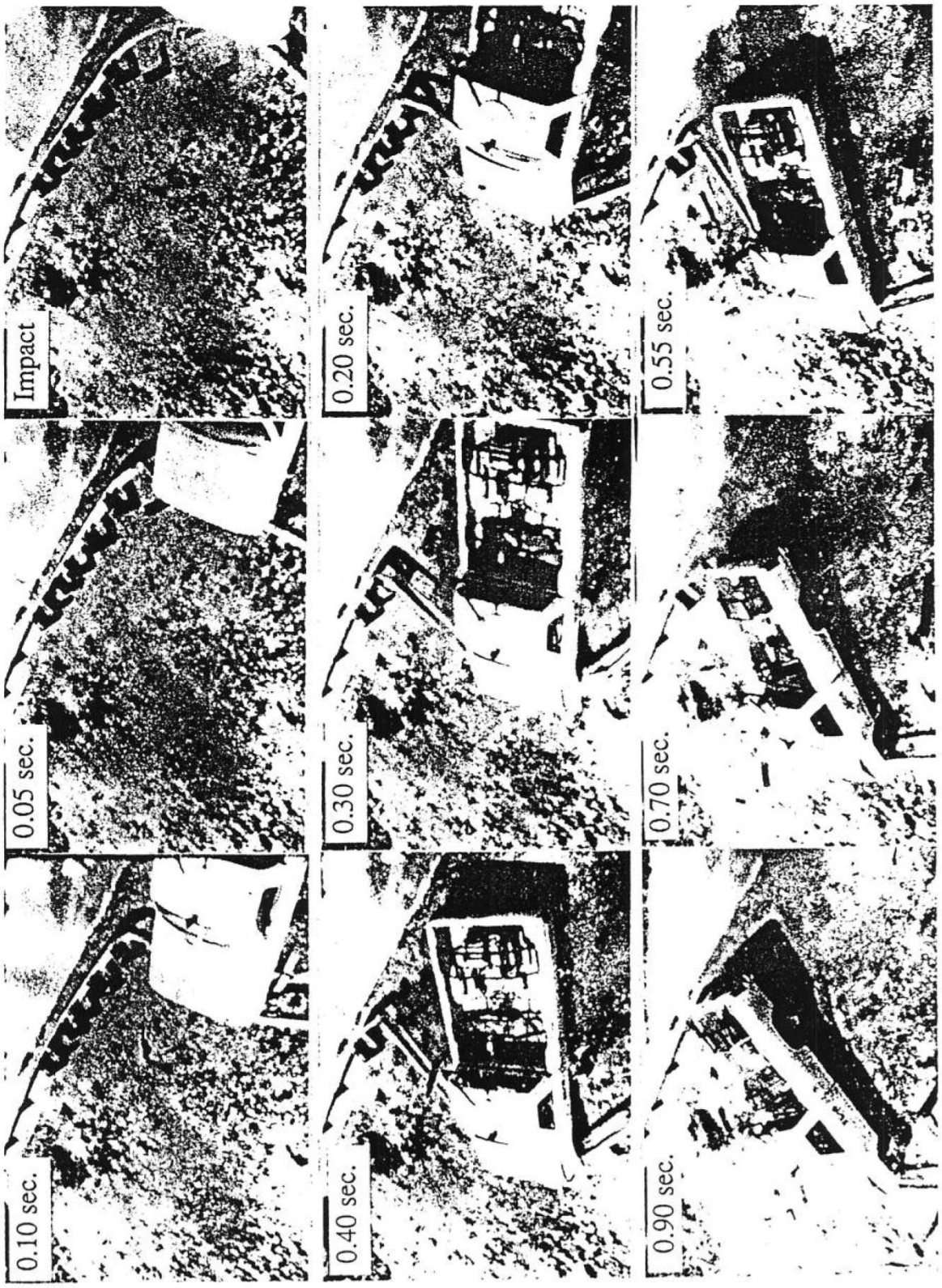

Figure 90. Time-Sequential Photographs of Test No. YC-4 [6]

Table 19. Comparison of Post Fracture Times, Test No. YC-4 and Simulation

Post No.	Fracture Time (ms)	
	Test (range)	Simulation
1	Did not fracture	Did not fracture
2	Did not fracture	Did not fracture
3	400-550	420-440
4	200-300	210-230
5	0-50	10-30
6	0-50	10-30
7	100-200	160-180
8	200-300	245-310
9	200-300	340-370
10	Did not fracture	Did not fracture
F1	0-50	30-40
F2	50-100	100-120

The stopping distance of the truck in the test was 12 ft (3.7 m) measured between the approximate impact location and the final vehicle CG location, as shown in Figure 91. The stopping distance of the truck in the simulation, measured from the initial impact point to the final CG position of the vehicle at 1.0 sec, was 12.96 ft (3.95 m). The final position of the pickup truck model was approximately 7% further downstream (measured parallel to the primary roadway) than the test vehicle. Measurement to vehicle final position in the test is sometimes subjective, and may incorporate significant unstated error. During the test, after reaching a maximum deflection, the truck rebounded and translated backward away from the rail. During the simulation, the tail slap into the transition arrested vehicle motion, and it did not rebound longitudinally. Thus, the maximum deflection of the truck may be very similar to the deflection observed in the simulation, since system damage, rail damage, and final deflected rail geometry were similar.

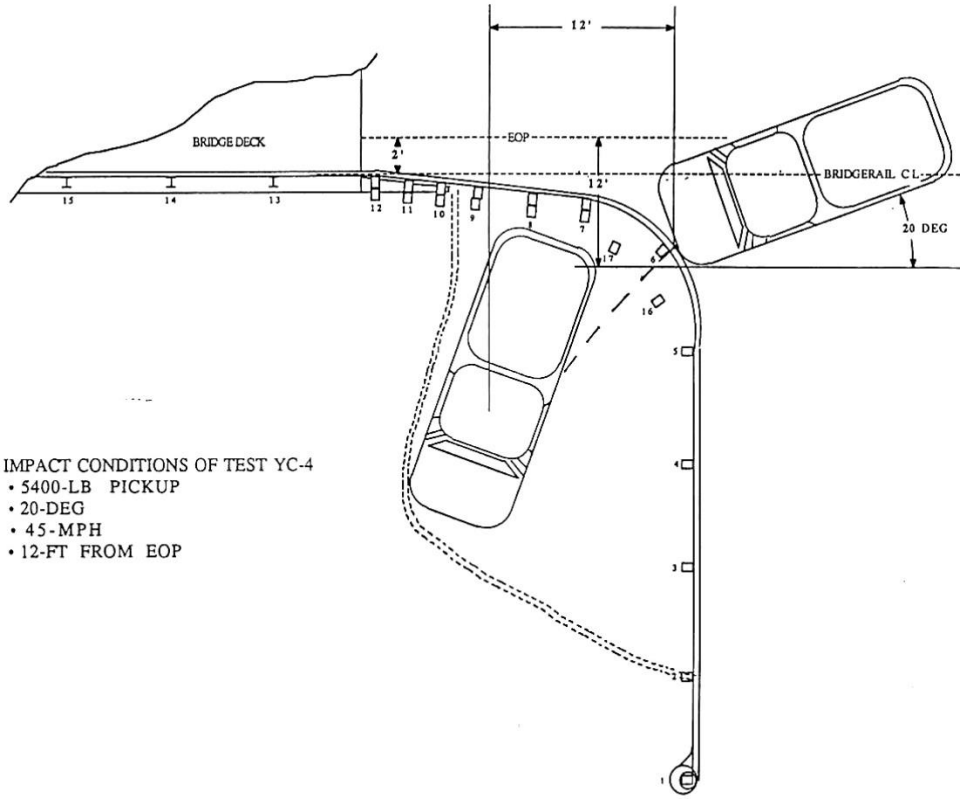

(a)

(b)

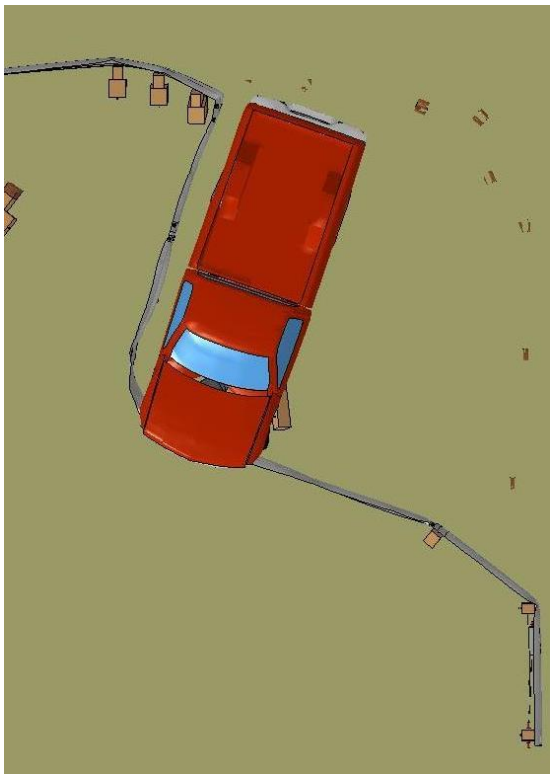

(c)

Figure 91. Final Vehicle Position after Crash (a) Reported [6] (b) Photograph [6] (c) Simulation

Unfortunately, more rigorous methods for evaluating the accuracy of the simulation in test no. YC-4 were not available. General similarities in system damage, stopping location, deformed system geometry, and vehicle crush damage indicated that the model of test no. YC-4 was considered representative of the full-scale crash test.

5.3 Modified 31-in. Yuma County System Simulation

The 31-in. (787-mm) tall short-radius guardrail system, which was a modified version of the model of the system in test no. YC-4, was simulated with an identical impact point test nos. YC-3 and YC-4. As previously stated, the modified BCT terminal with two spliced anchor cables was removed and replaced with an MGS end anchorage, the rail height was increased, and typical BCT posts were replaced with MGS BCT posts [13]. Sequential photographs of the simulation are shown in Figures 92 through 95. It was observed that initial bumper height and bumper-to-rail interactions were critical for this simulation; thus, the front bumper was colored red in the time-sequential photographs to distinguish the bumper from the guardrail.

At approximately 260 ms after impact, the guardrail engaged the radiator and grill, and became interlocked when the fenders crushed inward. Following rail engagement with the grill and fender, the vehicle was safely and smoothly brought to a controlled stop.

This contrasted with the unstable interaction observed in the simulation of test no. YC-4, in which only the top rail corrugation interacted with the test vehicle. At maximum deflection, the guardrail was engaged with the right-front wheel, and may not have captured a similar vehicle with slightly more initial kinetic energy at impact.

Unlike other systems with the rail mounted at 27 in. (686 mm), the short-radius system mounted at 31 in. (787 mm) was resistant to vaulting because the bumper restricted the rail from dropping. After impact, the bottom corrugation of the rail was crushed and the rail slid upward to

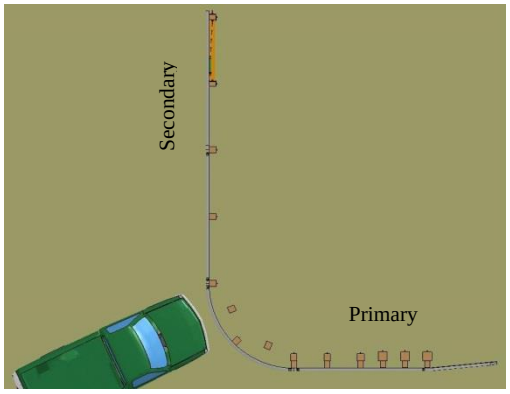

0 ms

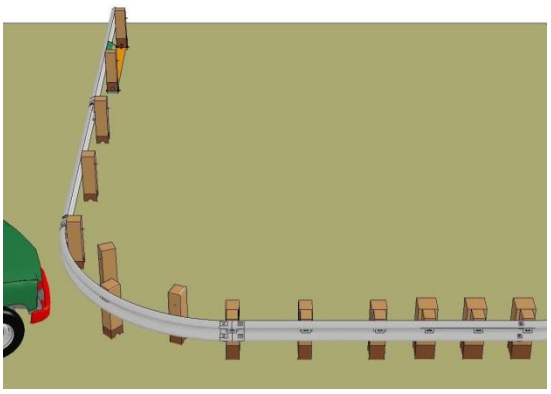

0 ms

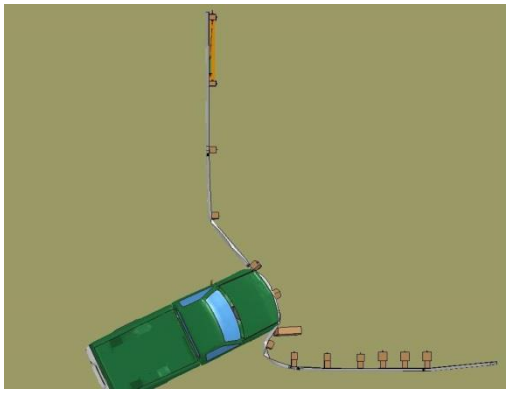

100 ms

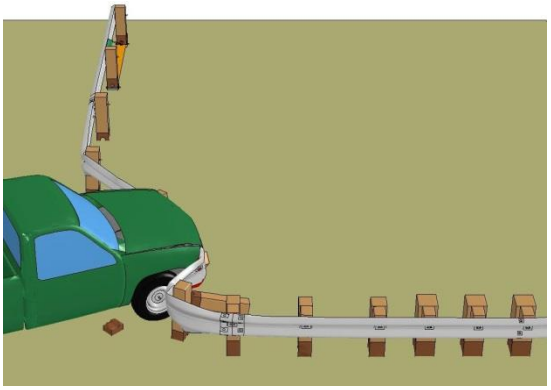

100 ms

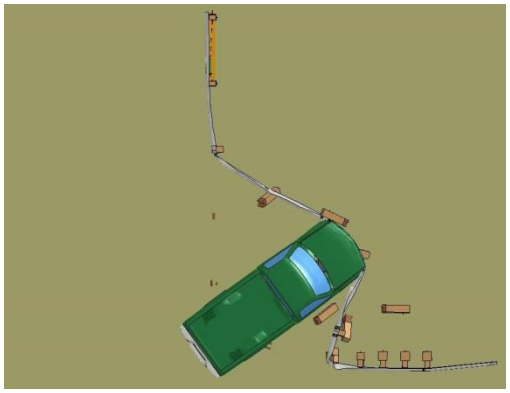

280 ms

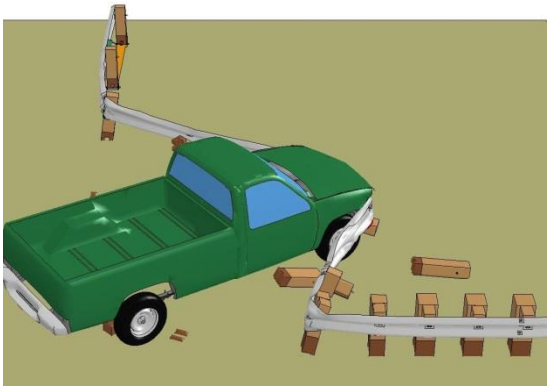

280 ms

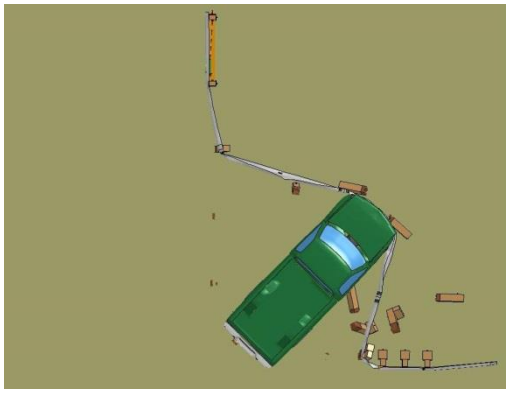

370 ms

370 ms

Figure 92. Time-Sequential Photographs, 31-in. (787-mm) Modification to Test No. YC-4

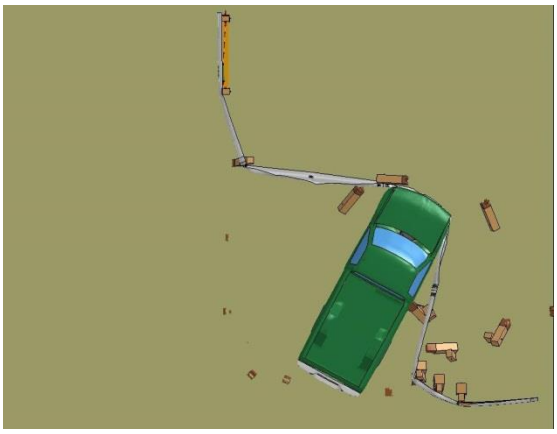
490 ms


490 ms

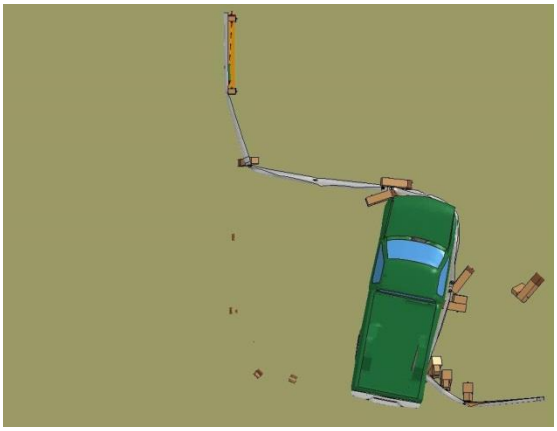
700 ms

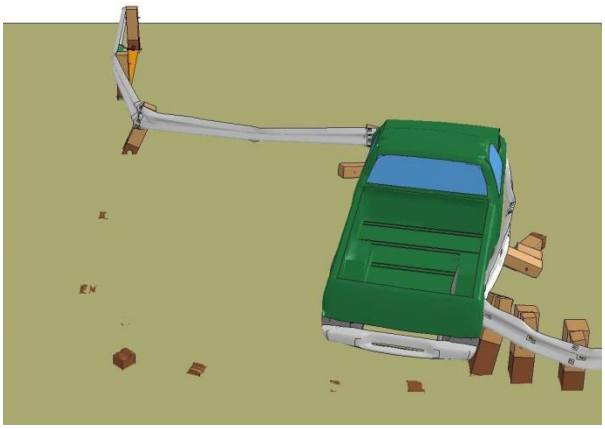
700 ms

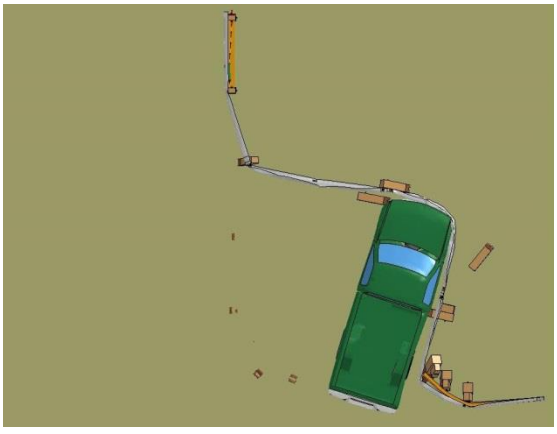
980 ms

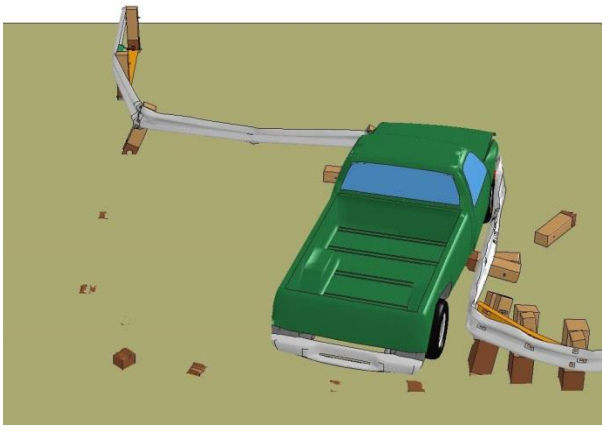
980 ms

Figure 93. Time-Sequential Photographs, 31-in. (787-mm) Modification to Test No. YC-4

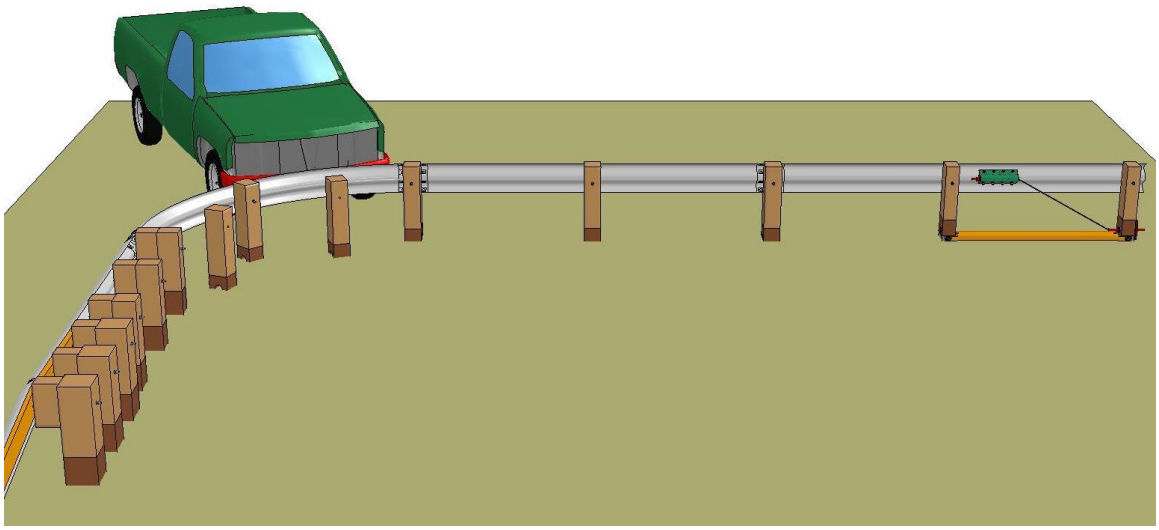

0 ms

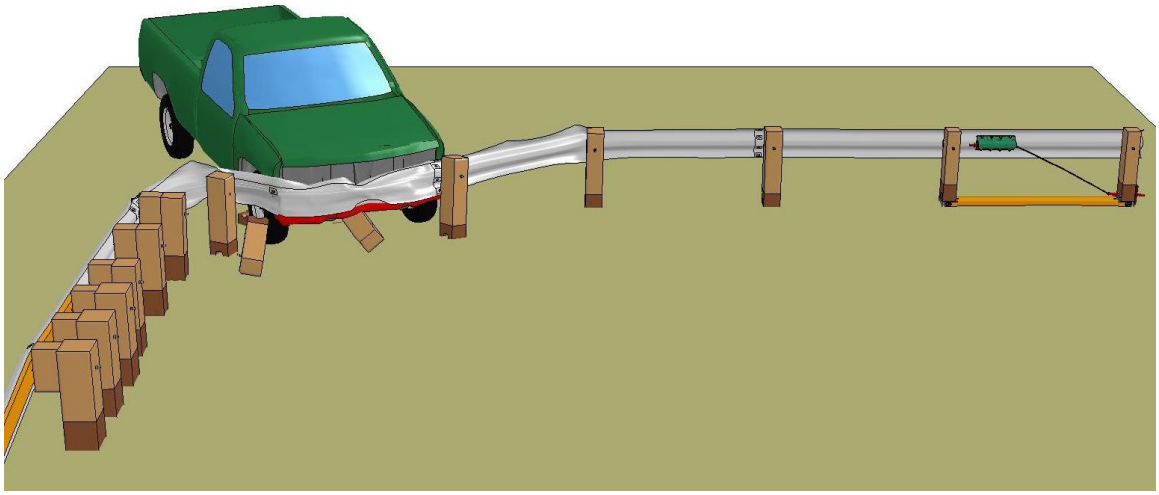

100 ms

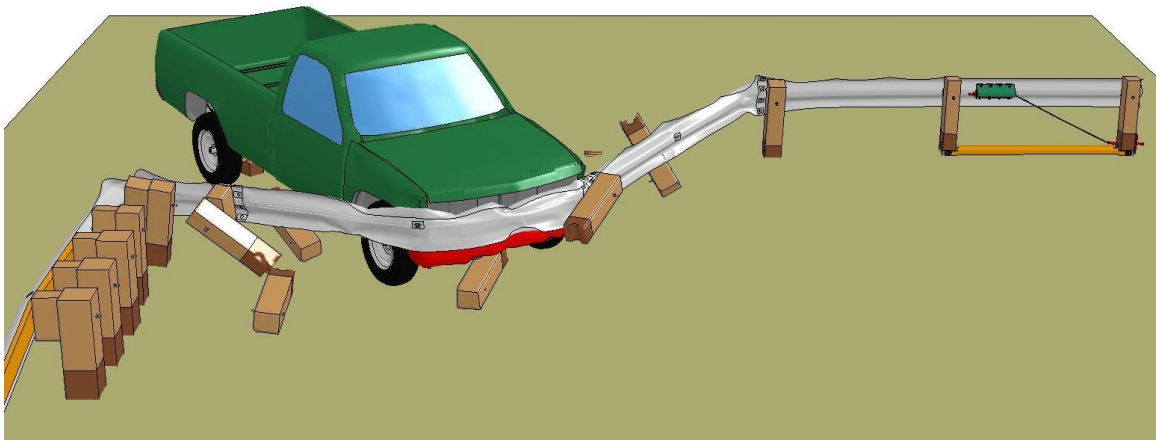

280 ms

Figure 94. Time-Sequential Photographs, 31-in. (787-mm) Modification to Test No. YC-4

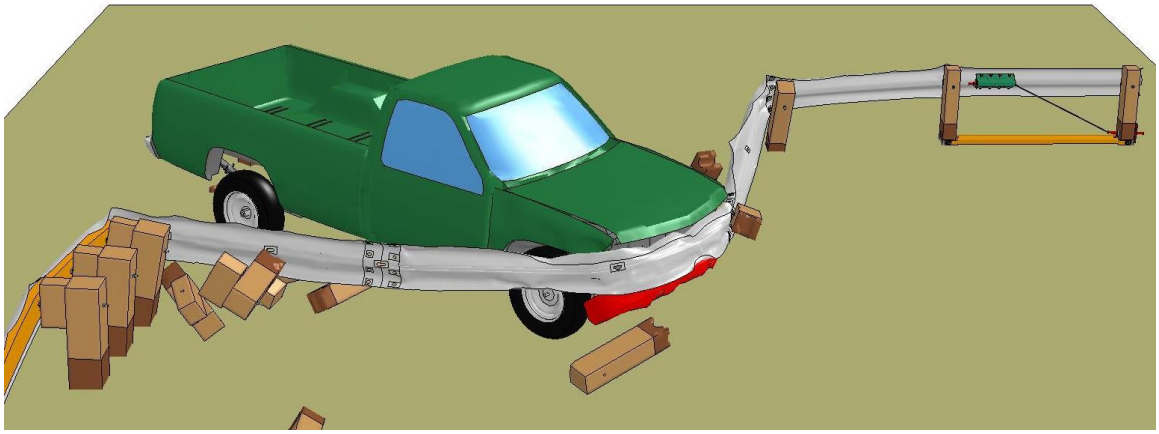

430 ms

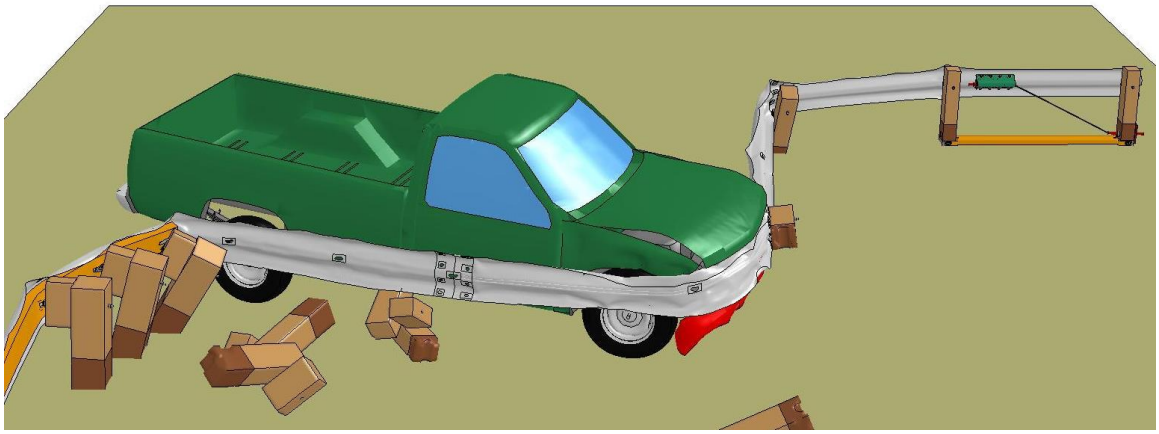

520 ms

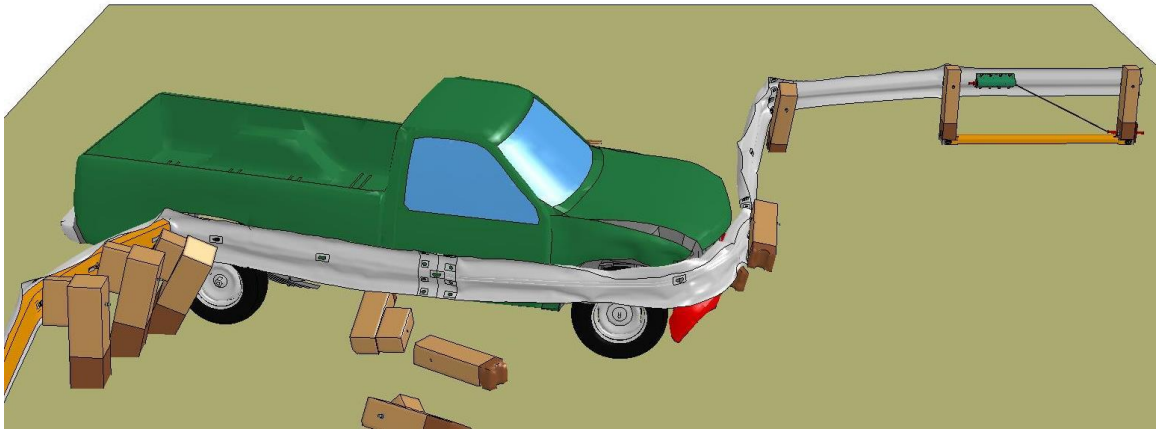

700 ms

Figure 95. Time-Sequential Photographs, 31-in. (787-mm) Modification to Test No. YC-4

engage the headlight, grill, radiator, and hood locations. Subsequent downward forces on the rail did not cause the rail to slide below the front bumper.

The 31-in. (787-mm) tall, modified Yuma County short-radius guardrail system performed as well as or better than the 27-in. (686-mm) tall Yuma County short-radius guardrail system when subjected to a 5,401-lb (2,450-kg) pickup truck at 45 mph (72 km/h) and 25.5 degrees (which included the flare from the bridge rail). Although post debris did accumulate in front of and around the vehicle during capture, the vehicle did not vault nor show the propensity to vault during the simulation. The vehicle was brought to a controlled stop with no occupant compartment penetrations nor excessive ridedown decelerations or OIV values.

Despite the excellent performance of the modified Yuma County short radius system with a 31-in. (787-mm) mounting height, the taller system has not been tested with a small car to assess underride performance. Short-radius guardrail systems have consistently demonstrated critical instability when impacted with small cars and pickup trucks. Full-scale crash test failures included small car underrides and pickup truck overrides. Although the simulated 31-in. (787-mm) tall system reduced the propensity for pickup truck overrides, there is significant concern that the system would fail to safely capture a small car. No full-scale tests have been conducted on a W-beam short-radius guardrail system with a top mounting height of 31 in. (787 mm).

5.4 Discussion

The Yuma County short radius model was validated by comparing simulation results to very limited test data. Despite the low precision for the few available metrics, system damage, stopping location, and limited photographic evidence were compared to simulation data. The simulations of test nos. YC-3 and YC-4 were determined to be representative of the full-scale crash tests conducted on the Yuma County short radius guardrail system through 310 ms for the system in test no. YC-3, because post no. 1 did not fracture, and throughout the event for the

system in test no. YC-4. A third simulation evaluating the performance of the system raised to a top mounting height of 31 in. (787 mm) was also evaluated, although no physical test data was available to assess the accuracy of the simulation.

The 31-in. (787-mm) tall guardrail system appeared to capture the impacting truck in a more stable and reliable manner than was observed when the system had a 27-in. (686-mm) mounting height. However, it is not recommended that the Yuma County short radius guardrail system be constructed with a top mounting height of 31 in. (787 mm) without full-scale crash testing using a small car to assess underride potential.

The 27-in. (686-mm) mounting height guardrail system was determined to be at the lower limit of stability for vehicle redirection. The rail remained engaged with the bumper throughout the impact event in the simulation of test no. YC-4, but the interaction was unstable. The system, as tested, could potentially perform differently with a lighter truck, if impacted in accordance with NCHRP Report No. 350.

6 SYSTEM DETAILS FOR SIMULATED LARGER-RADII SYSTEMS

The Wisconsin Department of Transportation (DOT) requested simulations of short-radius guardrail systems with radii as large as 70 ft (21 m). Only curved sections of guardrail encompassing 90-degree intersections were considered. The radius was terminated on the upstream and downstream ends at post locations to simplify rail bend requirements. These two factors discretized the number of guardrail-and-radius combinations to be simulated, based on discrete 6 ft – 3 in. (1,905 mm) post spans.

Three larger radii were selected for study: 23 ft – 10½ in. (7,277 mm), 47 ft – 9 in. (14,554 mm), and 71 ft – 7½ in. (21,831 mm), corresponding to 6, 12, and 18 CRT posts installed along the radius, respectively. For simplicity, the radii are rounded to the nearest foot (0.3 m), and are heretofore referenced as 24-ft (7.3-m), 48-ft (15-m), and 72-ft (22-m) radii, respectively. Each model contained one end anchorage system, one transition to stiff bridge rail, and one curved guardrail section. Schematic drawings of the Yuma County short radius system and three larger-radius systems simulated are shown in Figure 96. Finite element models of the systems are shown in Figures 97 through 99.

Two system heights were initially considered: a 27-in. (686-mm) tall guardrail top mounting height, similar to the system tested in Yuma County short-radius guardrail test nos. YC-1 through YC-7; and a 31-in. (787-mm) tall system based on the modified test no. YC-4 simulation. Because the 27-in. (686-mm) tall system demonstrated a propensity for override, a taller system was believed to reduce the risk of override and would be useful for investigating the performance limit of the system when override and vaulting did not occur.

Free-standing CRT posts placed behind the nose of the radius were eliminated for all increased-radius designs. Multiple posts were engaged to the curved radius rail for every increased-radius system considered. Any free-standing CRT posts utilized on these larger radii, if

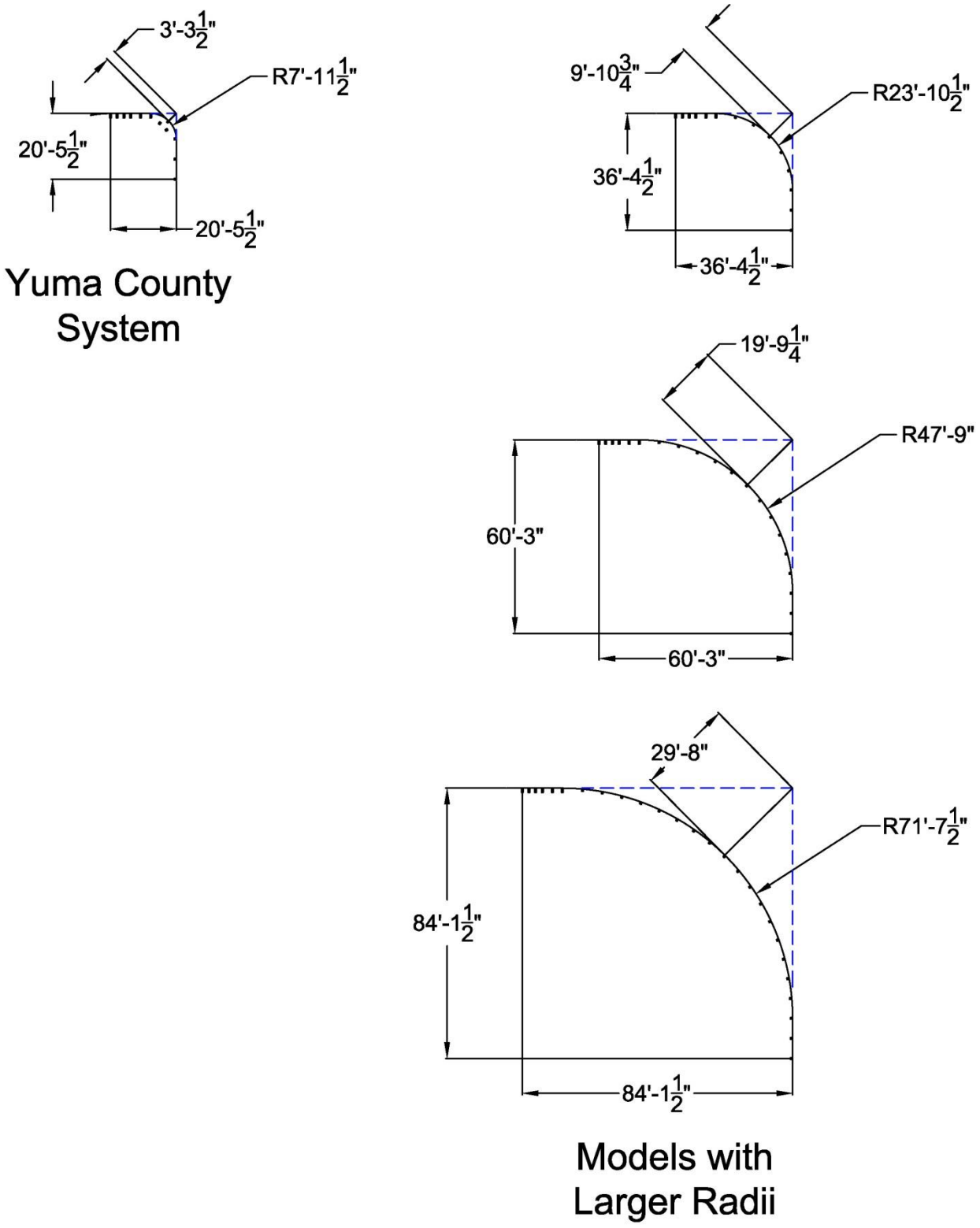

Figure 96. Schematic Drawings of Short Radius Simulation Models

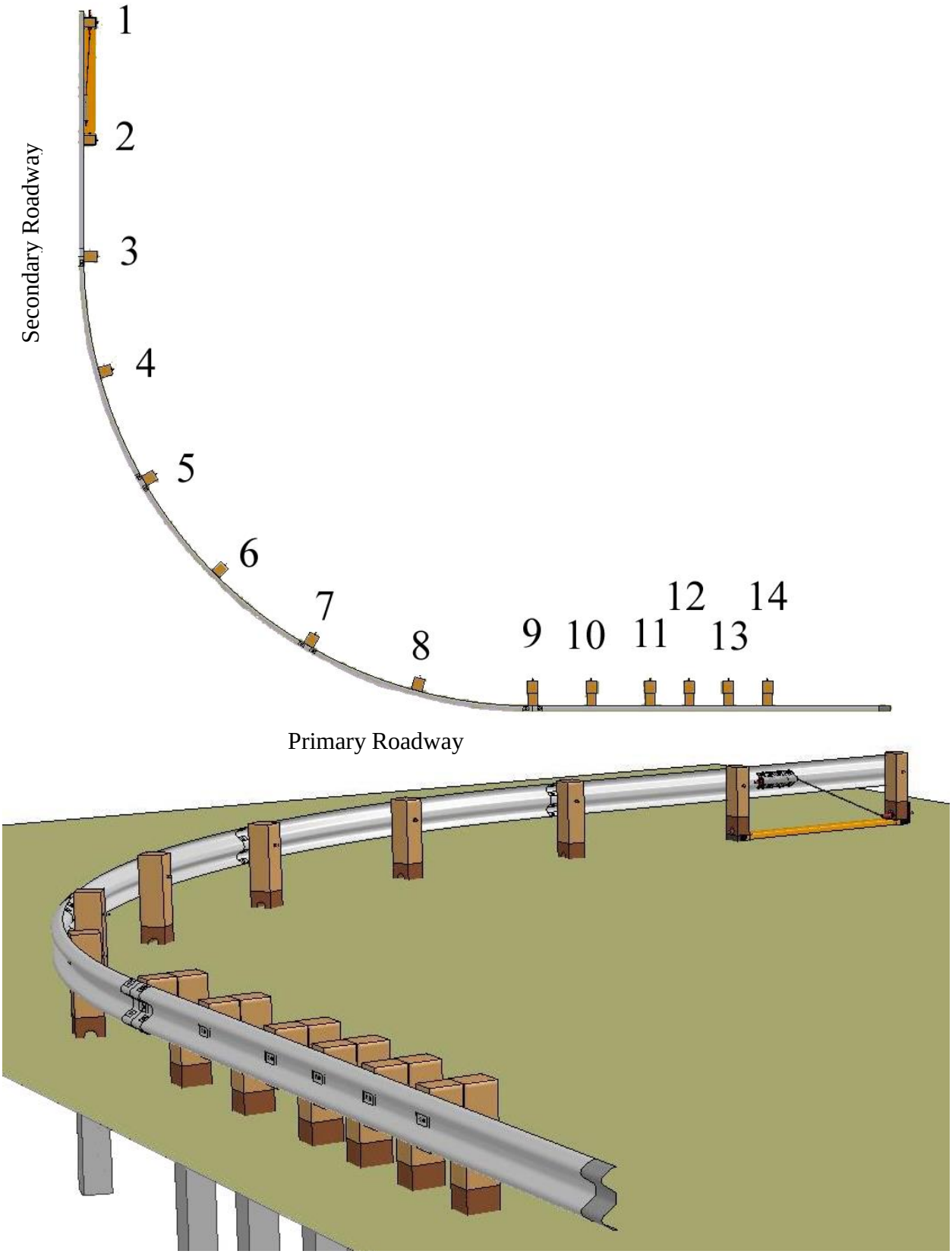

Figure 97. Simulation Model with Post Numbers, 24-ft (7.3-m) Radius

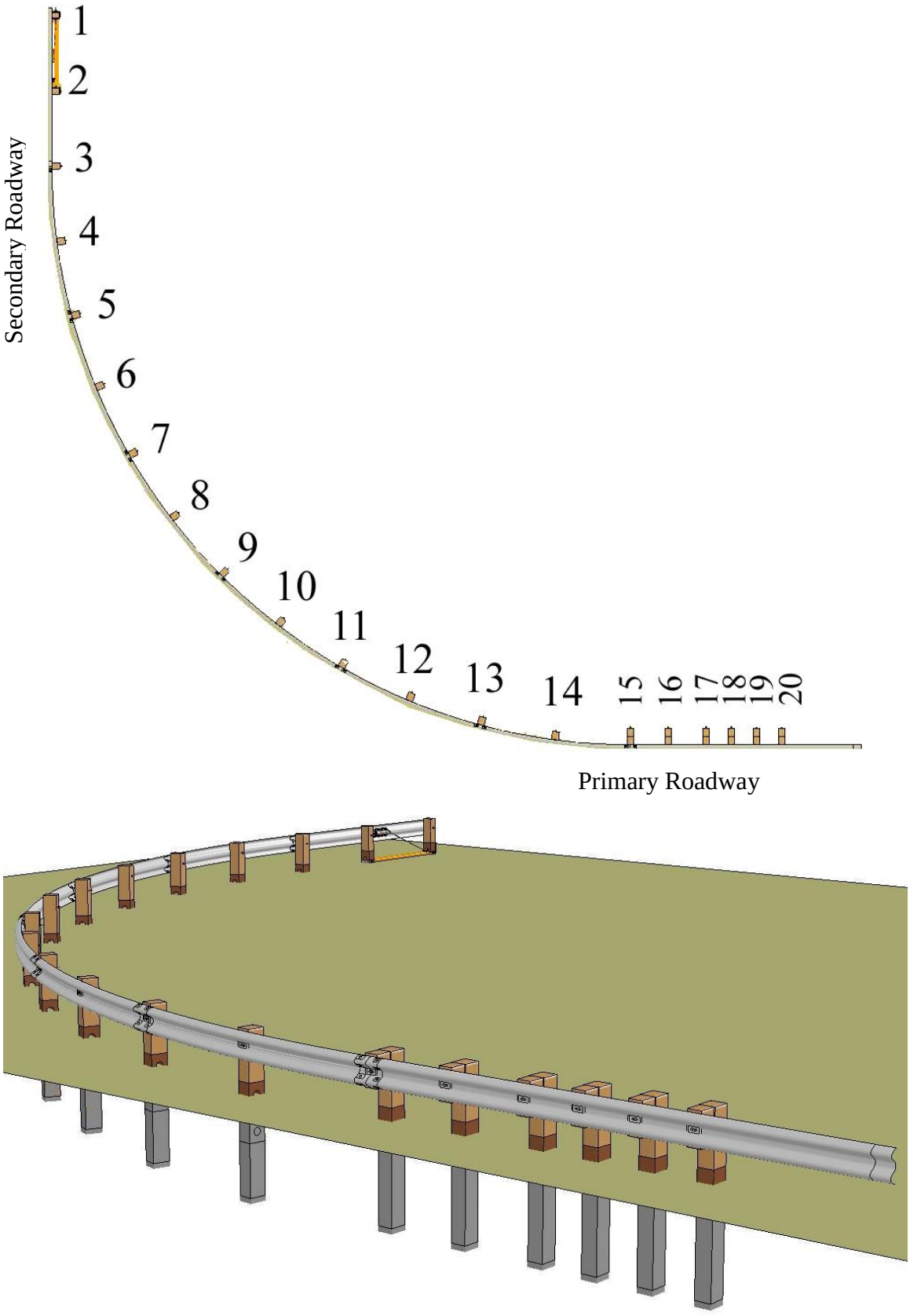

Figure 98. Simulation Model with Post Numbers, 48-ft (15-m) Radius

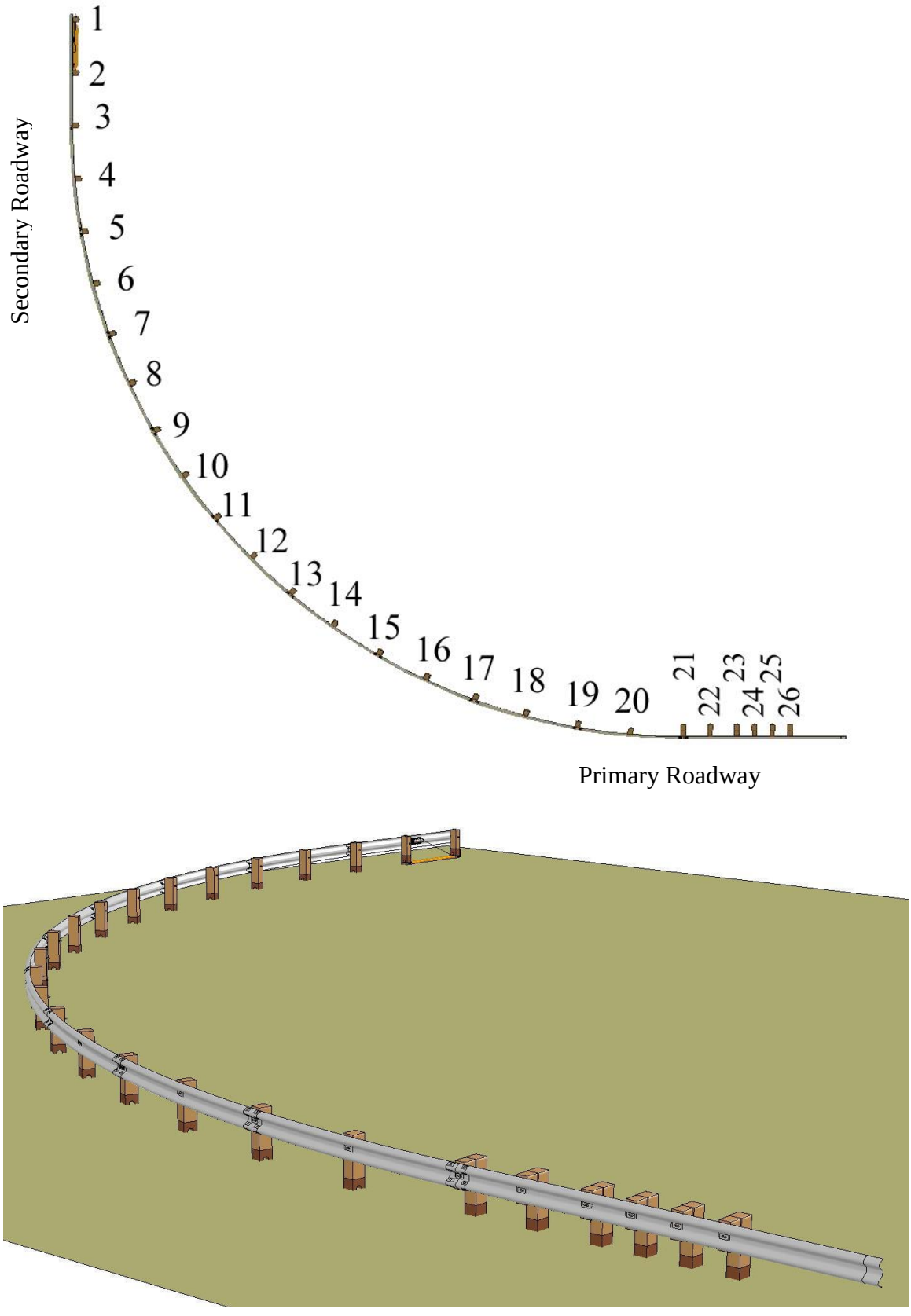

Figure 99. Simulation Model with Post Numbers, 72-ft (22-m) Radius

placed at the midspans between posts, could nearly double the required number of CRT posts for a single short-radius system installation, which would be both costly and difficult. These posts could also contribute to additional debris and adversely affect vehicle stability. In addition, the freestanding CRT posts were removed from recommended system details by researchers at TTI [27] based on component testing energy levels and estimated increased truck deflections.

Critical system elements, such as CRT post sizes and spacing, were not altered. The transition section also remained unchanged because it had already demonstrated crashworthy performance during impacts similar to TL-2 transition tests. Post locations, post-to-rail connections, rail shape and material parameters, and impact locations were identical for 27-in. (686-mm) and 31-in. (787-mm) tall short radius system variations of each radius size. The additional mass that was added to the C2500 model was removed, such that the weight of the vehicle was approximately 4,409 lb (2,000 kg).

For the 31-in. (787-mm) tall system, MGS CRT posts were utilized in lieu of standard CRT posts. MGS CRT posts are similar to standard CRTs, with the exception that the embedment depth is reduced by 4 in. (102 mm), the height of the top of the post was increased to 32 in. (813 mm), and the two CRT holes were shifted downward 4 in. (102 mm) such that the center of the top hole was still located at the ground line [13].

Standard 27-in. (686-mm) tall W-beam end anchorages and MGS end anchorages were used for all 27-in. (686-mm) and 31-in. (787-mm) tall simulations, respectively, in lieu of the two-cable system tested during Yuma County short-radius guardrail test nos. YC-1 through YC-7. The two-cable system simulated in the model of test no. YC-4 performed similarly to the strut and yoke assembly in the 31-in. (787-mm) top mounting height, modified YC-4 system simulation. Researchers at TTI similarly recommended substitution of the two-cable end anchorage assembly for a single-cable anchorage with a channel strut [27]. The MGS end

anchorage was similar to the strut-and-yoke system utilized on the 27-in. (787-mm) tall W-beam end anchorage, except that the rail height was increased, the BCT cable anchor cable was shifted to accommodate the increased distance between the cable anchor bracket and the rail, and MGS BCT posts were substituted for standard BCT posts. MGS BCT posts were similar to standard BCT posts, except that the embedment depth in the soil foundation tubes was decreased by 4 in. (102 mm), the top of the post was mounted at approximately 32 in. (813 mm), and the BCT hole was shifted downward by 4 in. (102 mm) such that it was at the same elevation as a BCT post used with the 27-in. (686-mm) tall system.

For all simulations, NCHRP Report No. 350 TL-2 impact conditions were selected to evaluate the rail propensity for override. Specifically, each simulation involved a pickup truck model impacting at 45 mph (72 km/h) and 25 degrees relative to the roadway, respectively. These impact conditions were selected based on the difficulty of passing this particular test scenario historically.

Of the 23 tests conducted with impact angles greater than or equal to 15 degrees on short-radius systems with NCHRP Report No. 230 or 350 or MASH impact conditions, ten tests, or 43% of impacts, passed evaluation criteria. Three of the passing tests, or 30%, were considered marginal. By eliminating angled impacts near the stiff bridge rail transitions, only six of 19 tests, or 32%, passed evaluation criteria, and half of those tests were considered marginal. In contrast, five of nine tests conducted with angles less than 15 degrees, or 56%, successfully passed evaluation criteria. These low-angle tests included three failed thrie beam short-radius tests conducted at MwRSF, and the only successful NCHRP Report No. 350 TL-3 thrie beam short radius test conducted to date [12-14].

7 NUMERICAL SIMULATIONS OF SYSTEMS WITH 24-FT (7.3-M) RADII

Impacts with the 27-in. (686-mm) and 31-in. (787-mm) short radius guardrail systems with 24-ft (7.3-m) radii were simulated by aligning the centerline of the truck with the third, fourth, fifth, sixth, and seventh posts, in addition to the midspans between the third and fourth, fourth and fifth, fifth and sixth, sixth and seventh, and seventh and eighth posts, respectively. Post numbers are shown in Figure 97. Results of the simulations are evaluated in Chapter 10.

7.1 Systems with 27-in. (686-mm) Top Mounting Height

The 27-in. (686-mm) tall, 24-ft (7.3-m) radius short radius system was simulated using a 4,409-lb (2,000-kg) pickup truck impacting at 45 mph (72 km/h) and 25 degrees, relative to a tangent line to the bridge rail. Because results with standard CRT posts indicated unacceptable performance of the curved guardrail system, 8-in. (203-mm) timber blockouts were added to the posts in an attempt to maintain the rail height after impact.

7.1.1 Systems without Blockouts Attached to Radius Posts

The pickup truck vaulted the system at every impact location selected with a 27-in. (686-mm) mounting height, when blockouts were not utilized. Typically, three or four posts fractured near impact before the rail slid below the bumper and the vehicle vaulted over the rail. The vehicle's bumper impacted and flattened the top corrugation of the guardrail, which permitted the bottom corrugation to twist below the bumper and engage the wheels. Rail twist was increased by a prolonged attachment between the posts and rail after post fracture, which tended to twist the top of the rail backward and away from impact and accentuating bottom rail corrugation deflection below the bumper. Results of the simulations are shown in Figures 100 through 102.

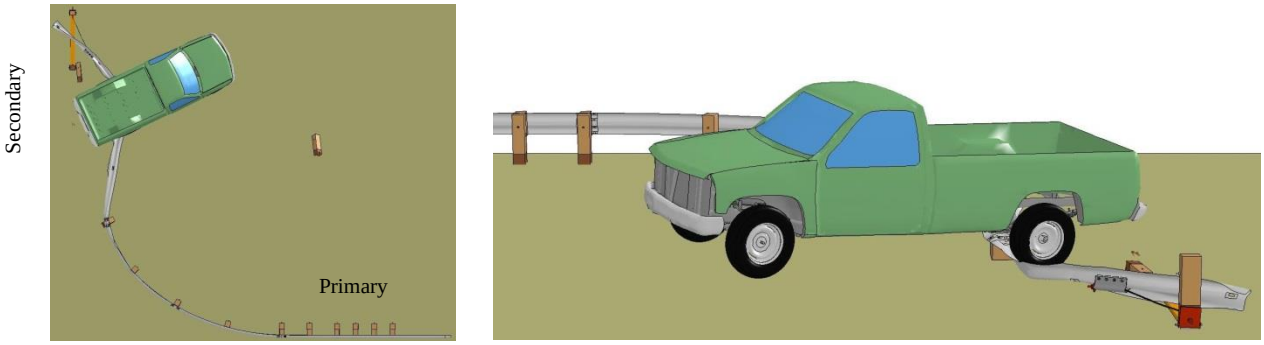

Impact at Post No. 3

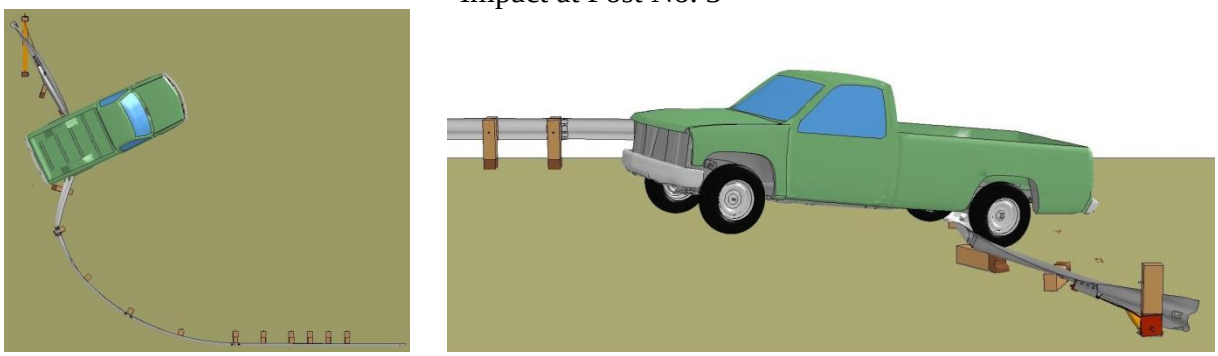

Impact at Midspan between Post Nos. 3 and 4

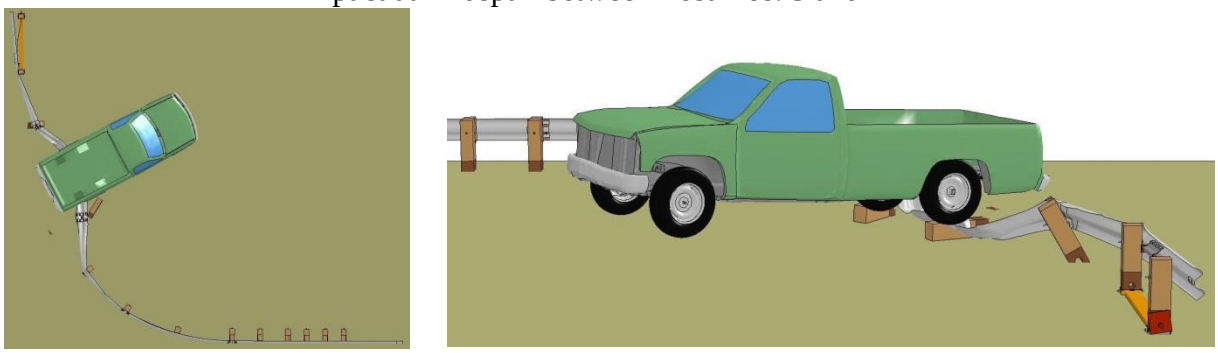

Impact at Post No. 4

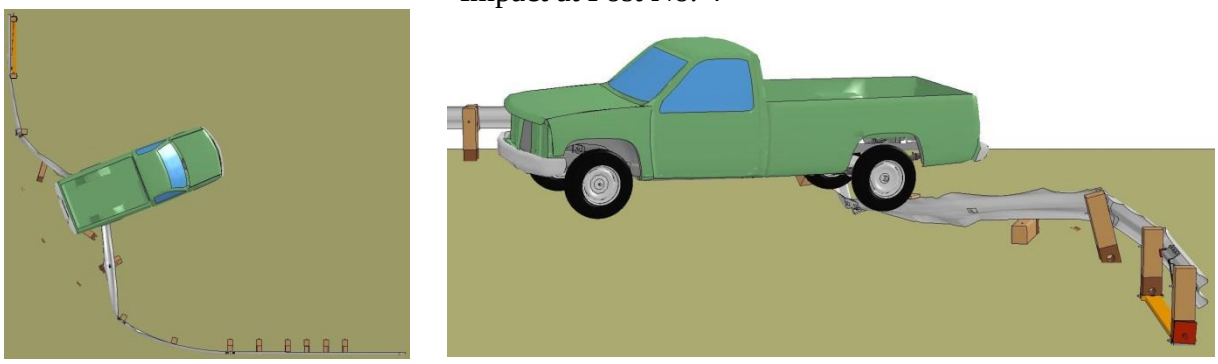

Impact at Midspan between Post Nos. 4 and 5

Figure 100. Images of Impacts with 27-in. (686-mm) Tall, 24-ft (7.3-m) Radius Systems without Blockouts Attached to Posts on Radius

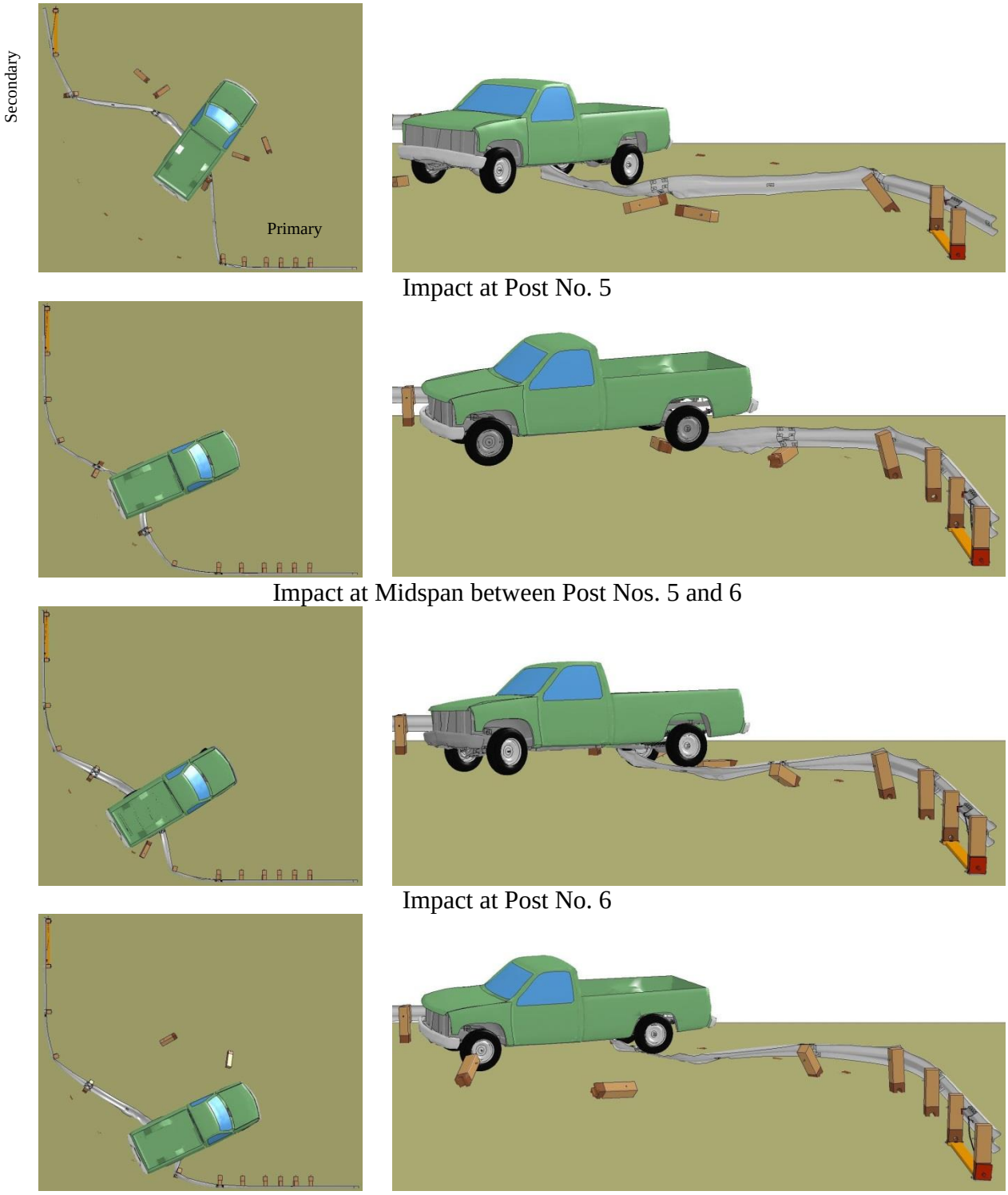

Impact at Post No. 5

Impact at Midspan between Post Nos. 5 and 6

Impact at Post No. 6

Impact at Midspan between Post Nos. 6 and 7

Figure 101. Images of Impacts with 27-in. (686-mm) Tall, 24-ft (7.3-m) Radius Systems without Blockouts Attached to Posts on Radius

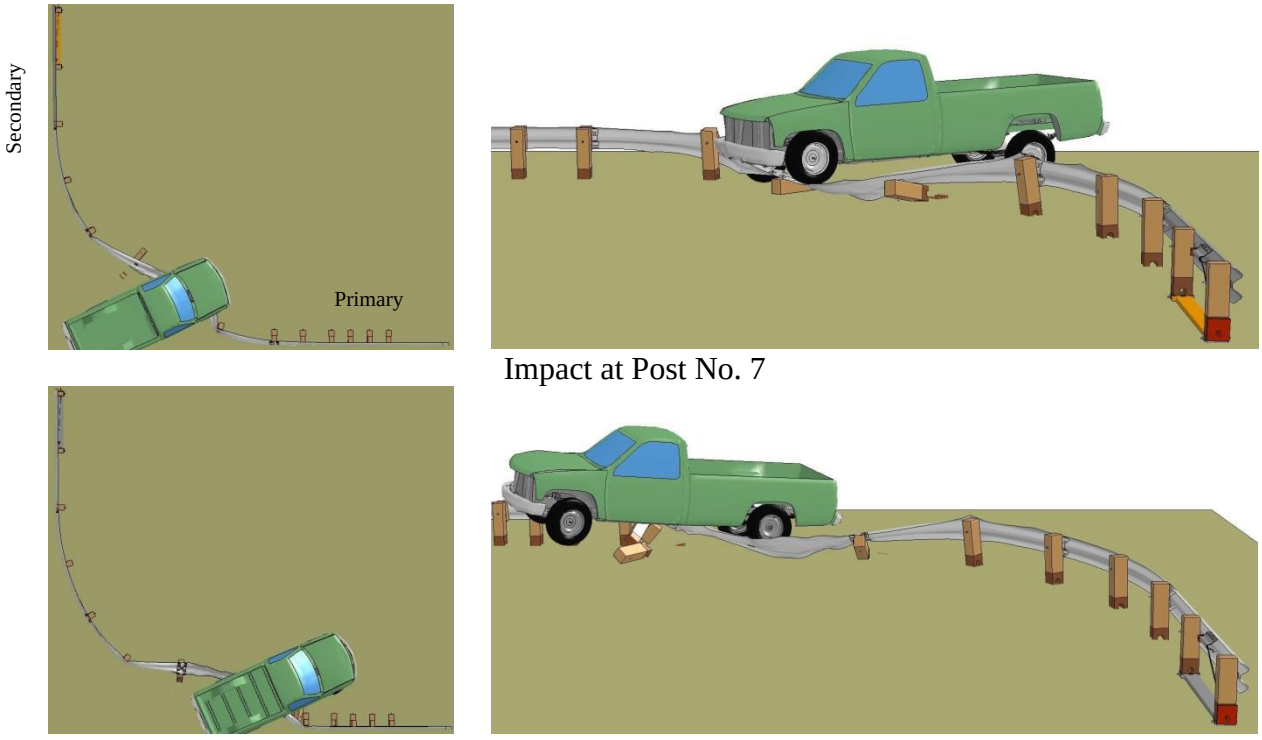

Figure 102. Images of Impacts with 27-in. (686-mm) Tall, 24-ft (7.3-m) Radius Systems without Blockouts Attached to Posts on Radius

Although it was expected that some of the impact locations would contribute to failure due to vaulting, the number of overrides and the low system damage prior to vaulting was concerning. It was determined that reduction in rail height due to post deflection and twisting may be mitigated, in part, by adding blockouts to the CRT posts. Previous research indicated blockouts may retain the rail at the impact height [33]. Also, posts with blockouts released more quickly from the guardrail than non-blocked posts.

7.1.2 Systems with Blockouts Attached to Radius Posts

The 24-ft (7.3-m) radius system was modified by adding 8-in. (203-mm) timber blockouts to the front sides of each post along the radius. The posts were shifted backward to maintain the same rail attachment locations. Summary images of the performance are shown in Figures 103 and 104.

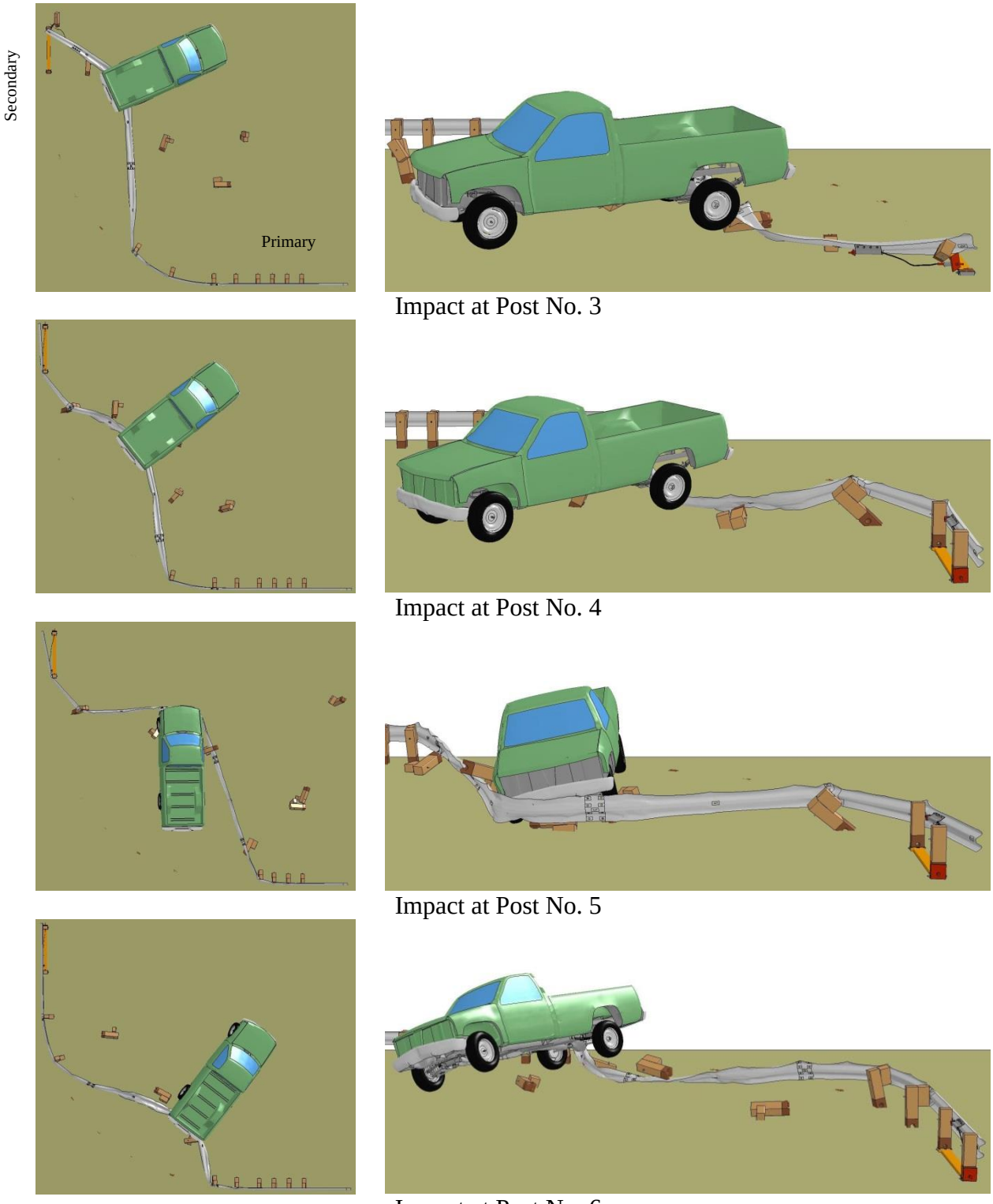

Figure 103. Images of Impacts with 27-in. (686-mm) Tall, 24-ft (7.3-m) Radius Systems with Blockouts Attached to Radius Posts

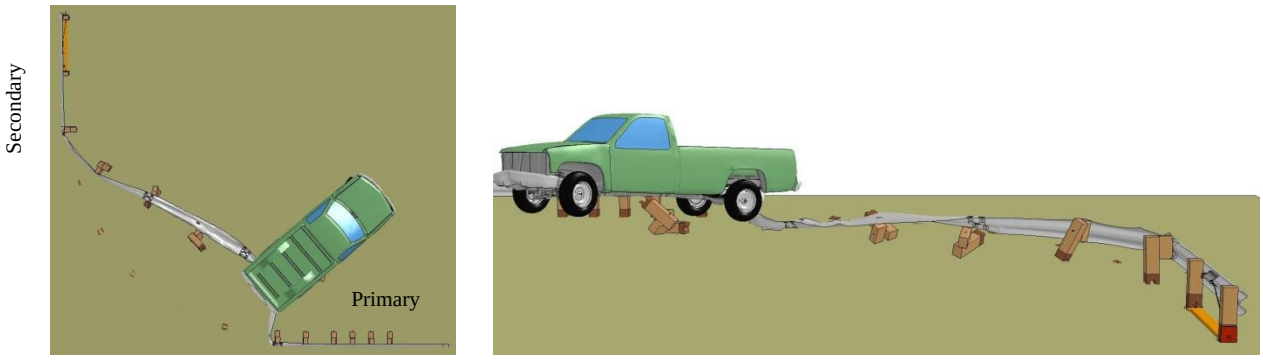

Figure 104. Images of Impacts with 27-in. (686-mm) Tall, 24-ft (7.3-m) Radius Systems with Blockouts Attached to Radius Posts

Results were improved over the non-blocked system, but only one impact condition resulted in acceptable vehicle capture. Five to seven posts were fractured prior to vaulting at each impact location. As with the simulation of the unblocked system, sustained post attachment to the rail and tire interaction with post debris contributed to vaulting, in addition to the rail flattening and sliding below the bumper without engaging the grill, radiator, or headlights.

7.2 Systems with 31-in. (787-mm) Top Mounting Height

7.2.1 Impacts at 45 mph (72 km/h)

The 31-in. (787-mm) tall barriers captured the pickups for each impact at or downstream of post no. 6, as shown in Figures 104 through 106. If one BCT post fractured during impact, simulation analysis was terminated because the end anchorage model was no longer considered validated, even if it appeared likely that the pickup would be captured. Four of the ten simulations acceptably captured the pickup. The major difference contributed by the taller system was that, after engaging the bumper, the rail slid upward and became interlocked with the headlight location, grill, and radiator. This interlock improved vehicle stability and reduced the vaulting tendency, even when the truck interacted with debris. The truck was captured at each impact location downstream of post no. 6 at NCHRP Report No. 350 TL-2 impact conditions.

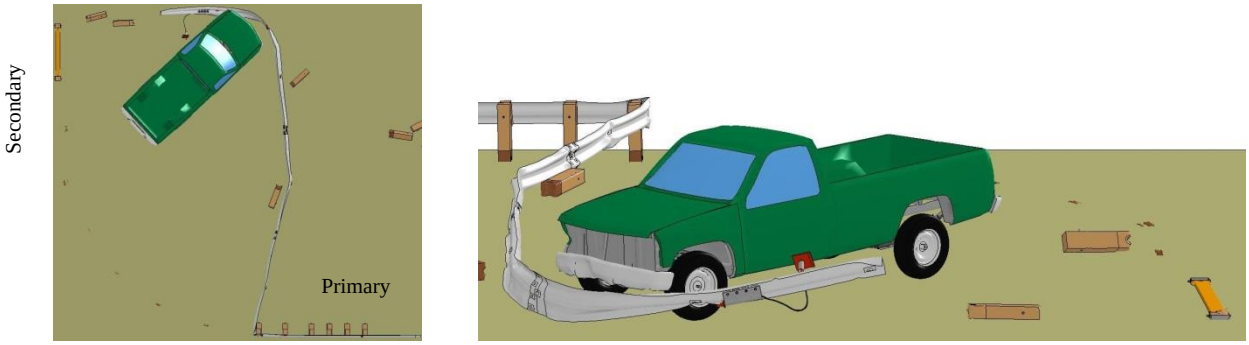

Impact at Post No. 3

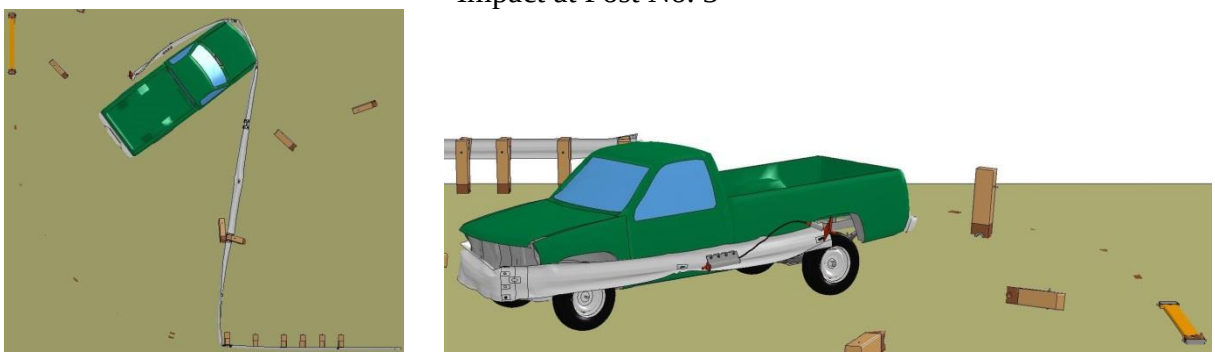

Impact at Midspan between Post Nos. 3 and 4

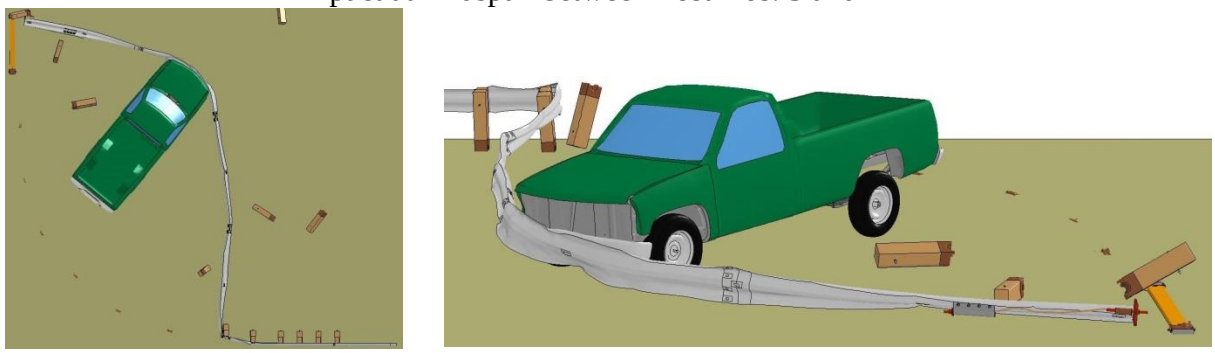

Impact at Post No. 4

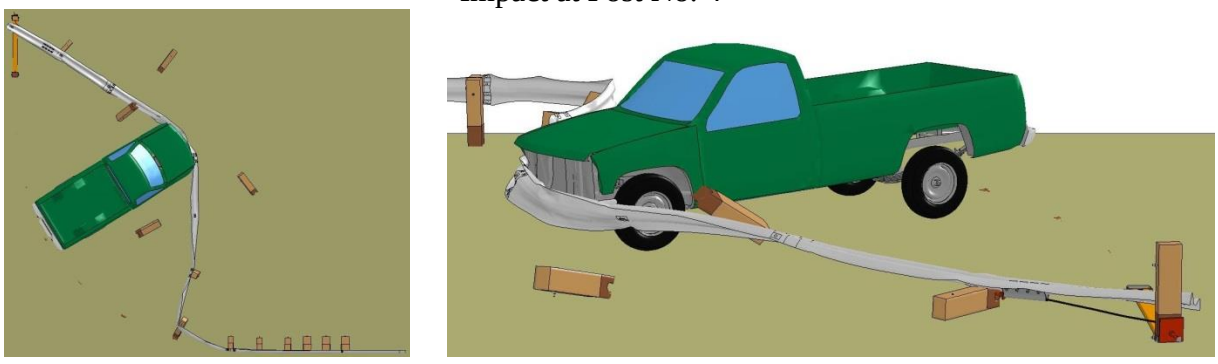

Impact at Midspan between Post Nos. 4 and 5

Figure 105. Images of Impacts with 31-in. (787-mm) Tall, 24-ft (7.3-m) Radius Systems at 45 mph (72 km/h)

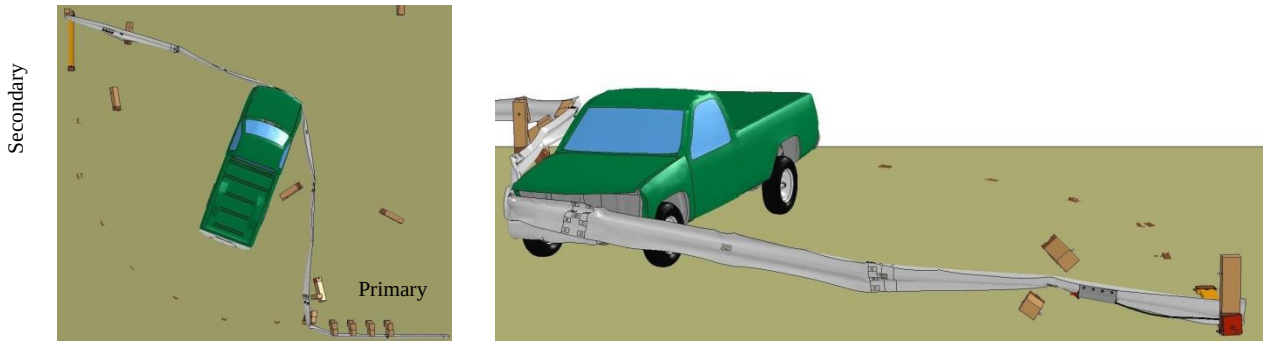

Impact at Post No. 5

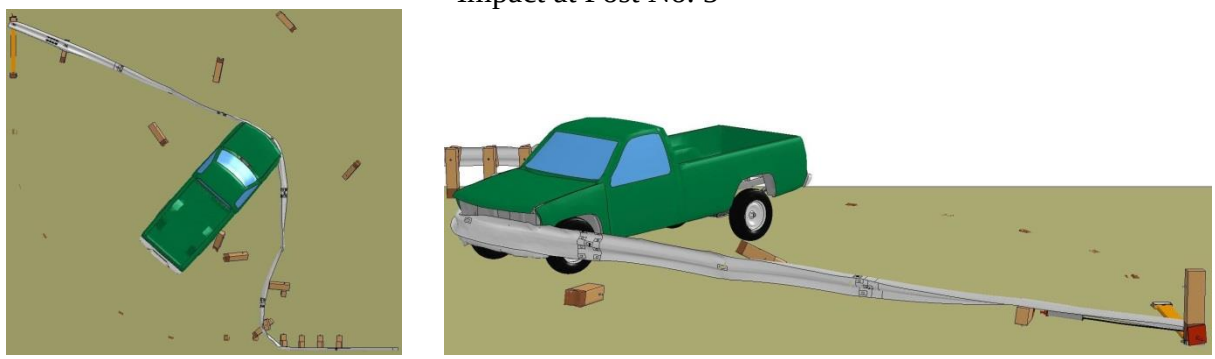

Impact at Midspan between Post Nos. 5 and 6

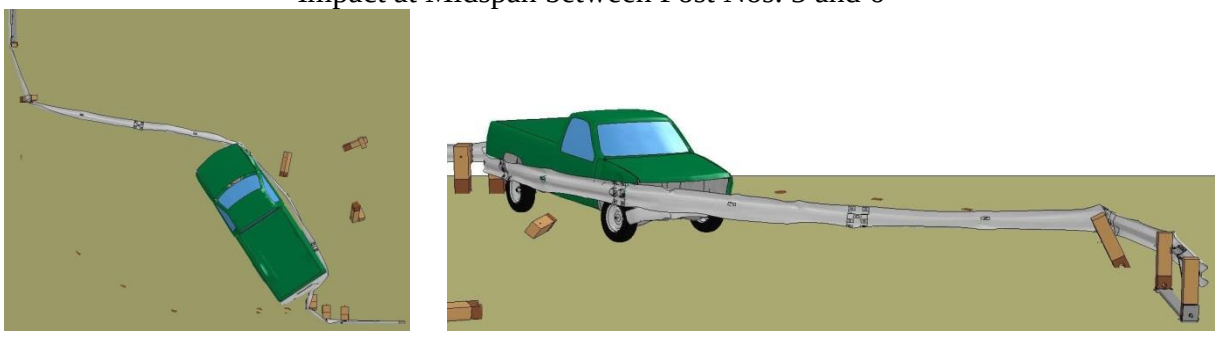

Impact at Post No. 6

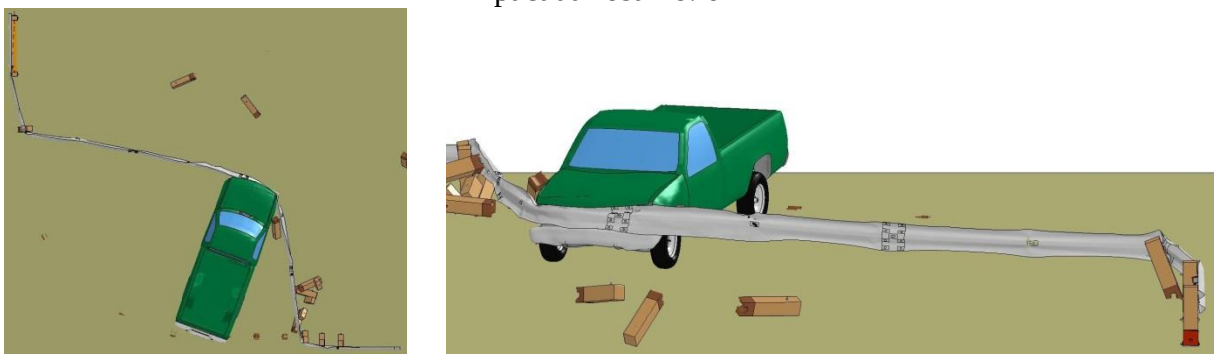

Impact at Midspan between Post Nos. 6 and 7

Figure 106. Images of Impacts with 31-in. (787-mm) Tall, 24-ft (7.3-m) Radius Systems at 45 mph (72 km/h)

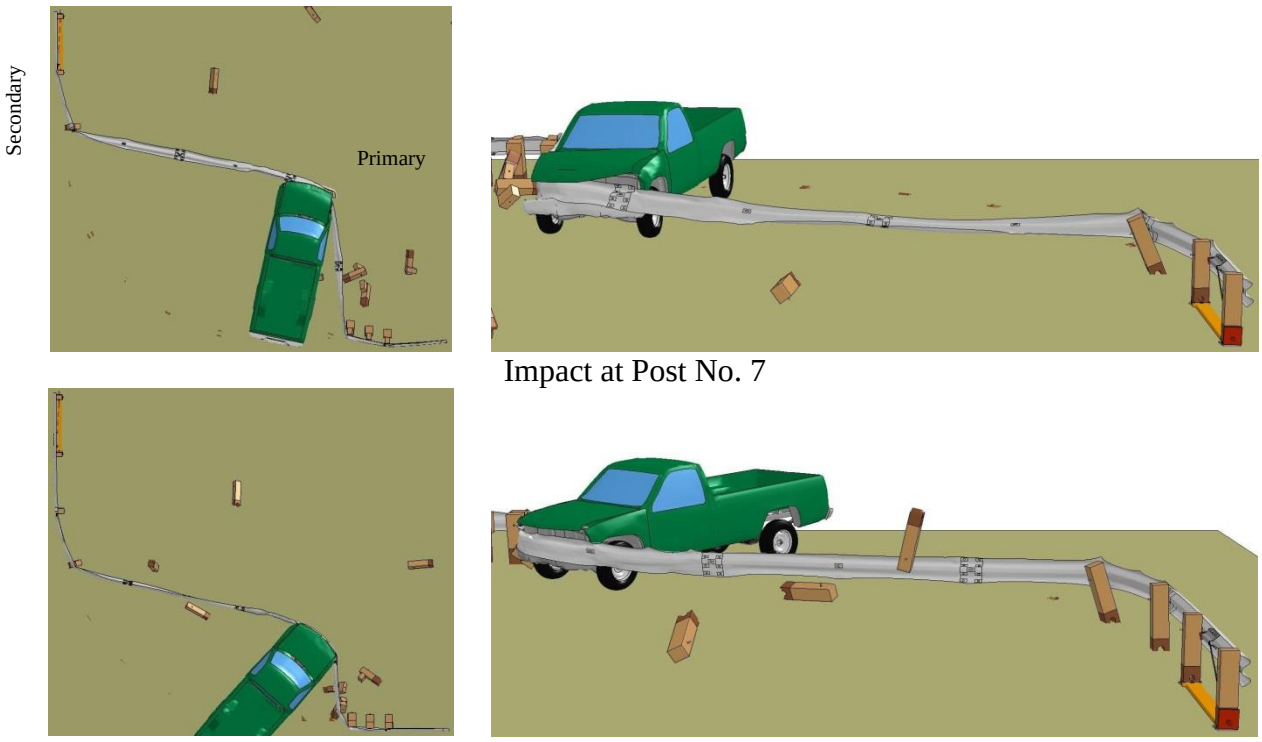

Impact at Post No. 7

Impact at Midspan between Post Nos. 7 and 8

Figure 107. Images of Impacts with 31-in. (787-mm) Tall, 24-ft (7.3-m) Radius Systems at 45 mph (72 km/h)

7.2.2 Impacts at 50 mph (80 km/h)

Based on the successful performance of the 31-in. (787-mm) tall short radius system at TL-2 impact conditions, impacts at each post location were simulated again with a 50-mph (80 km/h) impact speed to determine the maximum capacity of the system. Summary images of the performance are shown in Figure 108.

Each impact simulated between post nos. 4 and 7 resulted in the simulated vehicle gating through the system. Simulation data analysis, including evaluation of accelerations and forces, was terminated in each simulation after the downstream BCT post fractured. As stated, an MGS end anchorage was adapted to simulate the performance of the curved guardrail end anchorage. The model of the MGS end anchorage system has not been validated when an impact resulted in fracture of one BCT post, but the BCT cable remained engaged with the upstream BCT post.

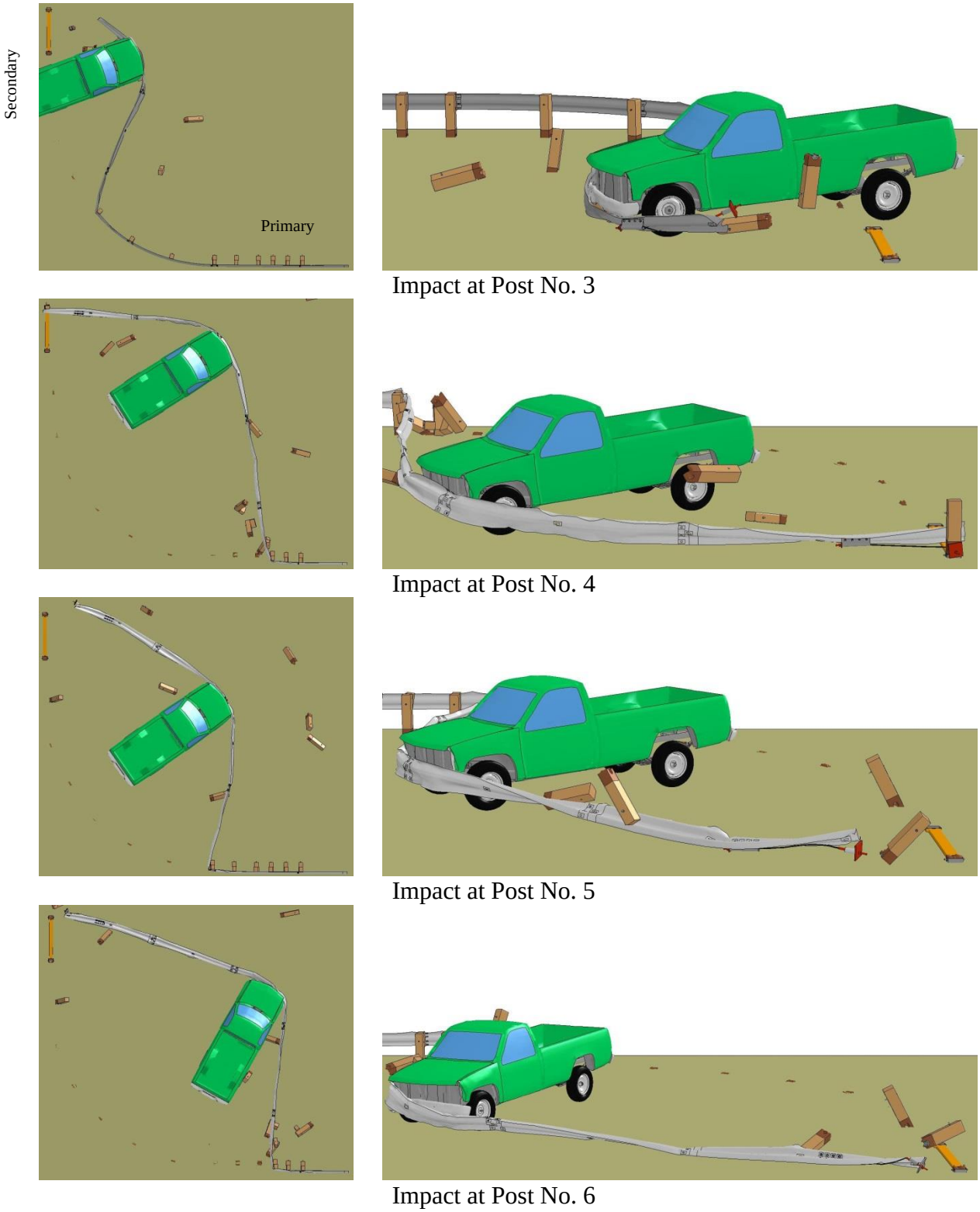

Figure 108. Images of Impacts with 31-in. (787-mm) Tall, 24-ft (7.3-m) Radius Systems at 50 mph (80 km/h)

It is possible that additional straight segments of W-beam guardrail with MGS CRT posts installed on the secondary side of the system at upstream end of the radius could result in some impact locations with acceptable capture. Additional posts on the secondary side of the roadway could be investigated in a subsequent simulation or full-scale crash testing study.

7.3 Discussion

The short-radius guardrail system with 24-ft (7.3-m) radius and 27-in. (686-mm) top rail height did not perform similarly to the Yuma County system. Whereas a 25-degree impact on the nose of the Yuma Co. system was determined to be acceptable and satisfactorily captured the vehicle, impacts into the larger radius resulted in unacceptable vaulting and penetration. By adding blockouts, rail performance improved and the pickup truck was captured in one simulation, but vaulting still occurred during impact at four other post locations.

Increasing the top rail mounting height from 27 in. (686 mm) to 31 in. (787 mm) resulted in acceptable capture of the simulated vehicle at or downstream from post no. 6. There was no tendency to vault observed in any simulation with a top rail mounting height of 31 in. (787 mm). The taller mounting height was also associated with increased deflections and lower vehicle accelerations, which may contribute to pocketing for impacts near the transition, and may increase the extent of system repairs required after an impact.

The system has not been evaluated using passenger cars, which was outside of the scope of the current study. There is some concern that a passenger car could underride or experience roof or windshield crush after impact with the guardrail mounted with a top height of 31 in. (787 mm). Nonetheless, the 31-in. (787-mm) top mounting height significantly improved rail interlock with the impacting truck. The maximum capacity of the system was exceeded for impacts occurring at 50 mph (80 km/h), resulting in vehicle penetration behind the rail. Thus, the system capacity is limited to 45 mph (72 km/h) impacts.

8 NUMERICAL SIMULATIONS OF SYSTEMS WITH 48-FT (15-M) RADII

Impacts with the 27-in. (686-mm) and 31-in. (787-mm) short radius guardrail systems with 48-ft (15-m) radii were simulated by aligning the centerline of the truck with the third, fourth, fifth, sixth, seventh, eighth, ninth, tenth, eleventh, twelfth, and thirteenth posts. Post numbers are shown in Figure 98. Results of the simulations are evaluated in Chapter 10.

8.1 Systems with 27-in. Top Mounting Height

The 27-in. (686-mm) tall, 48-ft (15-m) radius short radius system was simulated according to TL-2 impact using a 4,409-lb (2,000-kg) pickup truck impacting at 45 mph (72 km/h) and 25 degrees, relative to a tangent line to the bridge rail. After initial results with standard CRT posts indicated unacceptable performance of the curved guardrail system, 8-in. (203-mm) timber blockouts were added to the posts in an attempt to maintain the rail height after impact.

8.1.1 Systems Without Blockouts Attached to Radius Posts

The pickup truck vaulted the system at every impact location selected with a 27-in. (686-mm) mounting height, when blockouts were not utilized, as shown in Figures 109 through 111. Typically, four posts were fractured during impact before the vehicle overrode the guardrail. The best system performance occurred upstream of the center of the radius, where dynamic deflection was the largest before the vaulting occurred. Fractured post debris, posts which remained attached to the rail, flattening of the top corrugation of the W-beam, and rail twist contributed to vaulting.

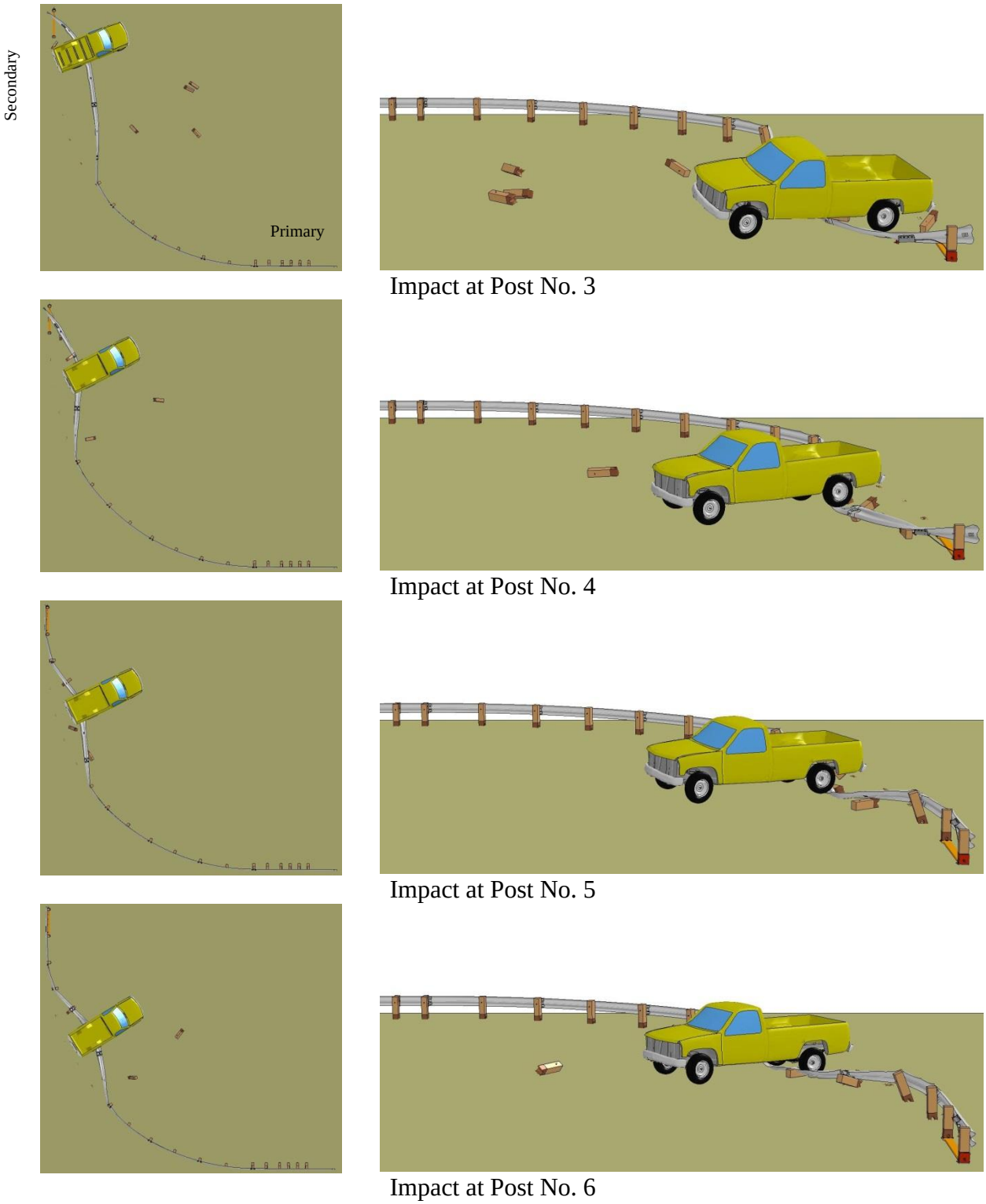

Figure 109. Images of Impacts with 27-in. (686-mm) Tall, 48-ft (15-m) Radius Systems without Blockouts Attached to Posts on Radius

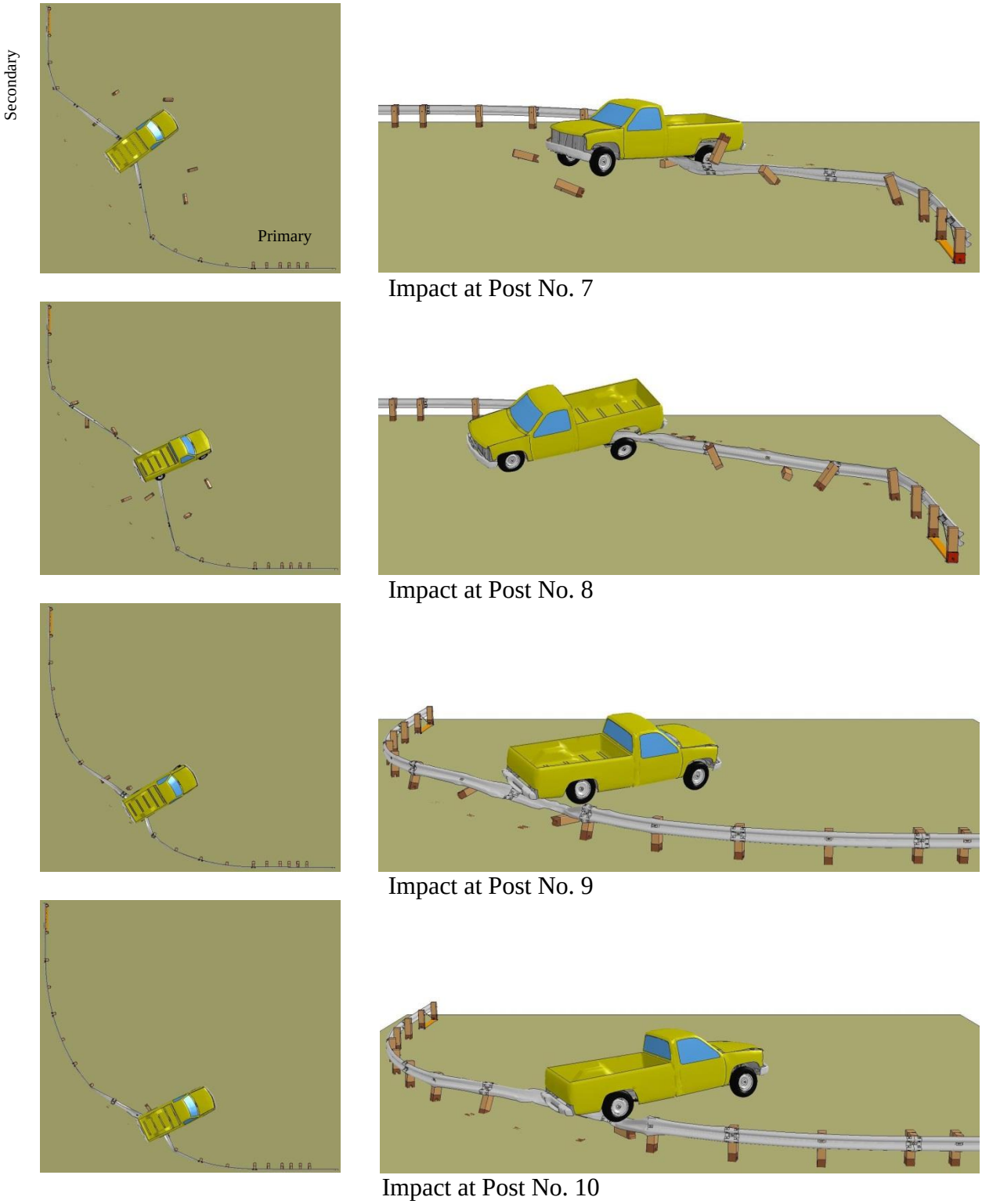

Figure 110. Images of Impacts with 27-in. (686-mm) Tall, 48-ft (15-m) Radius Systems without Blockouts Attached to Posts on Radius

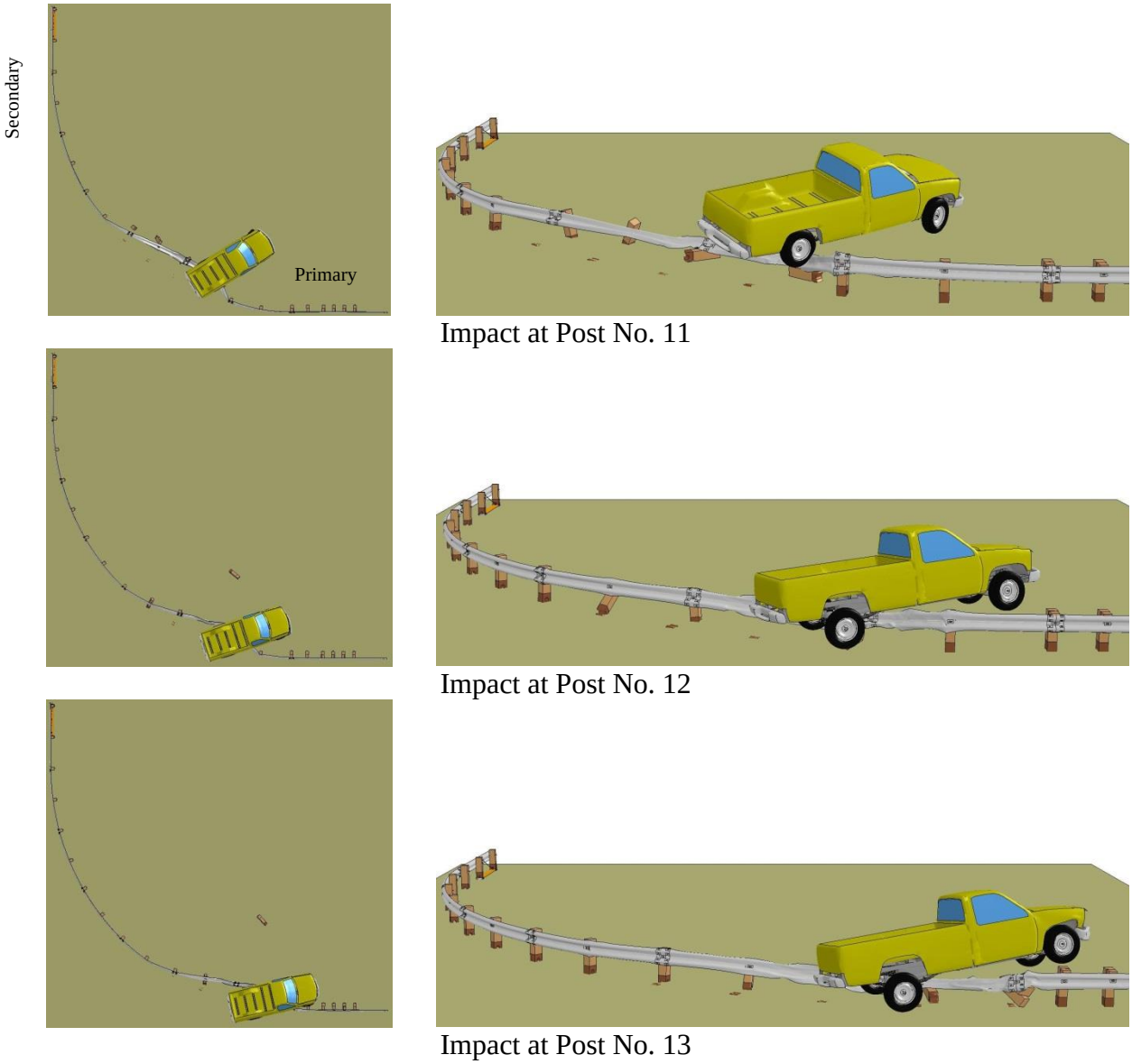

Figure 111. Images of Impacts with 27-in. (686-mm) Tall, 48-ft (15-m) Radius Systems without Blockouts Attached to Posts on Radius

8.1.2 Systems with Blockouts Attached to Radius Posts

Similar to the results of the 24-ft (7.3-m) radius, blockouts were added to the CRT posts to retain the rail height after impact and facilitate quicker post release from the rail after fracture. Simulations of the 27-in. (686-mm) tall, 48-ft (15-m) radius guardrail system with 8-in. (203-mm) blockouts are shown in Figures 112 through 114.

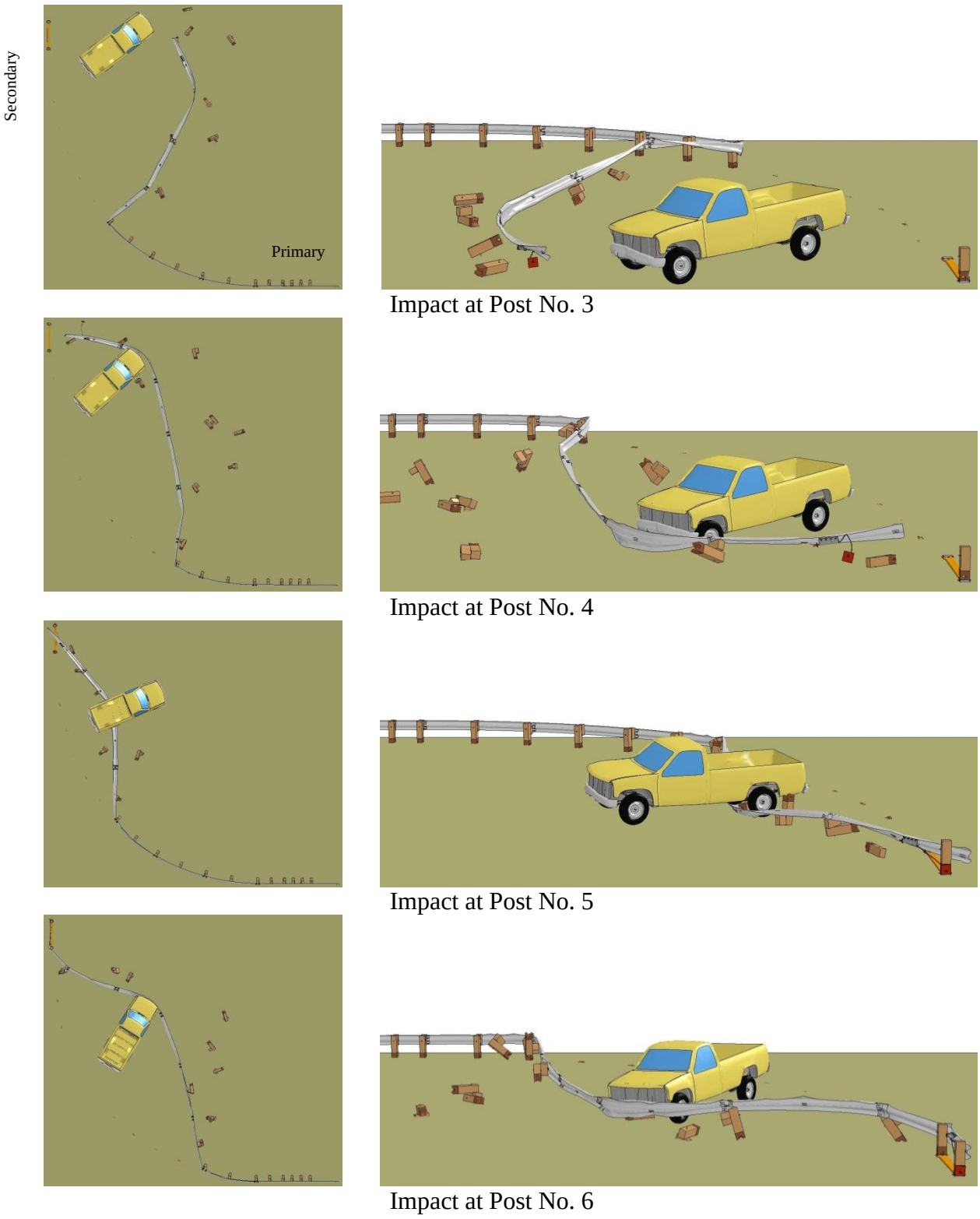

Figure 112. Images of Impacts with 27-in. (686-mm) Tall, 48-ft (15-m) Radius Systems with Blockouts Attached to Radius Posts

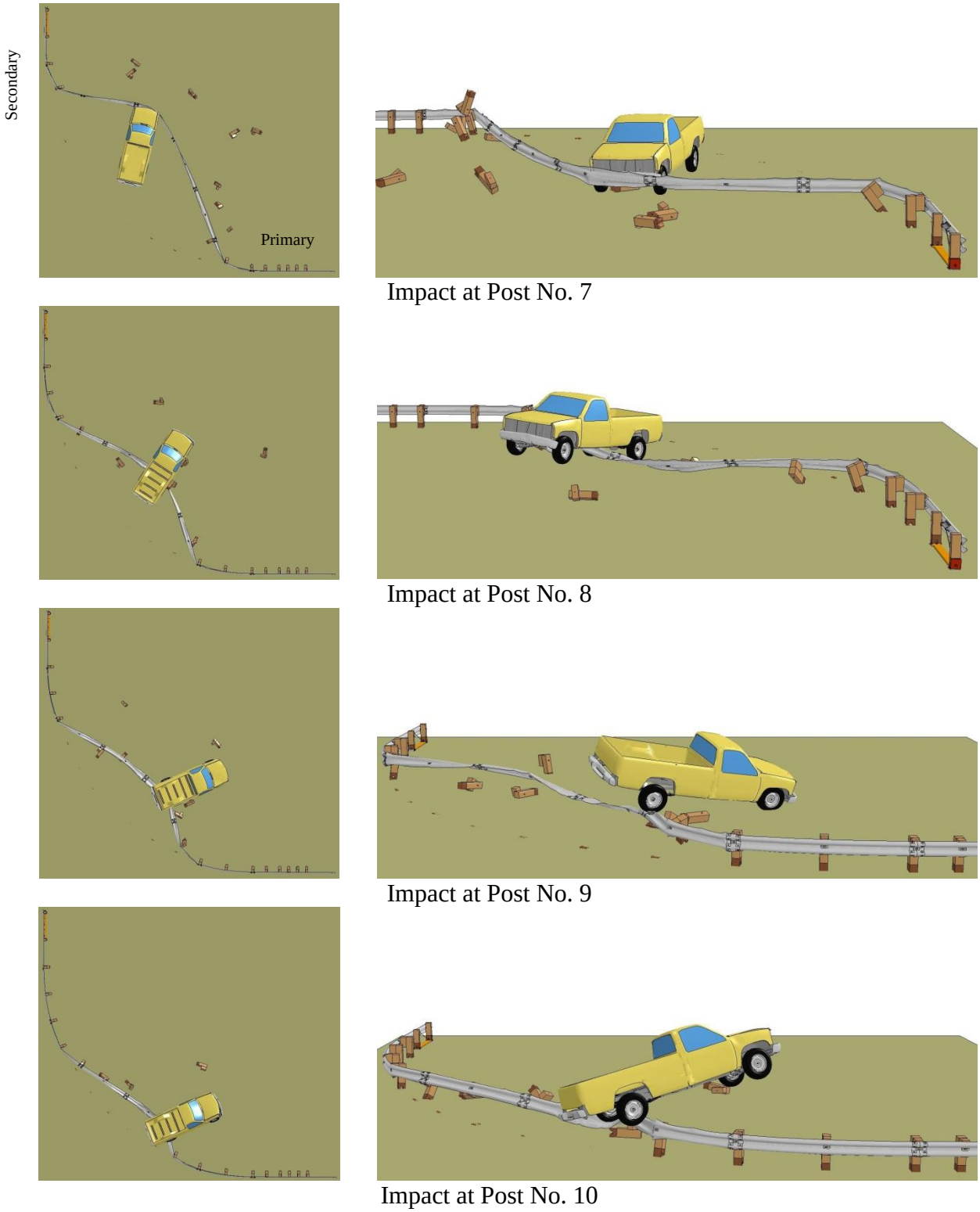

Figure 113. Images of Impacts with 27-in. (686-mm) Tall, 48-ft (15-m) Radius Systems with Blockouts Attached to Radius Posts

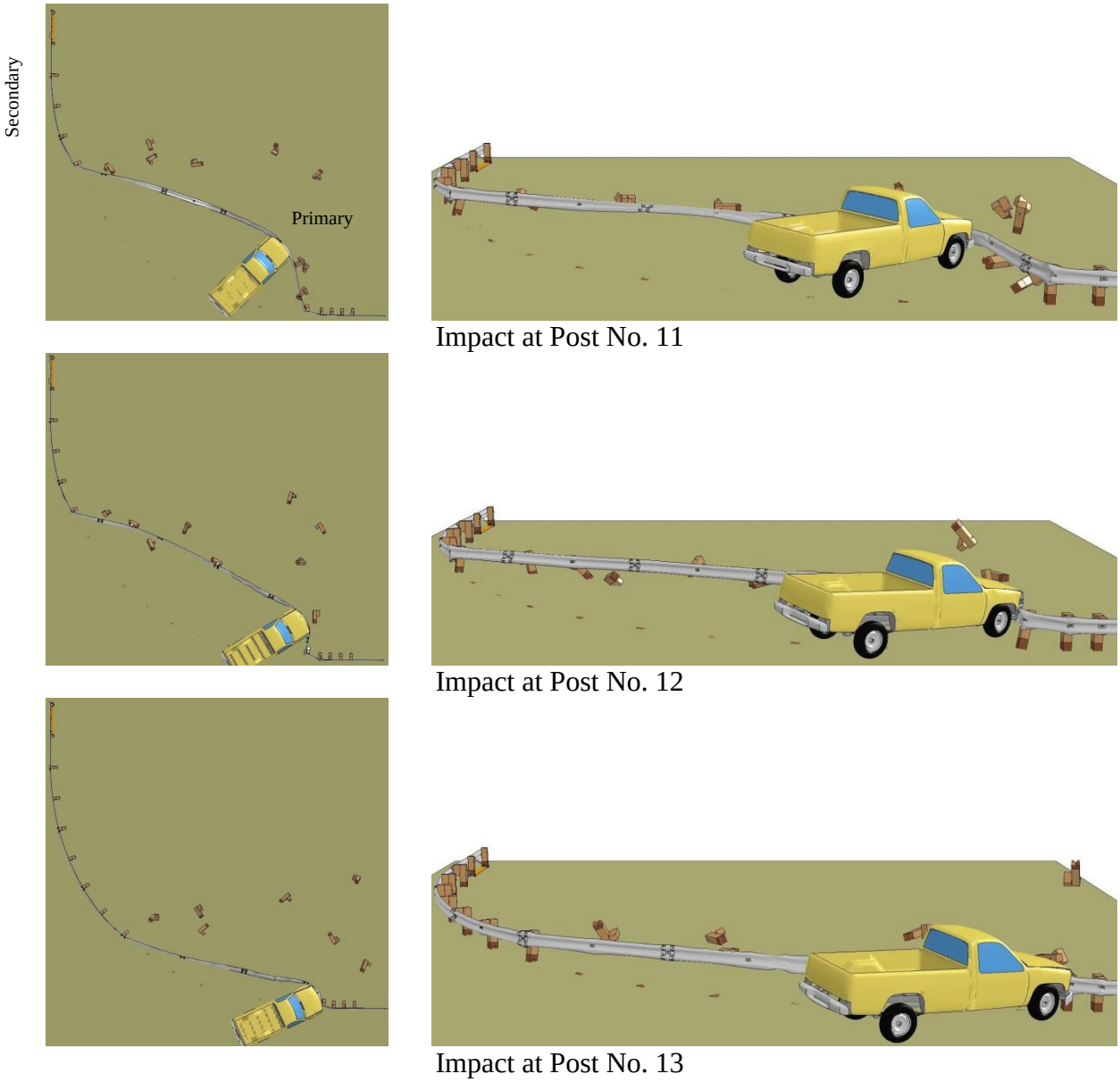

Figure 114. Images of Impacts with 27-in. (686-mm) Tall, 48-ft (15-m) Radius Systems with Blockouts Attached to Radius Posts

The system performance improved after blockouts were added. Five of the eight simulated impacts at post locations occurring downstream of post no. 5 resulted in capture. Impacts at post nos. 8, 9, and 10, which spanned between the centerpoint of the radius to two posts downstream, resulted in override and vaulting.

8.2 Systems with 31-in. (787-mm) Top Mounting Height

8.2.1 Impacts at 45 mph (72 km/h)

Results of the simulations are shown in Figures 115 through 117. Each impact downstream of post no. 6 resulted in vehicle capture, and impacts at or upstream from post no 6 resulted in at least one BCT post fracture and could result in gating during a crash.

After engaging the bumper, the rail flattened and slid upward and became interlocked with the headlight, grill, and radiator locations. This interlock improved vehicle stability and reduced the tendency to vault, even when the truck interacted with post debris. Between 8 and 12 posts fractured during each impact within the radius. The truck was captured upstream of post no. 13, and no impacts resulted in redirection.

8.2.2 Impacts at 50 mph (80 km/h)

The 31-in. (787-mm) tall short radius system was also simulated at a higher impact speed of 50 mph (80 km/h) based on the successful performance of the system at 45 mph (72 km/h). Summary images of the performance are shown in Figures 118 through 120. At least one BCT post fractured for each simulated impact location upstream of post no. 8. The vehicle was captured at and downstream from post no. 8. By the end of the simulations, a minimum of 10 posts fractured for each impact location between post nos. 7 and 11, and as many as 15 posts may fracture before vehicles come to a complete stop. The vehicle was not redirected at any impact location; each simulated impact resulted in either gating or capture.

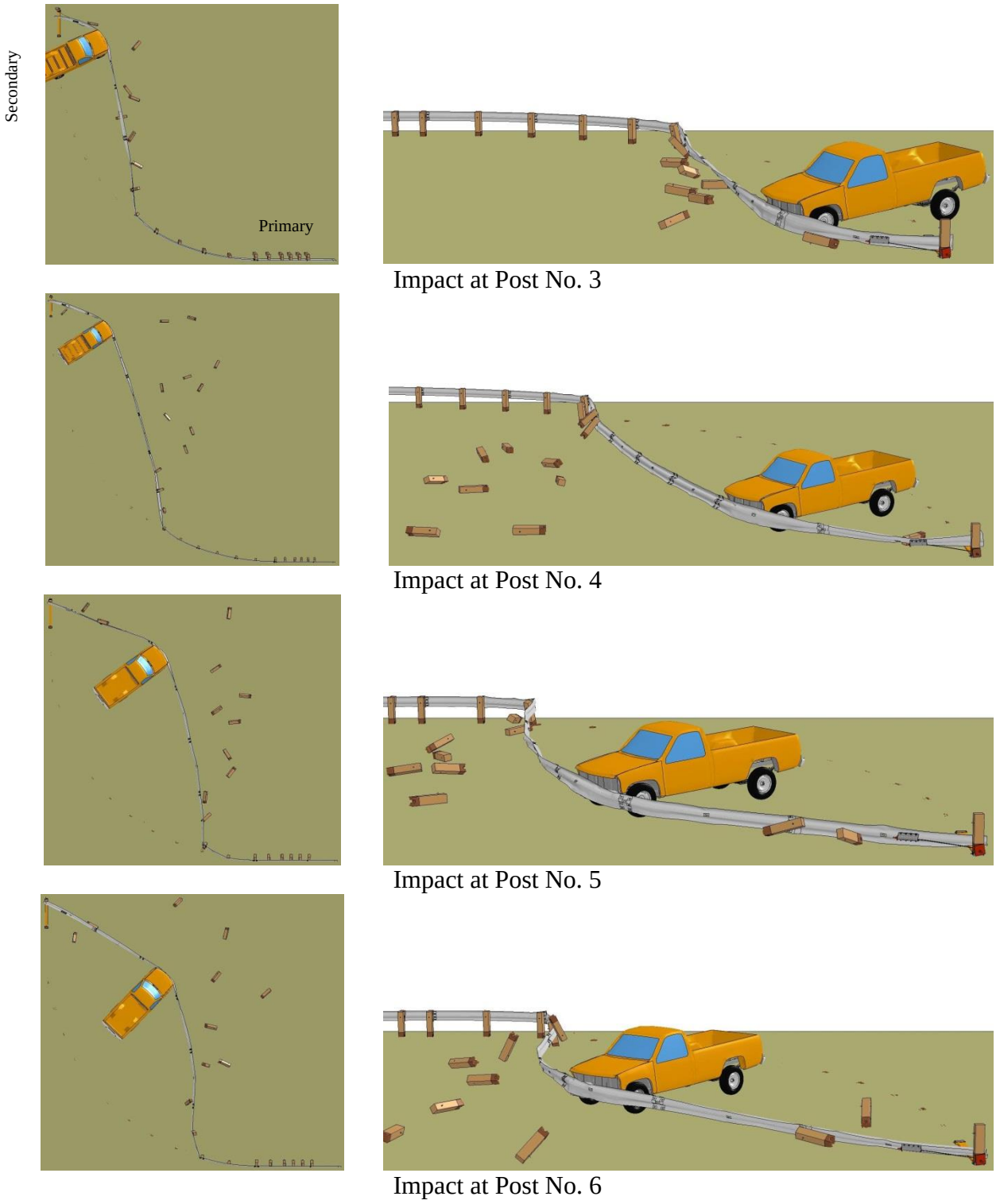

Figure 115. Images of Impacts with 31-in. (787-mm) Tall, 48-ft (15-m) Radius Systems at 45 mph (72 km/h)

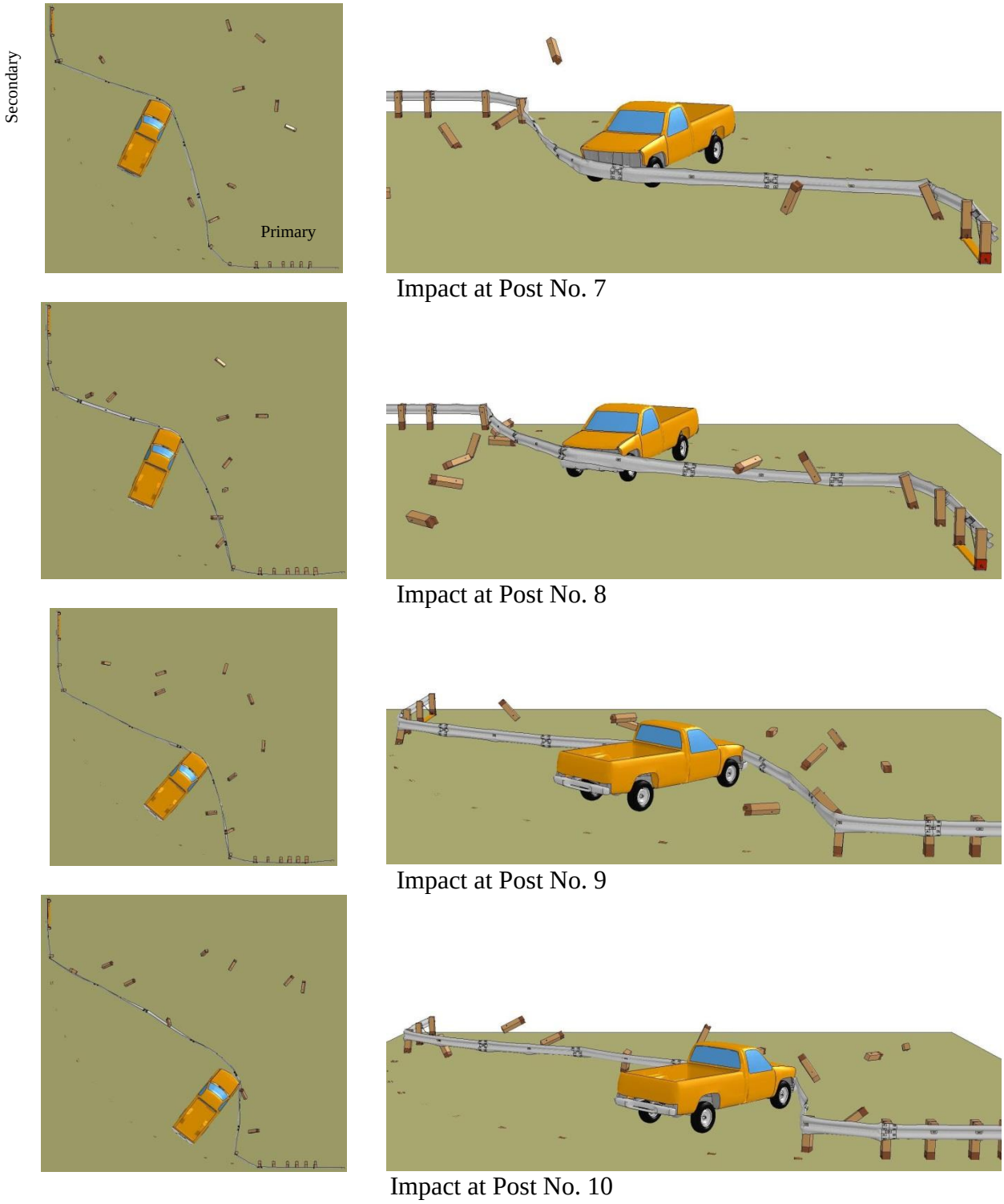

Figure 116. Images of Impacts with 31-in. (787-mm) Tall, 48-ft (15-m) Radius Systems at 45 mph (72 km/h)

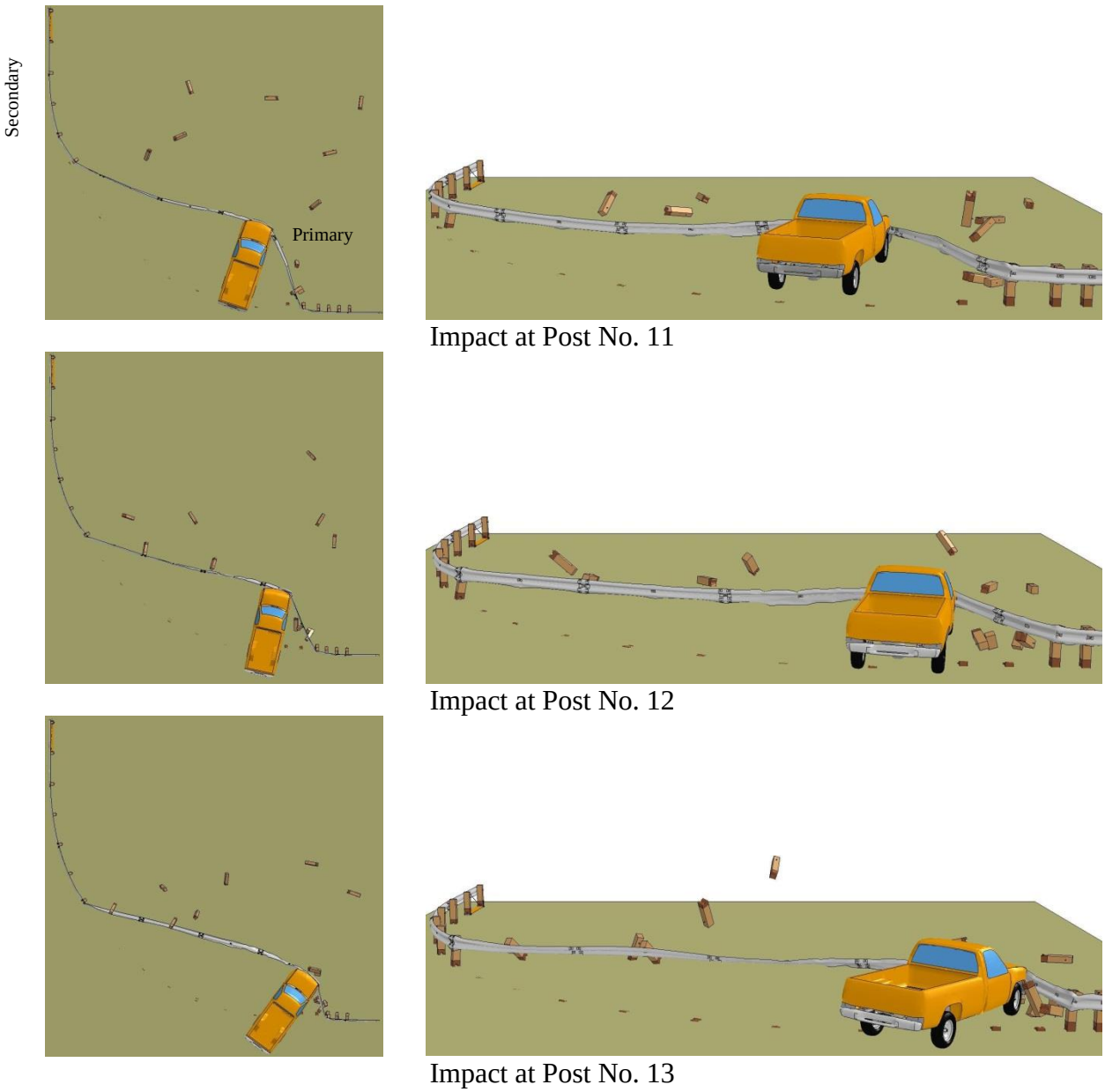

Figure 117. Images of Impacts with 31-in. (787-mm) Tall, 48-ft (15-m) Radius Systems at 45 mph (72 km/h)

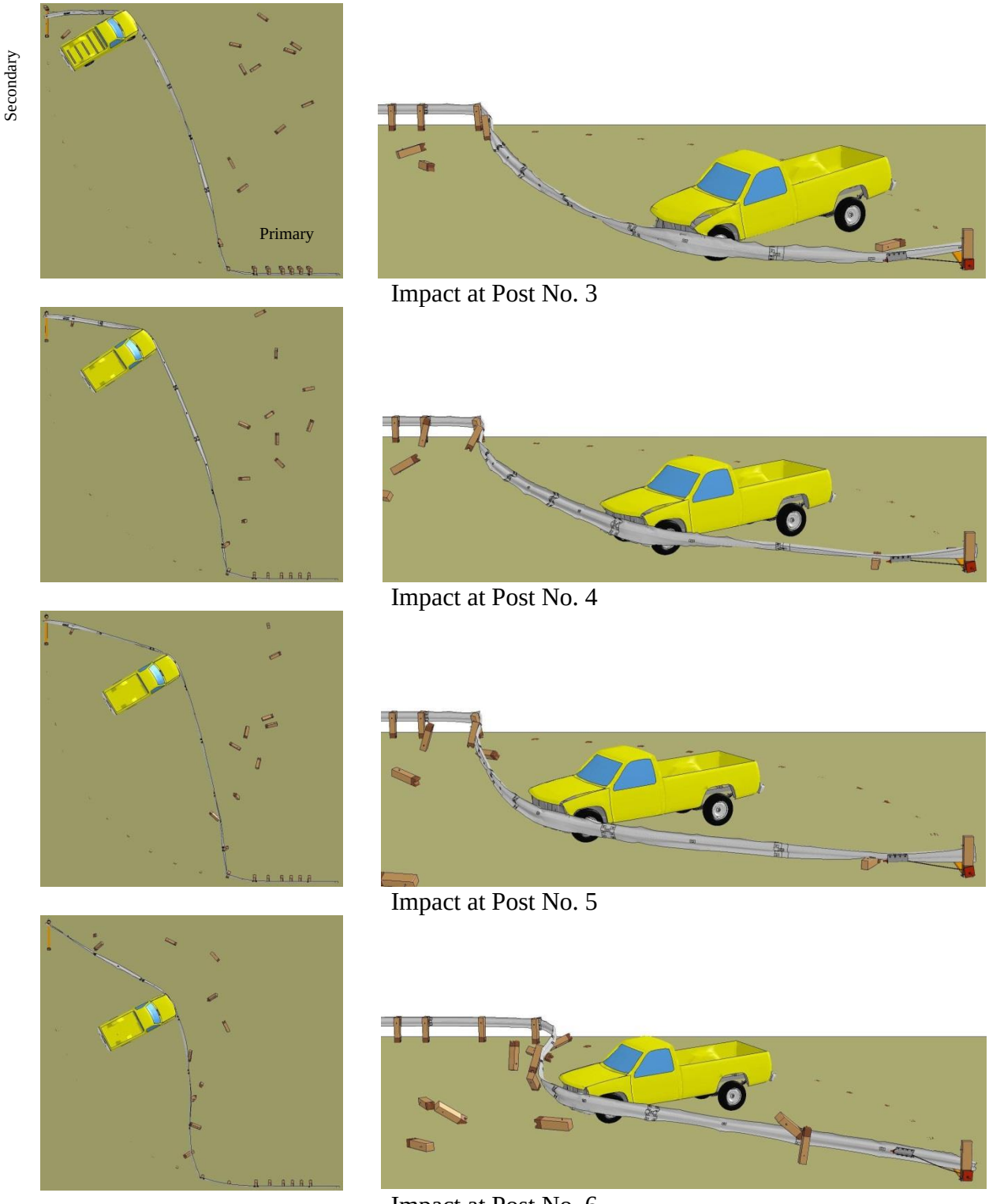

Figure 118. Images of Impacts with 31-in. (787-mm) Tall, 48-ft (15-m) Radius Systems at 50 mph (80 km/h)

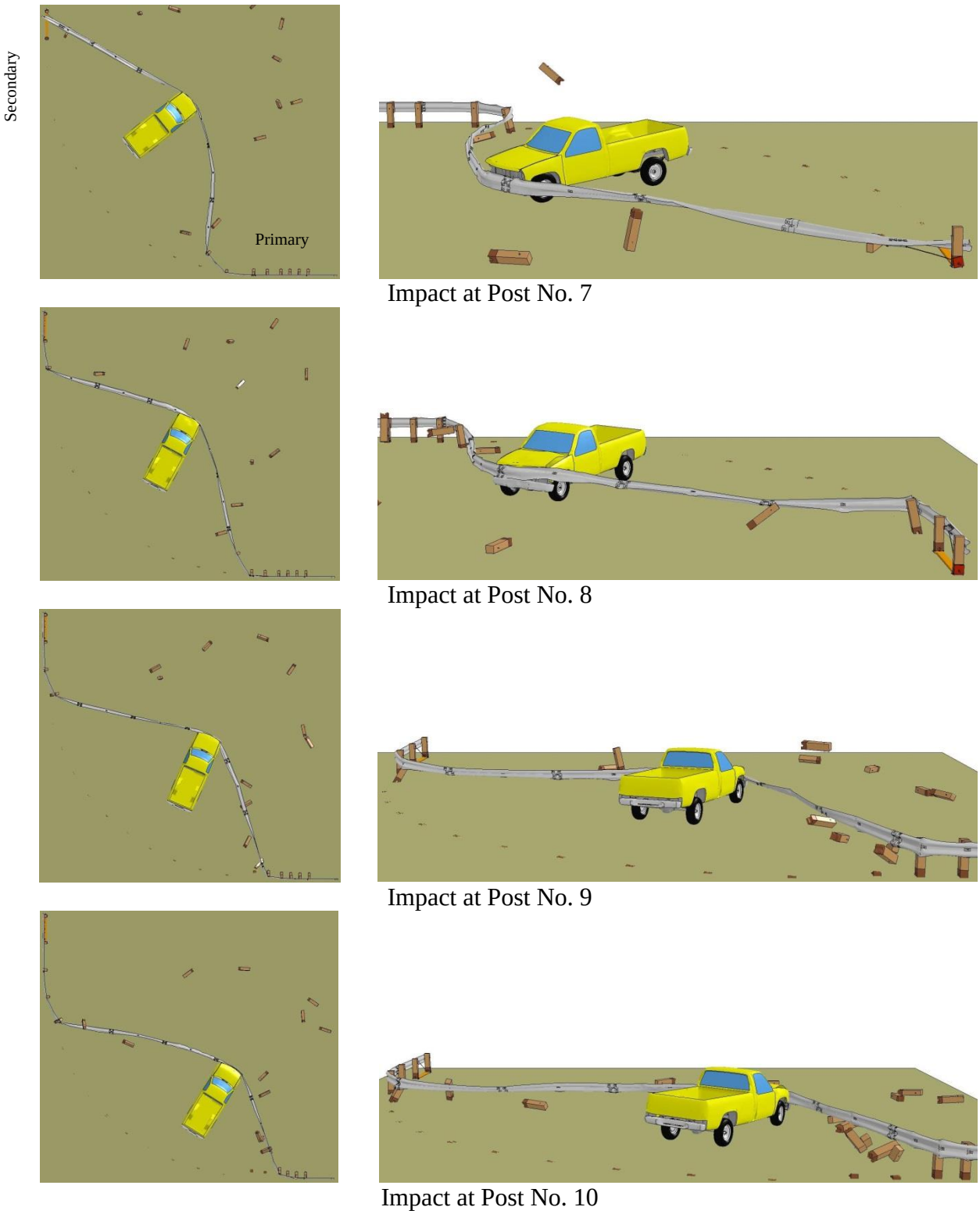

Figure 119. Images of Impacts with 31-in. (787-mm) Tall, 48-ft (15-m) Radius Systems at 50 mph (80 km/h)

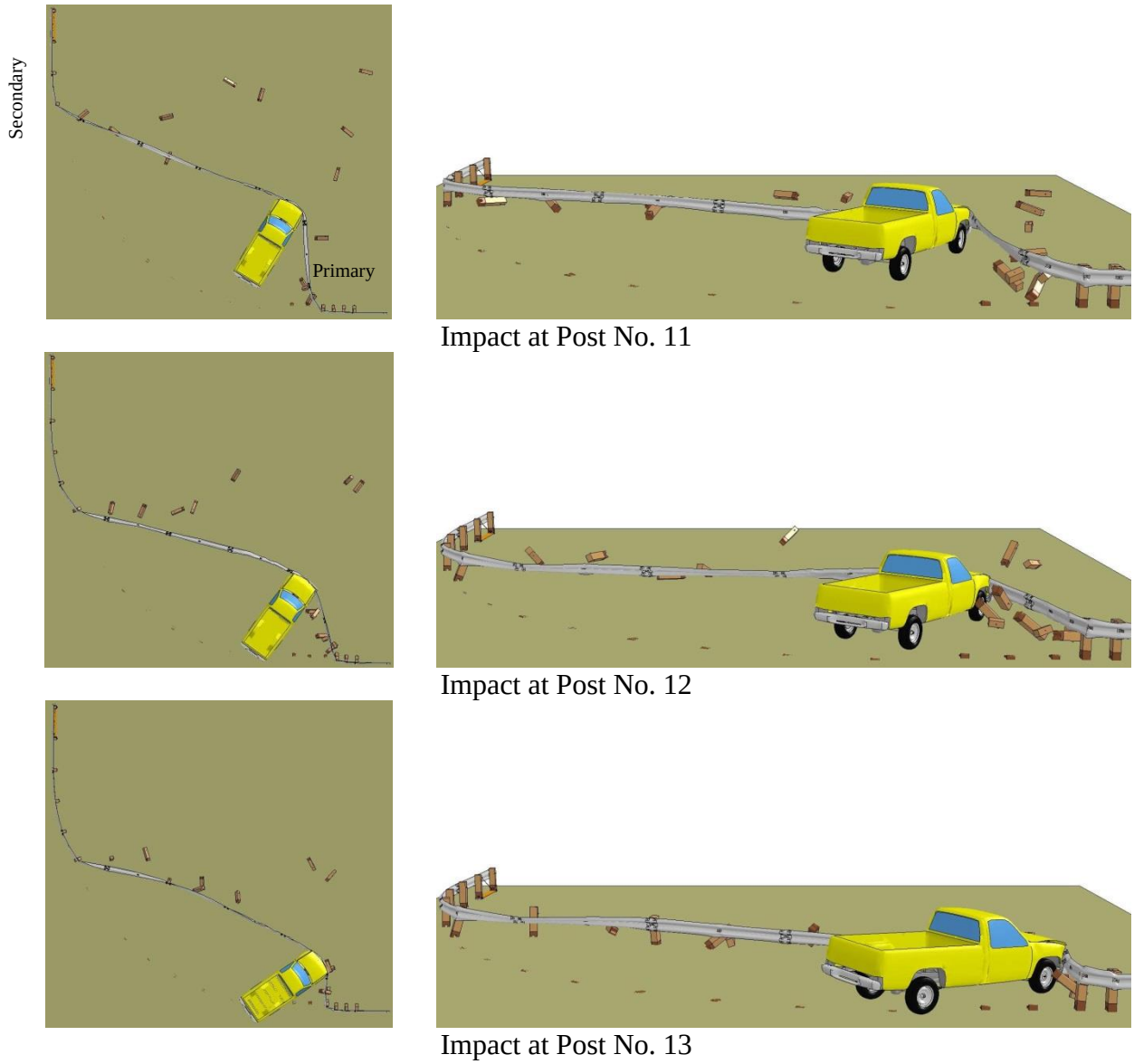

Figure 120. Images of Impacts with 31-in. (787-mm) Tall, 48-ft (15-m) Radius Systems at 50 mph (80 km/h)

8.3 Discussion

Higher guardrail installation heights contributed to improved capture and a reduced vaulting propensity for impacts with 2000P pickup truck vehicles. No simulations involving non-blocked 27-in. (686-mm) tall curved-guardrail resulted in vehicle capture or redirection, whereas five simulations of 27-in. (686-mm) tall systems with blockouts conducted at 45 mph (72 km/h) and 25 degrees captured the simulated vehicle. In comparison, nine of the 11 simulations

conducted at 45 mph (72 km/h) and 25 degrees into a non-blocked, 31-in. (787-mm) tall system successfully captured or redirected the vehicle, and the remaining two simulations involved the end terminal gating to allow the vehicle to pass by. Increased rail heights improved rail engagement with the bumper and decreased rail twisting tendencies which promoted vaulting at lower guardrail heights.

Vaulting and override times recorded for each impact indicated that impacts near the centerpoint of the radius demonstrated the greatest instability. Impacts at post no. 10 resulted in vaulting at 82 and 135 ms for 27-in. (686-mm) tall systems without and with blockouts, respectively. Between post nos. 8 and 10, the duration of rail engagement with the bumper was less than 300 ms for systems with blockouts, and less than 130 ms for systems without blockouts. These impact locations may be critical to the performance of this system.

Passenger car impacts were not within the scope of the current study. Passenger cars may experience underride or roof or windshield crush after impact with the guardrail with a top height of 31 in. (787 mm). Additional simulations and full-scale testing may be necessary to determine the underride propensity. Nonetheless the 31-in. (787-mm) tall guardrail system adequately captured the pickup truck for most impacts occurring at 45 mph (72 km/h), and all impacts at or downstream from post no. 8.

To capture the vehicle upstream from post no. 8, additional straight sections of guardrail to the upstream end of the radius between the end anchor and the end of the radius may be beneficial. If additional anchoring capacity is required, two end anchorages could be used: one at the upstream end of the radius and another anchorage installed upstream of the radius, with additional straight W-beam guardrail installed between the anchors.

9 NUMERICAL SIMULATIONS OF SYSTEMS WITH 72-FT (22-M) RADII

Impacts with the 27-in. (686-mm) and 31-in. (787-mm) short radius guardrail systems with 72-ft (22-m) radii were simulated by aligning the centerline of the truck with the center of post nos. 4, 5, 7, 9, 11, 13, 15, 17, and 19. Post numbers are shown in Figure 99. Results of the simulations are evaluated in Chapter 10.

9.1 Systems with 27-in. Top Mounting Height

The 27-in. (686-mm) tall short-radius system was simulated according to TL-2 impact using a 4,409-lb (2,000-kg) pickup truck impacting at 45 mph (72 km/h) and 25 degrees, relative to a tangent line to the bridge rail. After results with standard CRT posts indicated unacceptable performance of the short radius, 8-in. (203-mm) timber blockouts were added to the posts in an attempt to maintain the rail height after impact.

9.1.1 Systems Without Blockouts

At most impact locations, the pickup truck model overrode and vaulted the short-radius system, as shown in Figures 121 through 123. The truck was redirected during impact at post no. 19. During impact at post no. 9, which was slightly upstream from impact, the system captured the vehicle and slowed it to a controlled stop. Fractured post debris, posts which remained attached to the rail, and flattening of the upper rail corrugation and rail twisting, and subsequent rail slip below the bumper were the most common contributors to vaulting. Of the three radii simulated, 24, 48, and 72 ft (7.3, 15, and 22 m), posts remaining attached to the rail had the least effect on vehicle capture with the 72 ft (22 m) radius.

9.1.2 Systems with Blockouts Attached to Radius Posts

An effort was made to reduce the risk of override by placing 8-in. (203-mm) blockouts between the posts and guardrail. Simulation results are shown in Figures 124 through 126. Blockouts improved system performance compared to the unblocked system, with four

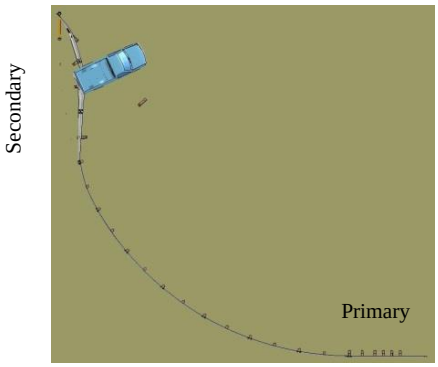

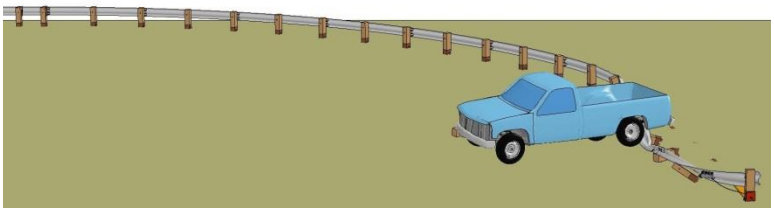

Impact at Post No. 4

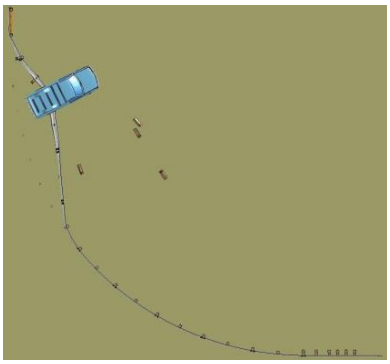

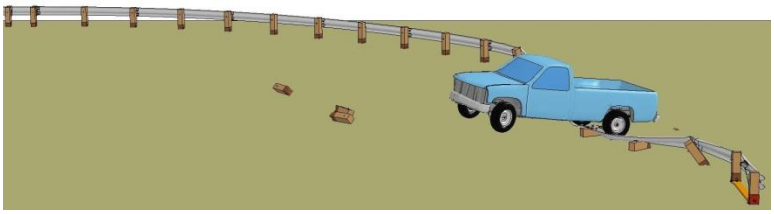

Impact at Post No. 5

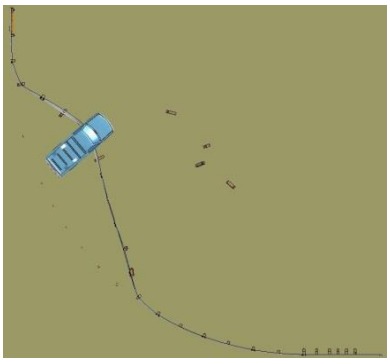

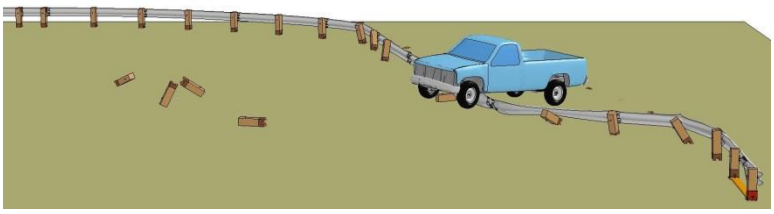

Impact at Post No. 7

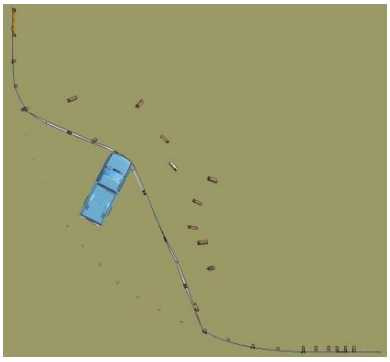

Impact at Post No. 9

Figure 121. Images of Impacts with 27-in. (686-mm) Tall, 72-ft (22-m) Radius Systems without Blockouts Attached to Posts on Radius

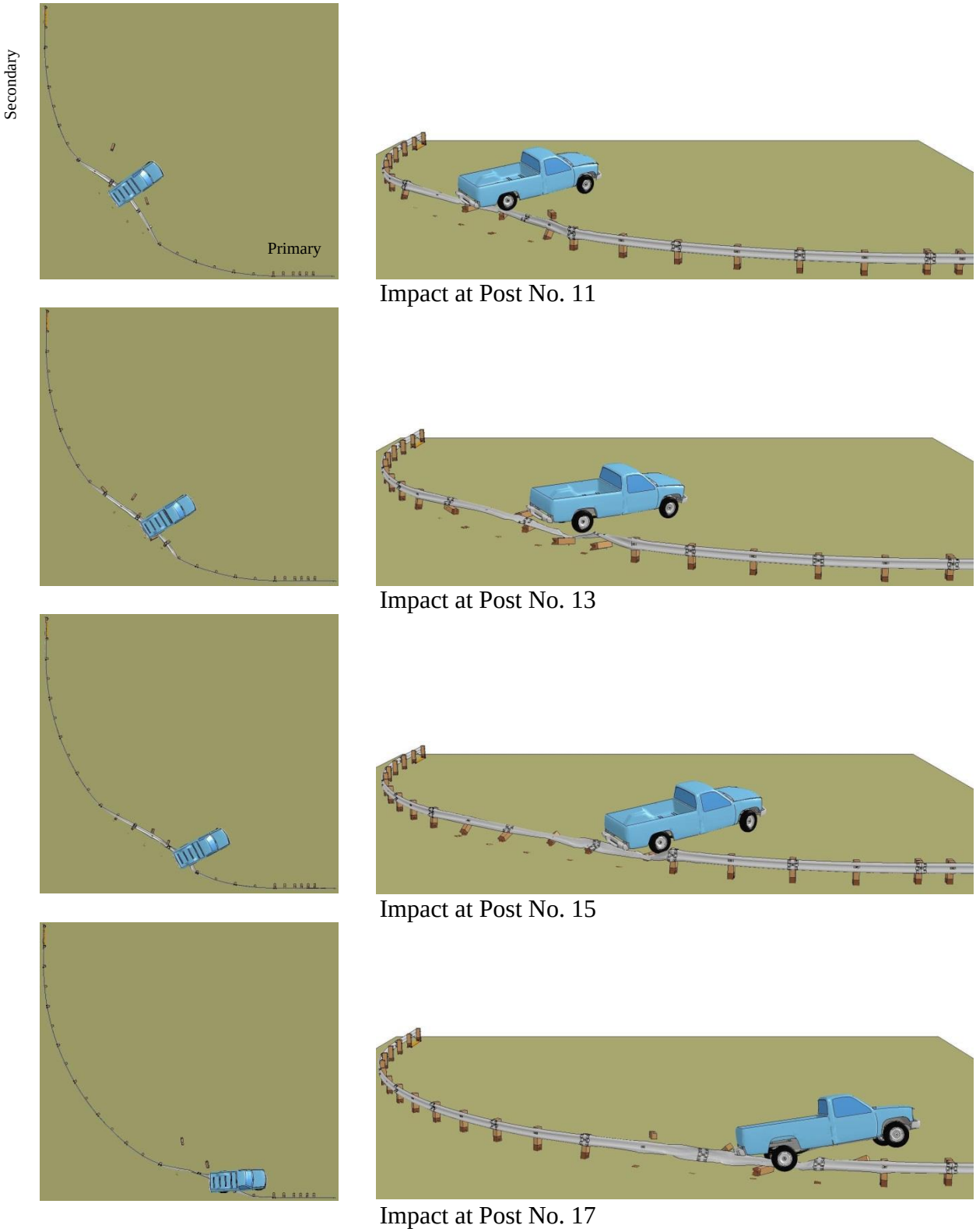

Figure 122. Images of Impacts with 27-in. (686-mm) Tall, 72-ft (22-m) Radius Systems without Blockouts Attached to Posts on Radius

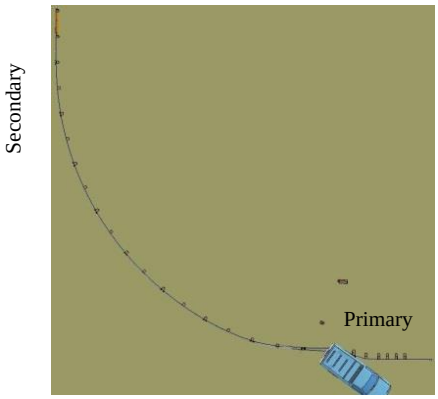

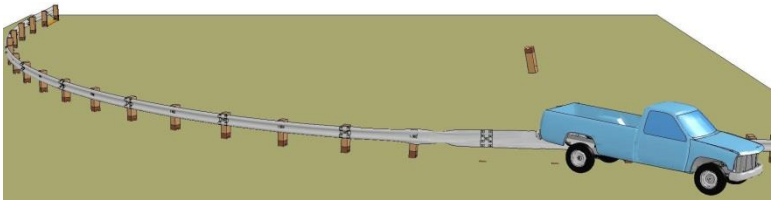

Impact at Post No. 19

Figure 123. Images of Impacts with 27-in. (686-mm) Tall, 72-ft (22-m) Radius Systems without Blockouts Attached to Posts on Radius

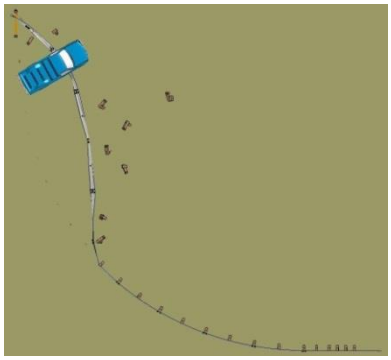

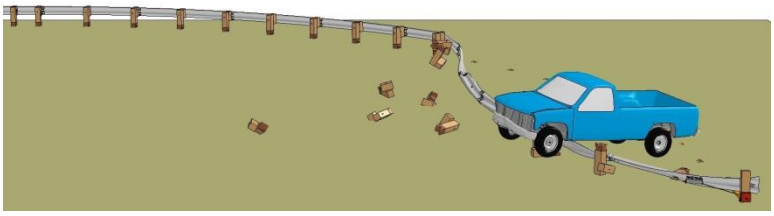

Impact at the Post No. 4

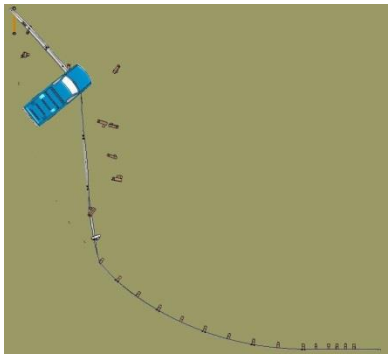

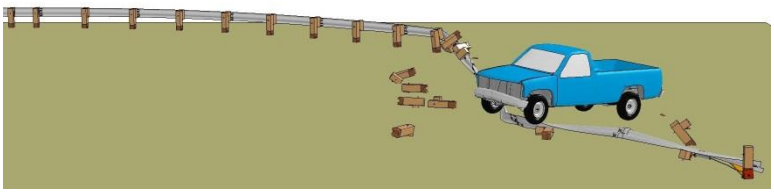

Impact at Post No. 5

Figure 124. Images of Impacts with 27-in. (686-mm) Tall, 72-ft (22-m) Radius Systems with Blockouts Attached to Radius Posts

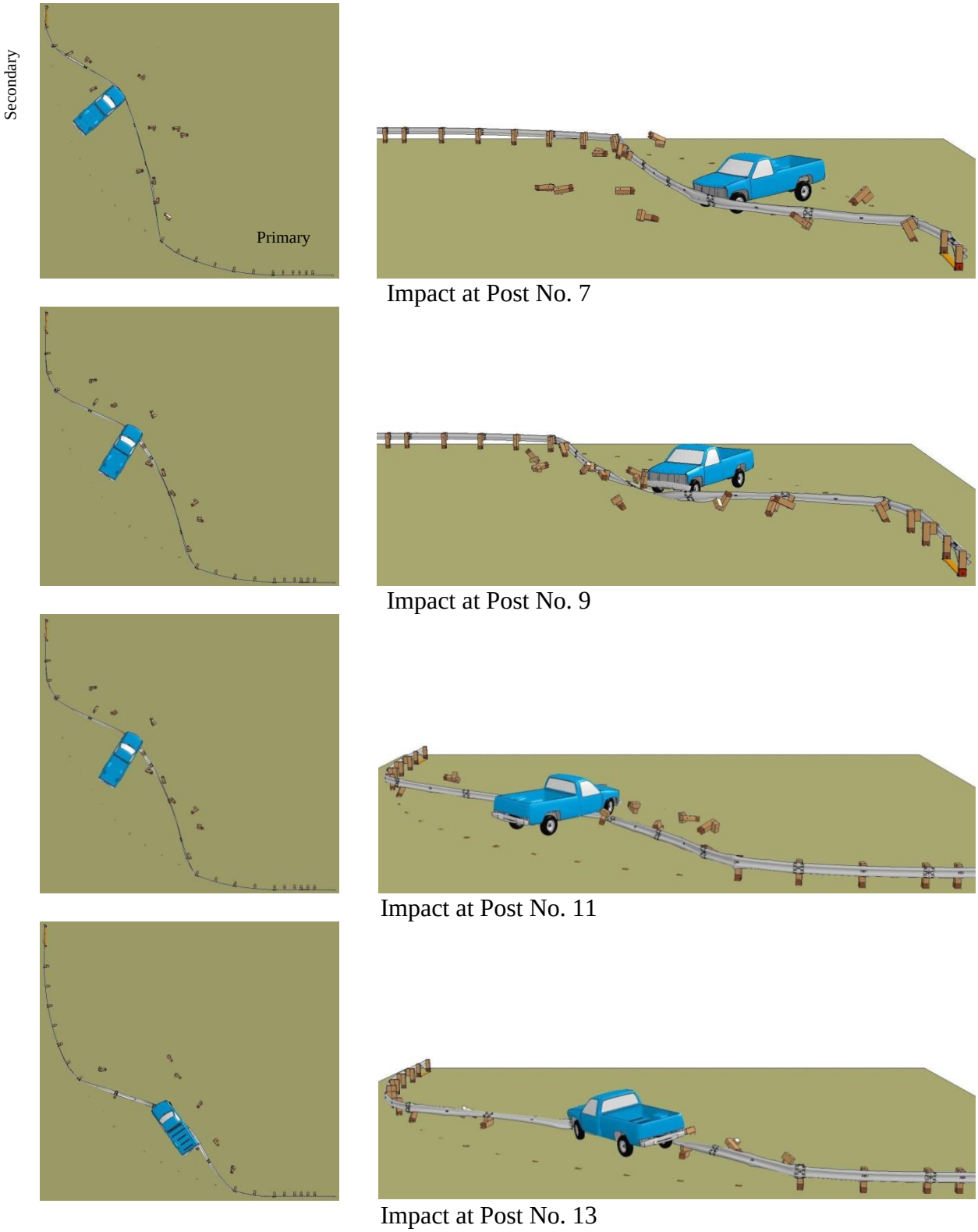

Figure 125. Images of Impacts with 27-in. (686-mm) Tall, 72-ft (22-m) Radius Systems with Blockouts Attached to Radius Posts

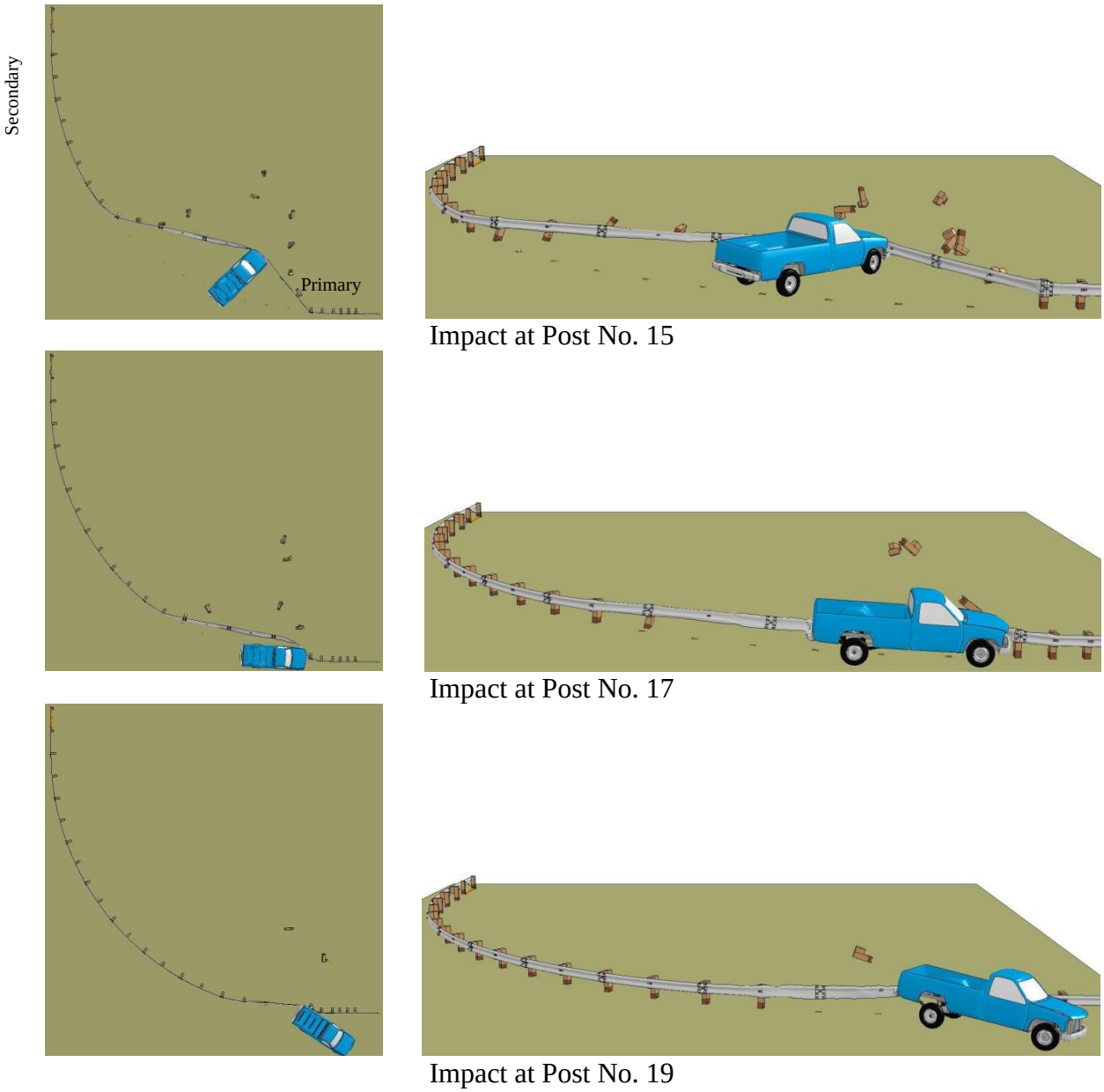

Figure 126. Images of Impacts with 27-in. (686-mm) Tall, 72-ft (22-m) Radius Systems with Blockouts Attached to Radius Posts

simulations resulting in acceptable system capture and one simulation resulting in redirection of the truck near the stiff bridge rail transition.

9.2 Systems with 31-in. (787-mm) Top Mounting Height

9.2.1 Impacts at 45 mph (72 km/h)

As observed with the 24-ft (7.3-m) and 48-ft (15-m) radii simulations, the 31-in. (787-mm) tall barriers were better able to capture or redirect the impacting pickup truck model, as shown in Figures 127 through 129. After engaging the bumper, the rail flattened and slid upward and became interlocked with the headlights, grill, and radiator locations. This interlock improved vehicle stability and reduced the tendency to vault, even when the truck interacted with post debris. Impacts downstream of post no. 7 resulted in acceptable vehicle capture or redirection when impacted at 45 mph (72 km/h) and 25 degrees, and impacts at or upstream of post no. 7 allowed the vehicle to gate through the upstream end of the system.

9.2.2 Impacts at 50 mph (80 km/h)

The 31-in. (787-mm) tall short radius system was simulated using a higher impact speed based on the successful performance of the system at 45 mph (72 km/h). Summary images of the performance are shown in Figures 130 and 131. Although the rail generally engaged the bumper at an acceptable height to capture the vehicle and no vaulting tendency was observed, the system either did not have sufficient capacity to redirect an errant vehicle impacting anywhere upstream of post no. 8, or results were inconclusive. Impact at post no. 11 resulted in unexpected fracture of the downstream BCT anchor post.

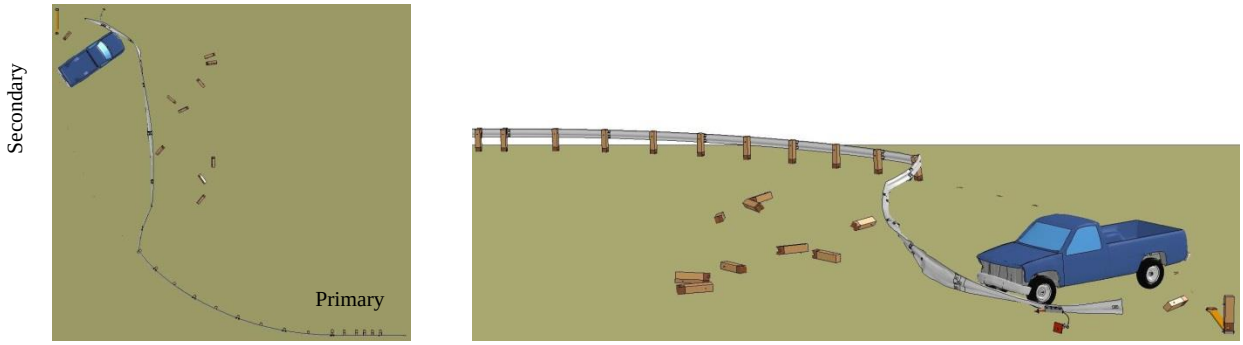

Impact at the Midspan between Post Nos. 3 and 4

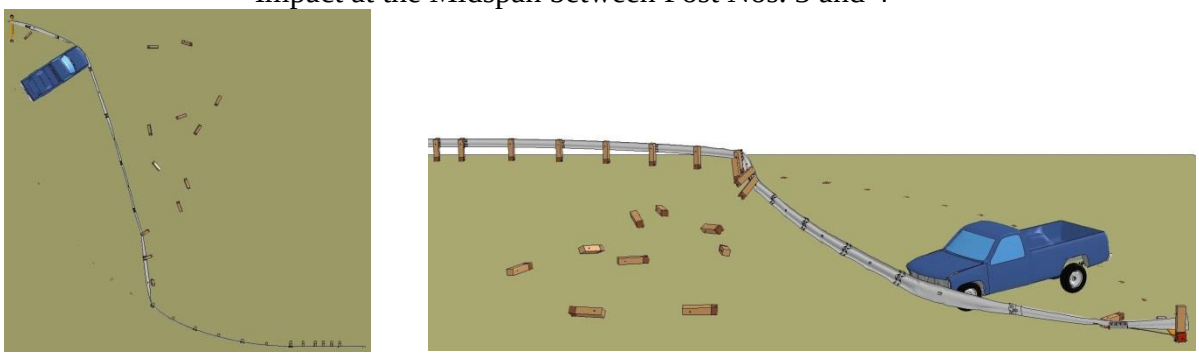

Impact at Post No. 4

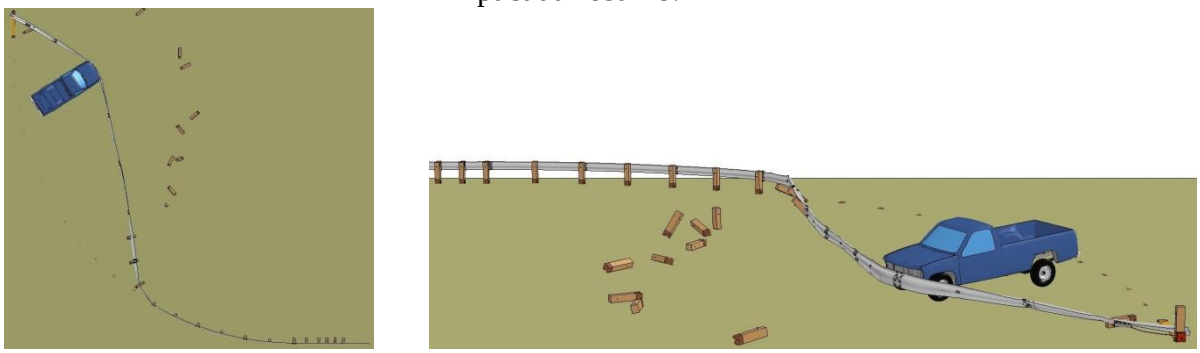

Impact at Post No. 5

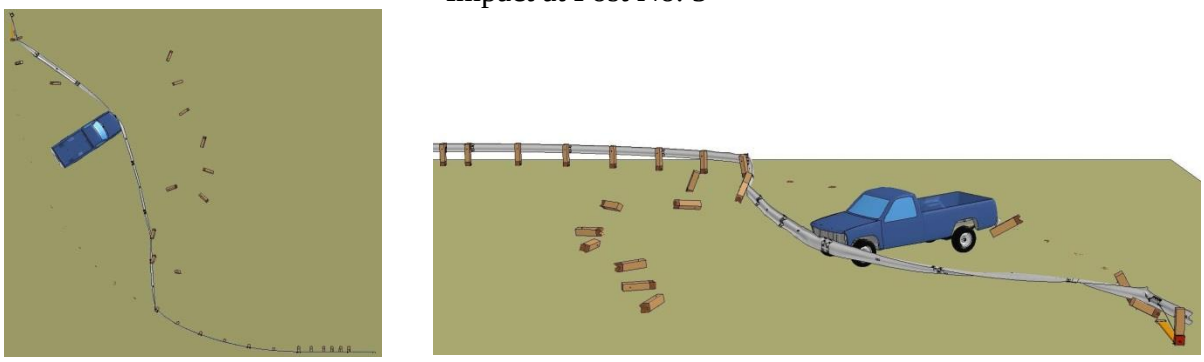

Impact at Post No. 7

Figure 127. Images of Impacts with 31-in. (787-mm) Tall, 72-ft (22-m) Radius Systems at 45 mph (72 km/h)

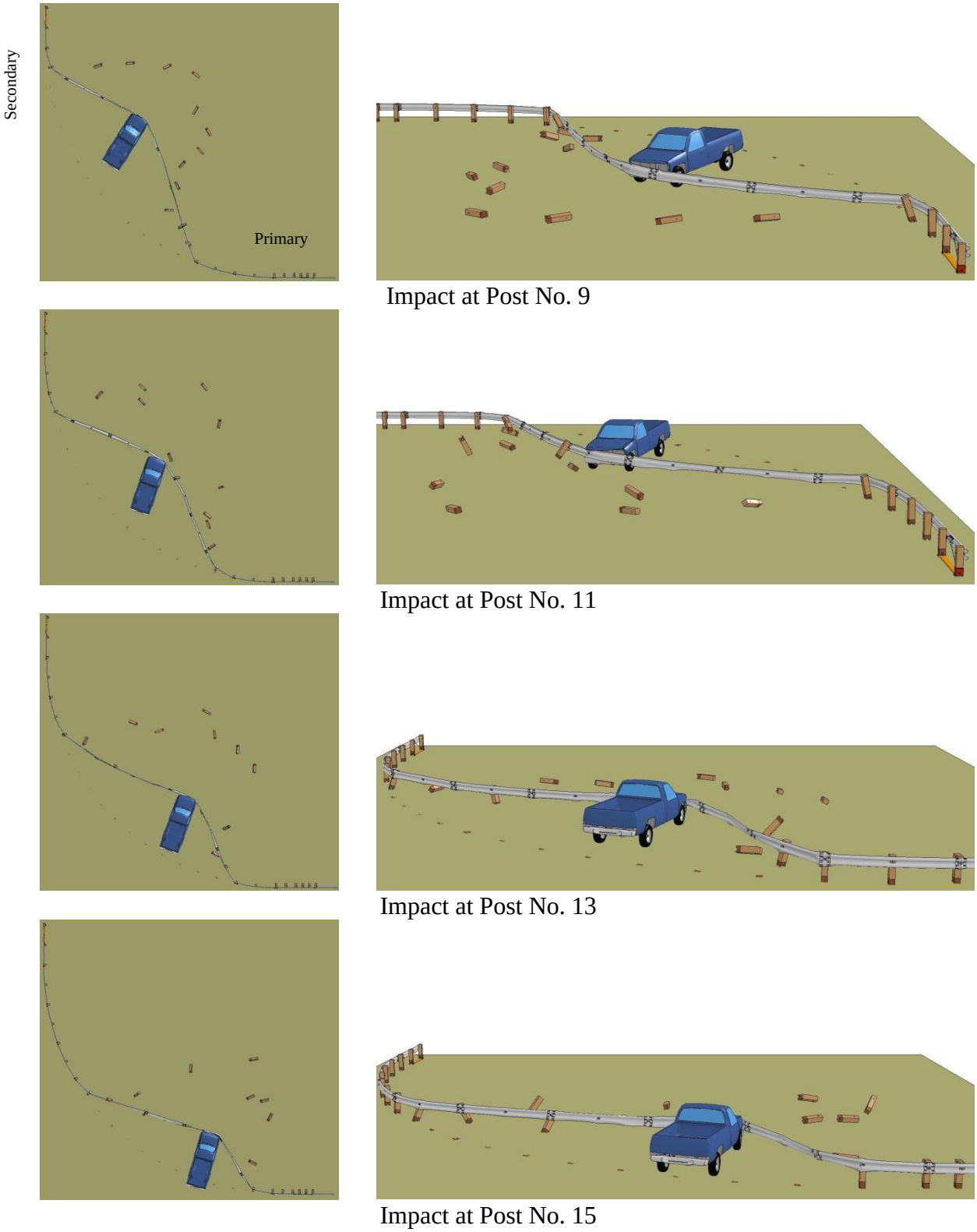

Figure 128. Images of Impacts with 31-in. (787-mm) Tall, 72-ft (22-m) Radius Systems at 45 mph (72 km/h)

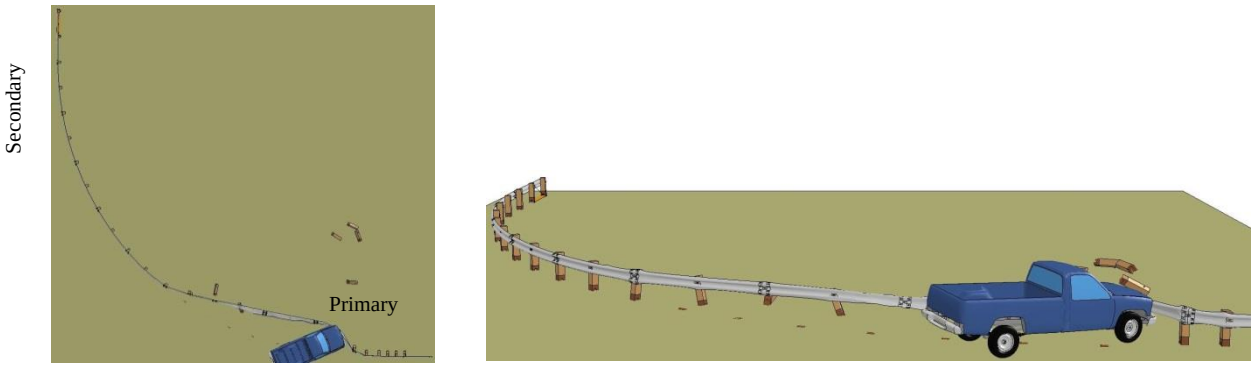

Impact at Post No. 17

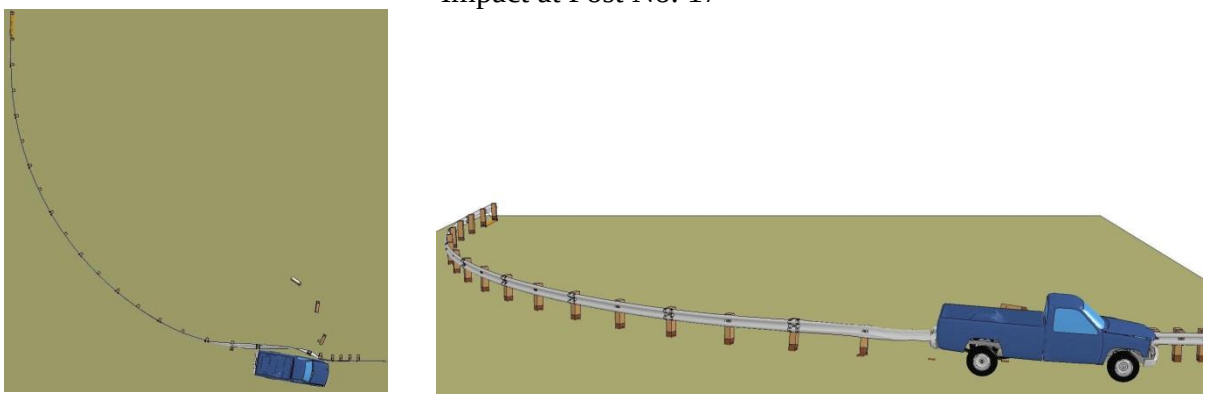

Impact at Midspan between Post Nos. 7 and 8

Figure 129. Images of Impacts with 31-in. (787-mm) Tall, 72-ft (22-m) Radius Systems at 45 mph (72 km/h)

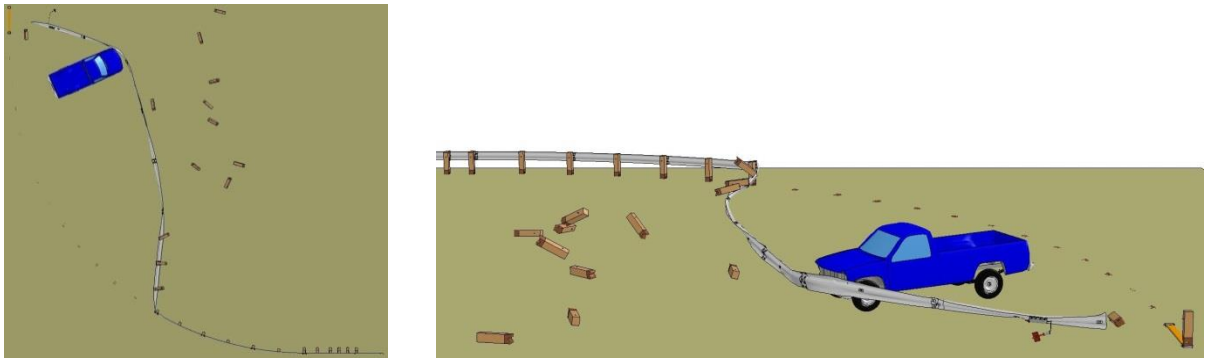

Impact at Post No. 5

Figure 130. Images of Impacts with 31-in. (787-mm) Tall, 72-ft (22-m) Radius Systems at 50 mph (80 km/h)

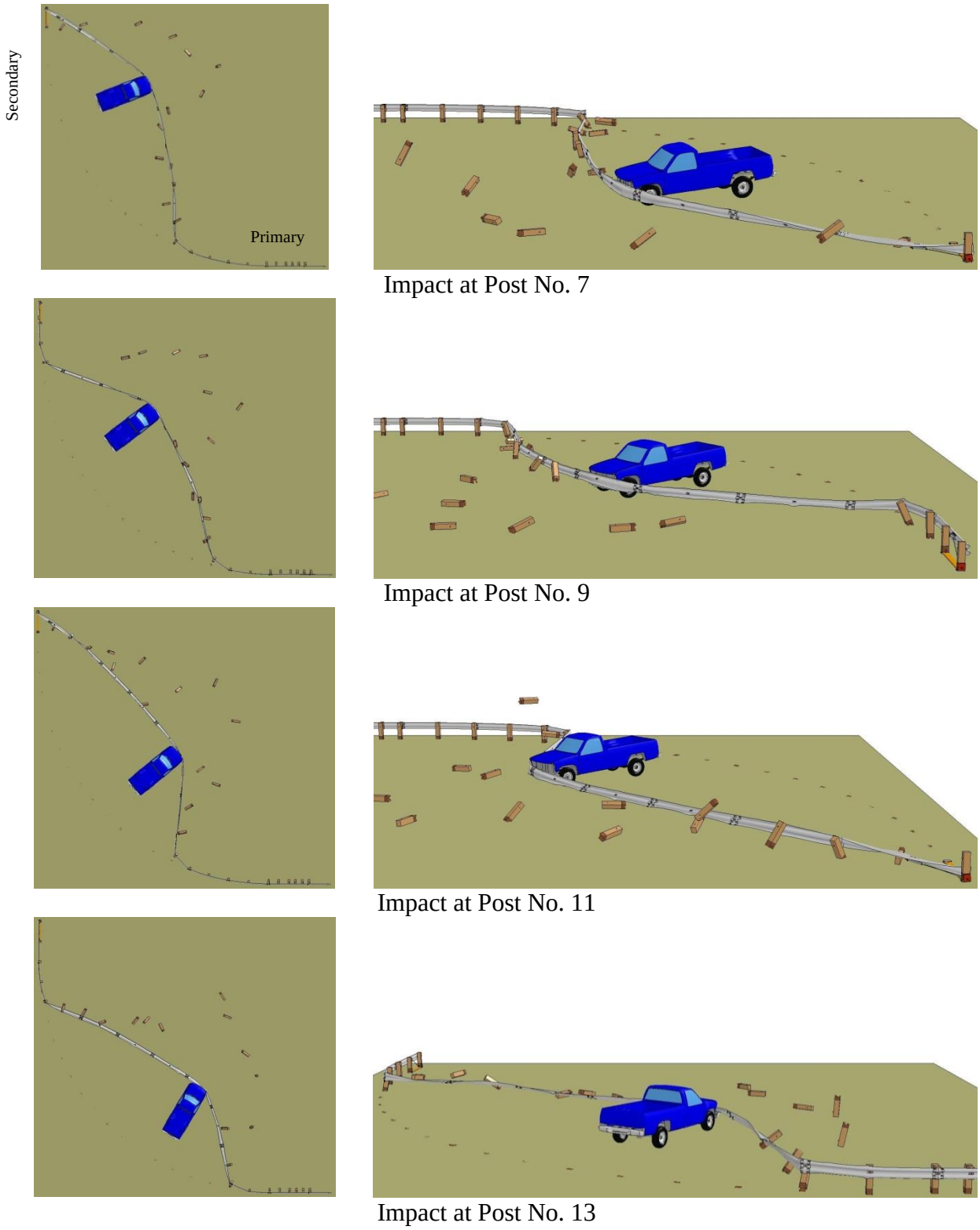

Figure 131. Images of Impacts with 31-in. (787-mm) Tall, 72-ft (22-m) Radius Systems at 50 mph (80 km/h)

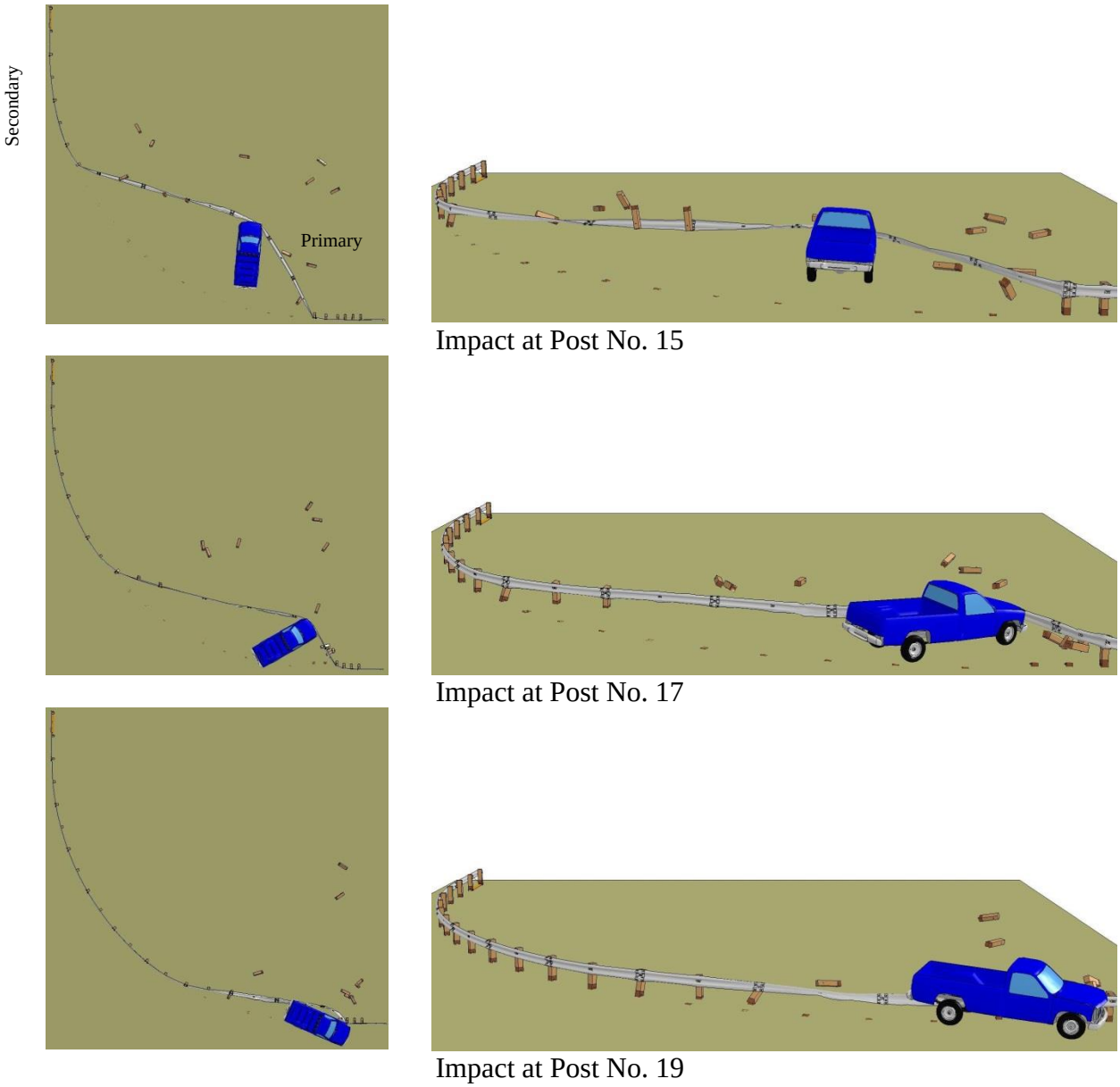

Figure 132. Images of Impacts with 31-in. (787-mm) Tall, 72-ft (22-m) Radius Systems at 50 mph (80 km/h)

9.3 Discussion

The 27-in. (686-mm) tall guardrail systems with a 72 ft (22 m) radius, with and without 8-in. (203-mm) timber blockouts, did not contain the impacting vehicle for each impact condition. For impacts at or downstream from post no. 7, or the beginning of the LON, two simulations of systems without blockouts resulted in acceptable capture or redirection of the

pickup truck, and four simulations with blockouts resulted in acceptable capture or redirection. The average energy dissipated prior to termination of the analysis was 47 percent for the non-blocked system, and 87 percent for the system with blockouts. This corresponded to better rail engagement with the front end of the truck, and was evidence that the blockouts assisted in retaining the rail height after impact.

Increasing the top rail mounting height from 27 in. (686 mm) to 31 in. (787 mm) resulted in acceptable capture of the simulated vehicle at or downstream from post no. 7. There was no tendency to vault observed in any simulation with a top rail mounting height of 31 in. (787 mm).

However, the system has not been evaluated using passenger cars, which was outside of the scope of the current study. There is some concern that a passenger car could underride or experience roof or windshield crush after impact with the guardrail mounted with a top height of 31 in. (787 mm). Further analysis, including simulation or full-scale crash testing, may be required to confirm or rebut these concerns.

Systems with 31-in. (787-mm) top mounting heights approached maximum capacity with 50 mph (80 km/h) impact speeds. Increased impact speeds may be beyond the performance capacity of this system. Additional sections of straight W-beam guardrail which spans between the upstream anchor and the upstream end of the radius may shift the beginning of the LON upstream from the modeled location.

With radii as large as 72 ft (22 m), it may be desired to span less than one entire 90-degree radius, either due to oblique intersection between two different roadways or to minimize the exposed area of guardrail installed. In these circumstances, the beginning of the LON should be determined, and a minimum of 8 posts upstream of the beginning of the LON should be used for roadways with speed limits of 45 mph (72 km/h), as shown in Figure 133. Location of the

Beginning of the LON for Non-Perpendicular Intersections. For roads with speed limits of 50 mph (80 km/h), at least 10 posts should be installed upstream of the beginning of the LON.

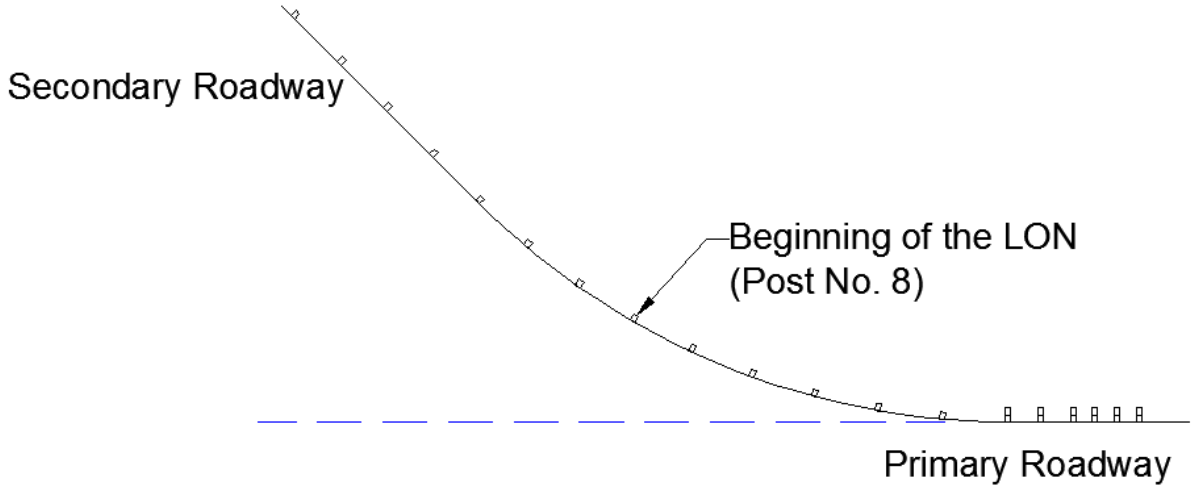

Figure 133. Location of the Beginning of the LON for Non-Perpendicular Intersections

10 EVALUATION OF SIMULATION RESULTS

10.1 Summary of Results

Results of the simulations with radii equal to 24, 48, and 72 ft (7.3, 15, and 22 m) at NCHRP Report No. 350 TL-2 impact conditions were examined in detail. A tabulated summary of pertinent simulation results is shown in Tables 20 through 25. Simulation termination times were determined when the rail was no longer in contact with the bumper (i.e., upon vaulting), when the vehicle came to a stop, or when the termination time was reached.

Simulations with 27-in. (686-mm) tall mounting heights frequently resulted in the light truck vaulting over the system. The 27-in. (686-mm) tall, unblocked systems with radii of 24, 48, and 72 m (7.3, 15, and 22 m) captured or redirected the vehicle in 0, 0, and 20 percent of simulations, respectively. The 27-in. (686-mm) tall, blocked systems with radii of 24, 48, and 72 m (7.3, 15, and 22 m) captured or redirected the vehicle in 20, 45, and 40 percent of simulations, respectively.

Each impact resulting in vehicle capture progressed through three phases: (1) forces predominantly transferred through membrane tension starting immediately after impact; (2) mixed membrane tension and guardrail pocketing forces; (3) and forces predominantly transferred through guardrail pocketing, as shown in Figure 134. Membrane tension is developed when a feature is impacted or deflected, and surface tension tangential to the face of the guardrail resists the deflection. Membrane tension forces are analogous to the restoring forces applied by bubbles or rubber bands when they are deformed. As a result, membrane tension forces remain relatively constant, regardless of post deflection or disengagement.

In contrast, when a pocket is formed in the guardrail in front of a vehicle, rail tension is primarily transferred to adjacent posts, and rail forces are mostly localized. Pockets are associated with large angular deflections of the rail. As a result, rail tension is transmitted to the

Table 20. Simulation Analysis Summary for 24-ft (7.3-m) Radius Systems

Impact Location	Rail Height (in.)	Blockouts?	Speed mph (km/h)	Angle (deg)	Result	Analysis End Time (ms)	Reason for Terminating Analysis	Anchor Posts Fracture Times	Posts on Radius Fractured/ Deflected	Transition Posts Fractured/ Deflected	Speed at End of Analysis mph (km/h)	Longitudinal Displacement at End of Analysis ft-in. (mm)	Lateral Displacement at End of Analysis ft-in. (mm)
Post 3	27 (686)	No	45 (72)	25	Fail - override	71 ms	Override	75 ms	2	0	38.5 (62)	4 ft-1 in. (1246)	1 ft-7 in. (477)
Midspan 3-4	27 (686)	No	45 (72)	25	Fail - override	75 ms	Override	84 ms	2	0	39.3 (63)	4 ft-4 in. (1319)	1 ft-7 in. (492)
Post 4	27 (686)	No	45 (72)	25	Fail - override	137 ms	Override	-	2	0	35.0 (56)	7 ft-6 in. (2274)	2 ft-10 in. (873)
Midspan 4-5	27 (686)	No	45 (72)	25	Fail - override	91 ms	Override	-	3	0	38.9 (63)	5 ft-2 in. (1585)	1 ft-10 in. (569)
Post 5	27 (686)	No	45 (72)	25	Fail - override	377 ms	Override	-	5	0	25.4 (41)	17 ft-2 in. (5241)	7 ft-1 in. (2159)
Midspan 5-6	27 (686)	No	45 (72)	25	Fail - override	88 ms	Override	-	3	0	40.0 (64)	5 ft-1 in. (1545)	1 ft-10 in. (569)
Post 6	27 (686)	No	45 (72)	25	Fail - override	151 ms	Override	-	3	0	36.2 (58)	8 ft-5 in. (2553)	3 ft-1 in. (939)
Midspan 6-7	27 (686)	No	45 (72)	25	Fail - override	113 ms	Override	-	4	0	38.3 (62)	6 ft-5 in. (1946)	2 ft-3 in. (695)
Post 7	27 (686)	No	45 (72)	25	Fail - override	53 ms	Override	-	3	0	41.1 (66)	3 ft-2 in. (960)	1 ft-2 in. (349)
Midspan 7-8	27 (686)	No	45 (72)	25	Fail - override	77 ms	Override	-	2	1	39.6 (64)	4 ft-6 in. (1367)	1 ft-7 in. (473)
Post 3	27 (686)	Yes	45 (72)	25	Fail - override	72 ms	Override	77 ms	3	0	37.7 (61)	4 ft-1 in. (1242)	1 ft-7 in. (474)
Post 4	27 (686)	Yes	45 (72)	25	Fail - override	193 ms	Override	-	5	0	29.2 (47)	9 ft-8 in. (2956)	3 ft-8 in. (1119)
Post 5	27 (686)	Yes	45 (72)	25	Captured	686 ms	End of Sim	-	5	2	9.3 (15)	22 ft-9 in. (6930)	9 ft-8 in. (2953)
Post 6	27 (686)	Yes	45 (72)	25	Fail - override	181 ms	Override	-	4	0	34.1 (55)	9 ft-7 in. (2932)	3 ft-8 in. (1106)
Post 7	27 (686)	Yes	45 (72)	25	Fail - override	156 ms	Override	-	5	0	33.7 (54)	8 ft-6 in. (2603)	3 ft-1 in. (949)
Post 3	31 (787)	No	45 (72)	25	Gated	67 ms	Gated	67, 336 ms	2	0	37.7 (61)	3 ft-10 in. (1162)	1 ft-5 in. (437)
Midspan 3-4	31 (787)	No	45 (72)	25	Gated	73 ms	Gated	73, 333 ms	3	0	38.2 (62)	4 ft-2 in. (1260)	1 ft-6 in. (468)
Post 4	31 (787)	No	45 (72)	25	Gated	179 ms	Gated	179, 498 ms	4	0	32.2 (52)	9 ft-2 in. (2785)	3 ft-6 in. (1078)
Midspan 4-5	31 (787)	No	45 (72)	25	No Conclusion	178 ms	End of Sim	178 ms	5	0	35.0 (56)	9 ft-5 in. (2859)	3 ft-6 in. (1061)
Post 5	31 (787)	No	45 (72)	25	No Conclusion	385 ms	End of Sim	385 ms	6	2	26.1 (42)	17 ft-3 in. (5269)	7 ft-5 in. (2252)
Midspan 5-6	31 (787)	No	45 (72)	25	Captured	619 ms	End of Sim	-	6	2	22.3 (36)	25 ft-10 in. (7871)	11 ft-10 in. (3619)
Post 6	31 (787)	No	45 (72)	25	Captured	674 ms	End of Sim	-	6	4	11.5 (19)	23 ft-9 in. (7236)	11 ft-0 in. (3362)
Midspan 6-7	31 (787)	No	45 (72)	25	Captured	678 ms	End of Sim	-	5	4	12.1 (20)	23 ft-9 in. (7247)	10 ft-2 in. (3110)
Post 7	31 (787)	No	45 (72)	25	Captured	650 ms	End of Sim	-	4	3	9.1 (15)	24 ft-0 in. (7306)	10 ft-4 in. (3141)
Midspan 7-8	31 (787)	No	45 (72)	25	Captured	583 ms	End of Sim	-	5	3	7.0 (11)	20 ft-4 in. (6201)	7 ft-9 in. (2371)
Post 3	31 (787)	No	50 (80)	25	Gated	59 ms	Gated	59, 155 ms	3	0	42.8 (69)	3 ft-8 in. (1111)	1 ft-9 in. (525)
Post 4	31 (787)	No	50 (80)	25	No Conclusion	125 ms	End Post Fracture	125 ms	4	0	38.3 (62)	7 ft-3 in. (2215)	3 ft-5 in. (1035)
Post 5	31 (787)	No	50 (80)	25	Gated	246 ms	Gated	246, 318 ms	6	3	34.8 (56)	13 ft-5 in. (4079)	6 ft-6 in. (1972)
Post 6	31 (787)	No	50 (80)	25	Gated	397 ms	Gated	397, 673 ms	6	2	29.5 (48)	19 ft-9 in. (6008)	10 ft-1 in. (3072)
Post 7	31 (787)	No	50 (80)	25	No Conclusion	521 ms	End Post Fracture	521 ms	6	3	21.2 (34)	24 ft-7 in. (7493)	12 ft-3 in. (3738)

Table 21. Simulation Analysis Summary for 24-ft (7.3-m) Radius Systems (cont)

Impact Location	Rail Height (in.)	Blockouts?	Speed mph (km/h)	Angle (deg)	Initial 50 ms Deceleration (g's)	Initial 100 ms Deceleration (g's)	% of Initial Energy Dissipated, 50 ms	% of Initial Energy Dissipated, 75 ms	% of Initial Energy Dissipated, 100 ms	% of Initial Energy Dissipated, 150 ms	% of Initial Energy Dissipated, 200 ms	% of Initial Energy Dissipated, 300 ms	% of Initial Energy Dissipated, 400 ms	% of Initial Energy Dissipated, End of Event
Post 3	27 (686)	No	45 (72)	25	3.7	3.4	17%	29%	30%	-	-	-	-	36%
Midspan 3-4	27 (686)	No	45 (72)	25	4.1	N/A	19%	24%	-	-	-	-	-	25%
Post 4	27 (686)	No	45 (72)	25	3.8	3.1	19%	23%	29%	-	-	-	-	39%
Midspan 4-5	27 (686)	No	45 (72)	25	3.7	N/A	17%	20%	-	-	-	-	-	25%
Post 5	27 (686)	No	45 (72)	25	3.0	3.0	14%	25%	27%	36%	50%	62%	-	68%
Midspan 5-6	27 (686)	No	45 (72)	25	3.7	N/A	17%	19%	-	-	-	-	-	21%
Post 6	27 (686)	No	45 (72)	25	2.9	2.6	14%	20%	24%	35%	-	-	-	35%
Midspan 6-7	27 (686)	No	45 (72)	25	3.6	2.7	17%	22%	25%	-	-	-	-	28%
Post 7	27 (686)	No	45 (72)	25	3.4	N/A	16%	-	-	-	-	-	-	17%
Midspan 7-8	27 (686)	No	45 (72)	25	3.1	N/A	15%	23%	-	-	-	-	-	23%
Post 3	27 (686)	Yes	45 (72)	25	4.4	3.5	21%	31%	32%	38%	-	-	-	42%
Post 4	27 (686)	Yes	45 (72)	25	4.4	4.0	20%	29%	35%	48%	-	-	-	58%
Post 5	27 (686)	Yes	45 (72)	25	3.4	3.3	16%	28%	30%	38%	49%	64%	77%	96%
Post 6	27 (686)	Yes	45 (72)	25	4.0	3.2	19%	25%	29%	37%	-	-	-	42%
Post 7	27 (686)	Yes	45 (72)	25	3.7	2.6	17%	20%	24%	42%	-	-	-	44%
Post 3	31 (787)	No	45 (72)	25	5.3	4.1	24%	32%	36%	49%	58%	67%	-	75%
Midspan 3-4	31 (787)	No	45 (72)	25	4.5	3.8	21%	28%	34%	42%	51%	61%	-	66%
Post 4	31 (787)	No	45 (72)	25	4.2	4.1	20%	28%	36%	46%	50%	62%	72%	78%
Midspan 4-5	31 (787)	No	45 (72)	25	4.5	3.7	22%	26%	33%	35%	42%	57%	-	67%
Post 5	31 (787)	No	45 (72)	25	4.2	3.2	20%	27%	29%	37%	49%	61%	69%	86%
Midspan 5-6	31 (787)	No	45 (72)	25	4.5	3.5	21%	23%	31%	43%	45%	53%	57%	76%
Post 6	31 (787)	No	45 (72)	25	4.3	3.9	20%	26%	35%	39%	44%	57%	72%	93%
Midspan 6-7	31 (787)	No	45 (72)	25	4.0	3.4	18%	27%	30%	41%	48%	62%	74%	93%
Post 7	31 (787)	No	45 (72)	25	4.3	3.2	20%	25%	29%	40%	45%	58%	68%	96%
Midspan 7-8	31 (787)	No	45 (72)	25	3.1	3.5	16%	27%	32%	40%	55%	70%	82%	98%
Post 3	31 (787)	No	50 (80)	25	5.7	4.1	24%	32%	33%	-	-	-	-	42%
Post 4	31 (787)	No	50 (80)	25	4.6	4.3	19%	28%	34%	42%	45%	58%	66%	85%
Post 5	31 (787)	No	50 (80)	25	4.6	3.3	19%	25%	27%	38%	46%	58%	-	64%
Post 6	31 (787)	No	50 (80)	25	4.7	3.7	20%	24%	30%	34%	44%	57%	65%	76%
Post 7	31 (787)	No	50 (80)	25	4.2	3.2	17%	20%	26%	32%	38%	51%	65%	90%

NOTE: "-" Analysis terminated; data was not collected

Table 22. Simulation Analysis Summary for 48-ft (15-m) Radius Systems

Impact Location	Rail Height (in.)	Blockouts?	Speed mph (km/h)	Angle (deg)	Result	Analysis End Time (ms)	Reason for Terminating Analysis	Anchor Posts Fracture Times	Posts on Radius Fractured/ Deflected	Transition Posts Fractured/ Deflected	Speed at End of Analysis mph (km/h)	Longitudinal Displacement at End of Analysis ft-in. (mm)	Lateral Displacement at End of Analysis ft-in. (mm)
Post 4	27 (686)	No	45 (72)	25	Fail - override	94 ms	Override	94 ms	3	0	35.9 (58)	5 ft-2 in. (1586)	2 ft-0 in. (611)
Post 5	27 (686)	No	45 (72)	25	Fail - override	113 ms	Override	-	4	0	36.8 (59)	6 ft-3 in. (1899)	2 ft-5 in. (729)
Post 6	27 (686)	No	45 (72)	25	Fail - override	128 ms	Override	-	4	0	33.9 (55)	6 ft-11 in. (2107)	2 ft-8 in. (815)
Post 7	27 (686)	No	45 (72)	25	Fail - override	224 ms	Override	-	6	0	31.3 (50)	11 ft-5 in. (3473)	4 ft-4 in. (1325)
Post 8	27 (686)	No	45 (72)	25	Fail - override	128 ms	Override	-	4	0	36.1 (58)	7 ft-1 in. (2162)	2 ft-7 in. (780)
Post 9	27 (686)	No	45 (72)	25	Fail - override	129 ms	Override	-	5	0	35.8 (58)	7 ft-2 in. (2185)	2 ft-6 in. (772)
Post 10	27 (686)	No	45 (72)	25	Fail - override	82 ms	Override	-	3	0	39.2 (63)	4 ft-9 in. (1457)	1 ft-8 in. (508)
Post 11	27 (686)	No	45 (72)	25	Fail - override	100 ms	Override	-	4	0	37.4 (60)	5 ft-9 in. (1757)	1 ft-11 in. (595)
Post 12	27 (686)	No	45 (72)	25	Fail - override	118 ms	Override	-	4	0	36.8 (59)	6 ft-9 in. (2056)	2 ft-2 in. (668)
Post 13	27 (686)	No	45 (72)	25	Fail - override	135 ms	Override	-	2	1	36.0 (58)	7 ft-8 in. (2345)	2 ft-4 in. (707)
Post 4	27 (686)	Yes	45 (72)	25	Gated	120 ms	Gated	120, 516 ms	5	0	34.1 (55)	6 ft-4 in. (1933)	2 ft-5 in. (744)
Post 5	27 (686)	Yes	45 (72)	25	Fail - override	178 ms	Override	178 ms	5	0	30.8 (50)	8 ft-12 in. (2743)	3 ft-5 in. (1053)
Post 6	27 (686)	Yes	45 (72)	25	Captured	685 ms	End of Sim	-	10	0	10.3 (17)	22 ft-7 in. (6895)	9 ft-8 in. (2954)
Post 7	27 (686)	Yes	45 (72)	25	Captured	684 ms	End of Sim	-	10	0	9.6 (15)	22 ft-7 in. (6882)	10 ft-0 in. (3036)
Post 8	27 (686)	Yes	45 (72)	25	Fail - override	276 ms	Override	-	9	0	26.5 (43)	13 ft-3 in. (4034)	5 ft-0 in. (1515)
Post 9	27 (686)	Yes	45 (72)	25	Fail - override	149 ms	Override	-	7	0	34.5 (56)	8 ft-0 in. (2440)	2 ft-10 in. (867)
Post 10	27 (686)	Yes	45 (72)	25	Fail - override	135 ms	Override	-	5	0	36.7 (59)	7 ft-5 in. (2270)	2 ft-6 in. (770)
Post 11	27 (686)	Yes	45 (72)	25	Captured	681 ms	End of Sim	-	8	2	8.7 (14)	25 ft-1 in. (7647)	6 ft-4 in. (1925)
Post 12	27 (686)	Yes	45 (72)	25	Captured	685 ms	Captured	-	8	2	3.0 (5)	23 ft-10 in. (7268)	4 ft-8 in. (1433)
Post 13	27 (686)	Yes	45 (72)	25	Captured	575 ms	End of Sim	-	5	2	5.7 (9)	20 ft-9 in. (6323)	2 ft-10 in. (858)
Post 4	31 (787)	No	45 (72)	25	No Conclusion	104 ms	End of Sim	104 ms	4	0	35.4 (57)	5 ft-7 in. (1714)	2.1 ft-0 in. (649)
Post 5	31 (787)	No	45 (72)	25	No Conclusion	159 ms	End of Sim	159 ms	6	0	33.6 (54)	8 ft-4 in. (2540)	3 ft-3 in. (979)
Post 6	31 (787)	No	45 (72)	25	No Conclusion	278 ms	End of Sim	278 ms	7	0	30.2 (49)	13 ft-8 in. (4160)	5 ft-6 in. (1675)
Post 7	31 (787)	No	45 (72)	25	Captured	681 ms	End of Sim	-	10	0	14.4 (23)	23 ft-3 in. (7093)	11 ft-1 in. (3375)
Post 8	31 (787)	No	45 (72)	25	Captured	593 ms	Numerical Instability	-	8	0	17.7 (28)	22 ft-6 in. (6861)	10 ft-6 in. (3188)
Post 9	31 (787)	No	45 (72)	25	Captured	598 ms	Numerical Instability	-	9	0	17.9 (29)	23 ft-7 in. (7196)	9 ft-7 in. (2918)
Post 10	31 (787)	No	45 (72)	25	Captured	683 ms	End of Sim	-	11	0	17.3 (28)	25 ft-10 in. (7873)	9 ft-1 in. (2767)
Post 11	31 (787)	No	45 (72)	25	Captured	682 ms	End of Sim	-	9	1	12.1 (19)	24 ft-4 in. (7405)	8 ft-4 in. (2535)
Post 12	31 (787)	No	45 (72)	25	Captured	685 ms	End of Sim	-	7	2	10.0 (16)	23 ft-11 in. (7285)	6 ft-9 in. (2051)
Post 13	31 (787)	No	45 (72)	25	Captured	692 ms	End of Sim	-	7	4	20.9 (34)	26 ft-10 in. (8177)	8 ft-3 in. (2508)
Post 6	31 (787)	No	50 (80)	25	No Conclusion	228 ms	Numerical Instability	228 ms	8	0	37.2 (60)	12 ft-8 in. (3861)	5 ft-10 in. (1785)
Post 7	31 (787)	No	50 (80)	25	No Conclusion	381 ms	End of Sim	381 ms	10	0	30.7 (49)	18 ft-9 in. (5718)	9 ft-1 in. (2757)
Post 8	31 (787)	No	50 (80)	25	Captured	680 ms	End of Sim	-	12	0	19.1 (31)	27 ft-7 in. (8412)	14 ft-8 in. (4461)
Post 9	31 (787)	No	50 (80)	25	Captured	684 ms	End of Sim	-	11	1	18.3 (29)	28 ft-4 in. (8635)	15 ft-5 in. (4702)
Post 10	31 (787)	No	50 (80)	25	Captured	684 ms	End of Sim	-	10	2	15.3 (25)	28 ft-8 in. (8743)	13 ft-2 in. (4005)
Post 11	31 (787)	No	50 (80)	25	Captured	685 ms	End of Sim	-	11	2	17.1 (28)	28 ft-6 in. (8696)	12 ft-8 in. (3866)
Post 12	31 (787)	No	50 (80)	25	Captured	603 ms	Numerical Instability	-	9	3	15.0 (24)	25 ft-8 in. (7833)	11 ft-0 in. (3352)
Post 13	31 (787)	No	50 (80)	25	Captured	484 ms	Numerical Instability	-	9	3	17.4 (28)	21 ft-9 in. (6641)	8 ft-8 in. (2629)

Table 23. Simulation Analysis Summary for 48-ft (15-m) Radius Systems (cont)

Impact Location	Rail Height (in.)	Blockouts?	Speed mph (km/h)	Angle (deg)	Initial 50 ms Deceleration (g's)	Initial 100 ms Deceleration (g's)	% of Initial Energy Dissipated, 50 ms	% of Initial Energy Dissipated, 75 ms	% of Initial Energy Dissipated, 100 ms	% of Initial Energy Dissipated, 150 ms	% of Initial Energy Dissipated, 200 ms	% of Initial Energy Dissipated, 300 ms	% of Initial Energy Dissipated, 400 ms	% of Initial Energy Dissipated, End of Event
Post 4	27 (686)	No	45 (72)	25	4.0	4.3	19%	31%	37%	-	-	-	-	41%
Post 5	27 (686)	No	45 (72)	25	4.3	3.5	20%	26%	31%	-	-	-	-	33%
Post 6	27 (686)	No	45 (72)	25	4.1	3.7	19%	29%	33%	-	-	-	-	43%
Post 7	27 (686)	No	45 (72)	25	4.0	3.5	19%	25%	31%	41%	49%	-	-	51%
Post 8	27 (686)	No	45 (72)	25	3.9	3.1	18%	25%	28%	-	-	-	-	36%
Post 9	27 (686)	No	45 (72)	25	3.3	3.2	16%	27%	29%	-	-	-	-	37%
Post 10	27 (686)	No	45 (72)	25	3.3	3.2	16%	22%	-	-	-	-	-	24%
Post 11	27 (686)	No	45 (72)	25	3.3	3.4	16%	24%	31%	-	-	-	-	31%
Post 12	27 (686)	No	45 (72)	25	3.4	3.0	16%	21%	27%	-	-	-	-	33%
Post 13	27 (686)	No	45 (72)	25	2.7	3.0	13%	20%	27%	-	-	-	-	36%
Post 4	27 (686)	Yes	45 (72)	25	4.9	4.3	23%	34%	38%	46%	53%	72%	80%	88%
Post 5	27 (686)	Yes	45 (72)	25	4.6	3.9	21%	30%	35%	49%	54%	-	-	58%
Post 6	27 (686)	Yes	45 (72)	25	4.8	4.1	22%	31%	36%	49%	54%	67%	78%	95%
Post 7	27 (686)	Yes	45 (72)	25	4.4	4.0	21%	29%	35%	43%	51%	68%	78%	95%
Post 8	27 (686)	Yes	45 (72)	25	4.5	3.8	21%	31%	34%	44%	50%	-	-	65%
Post 9	27 (686)	Yes	45 (72)	25	4.0	3.8	19%	29%	34%	-	-	-	-	41%
Post 10	27 (686)	Yes	45 (72)	25	4.0	3.7	18%	26%	33%	-	-	-	-	33%
Post 11	27 (686)	Yes	45 (72)	25	4.0	3.9	19%	27%	35%	39%	49%	64%	72%	96%
Post 12	27 (686)	Yes	45 (72)	25	3.7	3.6	18%	24%	32%	39%	49%	58%	74%	100%
Post 13	27 (686)	Yes	45 (72)	25	2.9	3.3	14%	24%	30%	42%	46%	69%	89%	98%
Post 4	31 (787)	No	45 (72)	25	5.0	4.2	23%	33%	37%	45%	54%	69%	77%	92%
Post 5	31 (787)	No	45 (72)	25	4.7	4.0	22%	28%	35%	42%	46%	57%	66%	86%
Post 6	31 (787)	No	45 (72)	25	4.8	3.7	22%	27%	33%	39%	45%	56%	67%	83%
Post 7	31 (787)	No	45 (72)	25	5.1	4.1	24%	32%	36%	48%	56%	62%	75%	90%
Post 8	31 (787)	No	45 (72)	25	4.9	4.1	23%	32%	36%	45%	51%	59%	70%	85%
Post 9	31 (787)	No	45 (72)	25	3.9	3.7	18%	29%	33%	44%	45%	62%	71%	84%
Post 10	31 (787)	No	45 (72)	25	4.0	3.7	19%	27%	33%	42%	46%	64%	74%	85%
Post 11	31 (787)	No	45 (72)	25	4.2	3.9	20%	27%	35%	41%	50%	63%	77%	93%
Post 12	31 (787)	No	45 (72)	25	4.3	4.0	20%	29%	36%	44%	52%	61%	78%	95%
Post 13	31 (787)	No	45 (72)	25	3.1	3.2	15%	22%	29%	42%	48%	65%	75%	78%
Post 6	31 (787)	No	50 (80)	25	5.1	4.0	21%	25%	32%	37%	41%	48%	58%	69%
Post 7	31 (787)	No	50 (80)	25	5.1	4.2	21%	28%	34%	42%	49%	58%	63%	85%
Post 8	31 (787)	No	50 (80)	25	5.2	4.0	22%	28%	32%	39%	46%	60%	72%	85%
Post 9	31 (787)	No	50 (80)	25	4.5	3.7	19%	26%	30%	39%	44%	53%	64%	87%
Post 10	31 (787)	No	50 (80)	25	4.4	3.5	19%	26%	29%	39%	44%	56%	65%	91%
Post 11	31 (787)	No	50 (80)	25	4.4	3.9	19%	26%	31%	39%	48%	56%	69%	88%
Post 12	31 (787)	No	50 (80)	25	4.1	3.8	17%	22%	30%	38%	45%	60%	74%	91%
Post 13	31 (787)	No	50 (80)	25	3.9	3.4	17%	20%	28%	37%	46%	67%	81%	88%

NOTE: "-" Analysis terminated; data was not collected

Table 24. Simulation Analysis Summary for 72-ft (22-m) Radius Systems

Impact Location	Rail Height (in.)	Blockouts?	Speed mph (km/h)	Angle (deg)	Result	Data Analysis End Time (ms)	Reason for Terminating Analysis	Anchor Posts Fracture Times	Posts on Radius Fractured/ Deflected	Transition Posts Fractured/ Deflected	Speed at End of Analysis mph (km/h)	Longitudinal Displacement at End of Analysis ft-in. (mm)	Lateral Displacement at End of Analysis ft-in. (mm)
Post 4	27 (686)	No	45 (72)	25	Fail - override	96	Override	333 ms	4	0	35.1 (56)	5 ft-2 in. (1586)	2 ft-0 in. (618)
Post 5	27 (686)	No	45 (72)	25	Fail - override	200	Override	-	7	0	25.0 (40)	9 ft-4 in. (2844)	3 ft-8 in. (1107)
Post 7	27 (686)	No	45 (72)	25	Fail - override	397	Override	-	9	0	17.6 (28)	15 ft-4 in. (4683)	6 ft-2 in. (1880)
Post 9	27 (686)	No	45 (72)	25	Captured	685	End of Sim	-	11	0	7.7 (12)	21 ft-3 in. (6470)	9 ft-0 in. (2755)
Post 11	27 (686)	No	45 (72)	25	Fail - override	123	Override	-	5	0	35.8 (58)	6 ft-9 in. (2058)	2 ft-5 in. (727)
Post 13	27 (686)	No	45 (72)	25	Fail - override	78	Override	-	5	0	38.3 (62)	4 ft-6 in. (1366)	1 ft-7 in. (479)
Post 15	27 (686)	No	45 (72)	25	Fail - override	99	Override	-	4	0	37.2 (60)	5 ft-8 in. (1728)	1 ft-10 in. (568)
Post 17	27 (686)	No	45 (72)	25	Fail - override	121	Override	-	3	0	36.2 (58)	6 ft-11 in. (2101)	2 ft-1 in. (644)
Post 19	27 (686)	No	45 (72)	25	Redirected	338	End of Sim	-	2	0	25.2 (41)	-	-
Post 4	27 (686)	Yes	45 (72)	25	Fail - override	84	Override	84 ms	4	0	34.3 (55)	4 ft-7 in. (1401)	1 ft-9 in. (537)
Post 5	27 (686)	Yes	45 (72)	25	Fail - override	470	Override	-	9	0	15.0 (24)	15 ft-6 in. (4736)	6 ft-5 in. (1949)
Post 7	27 (686)	Yes	45 (72)	25	Captured	688	End of Sim	-	11	0	8.8 (14)	20 ft-11 in. (6385)	9 ft-1 in. (2777)
Post 9	27 (686)	Yes	45 (72)	25	Fail - override	553	Override	-	11	0	14.3 (23)	19 ft-9 in. (6026)	8 ft-6 in. (2585)
Post 11	27 (686)	Yes	45 (72)	25	Fail - override	490	Override	-	10	0	18.0 (29)	19 ft-8 in. (5984)	6 ft-7 in. (2005)
Post 13	27 (686)	Yes	45 (72)	25	Fail - override	536	Override	-	11	0	16.0 (26)	19 ft-0 in. (5798)	8 ft-7 in. (2618)
Post 15	27 (686)	Yes	45 (72)	25	Captured	688	End of Sim	-	9	0	13.0 (21)	25 ft-0 in. (7618)	5 ft-5 in. (1646)
Post 17	27 (686)	Yes	45 (72)	25	Redirected	692	End of Sim	-	5	1	12.4 (20)	-	-
Post 19	27 (686)	Yes	45 (72)	25	Redirected	665	End of Sim	-	2	0	18.7 (30)	-	-
Post 4	31 (787)	No	45 (72)	25	No Conclusion	82	End of Sim	82 ms	4	0	35.7 (57)	4 ft-6 in. (1384)	1 ft-9 in. (528)
Post 5	31 (787)	No	45 (72)	25	No Conclusion	153	End of Sim	153 ms	6	0	31.3 (50)	7 ft-9 in. (2356)	3 ft-0 in. (916)
Post 7	31 (787)	No	45 (72)	25	No Conclusion	631	End of Sim	631 ms	12	0	13.8 (22)	22 ft-0 in. (6716)	9 ft-8 in. (2948)
Post 9	31 (787)	No	45 (72)	25	Captured	687	End of Sim	-	12	0	13.4 (22)	23 ft-5 in. (7129)	11 ft-4 in. (3447)
Post 11	31 (787)	No	45 (72)	25	Captured	689	End of Sim	-	11	0	11.3 (18)	23 ft-7 in. (7190)	9 ft-8 in. (2937)
Post 13	31 (787)	No	45 (72)	25	Captured	695	End of Sim	-	11	0	11.0 (18)	23 ft-9 in. (7249)	8 ft-3 in. (2506)
Post 15	31 (787)	No	45 (72)	25	Captured	693	End of Sim	-	9	0	8.5 (14)	23 ft-3 in. (7083)	6 ft-7 in. (2004)
Post 17	31 (787)	No	45 (72)	25	Captured	653	End of Sim	-	7	0	12.2 (20)	23 ft-11 in. (7290)	2 ft-4 in. (710)
Post 19	31 (787)	No	45 (72)	25	Redirected	433	Numerical Instability	-	3	1	18.7 (30)	-	-
Post 5	31 (787)	No	50 (80)	25	Gated	142	Gated	142, 441 ms	5	0	38.2 (61)	8 ft-0 in. (2446)	3.9 ft-0 in. (1179)
Post 7	31 (787)	No	50 (80)	25	No Conclusion	277	End of Sim	277 ms	12	0	32.5 (52)	14 ft-6 in. (4417)	6 ft-9 in. (2048)
Post 9	31 (787)	No	50 (80)	25	Captured	689	End of Sim	-	14	0	17.6 (28)	27 ft-7 in. (8411)	14 ft-1 in. (4288)
Post 11	31 (787)	No	50 (80)	25	No Conclusion	556	End of Sim	556 ms	14	0	21.3 (34)	24 ft-11 in. (7592)	11 ft-11 in. (3633)
Post 13	31 (787)	No	50 (80)	25	Captured	695	End of Sim	-	14	0	17.8 (29)	28 ft-2 in. (8591)	13 ft-6 in. (4118)
Post 15	31 (787)	No	50 (80)	25	Captured	689	End of Sim	-	12	0	15.9 (26)	26 ft-4 in. (8019)	13 ft-5 in. (4079)
Post 17	31 (787)	No	50 (80)	25	Captured	692	End of Sim	-	9	2	9.1 (15)	27 ft-0 in. (8240)	7 ft-11 in. (2423)
Post 19	31 (787)	No	50 (80)	25	Redirected	689	End of Sim	-	5	3	6.1 (10)	-	-

Table 25. Simulation Analysis Summary for 72-ft (22-m) Radius Systems (cont)

Impact Location	Rail Height (in.)	Blockouts?	Speed mph (km/h)	Angle (deg)	Initial 50 ms Deceleration (g's)	Initial 100 ms Deceleration (g's)	% of Initial Energy Dissipated, 50 ms	% of Initial Energy Dissipated, 75 ms	% of Initial Energy Dissipated, 100 ms	% of Initial Energy Dissipated, 150 ms	% of Initial Energy Dissipated, 200 ms	% of Initial Energy Dissipated, 300 ms	% of Initial Energy Dissipated, 400 ms	% of Initial Energy Dissipated, End of Event
Post 4	27 (686)	No	45 (72)	25	4.7	4.6	22%	35%	40%	-	-	-	-	46%
Post 5	27 (686)	No	45 (72)	25	5.2	5.0	24%	35%	43%	58%	-	-	-	69%
Post 7	27 (686)	No	45 (72)	25	5.1	4.7	23%	34%	41%	53%	65%	79%	-	85%
Post 9	27 (686)	No	45 (72)	25	5.1	4.7	24%	32%	42%	52%	60%	69%	81%	97%
Post 11	27 (686)	No	45 (72)	25	4.3	3.6	20%	29%	32%	-	-	-	-	37%
Post 13	27 (686)	No	45 (72)	25	3.5	3.3	17%	27%	-	-	-	-	-	27%
Post 15	27 (686)	No	45 (72)	25	3.6	3.6	17%	26%	-	-	-	-	-	32%
Post 17	27 (686)	No	45 (72)	25	3.3	3.5	16%	23%	31%	-	-	-	-	35%
Post 19	27 (686)	No	45 (72)	25	2.4	2.9	11%	20%	26%	39%	46%	62%	-	69%
Post 4	27 (686)	Yes	45 (72)	25	5.3	5.4	24%	39%	46%	55%	72%	85%	-	86%
Post 5	27 (686)	Yes	45 (72)	25	5.5	5.0	25%	37%	43%	57%	71%	85%	89%	89%
Post 7	27 (686)	Yes	45 (72)	25	5.5	4.8	25%	35%	42%	53%	64%	75%	81%	96%
Post 9	27 (686)	Yes	45 (72)	25	5.5	4.6	25%	36%	40%	52%	59%	69%	79%	90%
Post 11	27 (686)	Yes	45 (72)	25	5.0	4.0	23%	34%	35%	43%	54%	69%	78%	84%
Post 13	27 (686)	Yes	45 (72)	25	4.5	4.4	21%	29%	39%	52%	60%	73%	82%	87%
Post 15	27 (686)	Yes	45 (72)	25	4.1	4.3	19%	29%	38%	47%	57%	66%	76%	92%
Post 17	27 (686)	Yes	45 (72)	25	3.3	3.8	16%	25%	33%	43%	54%	66%	73%	92%
Post 19	27 (686)	Yes	45 (72)	25	2.5	3.0	12%	22%	28%	40%	49%	64%	73%	83%
Post 4	31 (787)	No	45 (72)	25	5.1	4.6	24%	35%	40%	50%	64%	78%	87%	98%
Post 5	31 (787)	No	45 (72)	25	5.2	4.8	24%	35%	42%	51%	57%	75%	82%	96%
Post 7	31 (787)	No	45 (72)	25	5.3	4.5	24%	33%	40%	49%	57%	69%	74%	91%
Post 9	31 (787)	No	45 (72)	25	5.5	4.5	25%	33%	40%	50%	57%	62%	72%	91%
Post 11	31 (787)	No	45 (72)	25	5.3	4.0	24%	34%	35%	43%	53%	64%	77%	94%
Post 13	31 (787)	No	45 (72)	25	4.3	3.9	20%	29%	35%	46%	53%	66%	79%	94%
Post 15	31 (787)	No	45 (72)	25	3.8	4.1	18%	27%	36%	44%	55%	68%	82%	96%
Post 17	31 (787)	No	45 (72)	25	3.9	3.9	18%	26%	35%	45%	55%	68%	76%	93%
Post 19	31 (787)	No	45 (72)	25	2.6	3.1	12%	21%	28%	42%	49%	66%	79%	83%
Post 5	31 (787)	No	50 (80)	25	5.6	4.6	23%	30%	36%	42%	51%	69%	75%	81%
Post 7	31 (787)	No	50 (80)	25	5.8	4.5	24%	30%	36%	42%	50%	60%	59%	84%
Post 9	31 (787)	No	50 (80)	25	5.6	4.7	23%	31%	37%	45%	49%	59%	69%	88%
Post 11	31 (787)	No	50 (80)	25	5.6	4.0	23%	30%	32%	39%	46%	57%	65%	84%
Post 13	31 (787)	No	50 (80)	25	4.7	4.1	20%	30%	33%	42%	48%	60%	69%	87%
Post 15	31 (787)	No	50 (80)	25	5.1	4.3	21%	29%	35%	45%	51%	60%	74%	90%
Post 17	31 (787)	No	50 (80)	25	4.2	4.1	18%	24%	33%	43%	49%	62%	75%	97%
Post 19	31 (787)	No	50 (80)	25	3.3	3.7	14%	23%	30%	39%	49%	70%	83%	99%

NOTE: "-" Analysis terminated; data was not collected

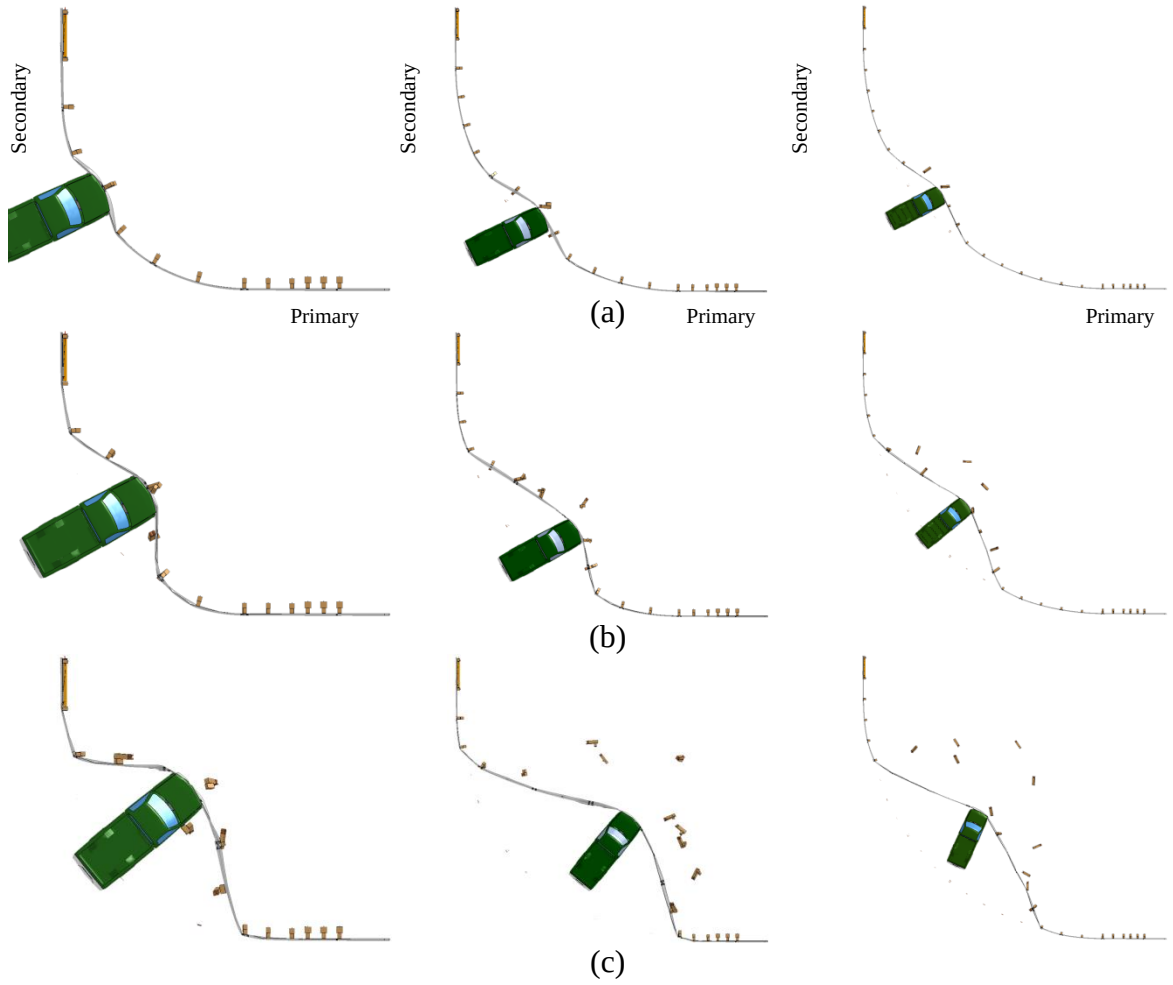

Figure 134. Phases in Vehicle Capture for 24, 48, and 72-ft (7.3, 15, and 22-m) Radii
(a) Membrane Tension (b) Mixed Membrane Tension and Pocketing (c) Fully-Developed Pocket

posts as a shear load and buckles form in the rail. After posts deflect or fracture, rail tension is temporarily reduced as another buckle is formed at the adjacent post, as shown in Figure 135.

Criteria were established to provide a quantitative comparison between the three phases observed during vehicle capture:

- Beginning of Phase II: guardrail deflected to at least 30 degrees to tangent line at radius
- Beginning of Phase III: the included angle of the 135 degrees

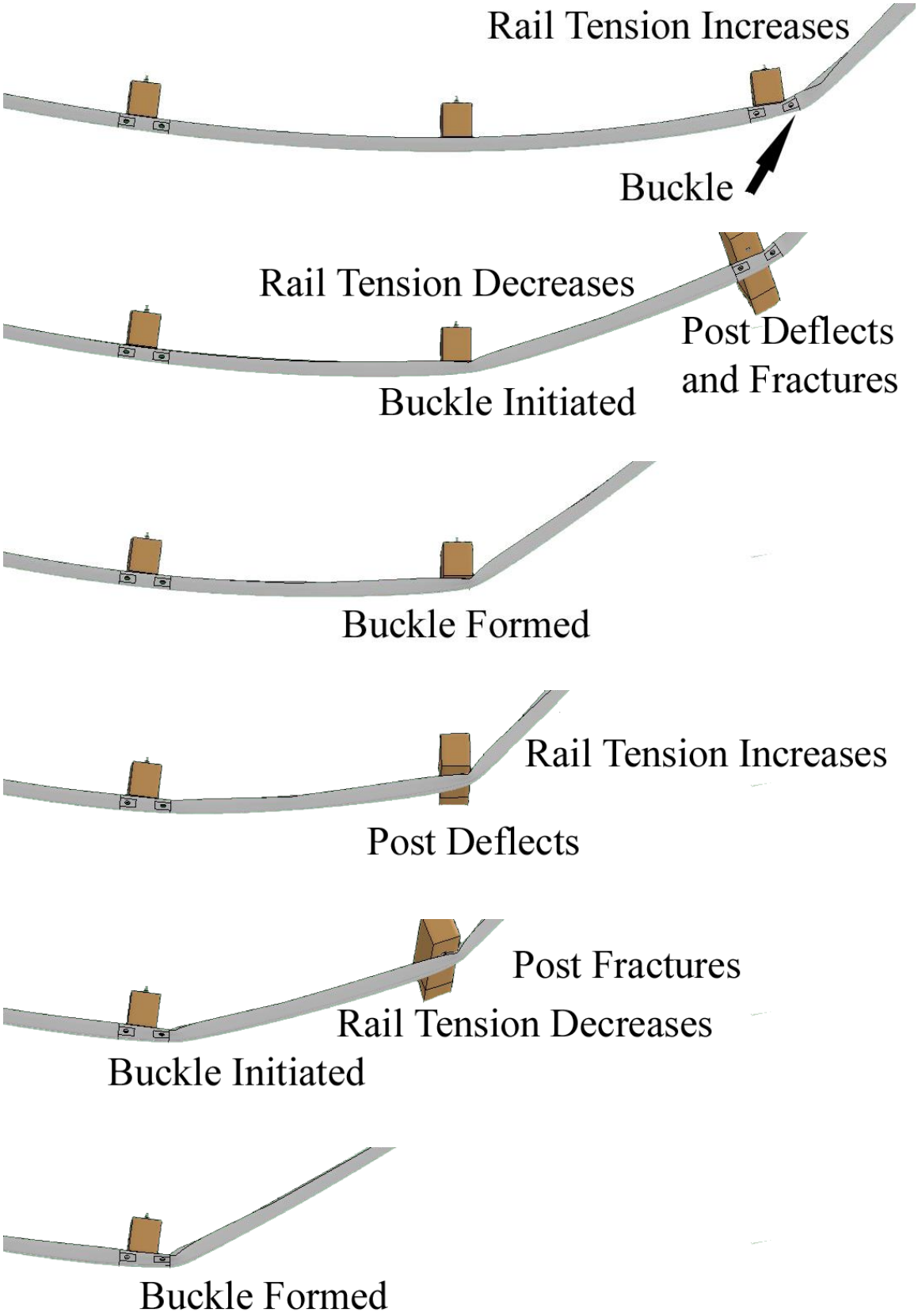

Figure 135. Progression of Rail Damage for Curved Guardrail

The criteria for determining the transitions between phases is shown in Figure 136. The duration of each phase for impacts involving systems with 31-in. (787-mm) top mounting heights is shown in Tables 26 through 28. Results were similar for successful simulations of the 27-in. (686-mm) tall systems.

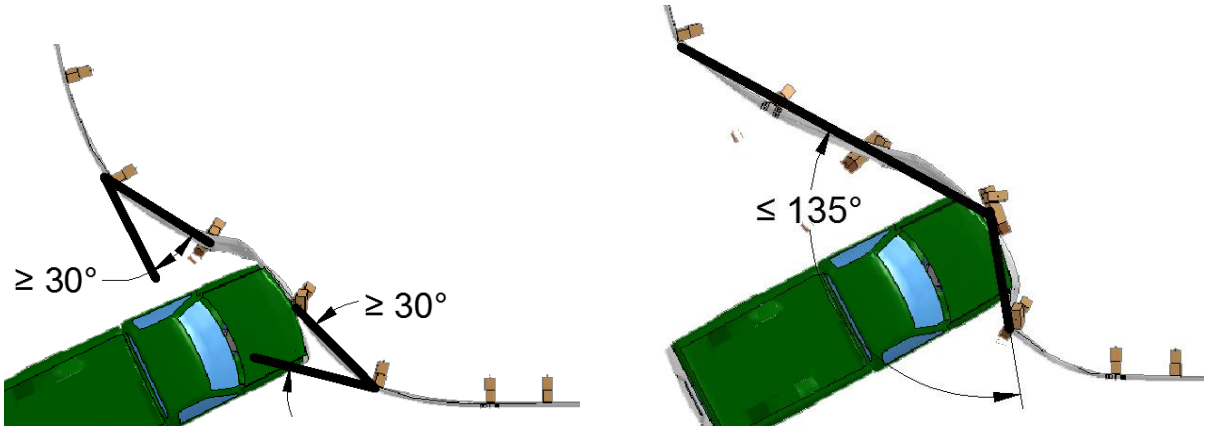

(a) (b)

Figure 136. Criteria for Identifying (a) Beginning and (b) End of Transition Between Membrane Tension and Guardrail Pocketing

Table 26. Phase Transitions for 45-mph (72-km/h), 25-degree Impacts into 24-ft (7.3-m) Radius Systems

Post No.	Phase I Membrane Tension	Phase II Mixed Tension and Pocketing		Phase III Pocketing	
		Interval	Duration	Interval	Duration
3	0-40 ms	40 ms - BCTF	27 ms	---	---
Mid 3-4	0-35 ms	35 ms - BCTF	38 ms	---	---
4	0-40 ms	40 ms - BCTF	139 ms	---	---
Mid 4-5	0-40 ms	40 ms - BCTF	138 ms	---	---
5	0-50 ms	50-135 ms	85 ms	135 ms - End	250 ms
Mid 5-6	0-50 ms	50-135 ms	85 ms	135 ms - End	485 ms
6	0-45 ms	45-185 ms	140 ms	185 ms - End	490 ms
Mid 6-7	0-85 ms	85-150 ms	65 ms	150 ms - End	530 ms
7	0-55 ms	55-160 ms	105 ms	160 ms - End	490 ms
Mid 7-8	0-45 ms	45-155 ms	110 ms	155 ms - End	430 ms

BCTF Analysis of simulation results terminated due to BCT post fracture
--- Pocket was not fully formed before analysis ended

Table 27. Phase Transitions for 45-mph (72-km/h), 25-degree Impacts into 48-ft (15-m) Radius Systems

Post No.	Phase I Membrane Tension	Phase II Mixed Tension and Pocketing		Phase III Pocketing	
		Interval	Duration	Interval	Duration
4	0-80 ms	80 ms - BCTF	24 ms	---	---
5	0-85 ms	85 ms - BCTF	74 ms	---	---
6	0-100 ms	100 ms - BCTF	178 ms	---	---
7	0-90 ms	90-325 ms	235 ms	325 ms - End	355 ms
8	0-90 ms	90-320 ms	230 ms	320 ms - End	275 ms*
9	0-85 ms	85-300 ms	215 ms	300 ms - End	300 ms*
10	0-100 ms	100-325 ms	225 ms	325 ms - End	360 ms
11	0-90 ms	90-305 ms	215 ms	305 ms - End	375 ms
12	0-95 ms	95-315 ms	220 ms	315 ms - End	370 ms
13	0-160 ms	160-230 ms	70 ms	230 ms - End	460 ms

BCTF Analysis of simulation results terminated due to BCT post fracture
--- Pocket was not fully formed before analysis ended
* Instability caused simulation to terminate early

Table 28. Phase Transitions for 45-mph (72-km/h), 25-degree Impacts into 72-ft (22-m) Radius Systems

Post No.	Phase I Membrane Tension	Phase II Mixed Tension and Pocketing		Phase III Pocketing	
		Interval	Duration	Interval	Duration
4	0-80 ms (End)	---	---	---	---
5	0-115 ms	115 ms - BCTF	38 ms	---	---
7	0-135 ms	135-525 ms	390 ms	525 ms - End	106 ms
9	0-170 ms	170-675 ms	505 ms	675 ms - End	12 ms
11	0-135 ms	135-590 ms	455 ms	590 ms - End	99 ms
13	0-150 ms	150 ms - End	545 ms	---	---
15	0-175 ms	175 ms - End	518 ms	---	---
17	0-330 ms	330 ms - End	323 ms	---	---

BCTF Analysis of simulation results terminated due to BCT post fracture
--- Pocket was not fully formed before analysis ended

An analysis of Tables 26 through 28 indicated that there was a nearly linear ratio of the increase in duration of Phase I (membrane tension) with increased radius size. The average durations of Phase I membrane tensions were 49, 92, and 147 ms for 24-, 48-, and 72-ft (7.3-, 15-, and 22-m) radii. By doubling or tripling the 24-ft (7.3-m) radius to 48 ft (15 m) or 72 ft (22

m), the duration of Phase I increased by factors of 1.88 and 3.00, respectively. Likewise the ratios of Phase I duration to radius size were 2.04, 1.92, and 2.04 ms/ft (6.70, 6.30, and 6.70 ms/m), respectively. In contrast, the duration of Phase II, or transition between which were predominantly membrane tension capture forces to predominantly guardrail pocketing capture forces, more closely resembled a quadratic relationship. The significance of these findings should be explored in future studies.

Overrides occurring downstream of the LON of the 27-in. (686-mm) tall systems were analyzed with respect to the three phases of guardrail deformation and capture noted above. For systems without blockouts, short-radius overrides occurred in disproportionately greater frequencies during Phase I deflections than for Phases II or III. Only one override was observed during Phase III guardrail deformation for 27-in. (686-mm) tall systems, for a 24-ft (7.3-m) radius system, although 80% of the failures occurring downstream of the LON of the 72-ft (22-m) radius system occurred during Phase I capture. All of the overrides observed involving the 27-in. (686-mm) tall system with blockouts occurred during the Phase II transition, regardless of radius size. Every impact in which a complete guardrail pocket was formed (i.e., the guardrail formed an included angle of less than 135 degrees around the vehicle, or Phase III deformation) involving a system with blockouts also resulted in vehicle capture. These results indicate that blockouts increased both the duration of acceptable guardrail contact with the vehicle and the likelihood of successful capture. Guardrail LONs are discussed in Section 10.2.

The process of rail tension rise, post deflection and fracture, and buckle formation and subsequent decrease in rail tension contributed to a stepwise plot of velocity vs. time. One plot of a successful impact occurring with all three radii at approximately the same impact location near the nose for each simulation is shown in Figure 137. For 24-ft (7.3-m) radii impacted at the midspan between post nos. 5 and 6, visible step-like changes in speed occurring near 100, 280,

and 460 ms, followed by periods in which speeds were relatively constant. The lags in speed reduction were related to the development of buckles in the guardrail and subsequent low rail tension, followed by increased tension prior to post fractures during times of vehicle slowing. Smaller step-like transitions in speed occurred during the 48-ft (15-m) radius system impacted at post no. 8 as well.

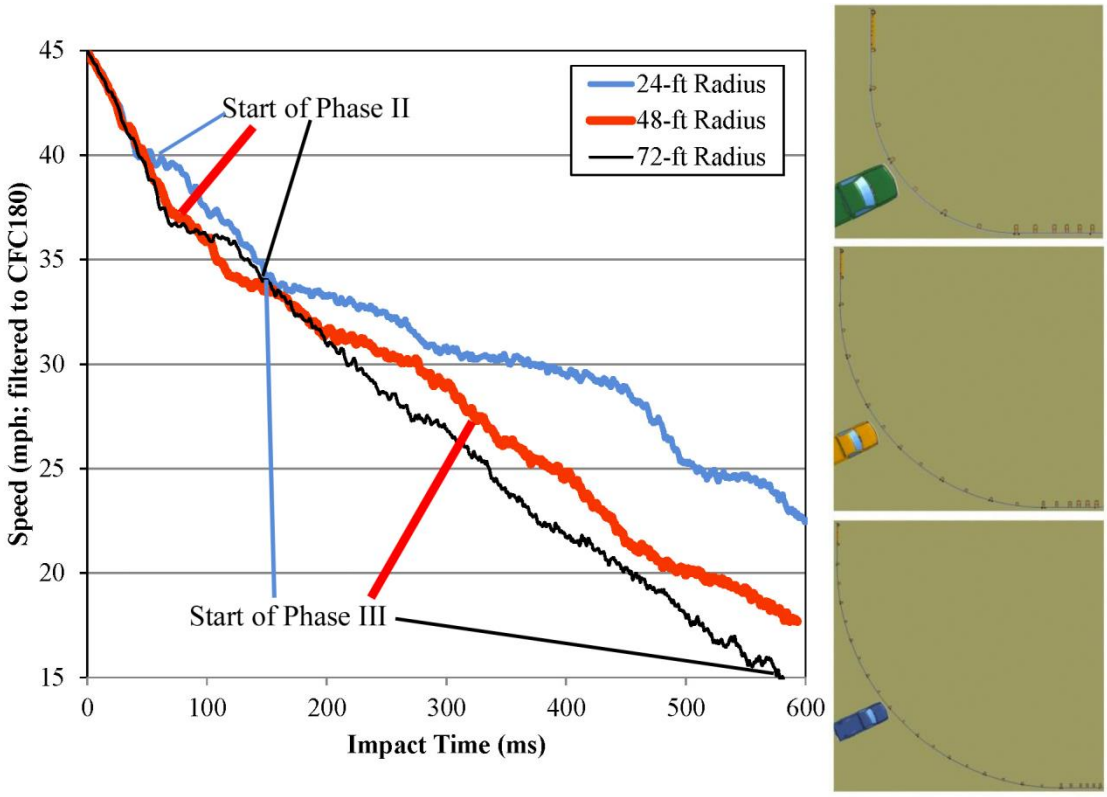

Figure 137. Vehicle Speed Comparison for Impacts near Center of Radius, 45 mph (72 km/h)

The rate of change of vehicle speed was greatest during Phase I capture and predominantly constant regardless of radius size. Rates of change of velocity decreased for Phases II and III capture. The 72-ft (22-m) radius system impacted at post no. 11 experienced smaller and less discernable speed perturbations because the phase transitions were much more gradual, and the effect of individual post fractures was not as distinctive.

As radius size increased, the duration of time in which membrane tension dominated guardrail capture increased. In addition, the duration of acceptable contacts, as well as number of

successful vehicle captures, increased for all radii for 27-in. (686-mm) tall systems. Phase transitions between predominantly membrane tension to predominantly guardrail pocketing forces were extended and became more gradual with increased radius size as well. Overall, increased radii performed better, on average, than smaller radii for most impact conditions. Also, blockouts significantly improved curved guardrail performance with a 27-in. (686-mm) tall top mounting height.

10.2 Maximum Practical Speeds for Short-Radius Guardrails

The maximum practical impact speed which will capture the majority of light truck impacts was estimated by examining the energy dissipated at the end of each simulations. Recall that analysis was terminated either when the system gated, the rail slipped below the bottom of the vehicle's front bumper, the termination time was reached, or the vehicle came to rest. For impacts occurring within the LON, in which the barrier could potentially capture or redirect a vehicle instead of gating, the maximum practical speed for non-blocked, 27-in. (686-mm) tall short radius guardrail ranged between 19 mph (31 km/h) and 22 mph (35 km/h) for radii of 24 ft (7.3 m) and 72 ft (22 m), respectively. When blockouts were added to the system, the acceptable impact speeds ranged between 29 mph (47 km/h) and 41 mph (66 km/h) for radii of 24 ft (7.3 m) and 72 ft (22 m), respectively. Impact speeds less than or equal to those indicated should result in vehicle capture, based on simulation results.

Based on system capacities and damage, it was estimated that the maximum impact speeds applicable for systems with 31-in. (787-mm) mounting heights were 45 mph (72 km/h) for systems with radii less than 45 ft (14 m) and 50 mph (80 km/h) for systems with radii greater than or equal to 45 ft (14 m). The maximum practical speeds and beginning of the LON of the 27-in. (686-mm) and 31-mm (787-mm) tall systems are shown in Table 29.

Table 29. Summary of Maximum Practical Speeds and Beginning of LON

System Configuration	24-ft (7.3-m) Radius		48-ft (15-m) Radius		72-ft (22-m) Radius	
	Max Practical Speed mph (km/h)	Beginning of LON	Max Practical Speed mph (km/h)	Beginning of LON	Max Practical Speed mph (km/h)	Beginning of LON
27-in. (686-mm) Tall No Blockouts	19 mph (30 km/h)	Post No. 5	22 mph (35 km/h)	Post No. 6	23 mph (38 km/h)	Post No. 7
27-in. (686-mm) Tall Blockouts	29 mph (47 km/h)	Post No. 5	26 mph (42 km/h)	Post No. 6	41 mph (66 km/h)	Post No. 7
31-in. (686-mm) Tall No Blockouts	45 mph (72 km/h)	Post No. 6	45 mph (72 km/h)	Post No. 7	45 mph (72 km/h)	Post No. 9
			50 mph (80 km/h)	Post No. 8	50 mph (80 km/h)	Post No. 9

NOTE: Post locations for 24, 48, and 72-ft (7.3, 15, and 22-m systems) are shown in Figures 97 through 99.

10.3 Critical Impact Locations

For all systems with 27-in. (686-mm) top rail height, the most severe impact occurred between the centerpoint of the nose and two posts downstream of the centerpoint, based on vaulting frequencies of the 27-in. (686-mm) tall systems. Vehicles which impacted up to two post spans upstream from the centerpoint of the nose remained engaged with the rail for a longer amount of time or were captured and brought to a controlled stop, as compared to vehicles impacting at or slightly downstream from the centerpoint of the nose. Although NCHRP Report 350 test conditions require vehicle impact with the center of the nose of a short-radius system, generally these test conditions have a line layout in which the centerline of the test vehicle is aligned with the centerpoint of the nose. The simulation modeling performed in this research suggested that impacts slightly downstream of the center of the radius may prove more difficult for all guardrail radii.

10.4 Causes of Vaulting and Penetration

Guardrail twisting and sliding beneath the impacting vehicle's bumper contributed to barrier override and vaulting. A comparison of the engagement of the vehicle's front end with

the rail with 27-in. (686-mm) and 31-in. (787-mm) tall guardrail curved systems is shown in Figures 138 and 139. Immediately after impact with a 27-in. (686-mm) tall guardrail, the top corrugation flattened and the bottom corrugation protruded beneath the bumper. As a result, the rail engagement with the bumper was unstable. Rail twisting occurred when posts rotated or fractured and were deflected backward before disengaging from the rail, and tended to accentuate rail slippage below the bumper. In addition, simulated pickup vehicles were more likely to vault during intermittent periods of low tension in the guardrail after post fractures.

In contrast, during impact with 31-in. (787-mm) tall systems, the bumper initially interacted with the bottom corrugation and the top corrugation protruded over the bumper. Because the region of the vehicle corresponding to the grill, radiator, and headlights was both recessed from the bumper and relatively broad and deformable, the rail tended to stably interact with the front of the vehicle and become interlocked. Although posts rotated or fractured, and some posts remained attached to the rail, due to bumper interaction the rail remained contact with the front of the vehicle until the vehicle came to rest.

Tire interaction with post debris also contributed to some vaulting overrides in the simulations. After posts fractured, posts which slid beneath the vehicle's wheels contributed to suspension compression and vehicle uplift. For example, during simulations of the 27-in. (686-mm) tall systems at and slightly downstream from the centerpoint of the radius for all radii, tire interaction with post debris contributed to vaulting. The orientation of the vehicle and impact direction caused fractured posts to fall directly in front of the front wheels, where they were overridden. Similar rail overrides due to debris interaction were noted during full-scale testing of the MwRSF TL-3 short-radius system [12-14]. Sequential images of impact at post no. 9 with a 27-in. (686-mm) tall system with a 48-ft (15-m) radius with blockouts are shown in Figure 140.

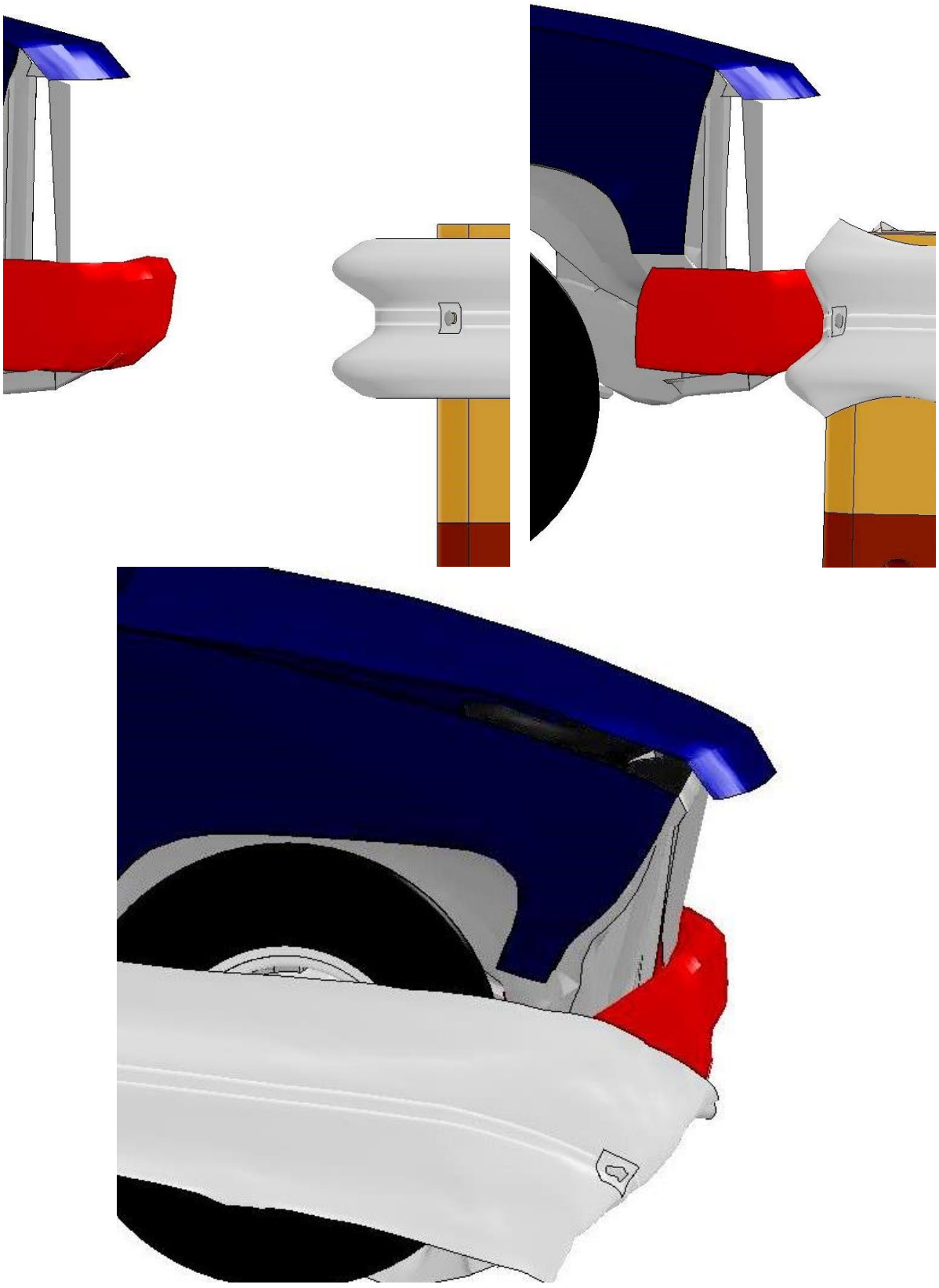

Figure 138. Upper Corrugation Flattening and Twisting Below Vehicle, 27-in. (686-mm) Rail Height

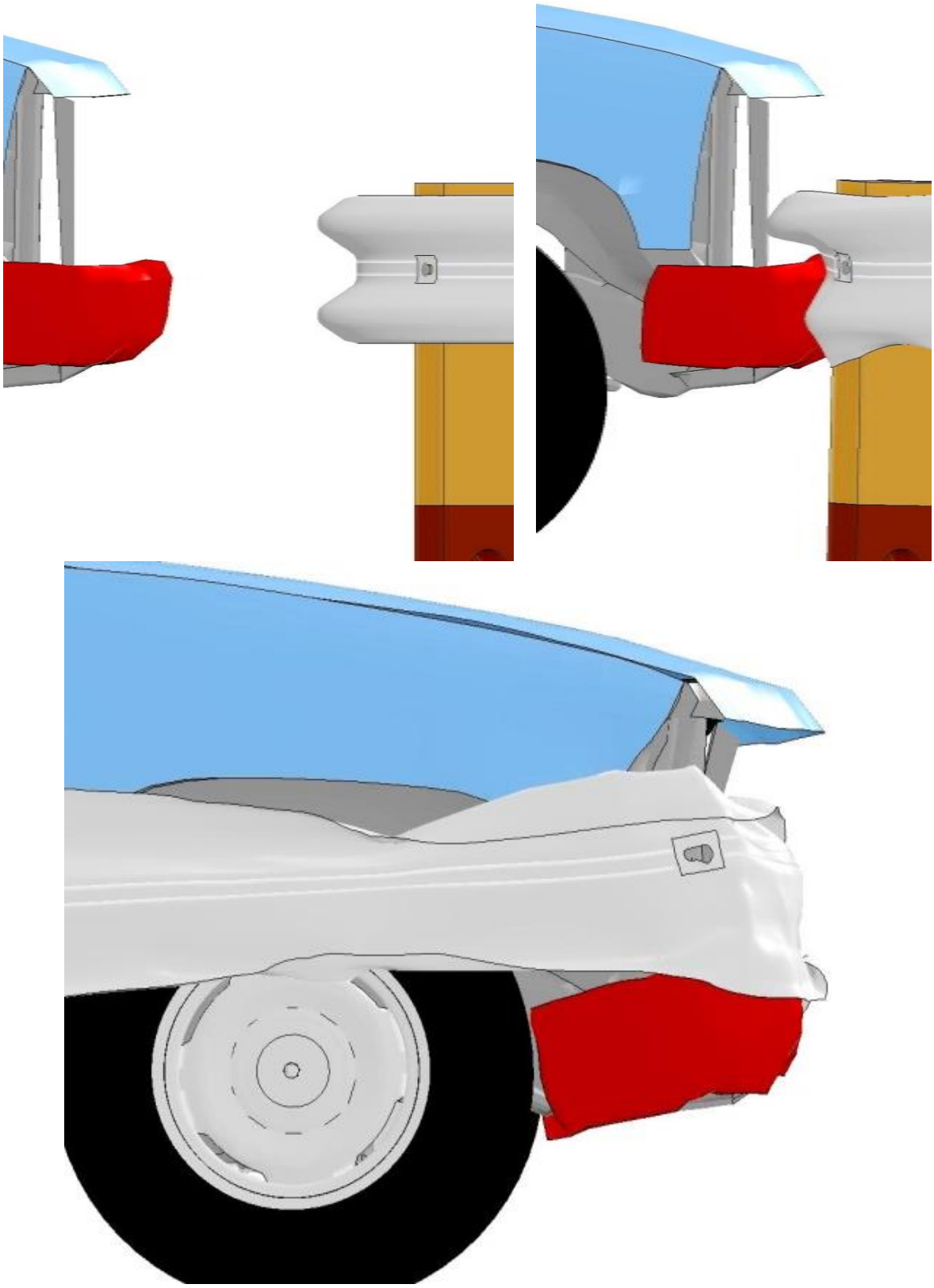

Figure 139. Lower Corrugation Flattening and Interlocking with Vehicle, 31-in. (787-mm) Rail Height (bumper colored red for clarity)

10.5 Additional Concerns

Because the 27-in. (686-mm) guardrail mounting height is impractical for most radii of interest, researchers believed that a taller guardrail mounting height was necessary to ensure acceptable interaction with light truck vehicles. For a 31-in. (787-mm) top rail height, passenger cars may underride the short radius systems if impacted with similar impact conditions. Without full-scale testing or simulation data, it is advised to proceed cautiously if a 31-in. (787-mm) tall rail height is utilized.

All short-radius guardrail designs, which have been approved according to criteria presented in NCHRP Report No. 230, were 27-in. (686-mm) tall. Taller short-radius systems have been installed. For example, researchers at Caltrans discussed Minnesota DOT's experience installing 29-in. (737-mm) W-beam bullnose systems in 1965 near the Minneapolis-St. Paul area [16]. The design was not tested to contemporary standards, but crash data collected by the Minnesota DOT indicated an overall acceptable performance between 1965 and 1970 [34]. Subsequent tests of the MN bullnose design conducted at TTI in 1975 utilized 27-in. (686-mm) tall W-beam for compliance testing with NCHRP Report 230 [15]. No W-beam short-radius system has been crash tested specifically for compliance with NCHRP Report No. 350 or MASH.

Of the failed short-radius guardrail tests, two testing agencies examined thrie beam short radius guardrail designs with a top rail height of at least 31 in. (787 mm): TTI [8] and MwRSF [12-14]. Both agencies began testing according to NCHRP Report No. 350 TL-3 impact conditions, but they to abandon further research and development due to lack of funds and frequent test failures. Small car underride occurred to some degree during tests with both systems. However, underride potential may be reduced when impacted with TL-2 impact conditions.

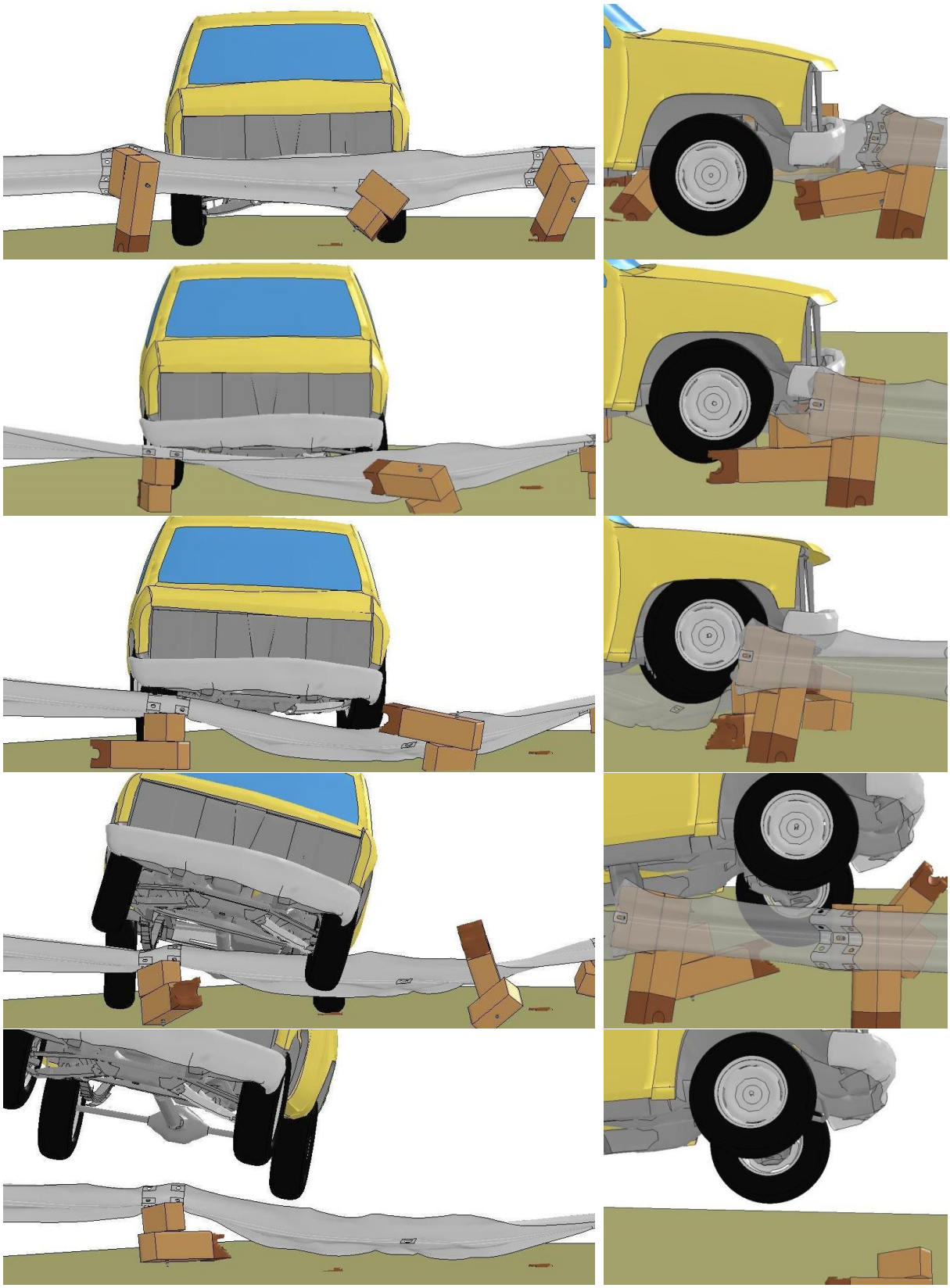

Figure 140. Wheel Interaction with Post Debris, 45 mph (72 km/h) impact with 27-in. (686-mm) Tall, 48-ft (15-m) Radius System with Blockouts at Post No. 10

Whereas thrie beam short-`radius systems failed multiple crash tests, a thrie beam bullnose system was successfully tested according to NCHRP Report No. 350 TL-3 impact conditions. The major difference between thrie beam bullnose and thrie beam short-radius guardrail is that, during head-on impacts, deflected guardrails in bullnose systems frequently undergo a nearly 180-degree bend over short radii of curvature. Because of this, redirective forces are transmitted through compressive resistance of the rails, and multiple, intermediate bends are formed, which retains rail tensions throughout impact. For short-radius systems, the angles between the primary and secondary roadway sides are typically less than 180 degrees, and the rails are loaded in a combination of tension and bending. Buckles and kinks form at post locations, but no intermediate buckles develop between adjacent post spans. Thus, little to no compressive loading occurs in short-radius guardrails, and the energy absorbed by the rail is decreased.

The 31-in. (787-mm) tall curved guardrail systems simulated have a potential for small car underride when impacted near a perpendicular orientation. There are fewer concerns that small cars will fail to be redirected or adequately captured by taller rails when impacts approach tangential to the rail. Recent testing of the MGS at very large flare rates indicated that for impact angles as high as 31 degrees into a 31-in. (787-mm) tall system, small cars did not underride beneath the guardrail [37]. Later tests conducted at MwRSF using an MGS guardrail with a 36-in. (914-mm) top mounting height successfully redirected an 1100C small car impacting with MASH TL-3 impact conditions [38]. Although small cars may be more susceptible to underride for near-perpendicular impacts into rails with a 31-in. (787-mm) top mounting height, acceptable performance has been demonstrated for less severe impacts. Thus, for radii as large as 72 ft (22 m), the 31-in. (787-mm) tall curved guardrail system may perform acceptable for most small car impacts occurring within the clear zone. Smaller radii may not perform as well as larger radii.

A proposed solution to reduce the risk of small car underride and retain the benefits of higher rail height for guardrail installed at intersecting roadways is to raise the guardrail by 2 in. (51 mm) to a top rail mounting height of 29 in. (737 mm). There is little historical precedent to estimate the ability of a 29-in. (737-mm) tall system to redirect both passenger cars and light trucks. However, because even 31-in. (787-mm) tall thrie beam short radius systems, which have bottom corrugation heights of approximately 13 in. (330 mm), still caused passenger car underride, researchers do not recommend installation of 31-in. (787-mm) tall W-beam short radius systems until crash testing can verify the crashworthiness of this system.

Another proposed solution to reduce the system deflection was to use half-post spacing. Although this solution may pose benefits in reduced dynamic deflection and better engagement with the pickup, half-post spacing may be excessively stiff for small car impacts and could cause occupant risk criteria to be violated or may promote underride. Further research and full-scale crash testing is recommended before reducing the post spacing of CRT posts on or adjacent to the radius.

11 CURVED GUARDRAIL EFFECTIVENESS EVALUATION

The performance of curved guardrail systems was determined, but it was uncertain as to what percentage of real-world crashes would be captured with these systems based on system performance limits. Researchers utilized the maximum practical impact speeds determined for each larger-radius, curved guardrail system to estimate the percentage of real-world crashes which researchers expected the curved guardrail systems to accommodate, using speed distributions on 45-mph (72-km/h) roadways. Distributions were obtained from a database of run-off-road (ROR) crashes assembled during completion of NCHRP Projects 17-22 and 17-11, which tabulated vehicle speed at roadside departure and at up to four unique impact locations, as well as CG trajectory angles, vehicle heading angles, and hazard locations [36]. A total of 186 crashes occurring on 45-mph (72-km/h) roadways were extracted and analyzed.

The 17-22 and 17-11 crash database overrepresented severe crashes. As a result, crash scaling factors extracted from SAS were applied to estimate globally-representative conditions as well. Problems with scale factors were noted, including that 4% of the crashes had weighting factors greater than 4,000, and several more above 2,000, whereas 55% of crashes had weighting factors less than 100. Therefore, the seven highest and lowest weighted crashes were excluded as outliers in both unweighted and weighted databases, to give adjusted data sets.

As a result, the adjusted, non-weighted database was considered to be representative of severe crashes, and the adjusted, weighted database was considered to be representative of most crashes occurring on 45-mph (72 km/h) roadways. The adjusted and non-adjusted distributions of roadway departure speeds and departure IS values are shown in Figures 141 and 142, respectively. Departure speeds frequently exceeded the nominal posted speed limit (PSL) in all data sets. Roadway departure speeds of 45 and 50 mph (72 and 80 km/h) represented the 58th and 68th percentile of severe crashes and the 72nd and 83rd percentiles of all crashes, respectively.

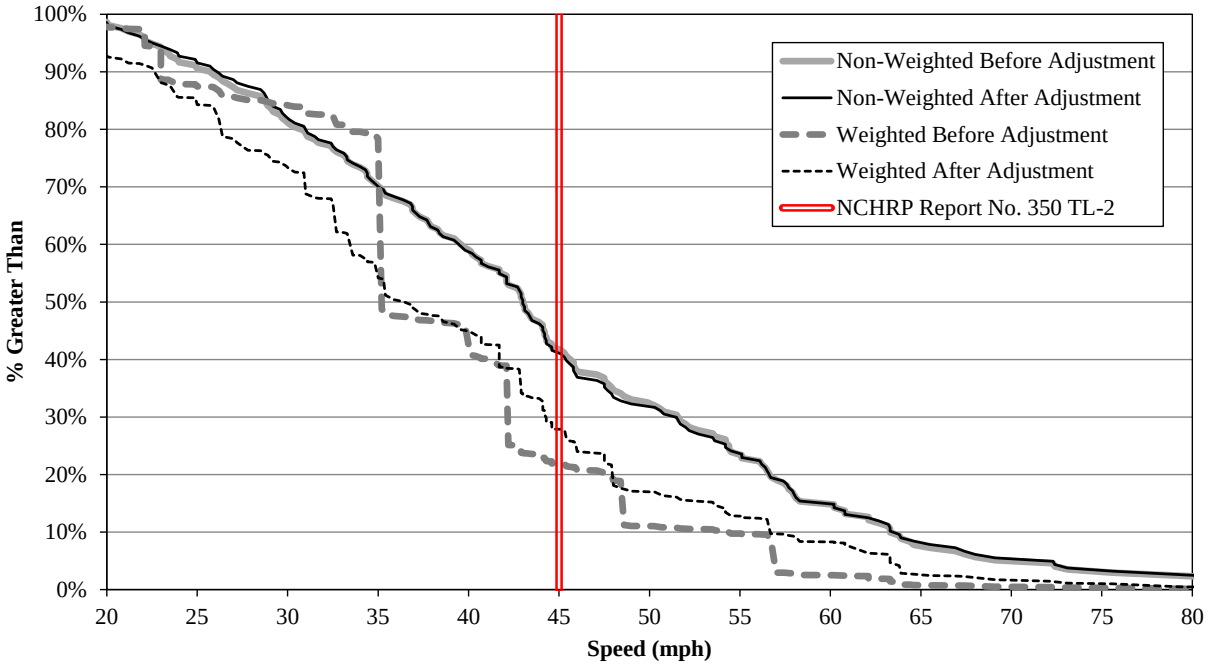

Figure 141. Departure Speed Distribution Comparison for 45-mph (72-km/h) Roadways using NCHRP Report No. 665 Data [36]

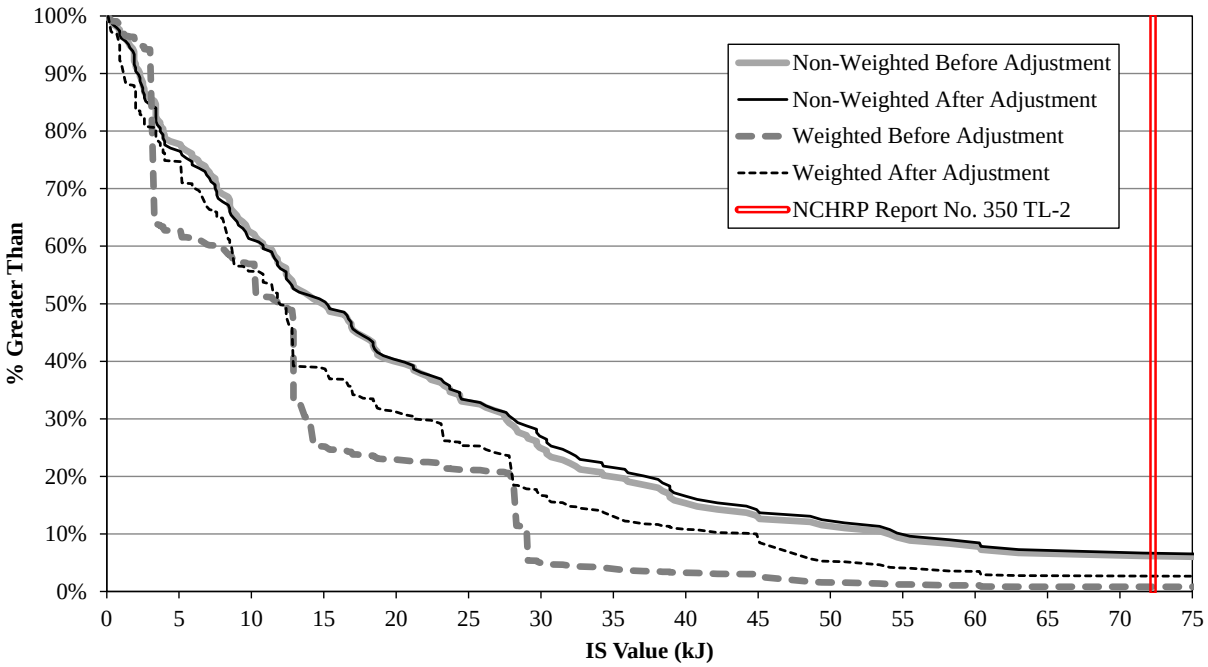

Figure 142. Roadway Departure IS-Value Distribution Comparisons for 45-mph (72-km/h) Roadways using NCHRP Report No. 665 Data [36]

To estimate the percentage of impacting vehicles which would be captured by each curved guardrail design, the maximum practical capture speed for each simulated system was

compared to the departure speed and IS-value distributions shown in Figures 141 and 142, as well as total vehicle energy at departure. Results of the analysis are shown in **Error! Not a valid bookmark self-reference.**. By evaluating only the impact speeds, passenger car impacts could be overweighted; thus the capture percentage calculated comparing vehicle real-world vehicle departure speeds and maximum practical system impact speeds was believed to underestimate the percentage of vehicle captures. Likewise, by only considering IS-value, the NCHRP Report No. 350 impact conditions are overweighted due to the 25-degree impact angle. Still, impact angle may be less critical during impact with curved guardrail systems within the radius and downstream of the LON, since the vehicle will be completely captured and come to a stop. Thus, evaluation based on IS-value was believed to overestimate the percentage of impacting vehicles captured, and would likely represent the upper bound of possible system performance. The average performance of the system was therefore correlated with the total vehicle energy at the point of departure, which factored in both vehicle size and speed. Most vehicles with less energy at impact than what was simulated would likely be captured, whereas some vehicles with more energy at impact than was simulated would likely penetrate behind the system. This is predominantly true for smaller-radius systems with limited secondary and primary side tangent guardrail lengths.

Using the adjusted 17-22 and 17-11 data to represent severe (non-weighted) and global (weighted) crash conditions, the average estimated capture percentages were plotted for systems with 24-, 48-, and 72-ft (7.3-, 15-, and 22-m) radii, as shown in . The plots did not take into account the potential reduction in capture frequency due to small car underride, but it is still believed to be reasonably accurate, in part because impact speeds may be much lower than departure speeds; thus the analysis may be considered conservative.

Table 30. Percentage of Crashes Captured by Curved Guardrail Designs

Curved Guardrail Configuration	Radius	Maximum Practical Speed	Maximum IS Value	NCHRP Report 665 Database [36] Capture Percentage Based on Speed (Lower Bound)	Capture Percentage Based on Energy (Expected Average)	Capture Percentage Based on IS Value (Upper Bound)
27 in. (686 mm) Tall No Blockouts	24 ft (7.3 m)	19 mph (30 km/h)	9.1 kip-ft (12.3 kJ)	2% Non-Adjusted 16% Adjusted	23% Non-Adjusted 37% Adjusted	42% Non-Adjusted 49% Adjusted
	48 ft (15 m)	22 mph (35 km/h)	12.8 kip-ft (17.3 kJ)	8.5% Non-Adjusted 22% Adjusted	26% Non-Adjusted 40% Adjusted	45% Non-Adjusted 52% Adjusted
	72 ft (22 m)	23 mph (38 km/h)	14.4 kip-ft (19.5 kJ)	11% Non-Adjusted 24% Adjusted	28% Non-Adjusted 41% Adjusted	46% Non-Adjusted 53% Adjusted
27 in. (686 mm) Tall With Blockouts	24 ft (7.3 m)	29 mph (47 km/h)	22.4 kip-ft (30.4 kJ)	22% Non-Adjusted 34% Adjusted	34% Non-Adjusted 48% Adjusted	52% Non-Adjusted 59% Adjusted
	48 ft (15 m)	26 mph (42 km/h)	17.6 kip-ft (23.9 kJ)	16% Non-Adjusted 28% Adjusted	30% Non-Adjusted 44% Adjusted	49% Non-Adjusted 55% Adjusted
	72 ft (22 m)	41 mph (66 km/h)	44.8 kip-ft (60.7 kJ)	44% Non-Adjusted 55% Adjusted	54% Non-Adjusted 65% Adjusted	70% Non-Adjusted 75% Adjusted
31 in. (787 mm) Tall With Blockouts	24 ft (7.3 m)	45 mph (72 km/h)	53.3 kip-ft (72.3 kJ)	51% Non-Adjusted 62% Adjusted	61% Non-Adjusted 71% Adjusted	76% Non-Adjusted 82% Adjusted
	48 ft (15 m)	50 mph (80 km/h)	65.8 kip-ft (89.2 kJ)	61% Non-Adjusted 71% Adjusted	72% Non-Adjusted 81% Adjusted	86% Non-Adjusted 91% Adjusted
	72 ft (22 m)	50 mph (80 km/h)	65.8 kip-ft (89.2 kJ)	61% Non-Adjusted 71% Adjusted	72% Non-Adjusted 81% Adjusted	86% Non-Adjusted 91% Adjusted

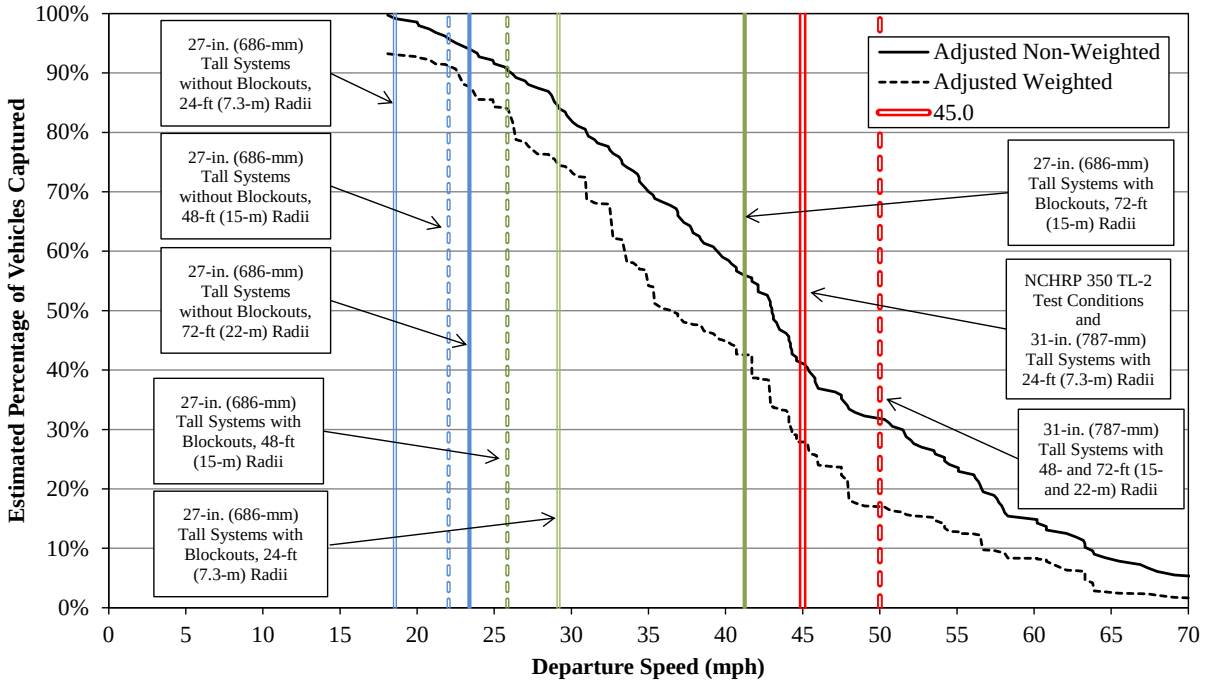

Figure 143. Distribution of Vehicle Speeds and Expected Lower Bound of Capture Frequency

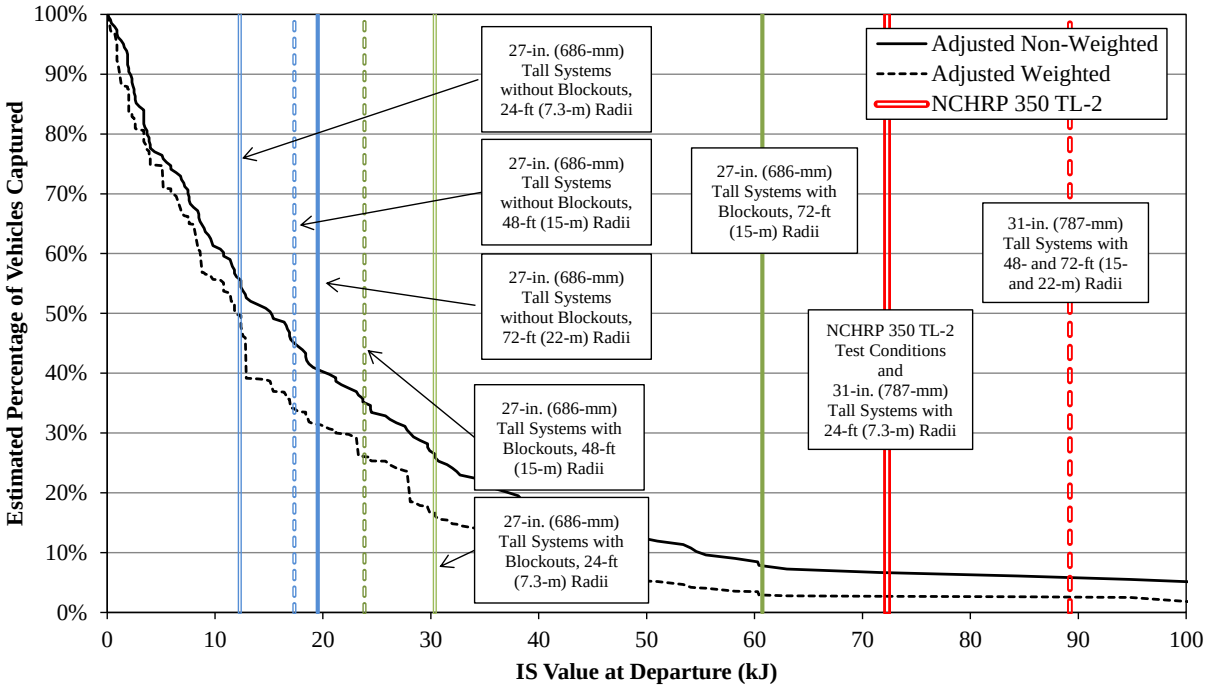

Figure 144. Vehicle IS Value at Departure and Expected Upper Bound of Capture Frequency

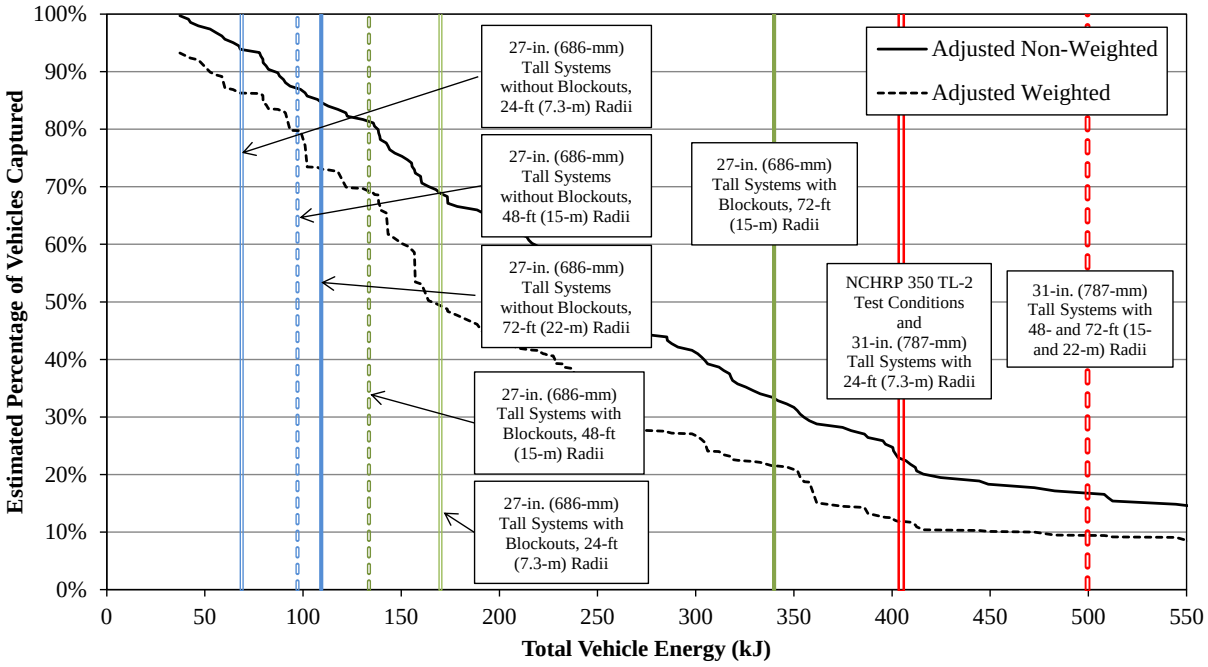

Figure 145. Total Vehicle Energy at Departure and Expected Average Guardrail Capture Frequency

12 SIMULATION OF SYSTEMS WITH 29-IN. (737-MM) MOUNTING HEIGHTS

12.1 Introduction

The 31-in. (787-mm tall curved guardrail satisfactorily captured the simulated C2500 pickup truck for many impact conditions. In contrast, the 27-in. (686-mm) tall system rarely captured the simulated vehicle and brought it to a controlled stop. However, in recognition of the risk that may be incurred by raising the guardrail mounting height by 4 in. (102 mm), an alternative large-radii solution with a 29-in. (737-mm) top mounting height was pursued. Although no short-radius guardrail has evern been tested at a top mounting height of 29 in. (737 mm), the geometry and height of a light truck bumper relative to the guardrail indicated likelihood for vehicle redirection or capture. In addition, the lowest practical guardrail height that could still redirect or contain an impacting 2000P light truck vehicle could reduce the propensity for small cars to underride beneath the barrier and maximize overall safety performance.

Based on the analysis of guardrail LON and critical impact locations of 27-in. (686-mm) tall systems impacted at 45 mph (72 km/h), simulations were conducted with 29-in. (737-mm) tall W-beam guardrail downstream from the centerpoint of each radius. Impacts upstream from the centerpoint were either less severe than impacts occurring at or downstream from the centerpoint, or resulted in vehicles gating through the end termination.

In addition, because blockouts significantly improved the guardrail-to-bumper interactions, 6-in. x 8-in. x 14½-in. (152-mm x 203-mm x 362-mm) blockouts were also added to each of the CRT posts. Blockouts could retain the rail at impact height for a longer amount of time, improving truck performance, while not adversely affecting small car underride potential and reducing the risk of a vehicle's wheel interacting with deflected posts.

12.2 Generation of 29-in. (737-mm) Tall System Models

The 29-in. (737-mm) tall short-radius system models were similar to the 27-in. (686-mm) guardrail models with blockouts. The rail height, transition posts, CRT and BCT posts, guardrail, and stiffening C-channel were all raised by 2 in. (51 mm), and the CRT and BCT holes were shifted downward by 2 in. (51 mm) to be in the same locations as the 27-in. (686-mm) tall system. The end anchorage BCT cable was adjusted for the increased height between the rail anchorage and the post. No other changes were made to the system models.

12.3 Simulation Results

12.3.1 Systems with 24-ft (7.3-m) Radius

Three simulations were conducted using the 24-ft (7.3-m) radius, corresponding to impacts at post nos. 5, 6, and 7. Impacts upstream from post no. 5 resulted in gating, and so were not critical to the performance of the system. Each impact was simulated with a 4,409-lb (2,000-kg) pickup truck impacting at 45 mph (72 km/h) and 25 degrees. Time-sequential images of the impacts are shown in Figures 146 through 148.

Upon impact, the top and bottom rail corrugations flattened around the front of the impacting pickup. The top of the upper corrugation extended above the top surface of the bumper. The bumper was crushed and deflected backward, and the vehicle pitched forward, which enabled the rail to slide upward and become interlocked with the headlight, grill, and radiator locations. Because of this, the vehicle was captured in each of the simulations. System damage was consistent with impacts at both the 27-in. (686-mm) system with blockouts and 31-in. (787-mm) system without blockouts, at similar impact times.

12.3.2 Systems with 48-ft (15-m) Radius

Five simulations were conducted using the 48-ft (15-m) radius, corresponding to impacts at post nos. 9, 10, 11, 12, and 13, and utilized a 4,409-lb (2,000-kg) pickup truck model

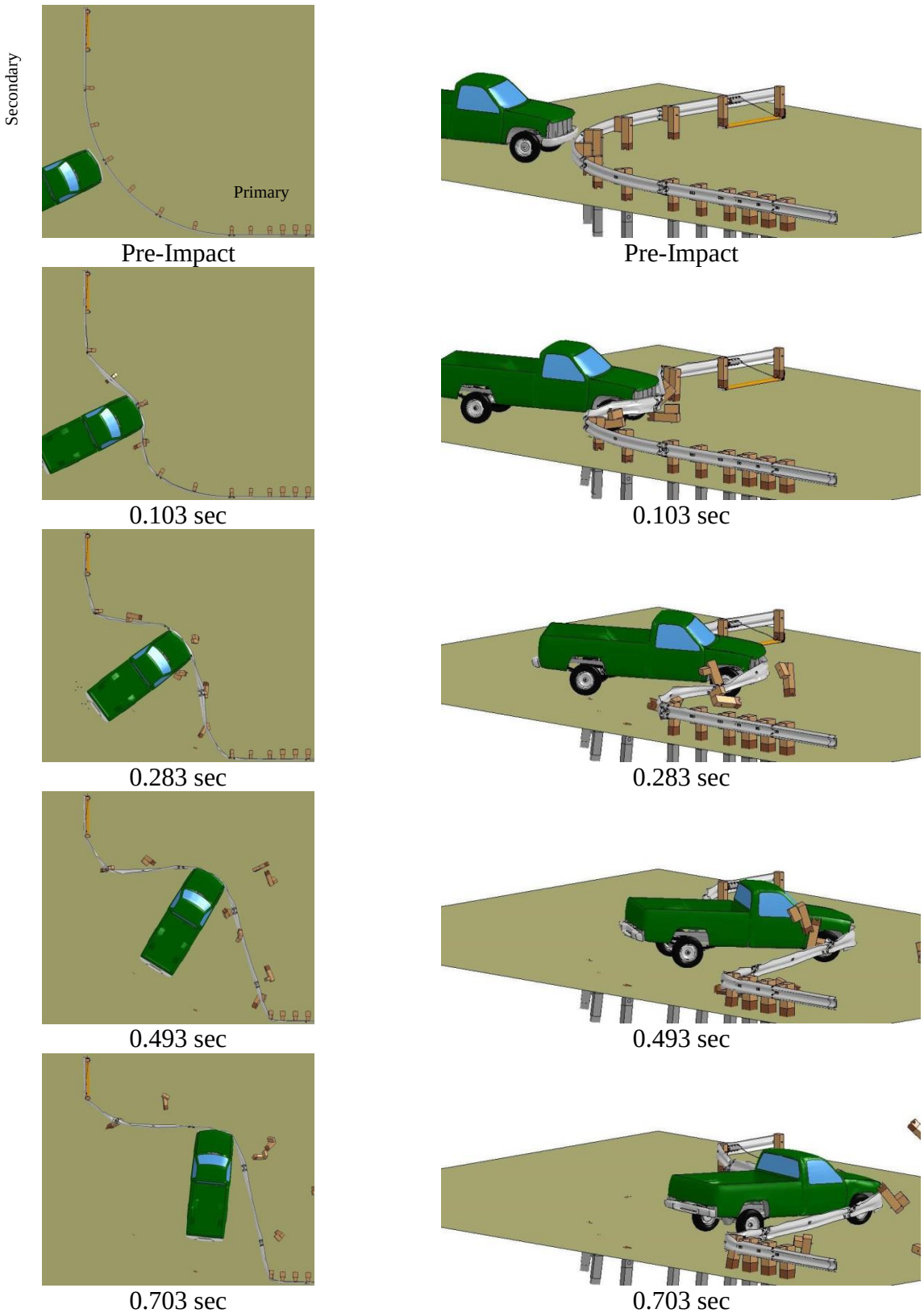

Figure 146. Time-Sequential Images of Impact at Post No. 5, 24-ft (7.3-m) Radius System with 29-in. (737-mm) Mounting Height

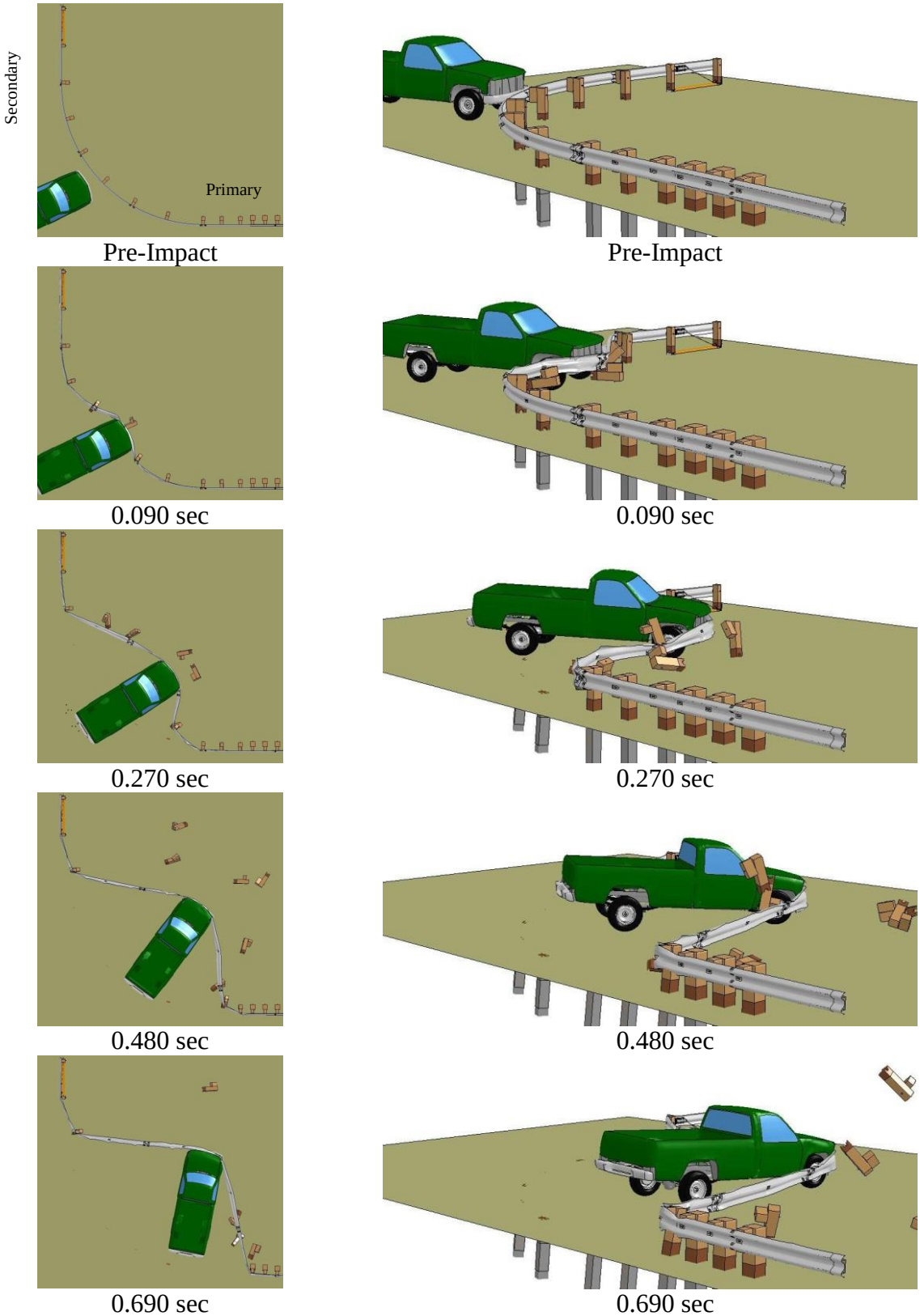

Figure 147. Time-Sequential Images of Impact at Post No. 6, 24-ft (7.3-m) Radius System with 29-in. (737-mm) Mounting Height

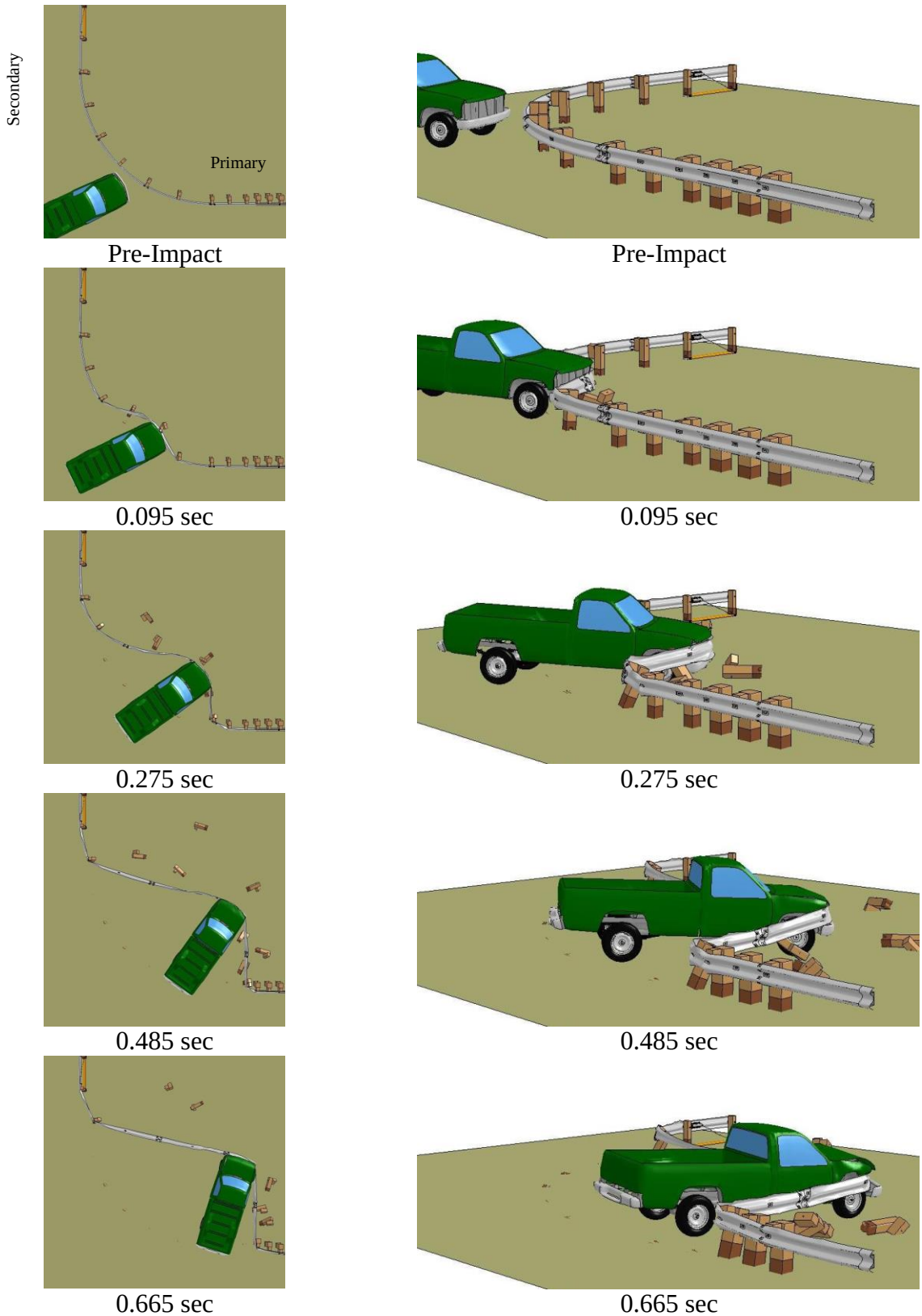

Figure 148. Time-Sequential Images of Impact at Post No. 7, 24-ft (7.3-m) Radius System with 29-in. (737-mm) Mounting Height

impacting at 45 mph (72 km/h) and 25 degrees. Time-sequential images of the impacts are shown in Figures 149 through 153. All five impacts resulted in acceptable vehicle capture. Impact results were similar to results of the 24-ft (7.3-m) radius, because the bottom corrugation flattened and the rail lifted upward to engage the front of the truck after approximately 500 ms.

The largest deflections observed in the simulations with a 48-ft (15-m) radius occurred near the center of the nose. Deflections decreased as the vehicle approached the transition to stiff bridge rail, and the pocketing propensity increased, as shown in Figures 152 and 153. However, vehicle decelerations were not excessive and were typically lower during pocketing than during the initial 50-ms of impact.

12.3.3 Systems with 72-ft (22-m) Radius

Four simulations were conducted with a 72-ft (22-m) radius, corresponding to impacts at post nos. 13, 15, 17, and 19 and utilized a 4,409-lb (2,000-kg) pickup truck model impacting at 45 mph (72 km/h) and 25 degrees. As with simulations of the 24-ft (7.3-m) and 28-ft (15-m) radii, the pickup truck was captured after the upper corrugation flattened and shifted above the bumper to become interlocked with the headlight, grill, and radiator locations, at approximately 500 ms.

Vehicle deflections were typically less than for impacts with smaller radii. Whereas the impacting truck was still engaged in the system and the vehicle continued to slow longitudinally for smaller-radius systems at approximately 850 ms, the pickup in the larger-radius simulations stopped all longitudinal deflection and was only yawing around the front end at the end for impacts at post nos. 13 and 15. During impact at post no. 17, the vehicle experienced very little yaw displacement, and came to rest after a pocket formed in the rail. The vehicle was redirected during impact at post no. 19.

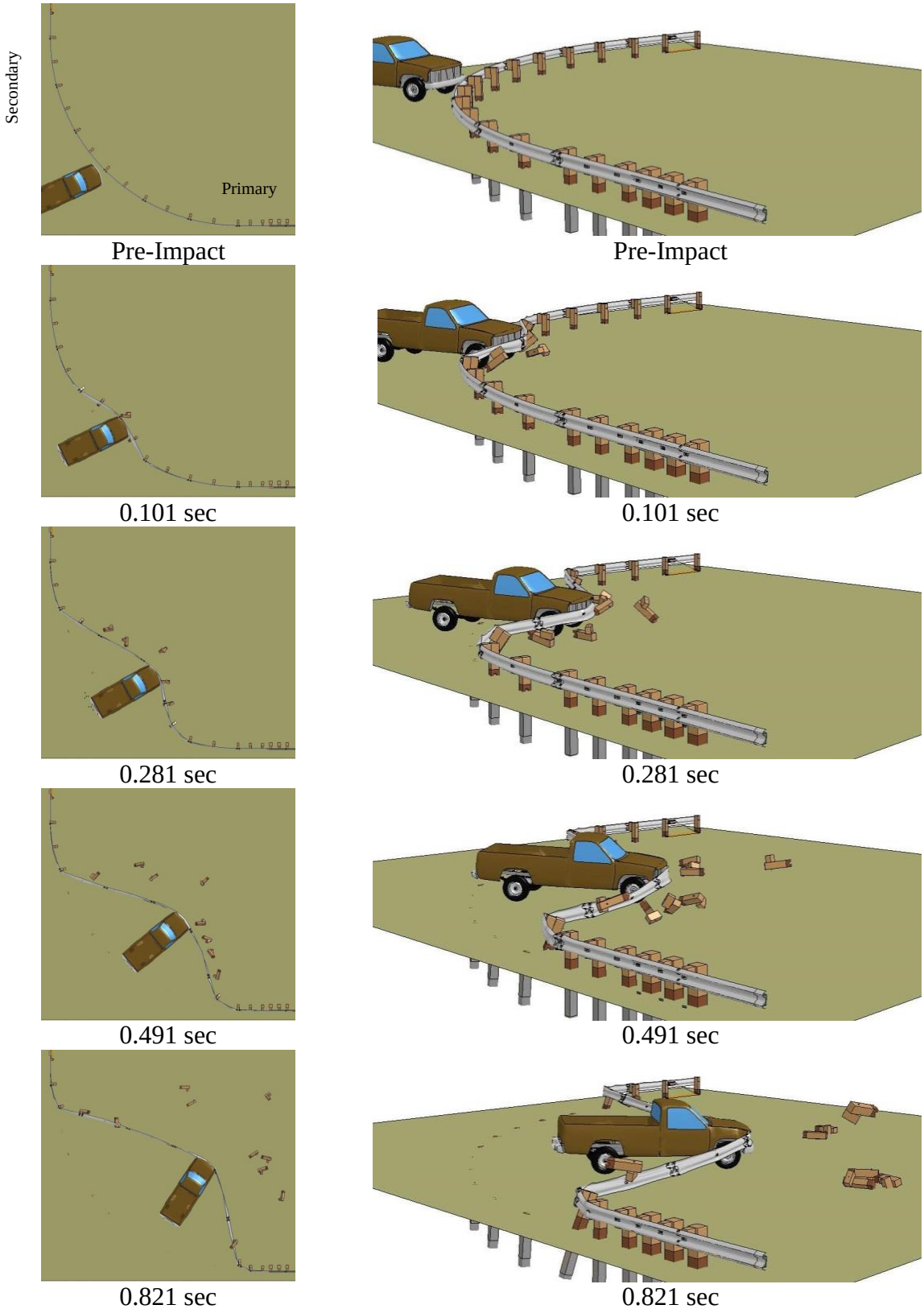

Figure 149. Time-Sequential Images of Impact at Post No. 9, 48-ft (15-m) Radius System with 29-in. (737-mm) Mounting Height

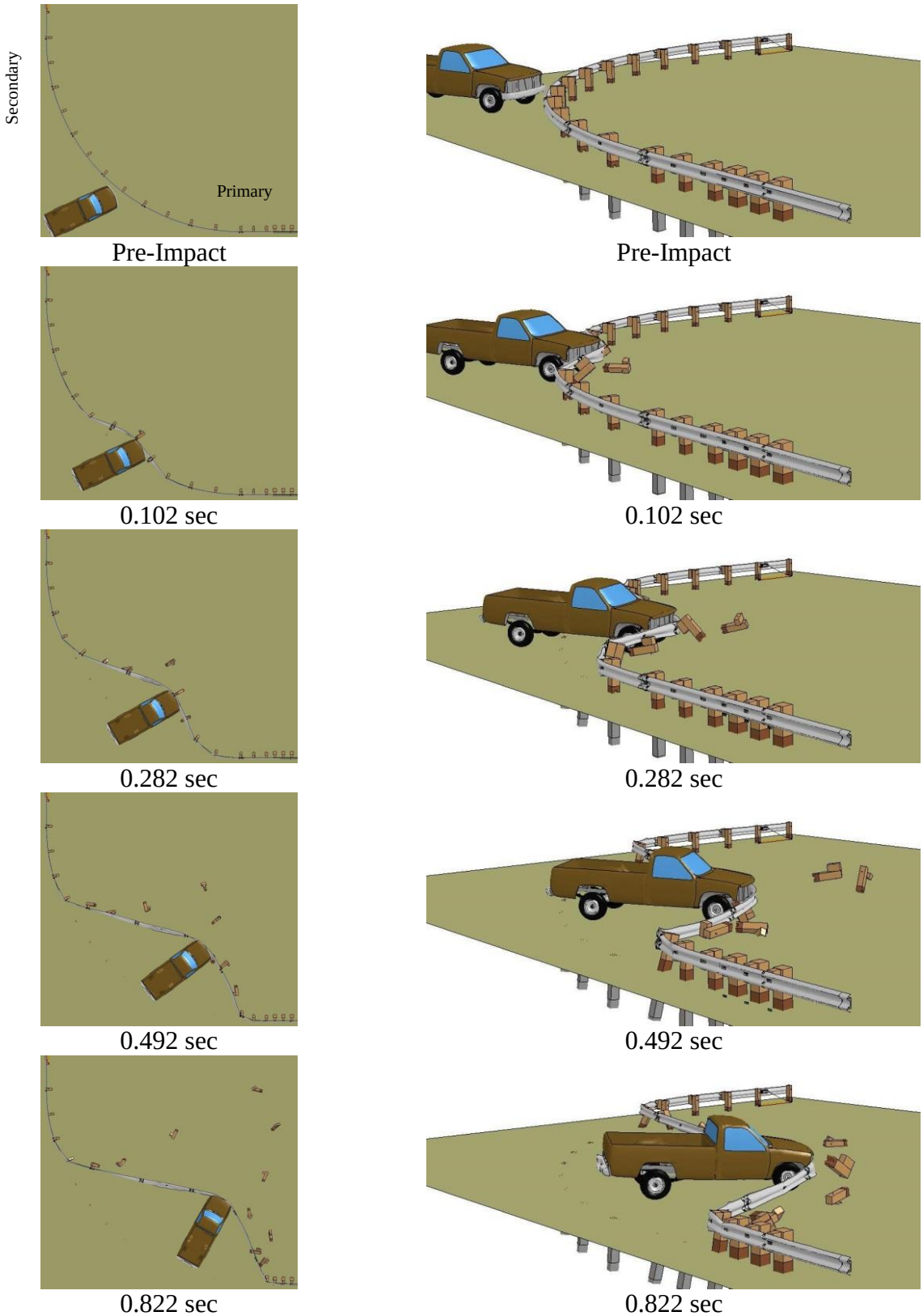

Figure 150. Time-Sequential Images of Impact at Post No. 10, 48-ft (15-m) Radius System with 29-in. (737-mm) Mounting Height

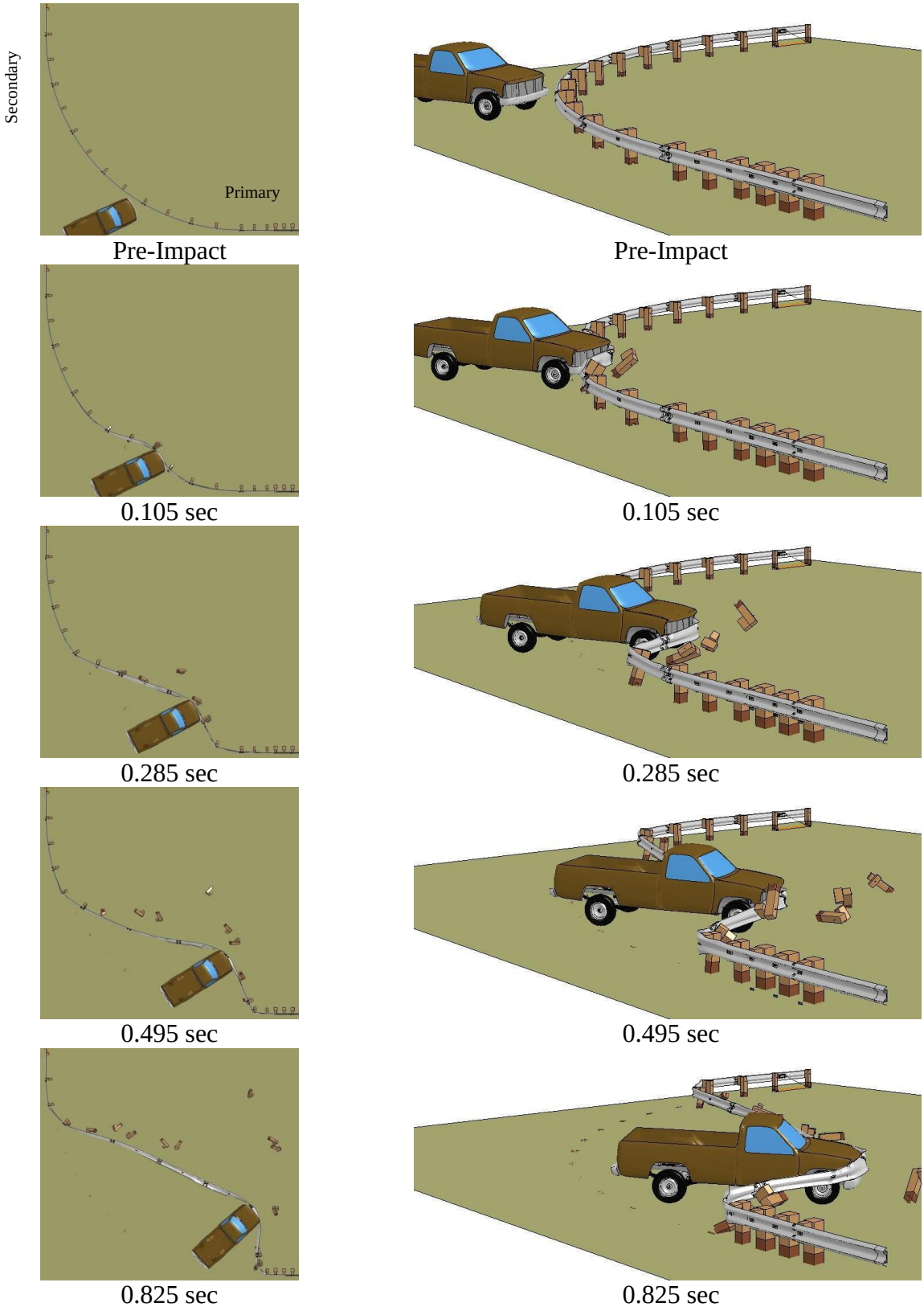

Figure 151. Time-Sequential Images of Impact at Post No. 11, 48-ft (15-m) Radius System with 29-in. (737-mm) Mounting Height

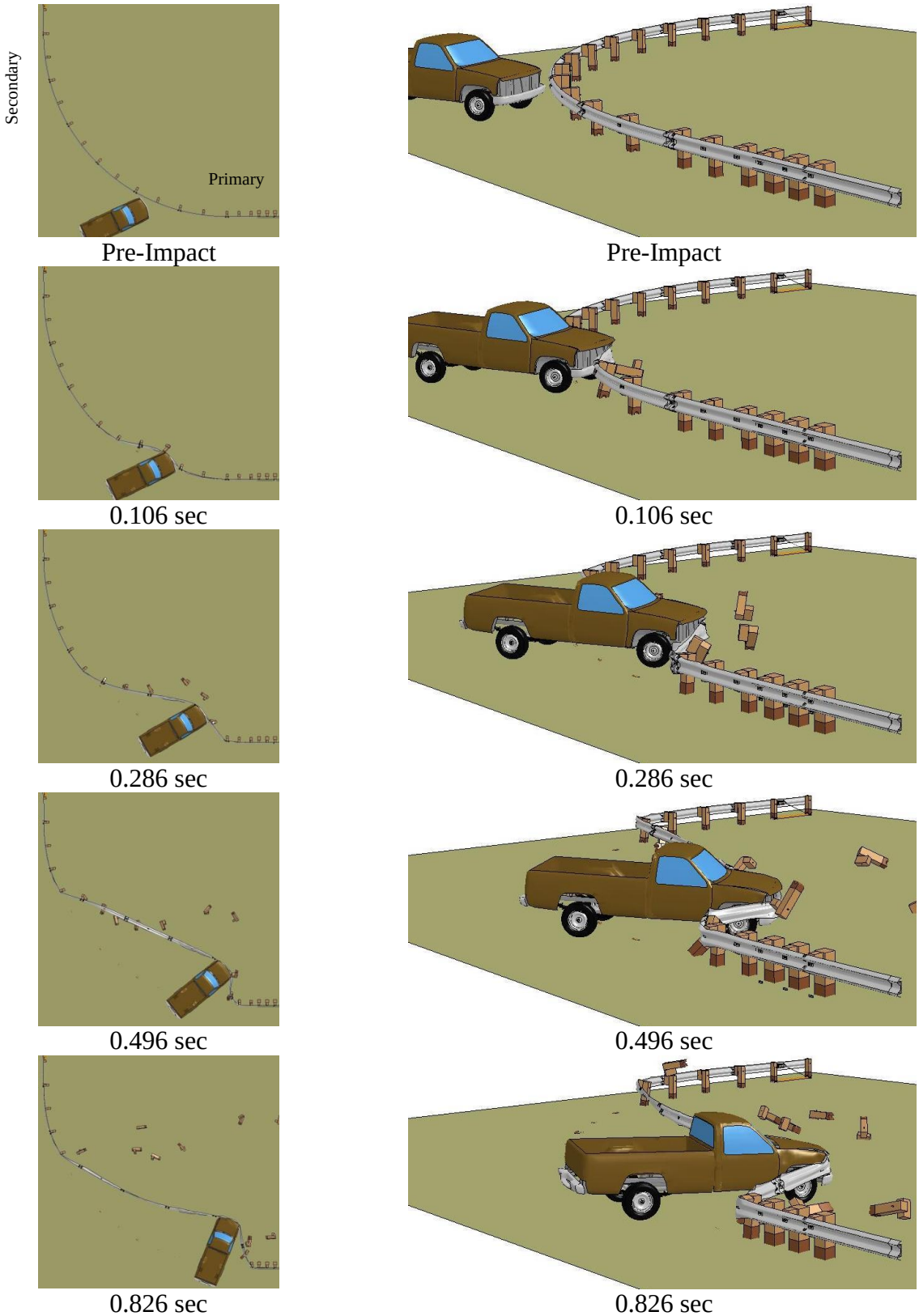

Figure 152. Time-Sequential Images of Impact at Post No. 12, 48-ft (15-m) Radius System with 29-in. (737-mm) Mounting Height

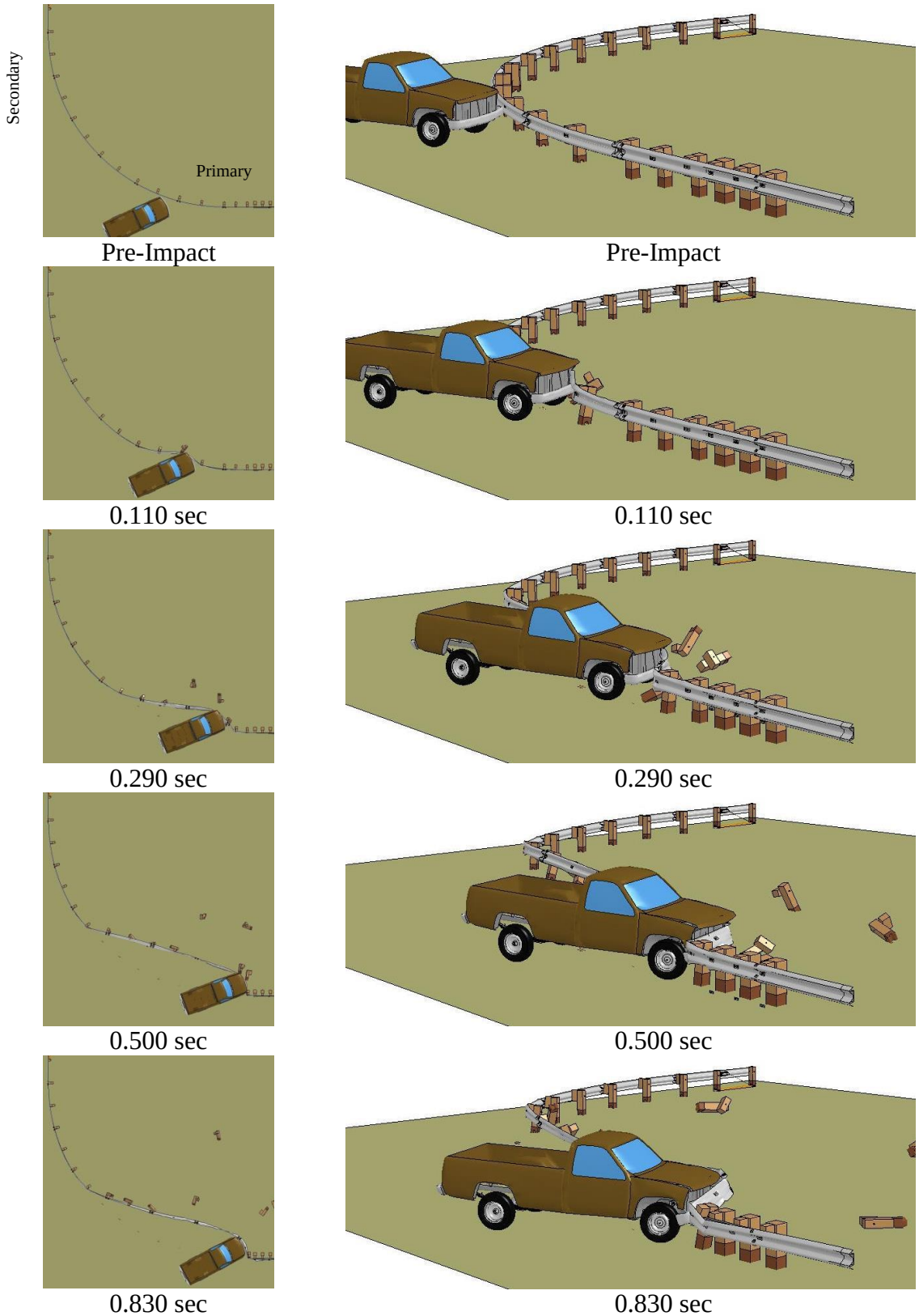

Figure 153. Time-Sequential Images of Impact at Post No. 13, 48-ft (15-m) Radius System with 29-in. (737-mm) Mounting Height

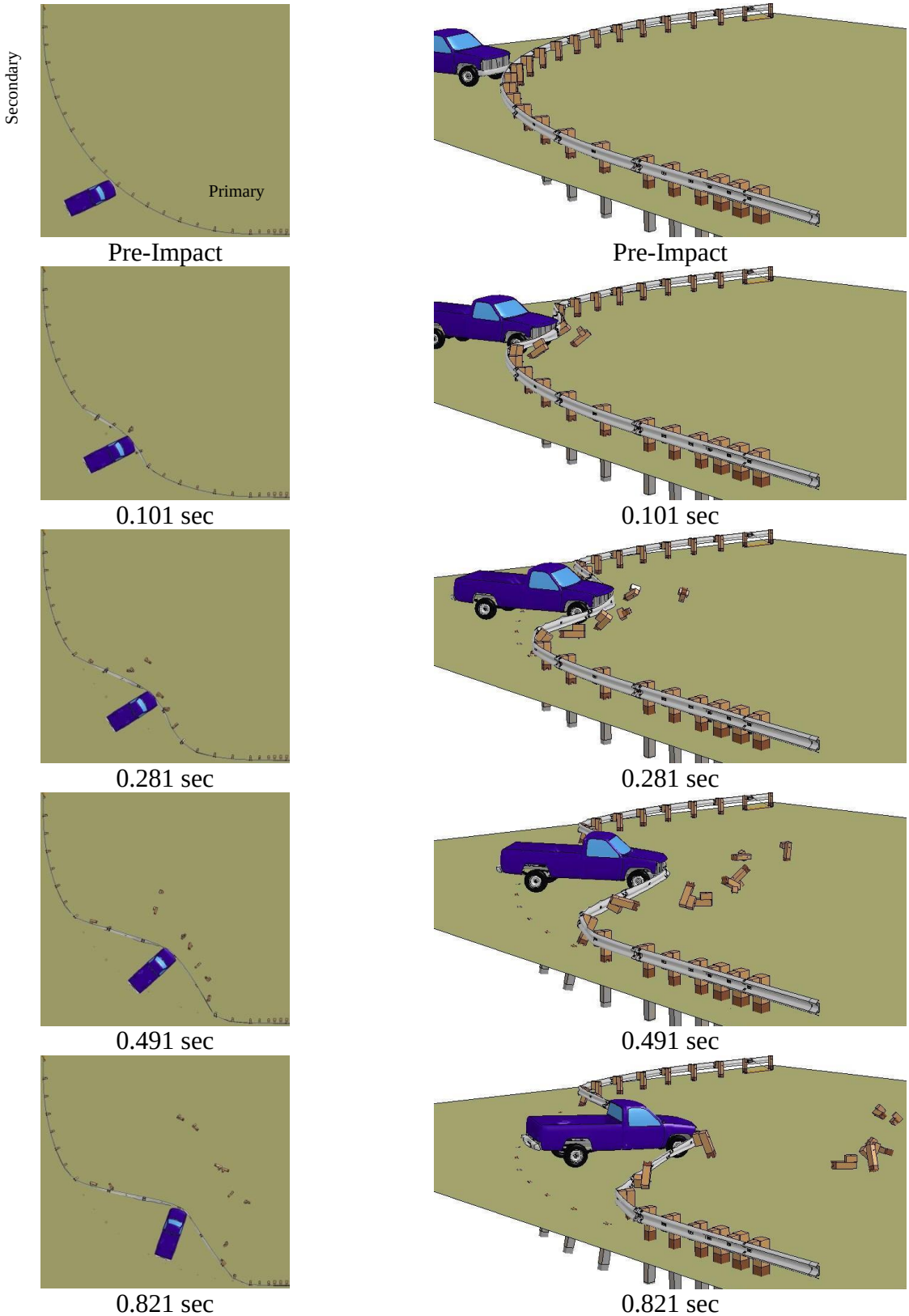

Figure 154. Time-Sequential Images of Impact at Post No. 9, 72-ft (22-m) Radius System with 29-in. (737-mm) Mounting Height

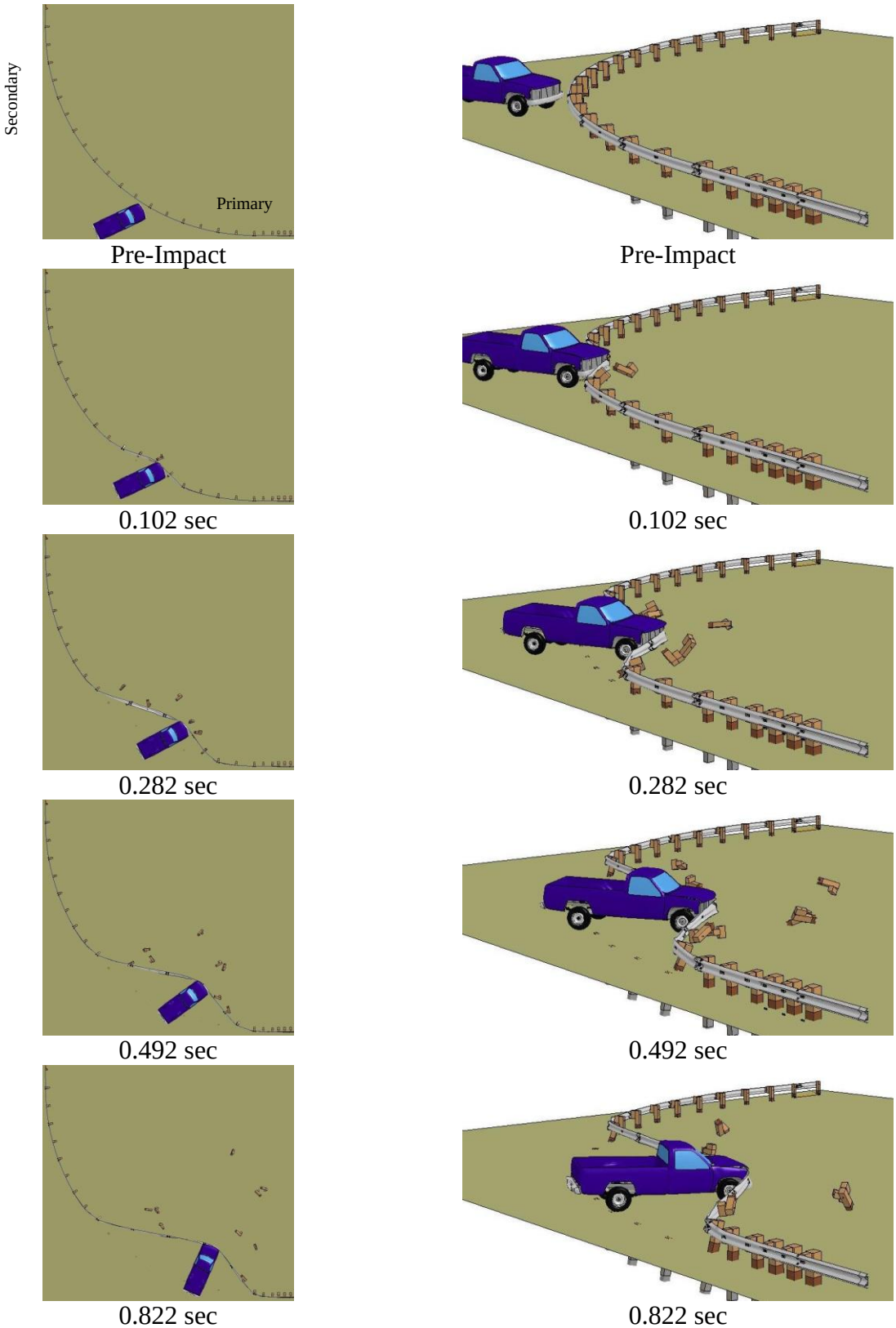

Figure 155. Time-Sequential Images of Impact at Post No. 10, 72-ft (22-m) Radius System with 29-in. (737-mm) Mounting Height

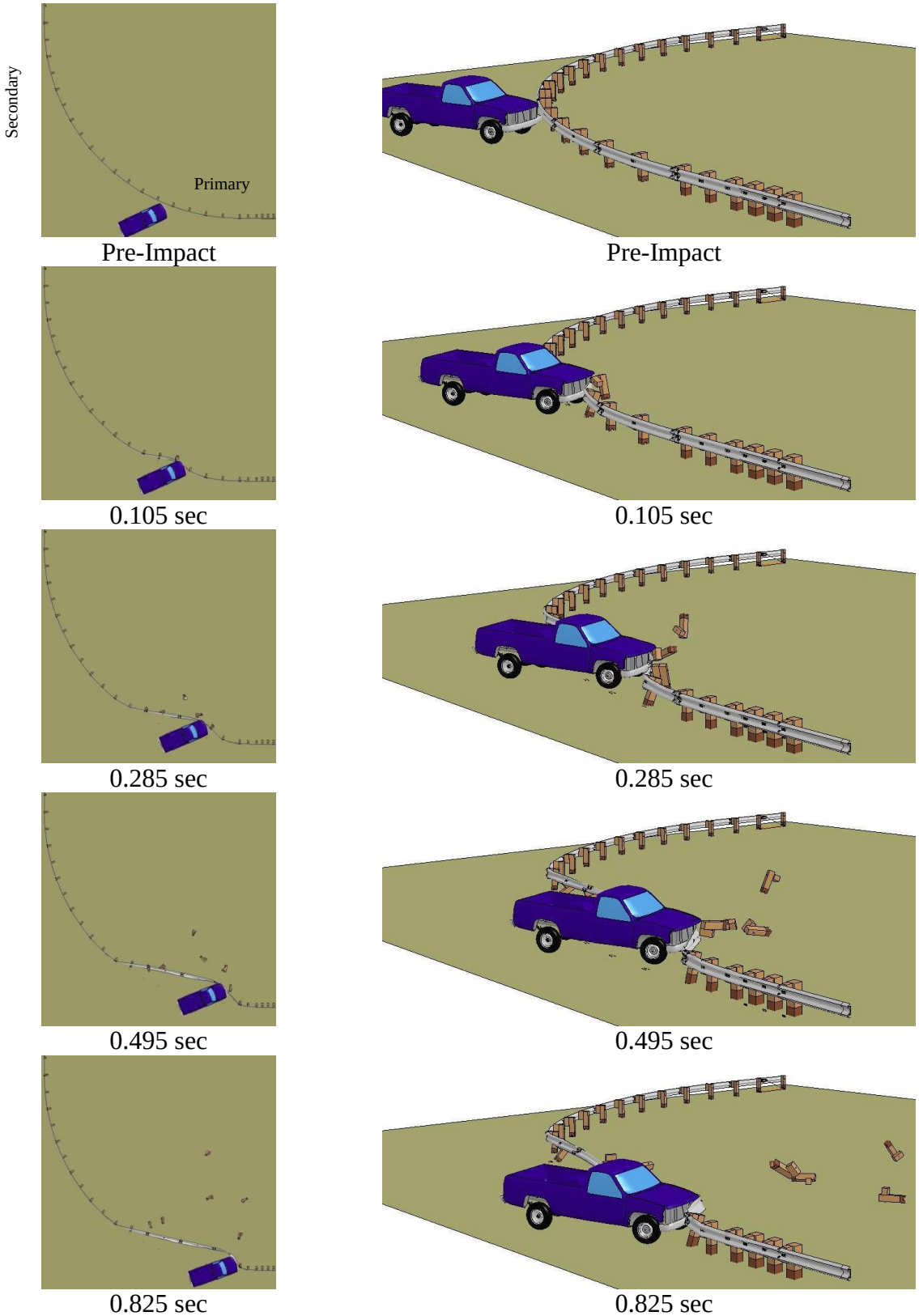

Figure 156. Time-Sequential Images of Impact at Post No. 11, 72-ft (22-m) Radius System with 29-in. (737-mm) Mounting Height

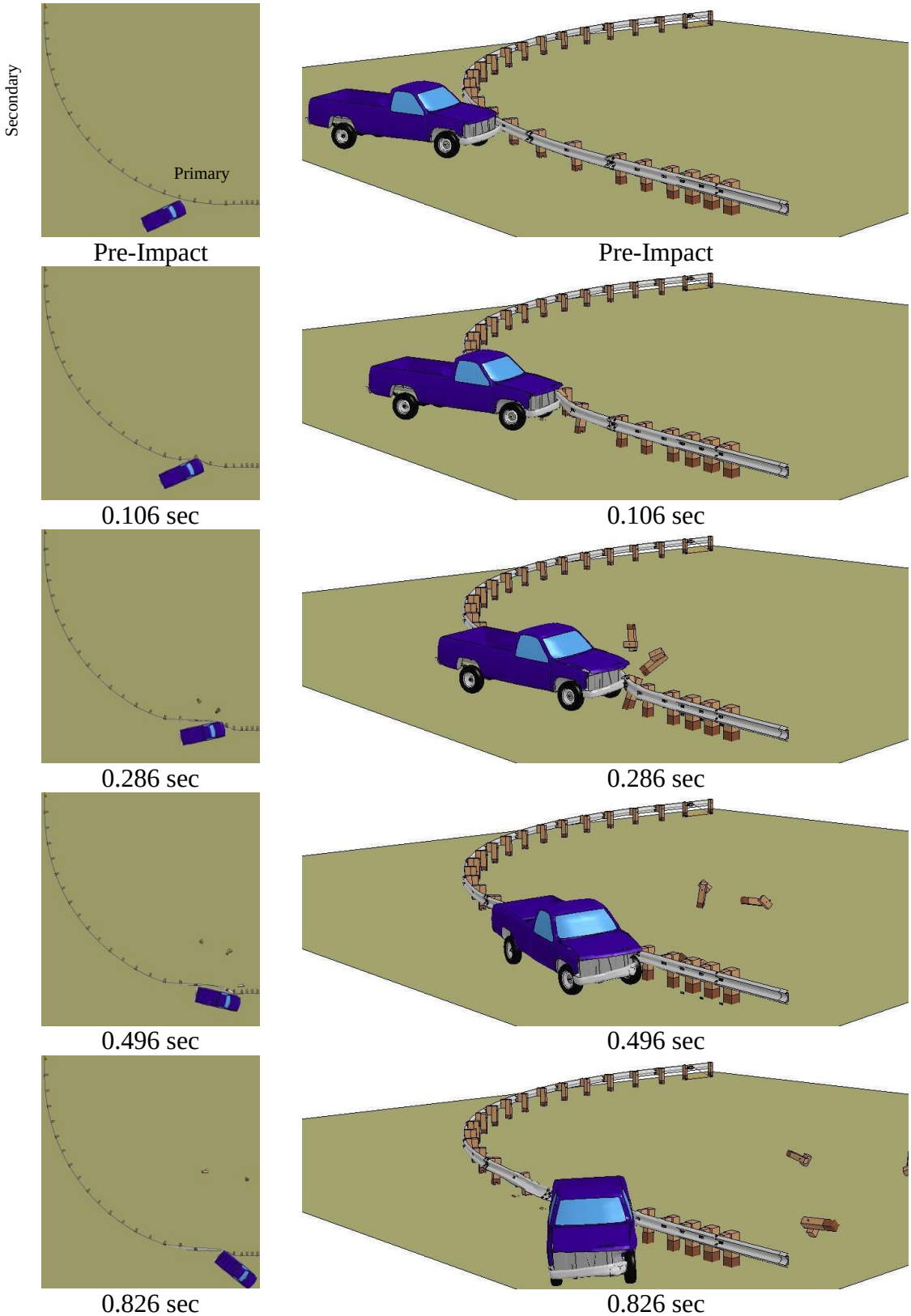

Figure 157. Time-Sequential Images of Impact at Post No. 12, 72-ft (22-m) Radius System with 29-in. (737-mm) Mounting Height

12.4 Discussion

Results of the 29-in. (737-mm) tall simulations are shown in Tables 31 and 32. Results were similar to the results of the 31-in. (787-mm) tall guardrail simulations, as shown in Tables 24 and 25. System damage was also similar, although more simulated posts fractured or deflected in the 29-in. (737-mm) tall system than in the 31-in. (787-mm) tall system.

This is believed to be related to the higher soil stiffness of the CRT posts in the 29-in. (787-mm) tall system, with a 2-in. (51-mm) deeper embedment depth. This also contributed to higher initial system stiffness with the lower rail height than the taller rail height.

12.5 Conclusions

The 29-in. (737-mm) tall short-radius systems with radii between 24 and 72 ft (7.3 and 22 m) satisfactorily captured or redirected vehicles in critical impact locations with TL-2 impact conditions. The propensity for passenger cars to underride beneath the system may be reduced with the 29-in. (737-mm) rail height used in combination with CRT posts and 6-in. x 8-in. x 14.25-in. (152-mm x 203-mm x 362-mm) blockouts, compared to 31-in. (787-mm) tall unblocked systems.

Likewise, fewer light truck overrides may occur with the 29-in. (737-mm) tall system than with the blocked or non-blocked 27-in. (686-mm) tall systems. The C2500 pickup model impacting with TL-2 impact conditions was redirected for every rail height and blockout configuration for 72-ft (22-m) radii at and downstream from post no. 19. Longitudinal (i.e., tangent) guardrail with English 27 in. (686 mm), metric 27.6 in. (700 mm), and modified metric 27¾ in. (705 mm) top mounting heights has historically had mixed performance for redirecting light trucks with TL-3 impact conditions [35]. Thus, with top mounting heights of may be critical to system performance with light trucks.

Table 31. Simulation Analysis Summary for 24-ft (7.3-m) Radius System, 29-in. (737-mm) Top Rail Height

Impact Location	Radius ft (m)	Rail Height (in.)	Speed mph (km/h)	Angle (deg)	Result	Analysis End Time (ms)	Reason for Terminating Analysis	Posts on Radius Fractured/ Deflected	Transition Posts Fractured/ Deflected	Speed at End of Analysis mph (km/h)	Longitudinal Displacement at End of Analysis ft-in. (mm)	Lateral Displacement at End of Analysis ft-in. (mm)
Post 5	24 (7.3)	29 (737)	45 (72)	25	Pass	717	End of Sim	6	2	10.2 (16)	24 ft-6 in. (7474)	8 ft-8 in. (2636)
Post 6	24 (7.3)	29 (737)	45 (72)	25	Pass	765	End of Sim	6	3	7.9 (13)	24 ft-7 in. (7490)	9 ft-6 in. (2898)
Post 7	24 (7.3)	29 (737)	45 (72)	25	Pass	689	End of Sim	6	4	8.5 (14)	24 ft-8 in. (7519)	9 ft-11 in. (3014)
Post 9	48 (15)	29 (737)	45 (72)	25	Pass	881	End of Sim	11	1	8.6 (14)	30 ft-0 in. (9151)	11 ft-5 in. (3474)
Post 10	48 (15)	29 (737)	45 (72)	25	Pass	882	End of Sim	9	2	7.2 (12)	28 ft-11 in. (8825)	7 ft-8 in. (2342)
Post 11	48 (15)	29 (737)	45 (72)	25	Pass	885	End of Sim	9	3	9.2 (15)	30 ft-6 in. (9294)	8 ft-2 in. (2497)
Post 12	48 (15)	29 (737)	45 (72)	25	Pass	886	End of Sim	8	2	4.0 (6)	25 ft-6 in. (7775)	6 ft-2 in. (1874)
Post 13	48 (15)	29 (737)	45 (72)	25	Pass	890	End of Sim	6	3	3.6 (6)	19 ft-11 in. (6069)	2 ft-7 in. (785)
Post 13	72 (22)	29 (737)	45 (72)	25	Pass	891	End of Sim	12	0	6.2 (10)	27 ft-1 in. (8253)	5 ft-10 in. (1779)
Post 15	72 (22)	29 (737)	45 (72)	25	Pass	885	End of Sim	10	1	8.1 (13)	26 ft-11 in. (8205)	4 ft-6 in. (1378)
Post 17	72 (22)	29 (737)	45 (72)	25	Pass	889	End of Sim	7	2	8.7 (14)	25 ft-3 in. (7708)	-1 ft-2 in. (-250)
Post 19	72 (22)	29 (737)	45 (72)	25	Pass	887	Redirected	3	1	15.3 (25)	-	-

Table 32. Simulation Analysis Summary for 24-ft (7.3-m) Radius System, 29-in. (737-mm) Top Rail Height

Impact Location	Radius ft (m)	Rail Height (in.)	Speed mph (km/h)	Angle (deg)	Initial 50 ms Deceleration (g's)	Initial 100 ms Deceleration (g's)	% of Initial Energy Dissipated, 50 ms	% of Initial Energy Dissipated, 75 ms	% of Initial Energy Dissipated, 100 ms	% of Initial Energy Dissipated, 150 ms	% of Initial Energy Dissipated, 200 ms	% of Initial Energy Dissipated, 300 ms	% of Initial Energy Dissipated, 400 ms	% of Initial Energy Dissipated, End of Event
Post 5	24 (7.3)	29 (737)	45 (72)	25	3.9	2.9	19%	26%	28%	38%	44%	58%	73%	95%
Post 6	24 (7.3)	29 (737)	45 (72)	25	3.6	3.6	17%	26%	33%	38%	49%	62%	74%	97%
Post 7	24 (7.3)	29 (737)	45 (72)	25	4.0	2.9	20%	22%	27%	38%	43%	57%	68%	96%
Post 9	48 (15)	29 (737)	45 (72)	25	4.0	3.7	19%	29%	33%	44%	47%	58%	66%	96%
Post 10	48 (15)	29 (737)	45 (72)	25	3.8	3.4	18%	27%	31%	40%	46%	54%	66%	97%
Post 11	48 (15)	29 (737)	45 (72)	25	3.8	3.5	18%	23%	32%	37%	44%	55%	65%	96%
Post 12	48 (15)	29 (737)	45 (72)	25	3.9	3.8	19%	27%	34%	41%	51%	59%	76%	99%
Post 13	48 (15)	29 (737)	45 (72)	25	3.4	3.5	16%	24%	31%	43%	47%	68%	83%	99%
Post 13	72 (22)	29 (737)	45 (72)	25	4.5	4.0	22%	31%	36%	48%	54%	65%	74%	98%
Post 15	72 (22)	29 (737)	45 (72)	25	4.3	4.0	20%	29%	36%	45%	55%	63%	75%	97%
Post 17	72 (22)	29 (737)	45 (72)	25	3.9	3.8	18%	24%	33%	42%	53%	68%	76%	96%
Post 19	72 (22)	29 (737)	45 (72)	25	2.7	2.9	13%	22%	27%	41%	48%	66%	80%	88%

When the stiff bridge transition is located downstream from the curved rail, intermediate sections of straight W-beam guardrail may be required between the stiff bridge transition and the downstream end of the radius. An FHWA memorandum issued May 17, 2010, summarized research which demonstrated that tangent, straight guardrail with mounting heights less than 27¾ in. (705 mm) were not recommended [39]. The recommended standard minimum mounting height for all future systems was 29 ± 1 in. (737 ± 25 mm), with a recommended height of 31 in. (787 mm). Thus, researchers believe that the 29-in. (737-mm) top rail height will perform acceptably when impacted along straight segments.

Although the 31-in. (787-mm) tall guardrail demonstrated acceptable performance with 50 mph (80 km/h) impact speeds for radii larger than or equal to 48 ft (15 m), the performance of the 29-in. (737-mm) tall guardrail has not been evaluated at these elevated speeds. It is believed that the performance of two systems would be similar with 50 mph (80 km/h) impact speeds, but further simulation and full-scale testing are required to validate this assumption.

It was observed that for 31-in. tall systems impacted at 50 mph (80 km/h), not more than 15 posts fractured or were deflected during impact. If the 29-in. (737-mm) tall system is installed on roads with a likelihood of 50 mph (80 km/h) impact speeds, it is recommended that a minimum of 16 CRT posts should be used. Not less than 10 posts should be installed upstream of the beginning of the LON, excluding the end anchorage posts. Adopting this simple approach should limit or prevent vehicles gating behind the system at the start of the LON.

13 SUMMARY, CONCLUSIONS, AND RECOMMENDATIONS

A literature review of short-radius guardrail systems was conducted to determine if there was a system well-suited for use with larger radii. It was observed that, unlike bullnose median barrier systems which are often doubly-symmetrical, short-radius systems are highly asymmetrical, and no short-radius system has ever been successfully crash-tested according to MASH or NCHRP Report No. 350 TL-3 impact conditions. A short-radius system was first tested according to AASHTO PL-1 test conditions at SwRI for use on an intersection in Yuma County, Arizona. This system was later analyzed, modified, and accepted for TL-2 conditions, as recommended by the Texas Transportation Institute.

A baseline model of the Yuma County short-radius system with a radius of 8 ft (2.4 m) was created and simulated using a modified model of a Chevrolet C2500. The baseline model of the system, with long and short overall lengths, was validated against the physical test data. A 31-in. (787-mm) tall modified version of the Yuma County system was created, and results of the simulation were compared to the 27-in. (686-mm) tall system. It was determined that the 31-in. (787-mm) tall system also performed acceptably.

Radii larger than 8 ft (2.4 m) were examined for perpendicular intersections. A total of three radii were selected for simulation: 24, 48, and 72 ft (7.3, 15, and 22 m). Systems with 27-in. (686-mm) tall top mounting heights were impacted at 45 mph (72 km/h) and 25 degrees, consistent with NCHRP Report No. 350 TL-2 impact conditions. Rail twisting, post debris interaction with wheels, and intermittent rail tension caused the impacting 4,409-lb (2,000-kg) pickup truck model to vault over the guardrail in 100, 100, and 80 percent of impact conditions simulated for 24, 48, and 72 ft (7.3, 15, and 22 m) radii, respectively. Blockouts were added to the CRT posts, and the vaulting override rates were reduced to 80, 36, and 50 percent of simulated impact conditions for 24, 48, and 72 ft (7.3, 15, and 22 m) radii, respectively.

Maximum practical impact speeds for 24, 48, and 72-ft (7.3, 15, and 22 m) radii were approximately 19, 22, and 23 mph (approximately 30, 35, and 38 km/h) for systems without blockouts and 29, 26, and 41 mph (47, 42, and 66 km/h) for systems with blockouts, respectively. Vehicle interaction with post debris caused the maximum acceptable speed of the 48-ft (15-m) radius with blockouts to be less than the 24-ft (7.3-m) radius system.

In contrast, the 31-in. (787-mm) tall systems adequately captured or redirected the 2000P vehicle for each impact conditions downstream of post nos. 4, 5, and 7 for radii of 24, 48, and 72 ft (7.3, 15, and 22 m), respectively, when impacted at modified NCHRP Report No. 350 TL-2 conditions of 45 mph (72 km/h) and 25 degrees. The systems captured the vehicles downstream from post nos. 8 and 9 for 48-ft (15-m) and 72-ft (22-m) systems, respectively, with impact speeds of 50 mph (80 km/h). Systems also successfully redirected the vehicle upstream of the stiff bridge rail transition for each of the radii at both 45 and 50 mph (72 and 80 km/h). However, the small car performance was not evaluated, and there is concern that small cars may underride a 31-in. (787-mm) tall barrier.

Limited experience with 29-in. (737-mm) tall W-beam short-radius systems in Minnesota during the 1960s suggested that 29-in. (737-mm) top mounting heights could be a feasible alternative to the 31-in. (787-mm) tall simulated systems. Models of 29-in. (737-mm) rail were generated and simulated for various impact conditions. Similar deflections, decelerations, and system damage were observed for 29-in. (737-mm) tall systems as compared to 31-in. (787-mm) tall systems when impacted at 45 mph (72 km/h) and 25 degrees between the center of the nose to the start of the stiff bridge transition.

The guardrail length-of-need (LON) for each radius system was determined for an impact speed of 45 mph (72 km/h). Recommendations for the 31-in. (787-mm) tall system were used for all guardrail heights, and occurred at post nos. 6, 7, and 8 for radii of 24, 48, and 72 ft (7.3, 14.6,

and 21.8 m), respectively. For 50 mph (80 km/h) impacts upstream of the transition, between 12 and 14 posts fractured before the vehicle came to rest. It is recommended that post no. 9 be considered the beginning of the LON for all radii larger than 16 ft (4.9 m). Not less than 7 CRT posts (or 9 posts total) should be installed upstream of the beginning of the LON in any system installed on roadways with speed limits of 50 mph (80 km/h). System performance at higher speeds is currently unknown, and the 29-in. (713-mm) tall system performance has not yet been evaluated at 50 mph (80 km/h). System recommendations are shown in Table 33. Increased guardrail length on the secondary roadway side of the system could shift the start of the LON such that it remains at the post number identified in Table 33.

Table 33. Summary of 29-in. (713-mm) Tall Curved Guardrail System Recommendations

Impact Speed mph (km/h)	Beginning of LON		
	24-ft (7.3-m) Radius	48-ft (15-m) Radius	72-ft (22-m) Radius
45 (72)	4th CRT Post	5th CRT Post	6th CRT Post
50 (80)	7th CRT Post	7th CRT Post	7th CRT Post

Throughout this research report, only 25-degree impact angles were simulated. No impacts were performed at 0-degree or 15-degree impact angles, although these impact conditions are also evaluated in full-scale crash testing. Historically, the 25-degree impact condition near the nose has been the most difficult impact condition to meet. Additional simulations could be used to further validate or rebut these observations.

Passenger cars may underride the rail if a 31-in. (787-mm) mounting height is used despite a beneficial interaction with pickup truck vehicles. Previous thrie beam short-radius systems with 31-in. (787-mm) mounting heights culminated in small car underride and roof or windshield crush. No W-beam short-radius system has been tested and approved with a top mounting height higher than 27 in. (686 mm). Nonetheless, tangent guardrails as tall as 36 in.

(914 mm) have redirected small cars at MASH TL-3 impact conditions [38]. Taller rail heights are most advantageous for larger radii, which could reduce the small car . Full-scale testing is highly recommended if a 31-in. (787-mm) tall system is to be used.

Unfortunately, it is currently unknown what percentage of vehicles will be captured by the 27-in., 29-in., or 31-in. (686-mm, 737-mm, or 787-mm) tall guardrail systems simulated during this research effort. Based on recent crash studies, it is estimated that approximately 40% of the vehicle fleet impacting roadside systems are high-CG vehicles such as pickups, SUVs, or vans. Approximately 55% of impacting vehicles are passenger cars, and the remainder are heavy trucks including single-unit trucks. The exact composition of impacting vehicle fleet will change based on roadway type, function, and traffic volumes encountered. It is believed that the lower guardrail height may have the best probability of capturing passenger cars, whereas the highest guardrail height is most suitable for large vehicles such as pickup trucks. The 29-in. (737-mm) tall guardrail may be an ideal balance between the two. Further research is needed to corroborate or reject these assumptions.

14 FUTURE WORK

It is recommended that further simulation analysis be conducted using passenger cars to analyze the safety of the 29-in. (737-mm) and 31-in. (787-mm) tall short-radius systems and evaluate underride propensity. Although computer simulations may be an effective estimating tool, full-scale crash tests should be conducted to determine the crashworthiness of increased rail height and larger radii.

All systems in this research report spanned a 90-degree angle. Many secondary roadways intersect obliquely with primary roadways, which would result in a short radius that could encompass more or less than 90 degrees. Further analysis may be required to estimate the effect of oblique intersections on short-radius guardrail performance.

Traditionally, the beginning of the LON was defined based on AASHTO RDG recommendations, dependent on hazard and guardrail configurations. For the Yuma County short-radius guardrail system, the farthest upstream location on the guardrail that could still redirect or capture a vehicle occurred at the centerpoint of the radius. According to the definition of LON, this impact location would suggest that this system has a very limited window of effectiveness, because the beginning of the LON of the system is very close to the centerpoint of the radius. The centerpoint of the radius is located nearly tangential with the bridge rail. Thus, very little is gained by using a short-radius system if traditional methods of LON are used. New techniques for determining guardrail LON, or modifications to the system to accommodate impacts upstream of the centerpoint of the nose, may require future consideration.

15 REFERENCES

1. *Roadside Design Guide*, American Association of State Highway and Transportation Officials, Issue 4, Washington, D.C., 2011.

2. Ross, H.E., Sicking, D.L., Zimmer, R.A., and Michie, J.D., *Recommended Procedures for the Safety Performance Evaluation of Highway Features*, National Cooperative Highway Research Program (NCHRP) Report 350, Transportation Research Board, Washington, D.C., 1993.

3. *Manual for Assessing Safety Hardware (MASH)*, American Association of State Highway and Transportation Officials (AASHTO), Washington, D.C., 2009.

4. Michie, J.D., *Recommended Procedures for the Safety Performance Evaluation of Highway Appurtenances*, National Cooperative Highway Research Program (NCHRP) Report No. 230, Transportation Research Board, Washington, D.C., March 1981.

5. *Guide Specifications for Bridge Railings*, American Association of State Highway Transportation Officials, Washington, D.C., 1989.

6. Mayer, J.B, *Full-Scale Crash Testing of Approach Guardrail for Yuma County Public Works Department*, Final Report, Project No.06-2111, Southwest Research Institute, San Antonio, Texas, 1989.

7. *Curved W-Beam Guardrail Installations at Minor Roadway Intersections*, Federal Highway Administration (FHWA), U.S. Department of Transportation, Technical Advisory T5040.32, April 13, 1992.

8. Bligh, R.P., Ross, H.E. Jr., and Alberson, D.C., *Short Radius Thrie Beam Treatment for Intersecting Streets and Drives*, Final Report to the Texas Department of Transportation, Report No. FHWA/TX-95/1442-1F, Texas Transportation Institute, Texas A&M University, College Station, Texas, November 1994.

9. Bielenberg, R.W., Reid, J.D., Faller, R.K., Rohde, J.R., Sicking, D.L., and Keller, E.A., *Concept Development of a Short-Radius Guardrail System for Intersecting Roadways*, Final Report to the Midwest States Regional Pooled Fund, Midwest Research Report No. TRP-03-100-00, Midwest Roadside Safety Facility, University of Nebraska-Lincoln, Lincoln, Nebraska, September 2000.

10. Bronstad, M.E., Calcote, L.R., Ray, M.H.; and Mayer, J.B., *Guardrail-Bridge Rail Transition Designs*, Volume I, Report No. FHWA/RD-86/178, Southwest Research Institute, San Antonio, Texas, April 1988.

11. Ross, H.E. Jr., Bligh, R.P., Parnell, C.B., *Bridge Railing End Treatments at Intersecting Streets and Drives*, Report No. FHWA TX-91/92-1263-1F, Texas Transportation Institute, College Station, Texas, August 1992.

12. Bielenberg, R.W., Faller, R.K., Holloway, J.C., Reid, J.D., Rohde, J.R., and Sicking, D.L., *Phase II Development of a Short-Radius Guardrail for Intersecting Roadways*, Final Report to the Midwest States' Pooled Fund Program, MwRSF Research Record No. TRP-03-137-03, Midwest Roadside Safety Facility, University of Nebraska-Lincoln, Lincoln, Nebraska, 2003.

13. Stolle, C.S., Polivka, K.A., Bielenberg, R.W., Reid, J.D., Faller, R.K., Rohde, J.D., and Sicking, D.L., *Phase III Development of a Short-Radius Guardrail for Intersecting Roadways*, Final Report to the Midwest States' Pooled Fund Program, MwRSF Research Report No. TRP-03-183-07, Midwest Roadside Safety Facility, University of Nebraska-Lincoln, Lincoln, Nebraska, August 2007.

14. Stolle, C.S., Polivka, K.A., Bielenberg, R.W., Reid, J.D., Faller, R.K., Rohde, J.D., and Sicking, D.L., *Phase IV Development of a Short-Radius Guardrail for Intersecting Roadways*, Final Report to the Midwest States' Pooled Fund Program, MwRSF Research Report No. TRP-03-199-08, Midwest Roadside Safety Facility, University of Nebraska-Lincoln, Lincoln, Nebraska, February 2008.

15. Button, J.W., Buth, E., and Olson, R.M., *Crash Tests of Five-Foot Radius Plate Beam Guardrail*, Final Report to the Minnesota Department of Transportation, Texas Transportation Institute, Texas A&M University, College Station, Texas, June 1975.

16. Parks, D.M., Stoughton, R.L., Stoker, J.R., and Nordlin, E.F., *Vehicular Crash Tests of Four Bullnose Traffic Barrier Designs*, Final Report to the California Department of Transportation, Caltrans Report No. FHWA-CA-DOT-TL-6392-5-76-35, California Department of Transportation, Sacramento, California, June 1976.

17. Robertson, R.G., and Ross, H.E. Jr., *Colorado Median Barrier End Treatment Tests*, Final Report to the Colorado Department of Transportation, TTI Research Report No. CDOH-TTI-R-81-2, Texas Transportation Institute, Texas A&M University, College Station, Texas, May 1981.

18. Bronstad, M.E., Ray, M.H., Mayer, J.B. Jr., and Brauer, S.K., *Median Barrier Terminals and Median Treatments: Volume I*, Final Report to the Federal Highway Administration, SwRI Research Report No. FHWA/RD-88/004, Southwest Research Institute, San Antonio, Texas, October 1987.

19. Bielenberg, R.W., Faller, R.K., Reid, J.D., Sicking, D.L., Rohde, J.R., and Keller, E.A., *Concept Development of a Bullnose Guardrail System for Median Applications*, Final Report to the Midwest States Regional Pooled Fund Program, Midwest Research Report No. TRP-03-73-98, Midwest Roadside Safety Facility, University of Nebraska-Lincoln, Lincoln, Nebraska, May 1998.

20. Bielenberg, R.W., Reid, J.D., Faller, R.K., Sicking, D.L., Rohde, J.R., Keller, E.A., and Holloway, J.C., *Phase II Development of a Bullnose Guardrail System for Median Applications*, Final Report to the Midwest States Regional Pooled Fund Program, Midwest Research Report No. TRP-03-78-98, Midwest Roadside Safety Facility, University of Nebraska-Lincoln, Lincoln, Nebraska, December 1998.

21. Bielenberg, R.W., Reid, J.D., Faller, R.K., Rohde, J.R., Sicking, D.L., Keller, E.A., Holloway, J.C., and Supencheck, L., *Phase III Development of a Bullnose Guardrail System for Median Applications*, Final Report to the Midwest States Regional Pooled Fund Program, Midwest Research Report No. TRP-03-95-00, Midwest Roadside Safety Facility, University of Nebraska-Lincoln, Lincoln, Nebraska, June 2000.

22. Arens, S.W., Sicking, D.L., Faller, R.K., Reid, J.D., Bielenberg, R.W., Rohde, J.R., and Lechtenberg, K.A., *Investigating the Use of a New Breakaway Steel Post*, Letter Report to the Midwest States Regional Pooled Fund Program, Midwest Research Report No. TRP-03-218-09, Midwest Roadside Safety Facility, University of Nebraska-Lincoln, Lincoln, Nebraska, August 2009.

23. Arens, S.W., Sicking, D.L., Faller, R.K., Reid, J.D., Bielenberg, R.W., Rohde, J.R., and Lechtenberg, K.A., *Investigating the Use of a New Universal Breakaway Steel Post*, Final Report to the Midwest States Regional Pooled Fund Program, Midwest Research Report No. TRP-03-281-09, Midwest Roadside Safety Facility, University of Nebraska-Lincoln, Lincoln, Nebraska, August 2009.

24. Schmidt, J.D., Sicking, D.L., Faller, R.K., Reid, J.D., Bielenberg, R.W., and Lechtenberg, K.A., *Investigating the Use of a New Breakaway Steel Post – Phase 2*, Final Report to the Midwest States Regional Pooled Fund Program, Midwest Research Report No. TRP-03-230-10, Midwest Roadside Safety Facility, University of Nebraska-Lincoln, Lincoln, Nebraska, August 2010.

25. Mongiardini, M., Faller, R.K., Reid, J.D., Sicking, D.L., Stolle, C.S., and Lechtenberg, K.A., *Downstream Anchoring Requirements for the Midwest Guardrail System*, Final Report to the Wisconsin Department of Transportation, Midwest Research Report No. TRP-03-279-13, Midwest Roadside Safety Facility, University of Nebraska-Lincoln, Lincoln, Nebraska, June 2013.

26. *Guardrail Placement, Weak Post Intersection Design (35 ft Max Radius) (Cases 13AC, 13AD, 13BC & 13BD), Standard Plans*, Washington State Department of Transportation, Updated July 27, 2001, Accessed September 24, 2013.
< http://www.wsdot.wa.gov/publications/fulltext/Standards/english/PDF/c02g_eng.pdf>

27. Abu-Odeh, A., and Kim, K., *Evaluation of Existing T-Intersection Guardrail Systems for Equivalency with NCHRP Report 350 TL-2 Test Conditions*, Final Report to the Roadside Safety Research Pooled Fund Program, TTI Research Report No. 405160-10, Texas Transportation Institute, Texas A&M University, College Station, Texas, August, 2010.

28. *LS-DYNA Keyword User's Manual*, Version 971 R6.0.0, Livermore Software Technology Corporation, Livermore, California, February 2012.

29. Stolle, C.S., Reid, J.D., and Lechtenberg, K.A., *Development of Advanced Finite Element Material Models for Cable Barrier Wire Rope*, Final Report to the Mid-America Transportation Center, FHWA Region VII University Transportation Center, MwRSF Report No. TRP-03-233-10, August 2010.

30. *Finite Element Model Archive*, National Crash Analysis Center, George Washington University, Updated December 2011. < http://www.ncac.gwu.edu/vml/models.html>.

31. Society of Automotive Engineers (SAE), *Instrumentation for Impact Test – Part 1 – Electronic Instrumentation*, SAE J211/1 MAR95, New York City, NY, July 2007.

32. "1984 Ford Pickup", Posted August 5, 2012, Accessed May 30, 2013. < http://ford.cararchives.net/1984-ford-pickup/>.

33. Polivka, K. A., Faller, R. K., Sicking, D. L., Reid, J. D., Rohde, J. R., Holloway, J. C., Bielenberg, R. W., and Kuipers, B. D., *Development of the Midwest Guardrail System (MGS) for Standard and Reduced Post Spacing and in Combination with Curbs*, Final Report to the Midwest States Regional Pooled Fund Program, MwRSF Research Report No. TRP-03-139-04, Midwest Roadside Safety Facility, University of Nebraska–Lincoln, Lincoln, Nebraska, 2004.

34. Thorstenson, F. W., Minnesota State Department of Highways. Letter to John L. Beaton, Materials and Research Engineer, California State Division of Highways, July 14, 1971.

35. Polivka, K. A., Faller, R. K., Sicking, D. L., Reid, J. D., Rohde, J. R., Holloway, J. C., Bielenberg, R. W., and Kuipers, B. D., *Development of the Midwest Guardrail System (MGS) for Standard and Reduced Post Spacing and in Combination with Curbs*, Final Report to the Midwest States Regional Pooled Fund Program, MwRSF Research Report No. TRP-03-139-04, Midwest Roadside Safety Facility, University of Nebraska–Lincoln, Lincoln, Nebraska, 2004.

36. Mak, K.K., Sicking, D.L., de Albuquerque, F.D.B., and Coon, B.A., *Identification of Vehicular Impact Conditions Associated with Serious Ran-Off-Road Crashes*, National Cooperative Highway Research Program Report No. 665, Transportation Research Board,. Washington, D.C., 2010.

37. Stolle, C.S., Polivka, K.A., Reid, J.D., Faller, R.K., Sicking, D.L., Bielenberg, R.W., and Rohde, J.R., *Evaluation of Critical Flare Rates for the Midwest Guardrail System (MGS)*, Final Report to the Midwest States Regional Pooled Fund Program, Transportation Research Report No. TRP-03-191-08, Project No.: SPR-3(017), Project Code: RPFP-04-03 and RPFP-05-05 - Years 14 and 15, Midwest Roadside Safety Facility, University of Nebraska-Lincoln, Lincoln, Nebraska, July 15, 2008.

38. Stolle, C.J., Lechtenberg, K.A., Reid, J.D., Faller, R.K., Bielenberg, R.W., Rosenbaugh, S.K., Sicking, D.L., and Johnson, E.A., *Determination of the Maximum MGS Mounting Height – Phase I Crash Testing*, Final Report to the Midwest States Pooled Fund Program, Report No. TRP-03-255-11, Midwest Roadside Safety Facility, University of Nebraska-Lincoln, March 9, 2012.

39. Nicol, D.A., *Action - Roadside Design: Steel Strong-Post W-Beam Guardrail*, Federal Highway Administration, May 17, 2010.

16 APPENDIX

Appendix A. Modified Yuma Co. Design Drawings [27]

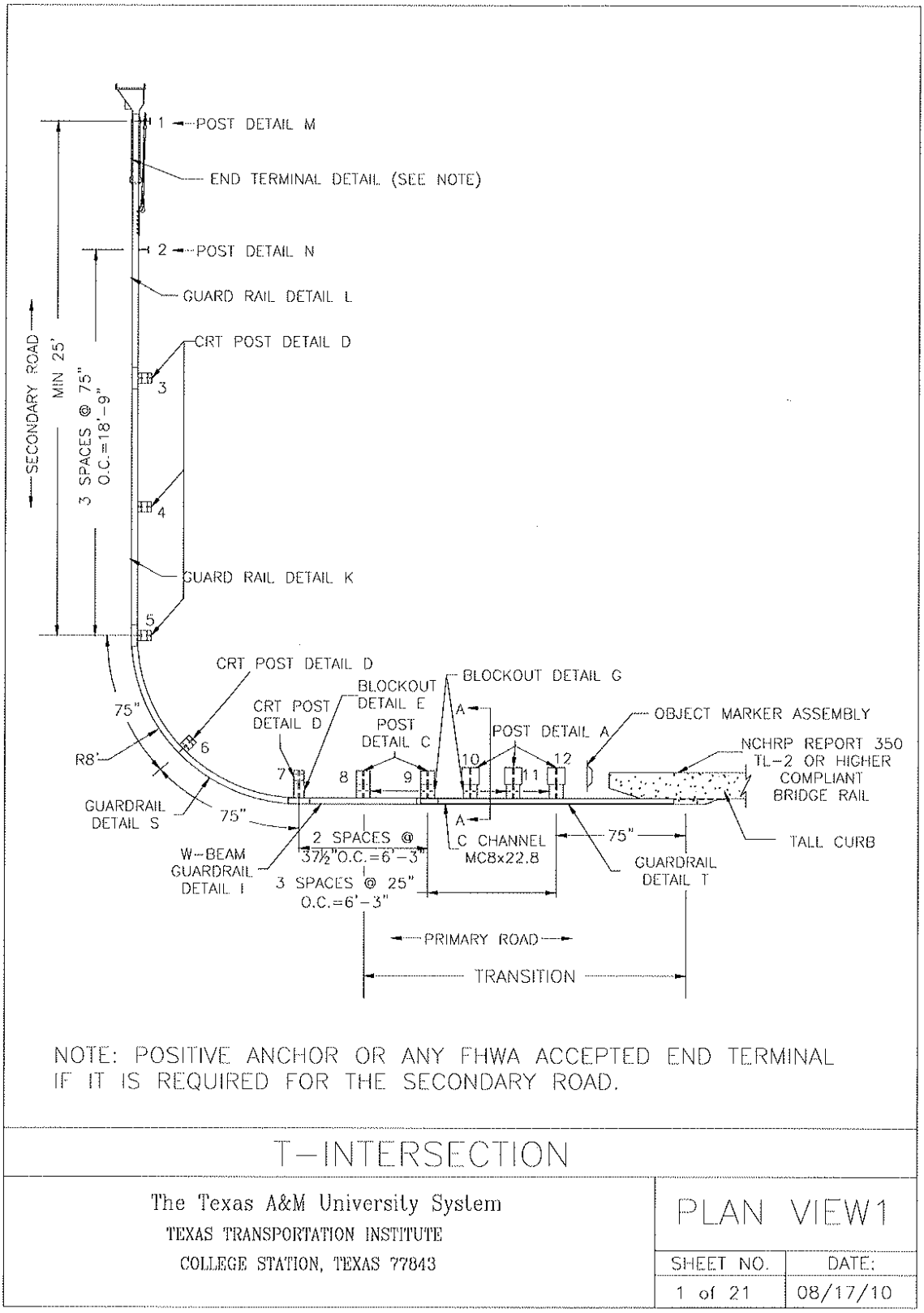

Figure A-1. Recommended Design Details for Yuma County Short-Radius System [27]

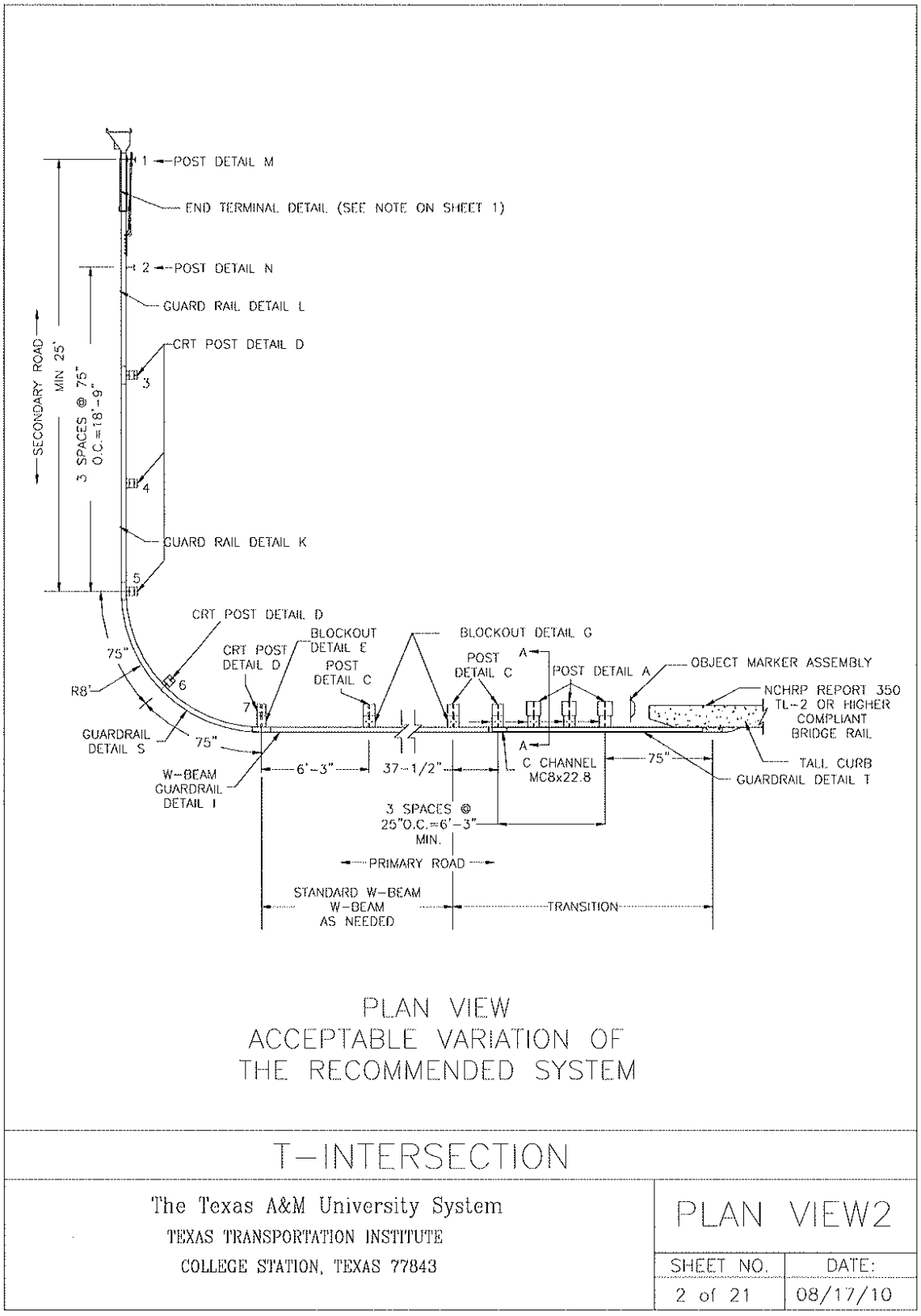

Figure A-2. Alternative Design Details for Yuma County Short-Radius System [27]

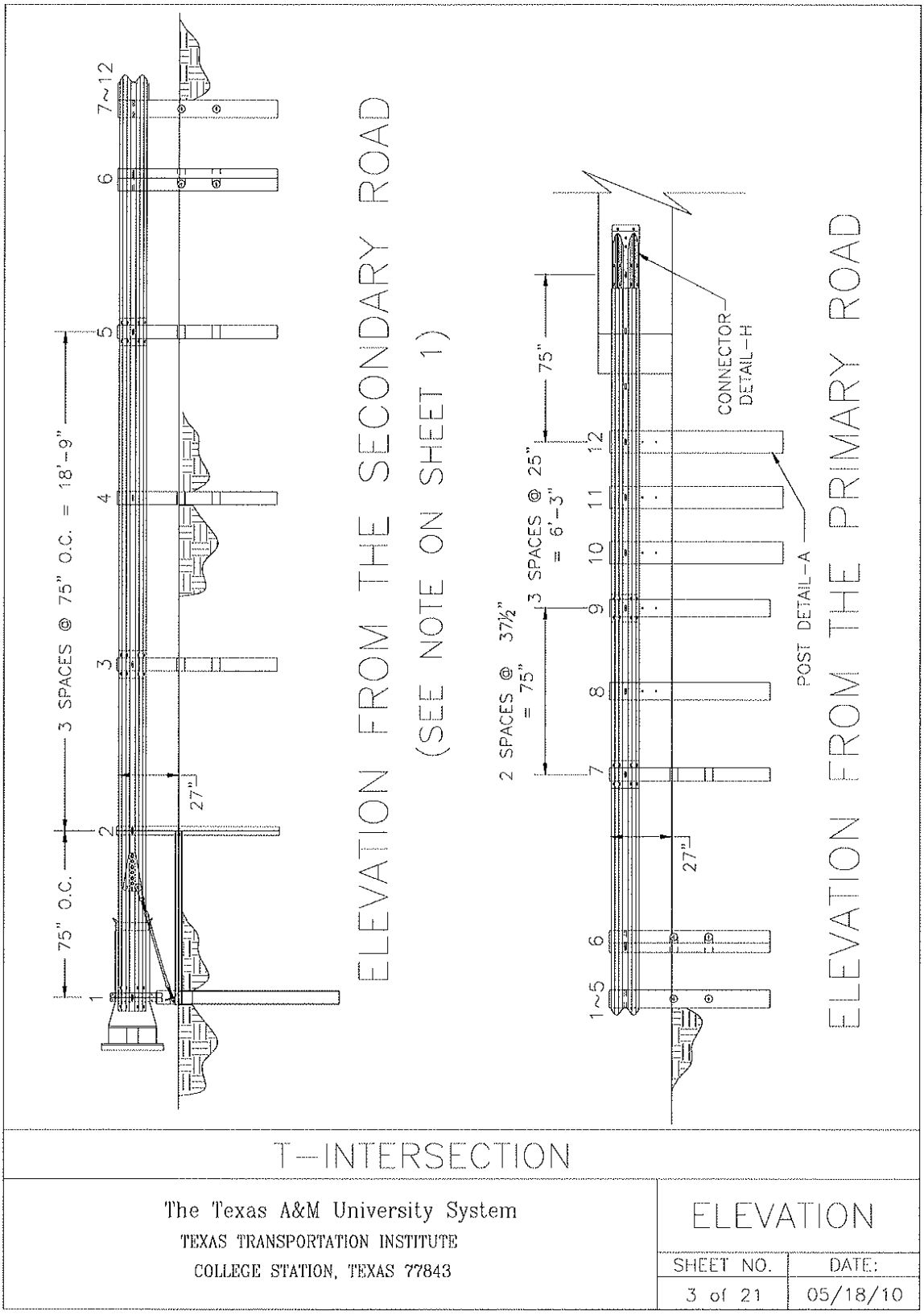

Figure A-3. Rail Elevation, Post Spacing, and Post Details [27]

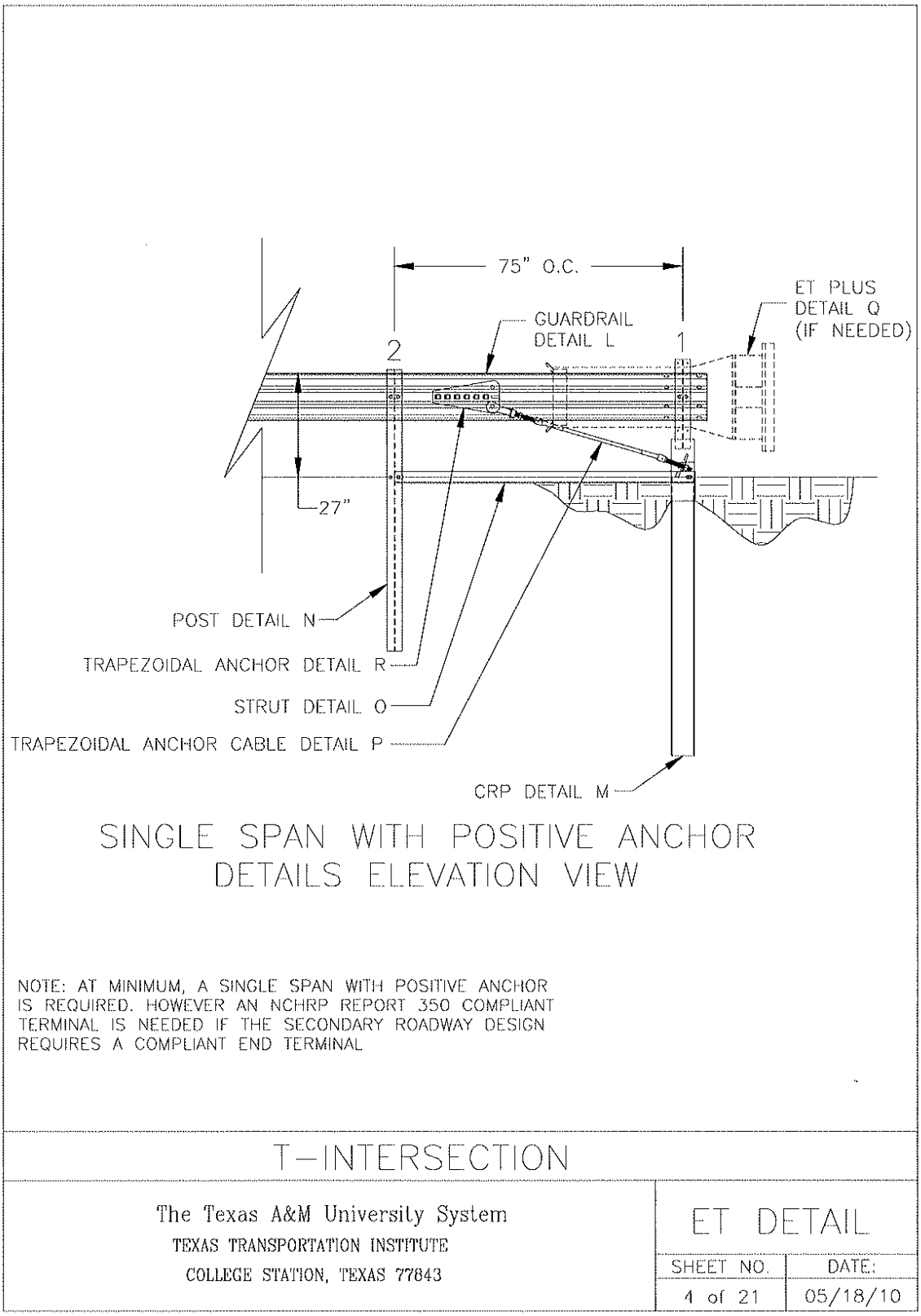

Figure A-4. Upstream End Anchorage Details [27]

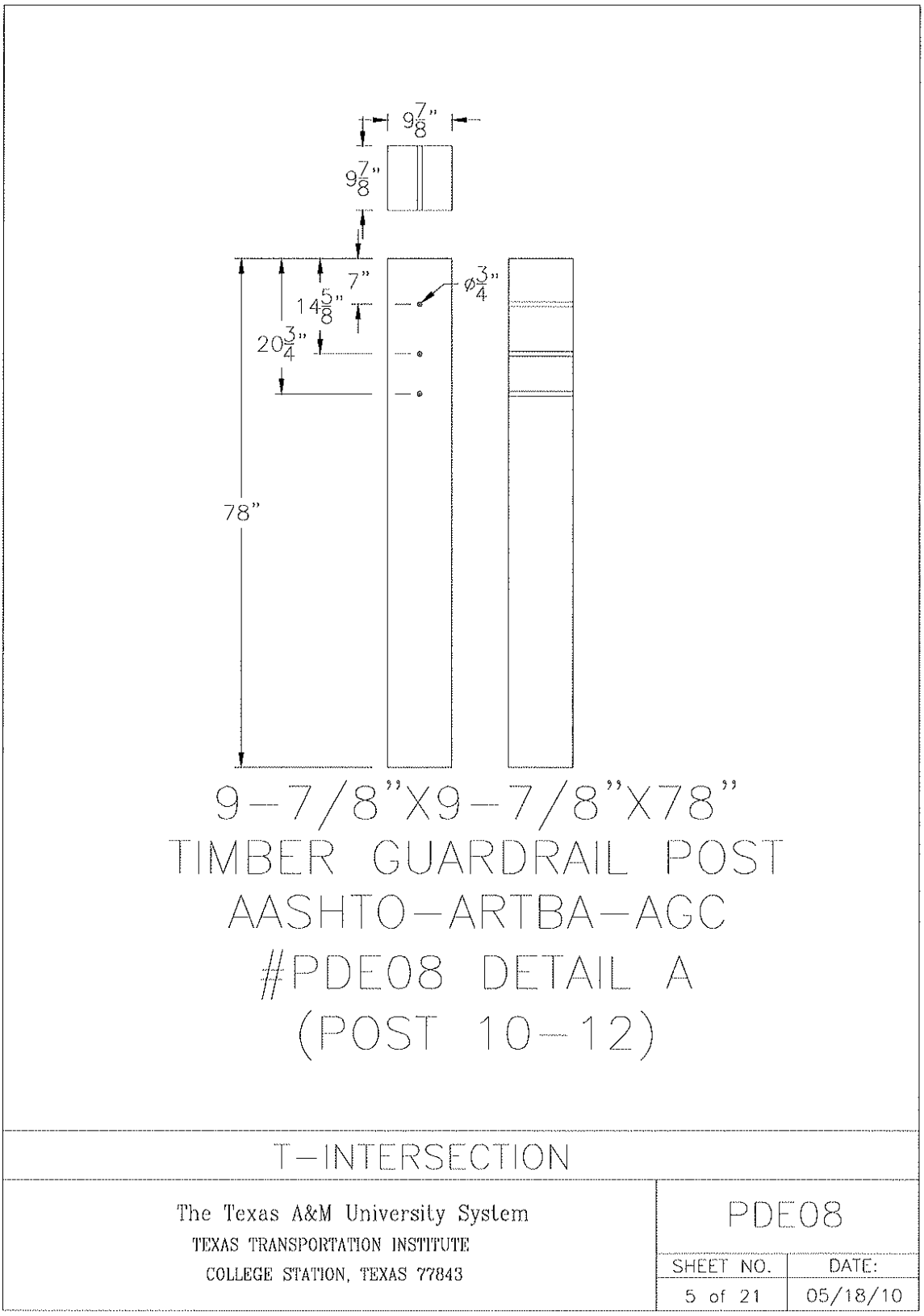

Figure A-5. Timber Post Details, Transition Post Nos. 10 through 12 [27]

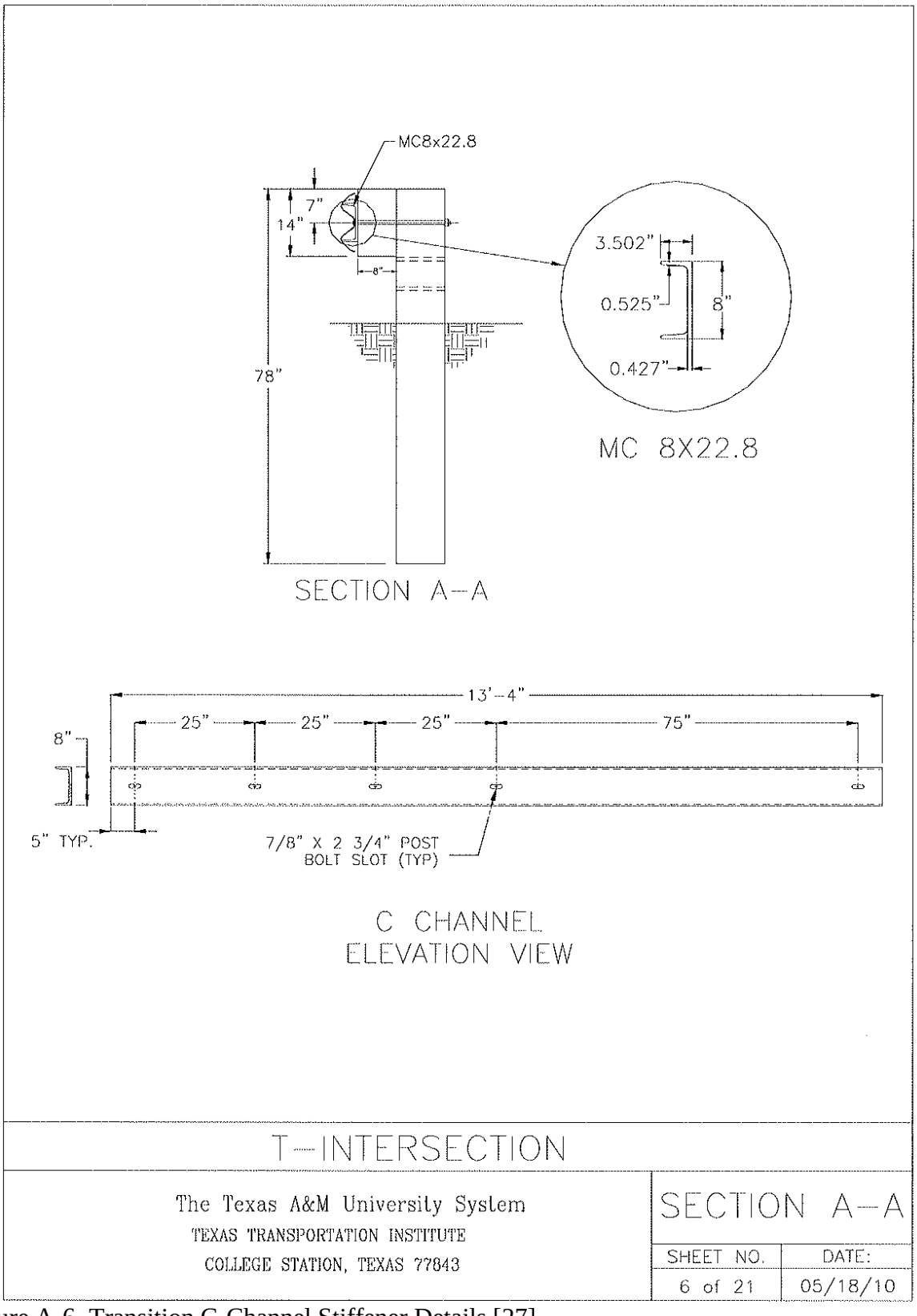

Figure A-6. Transition C-Channel Stiffener Details [27]

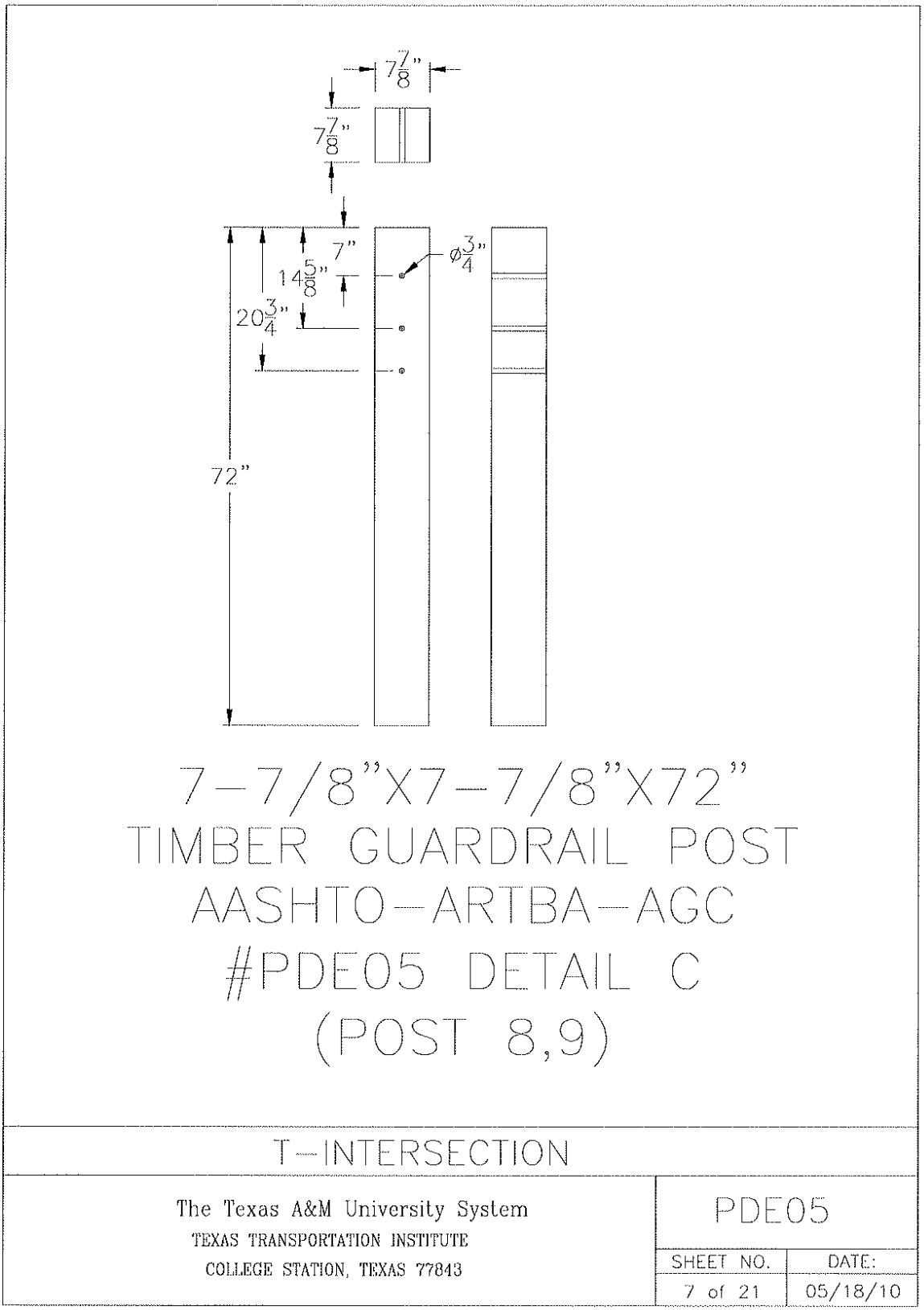

Figure A-7. Transition Timber Post Details, Post Nos. 8 and 9 [27]

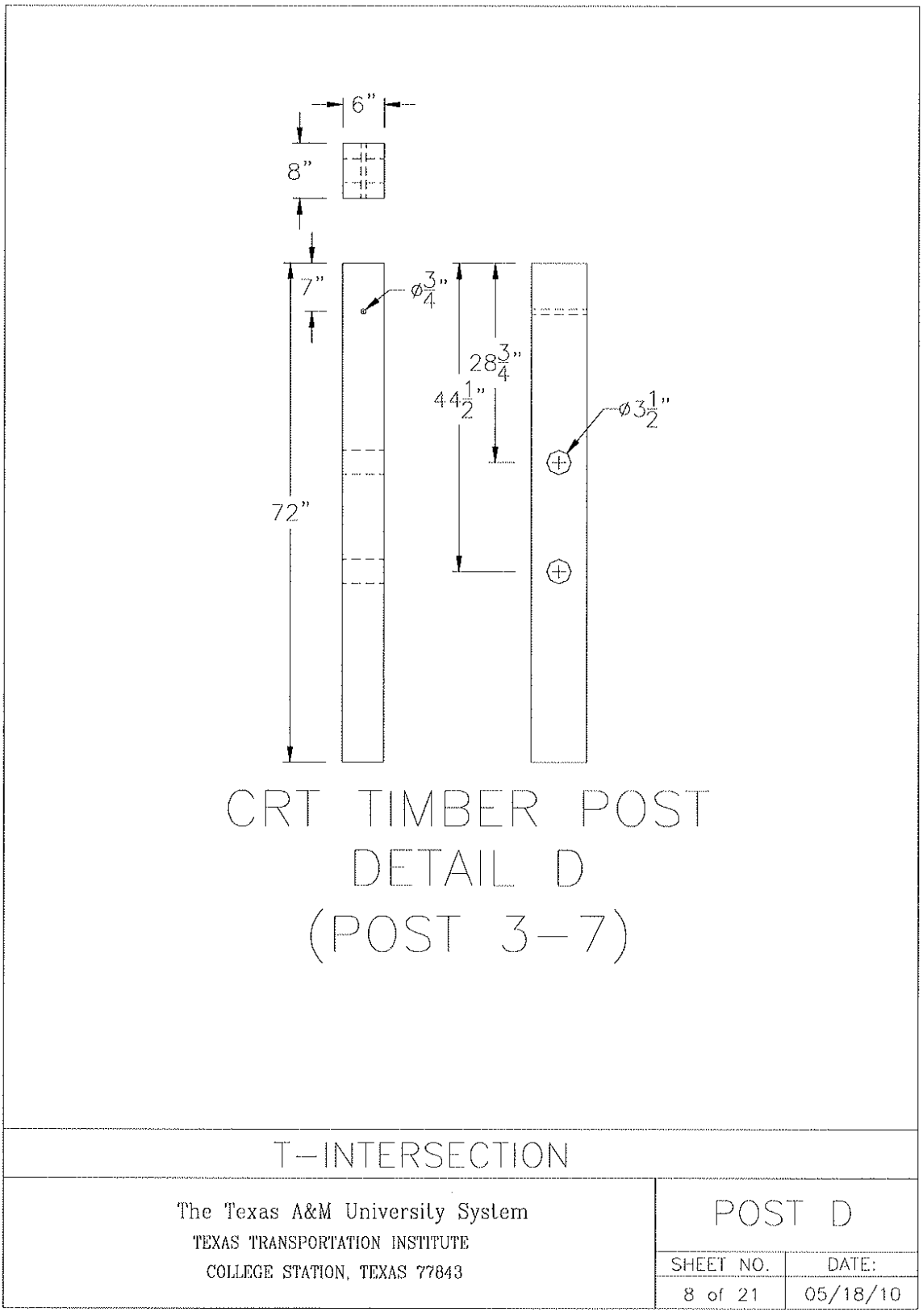

Figure A-8. CRT Post Details, Post Nos. 3 through 7 [27]

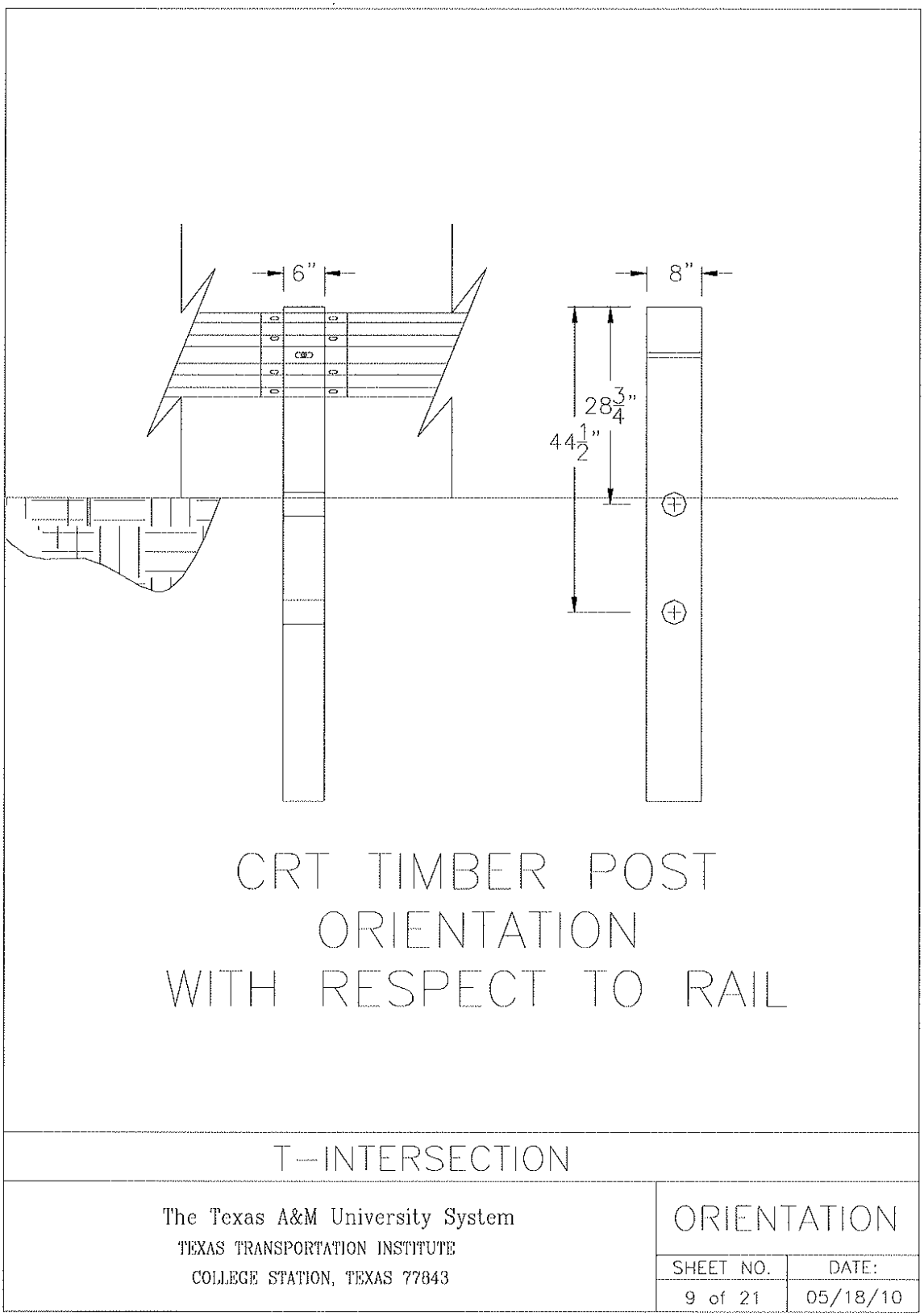

Figure A-9. CRT Post Details [27]

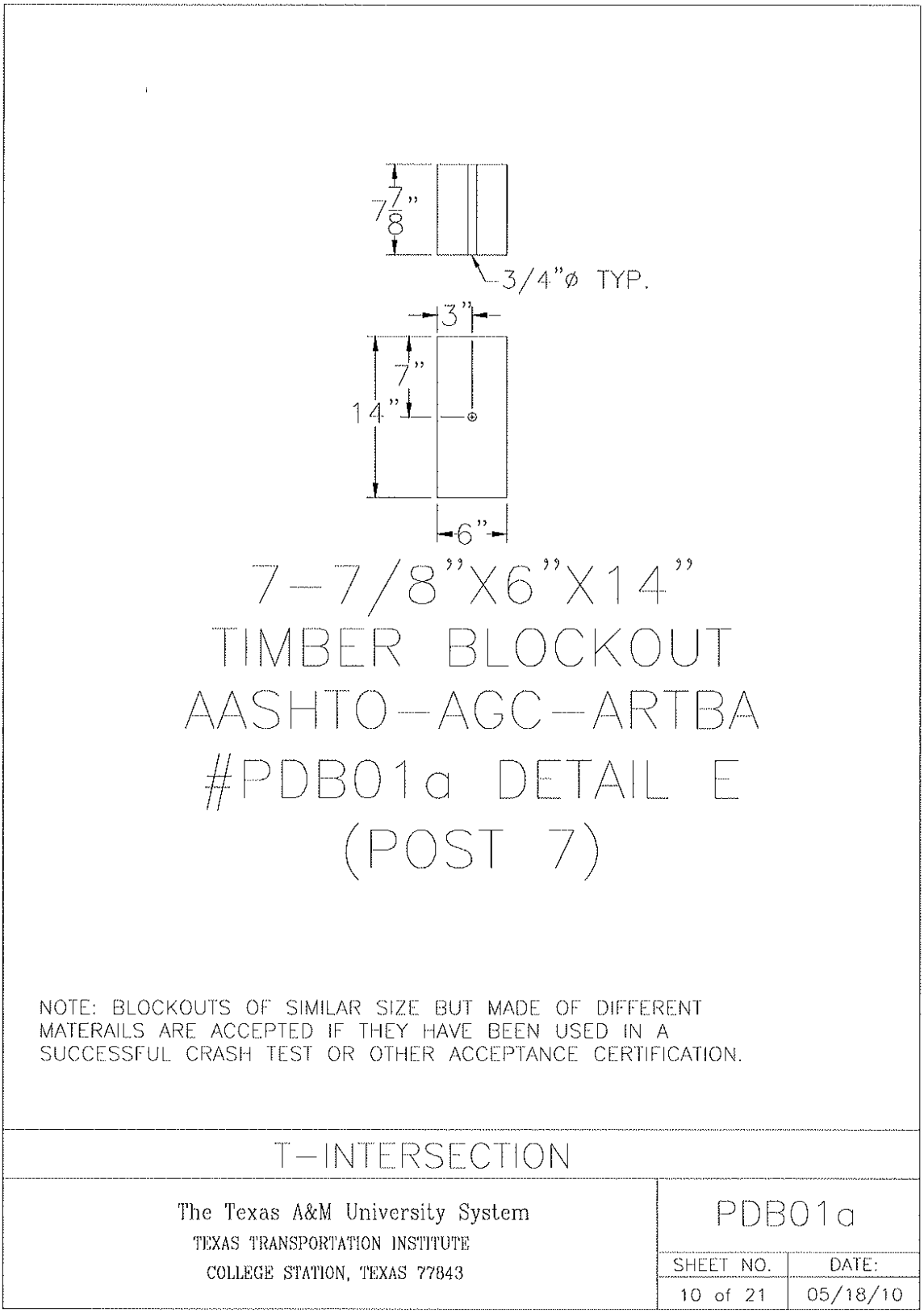

Figure A-10. Transition Post Blockout Details, Post No. 7 [27]

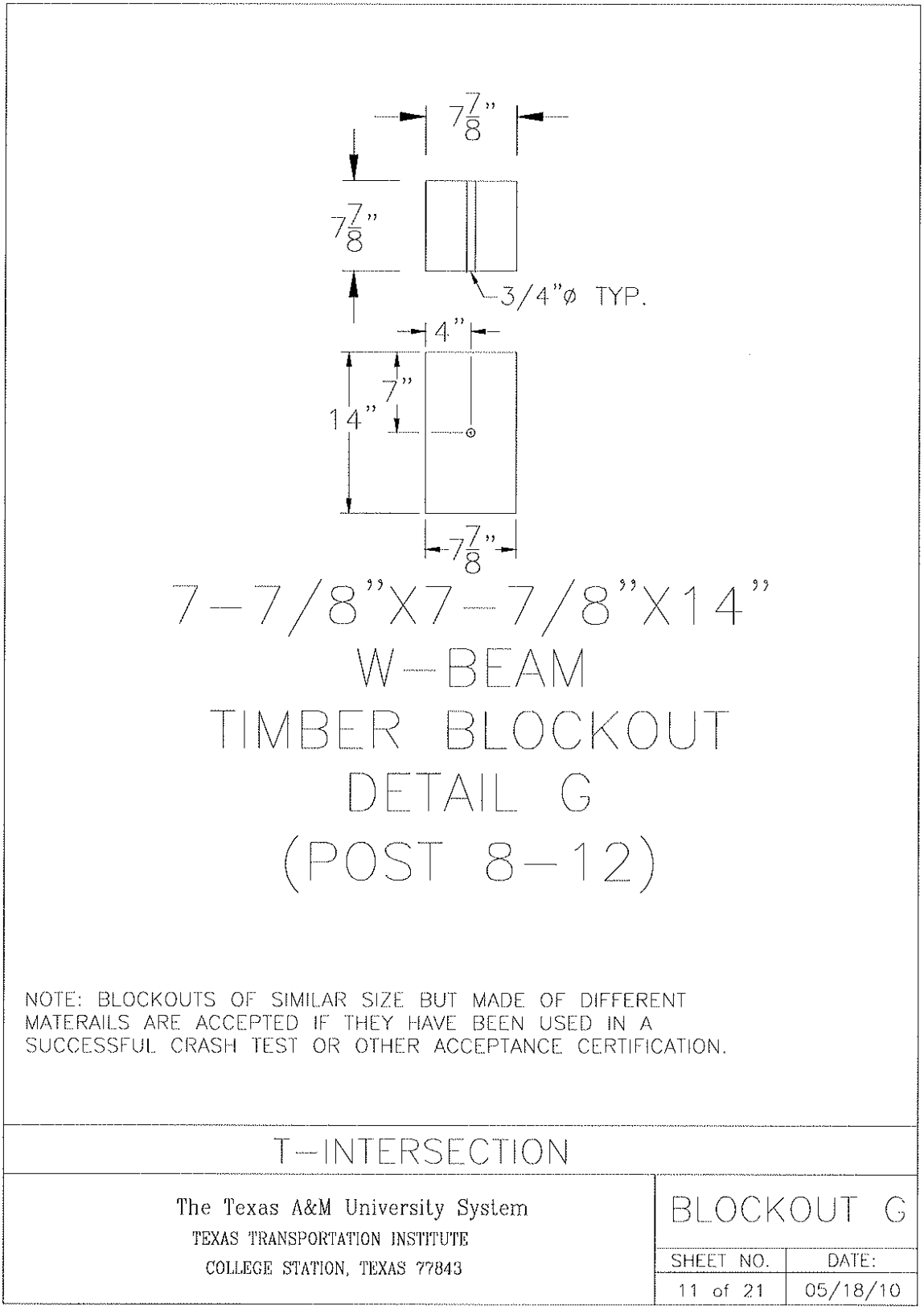

Figure A-11. Transition Post Blockout Details, Post Nos. 8 through 12 [27]

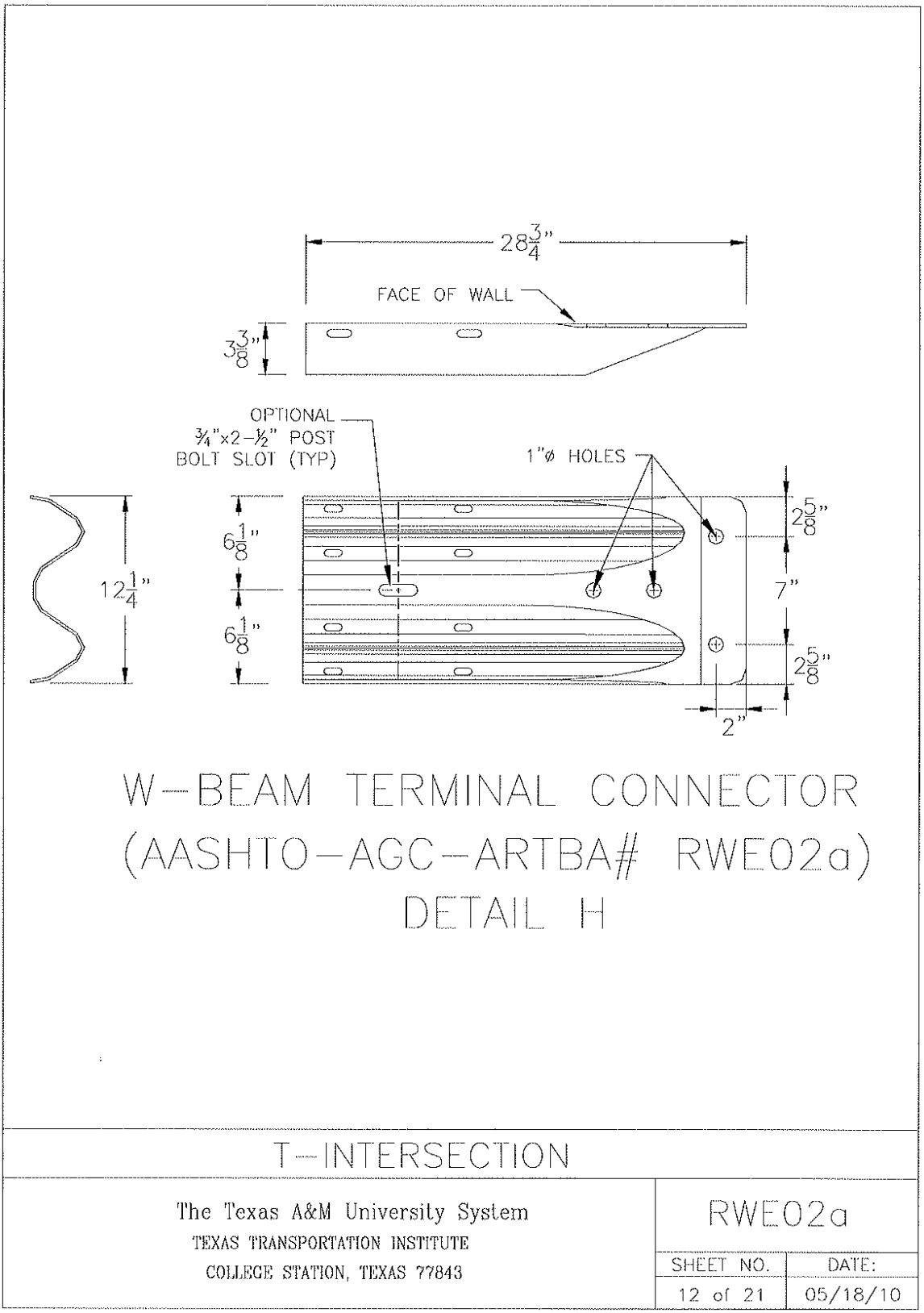

Figure A-12. End Shoe Details for W-beam Connector to Concrete Barrier [27]

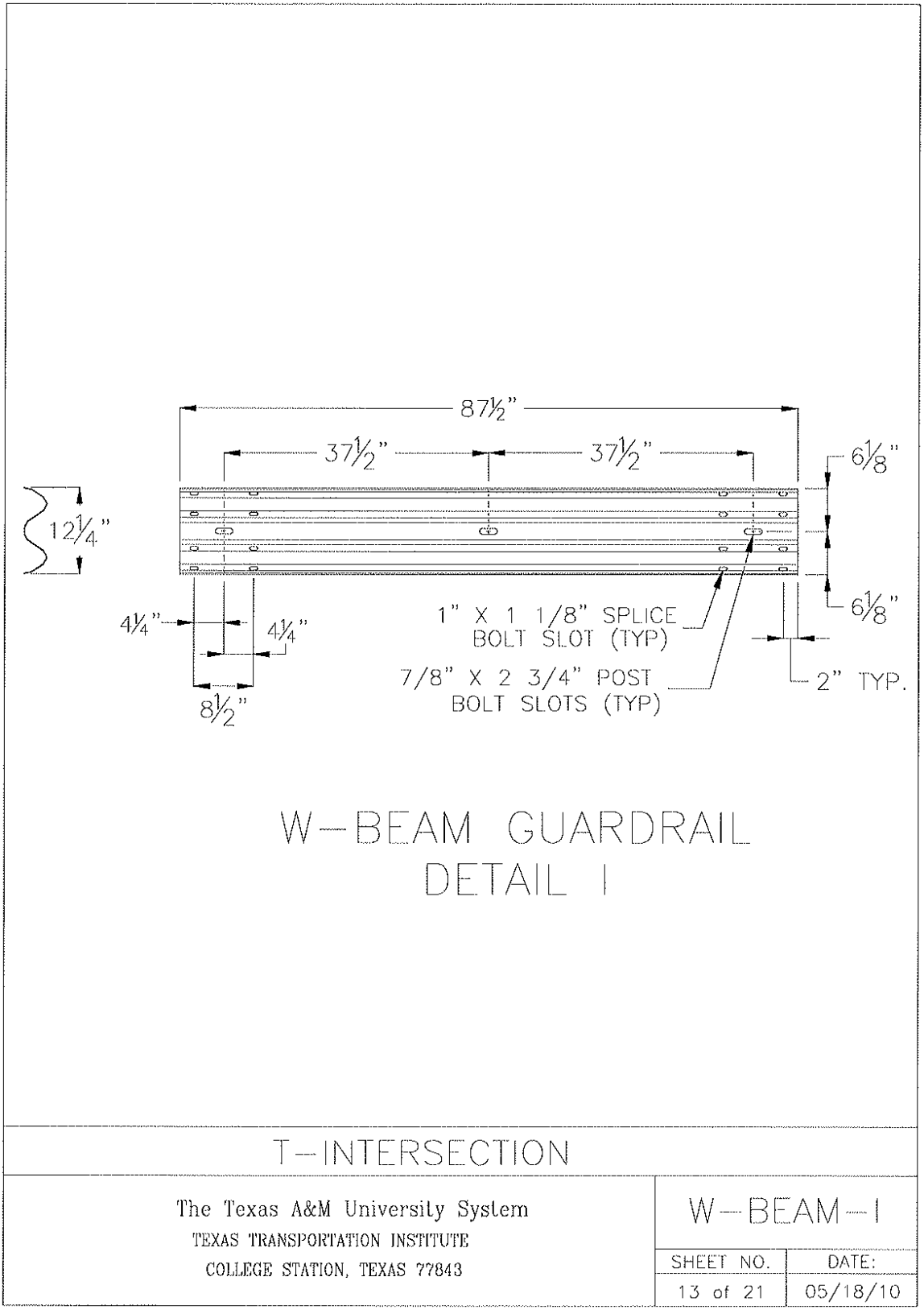

Figure A-13. Rail Punch Details for W-Beam Near Transition [27]

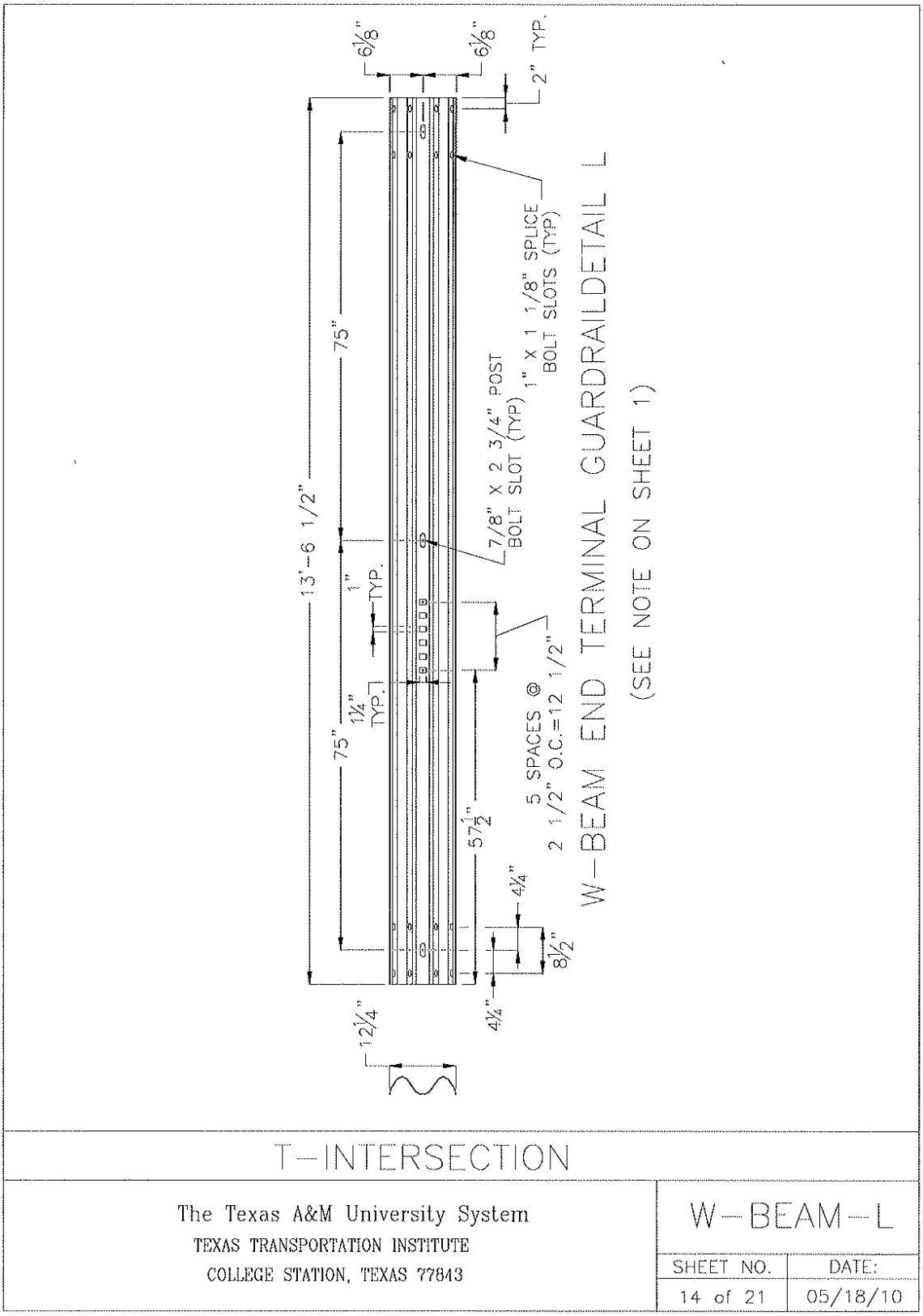

Figure A-14. Rail Punch Details for W-Beam at End Anchorage [27]

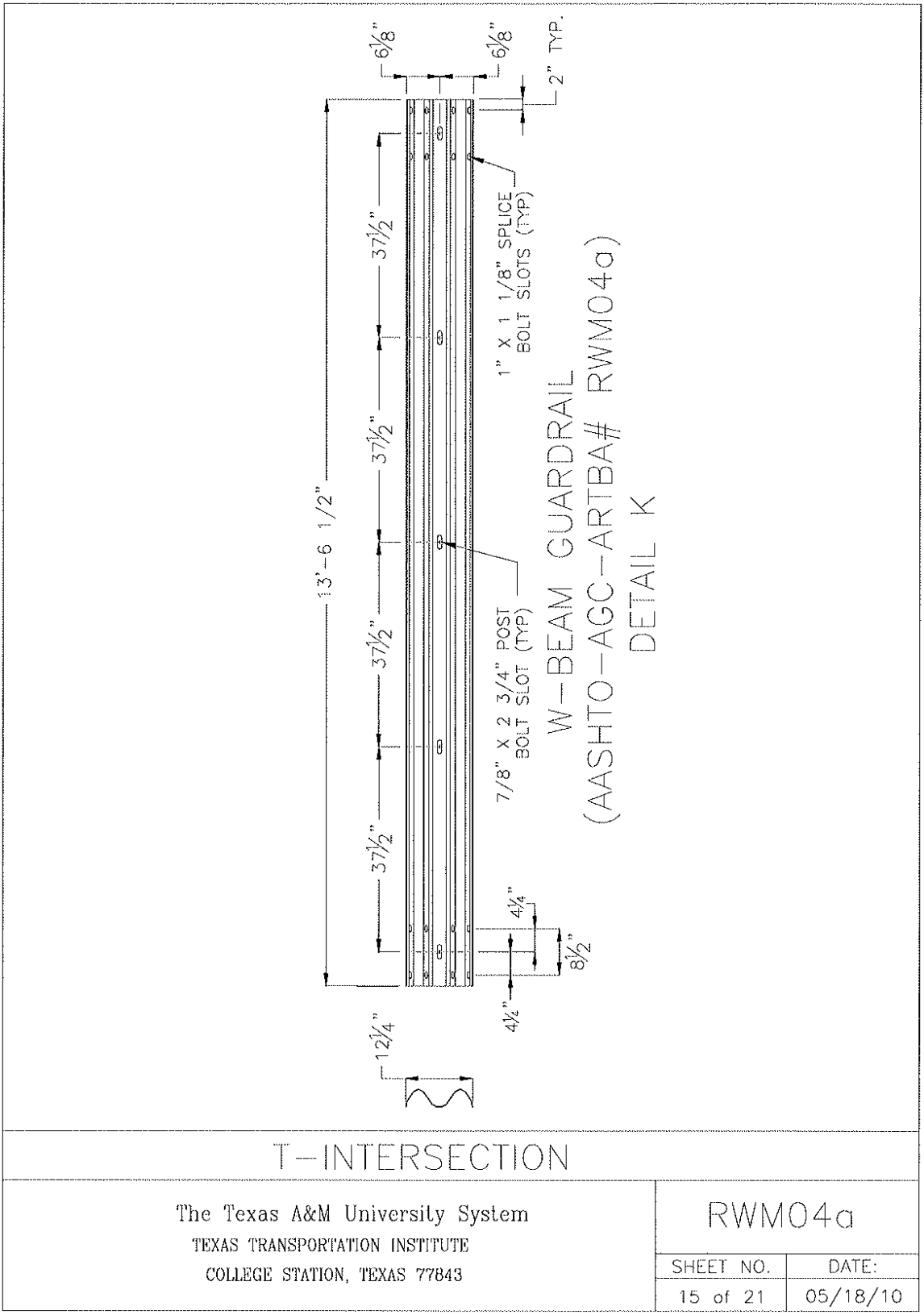

Figure A-15. Rail Punch Details for Straight Guardrail Upstream of Radius [27]

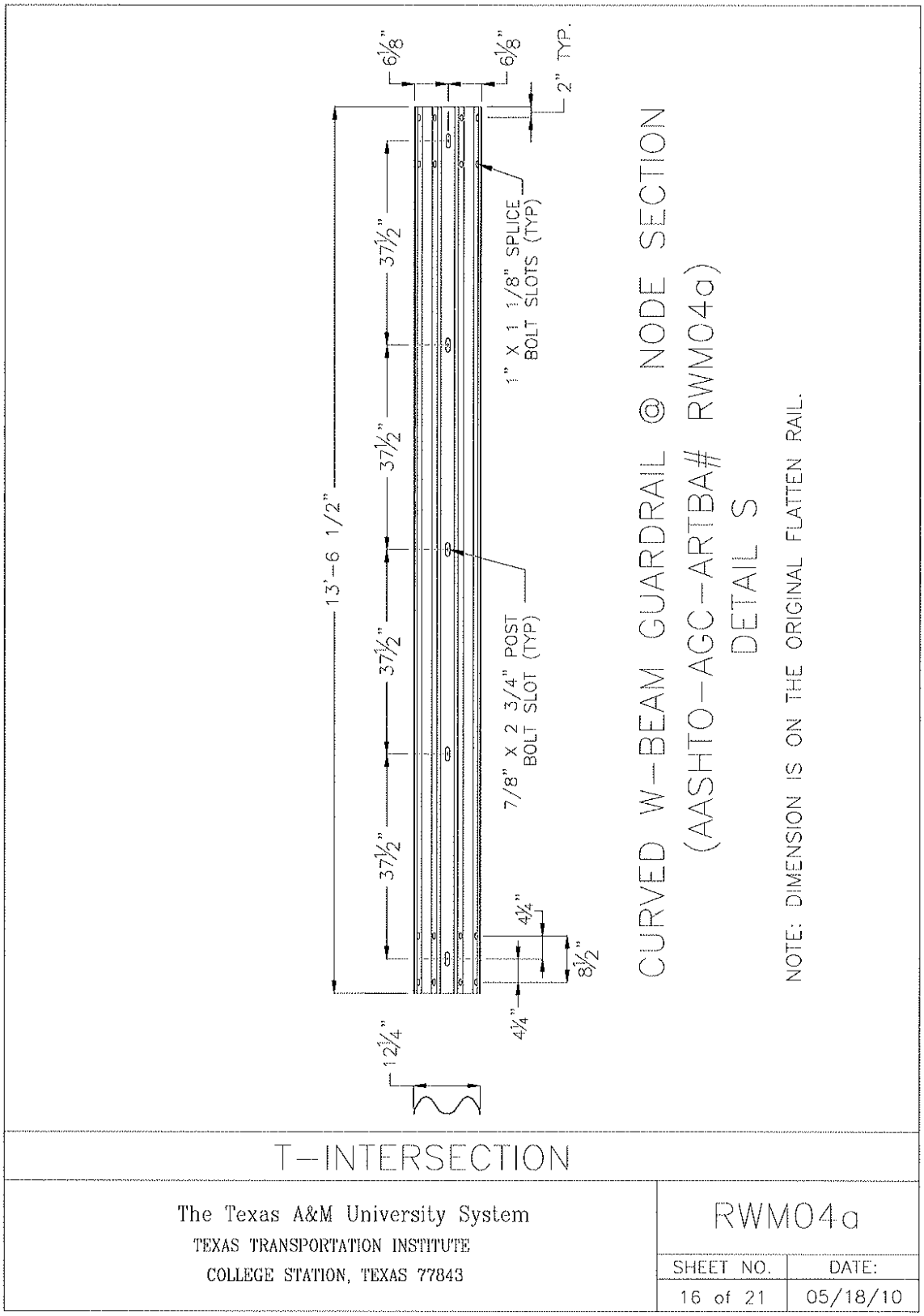

Figure A-16. Rail Punch Details for Curved W-beam Nose Section [27]

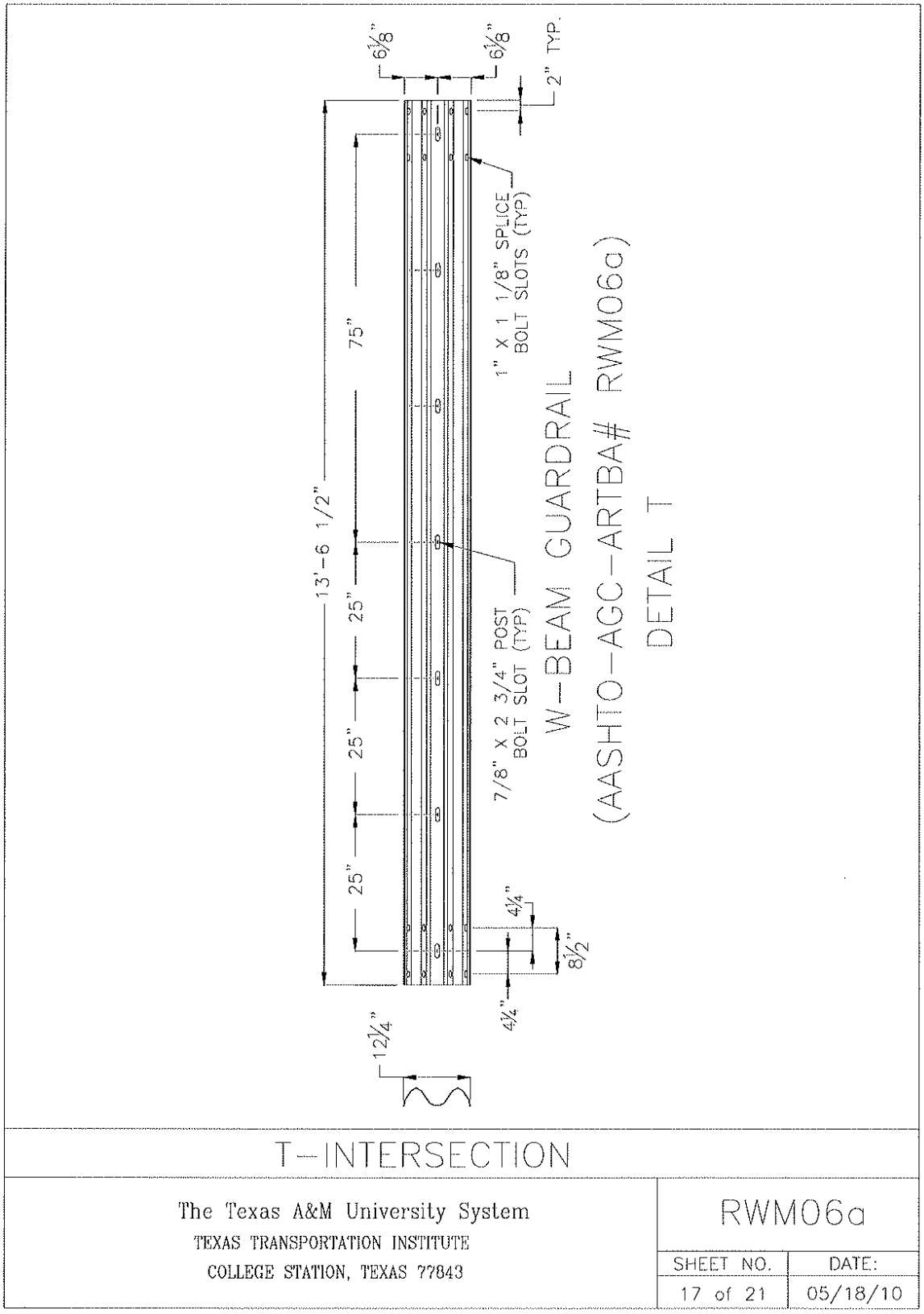

Figure A-17. Rail Punch Details for W-beam at Transition [27]

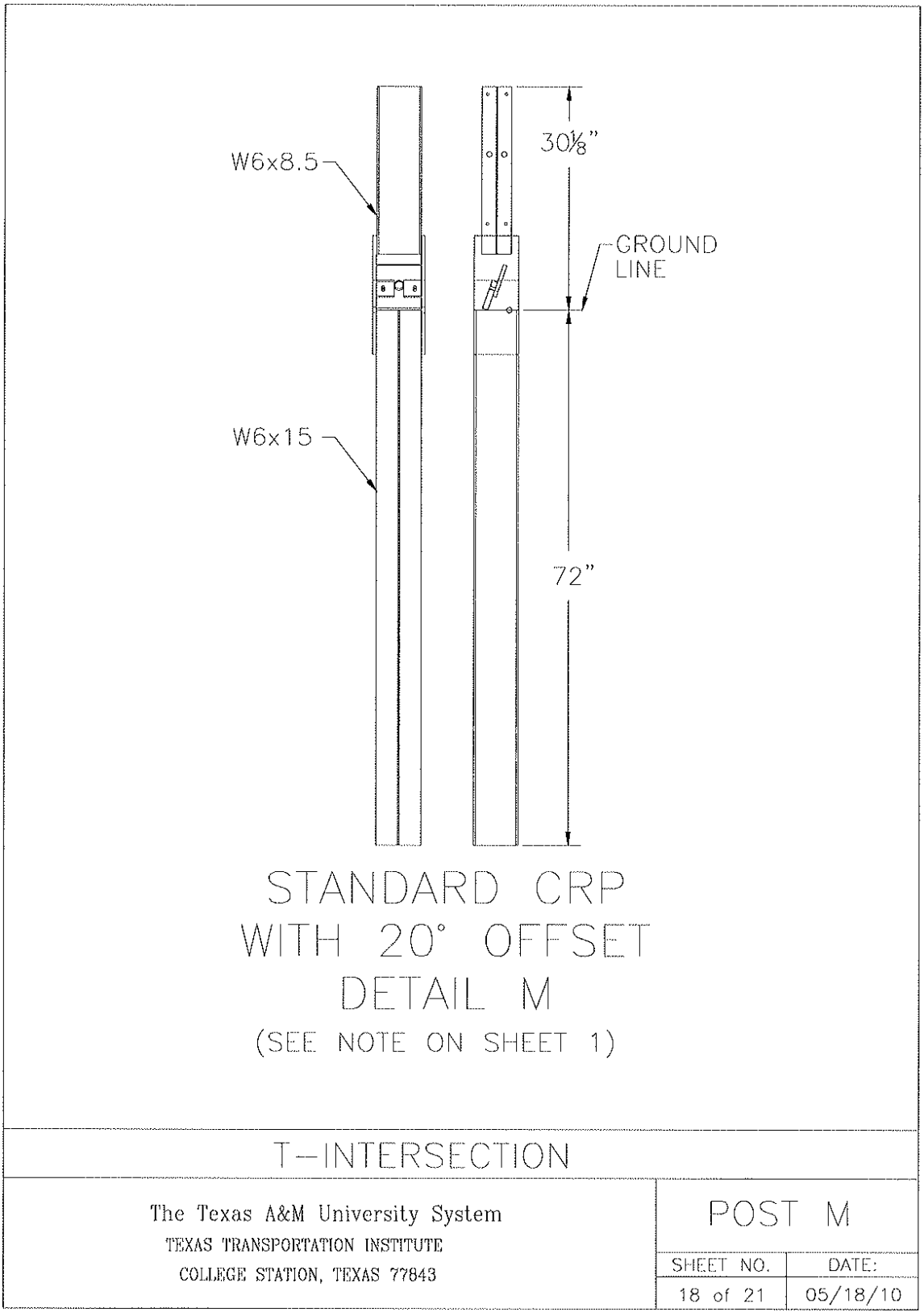

Figure A-18. Post Details [27]

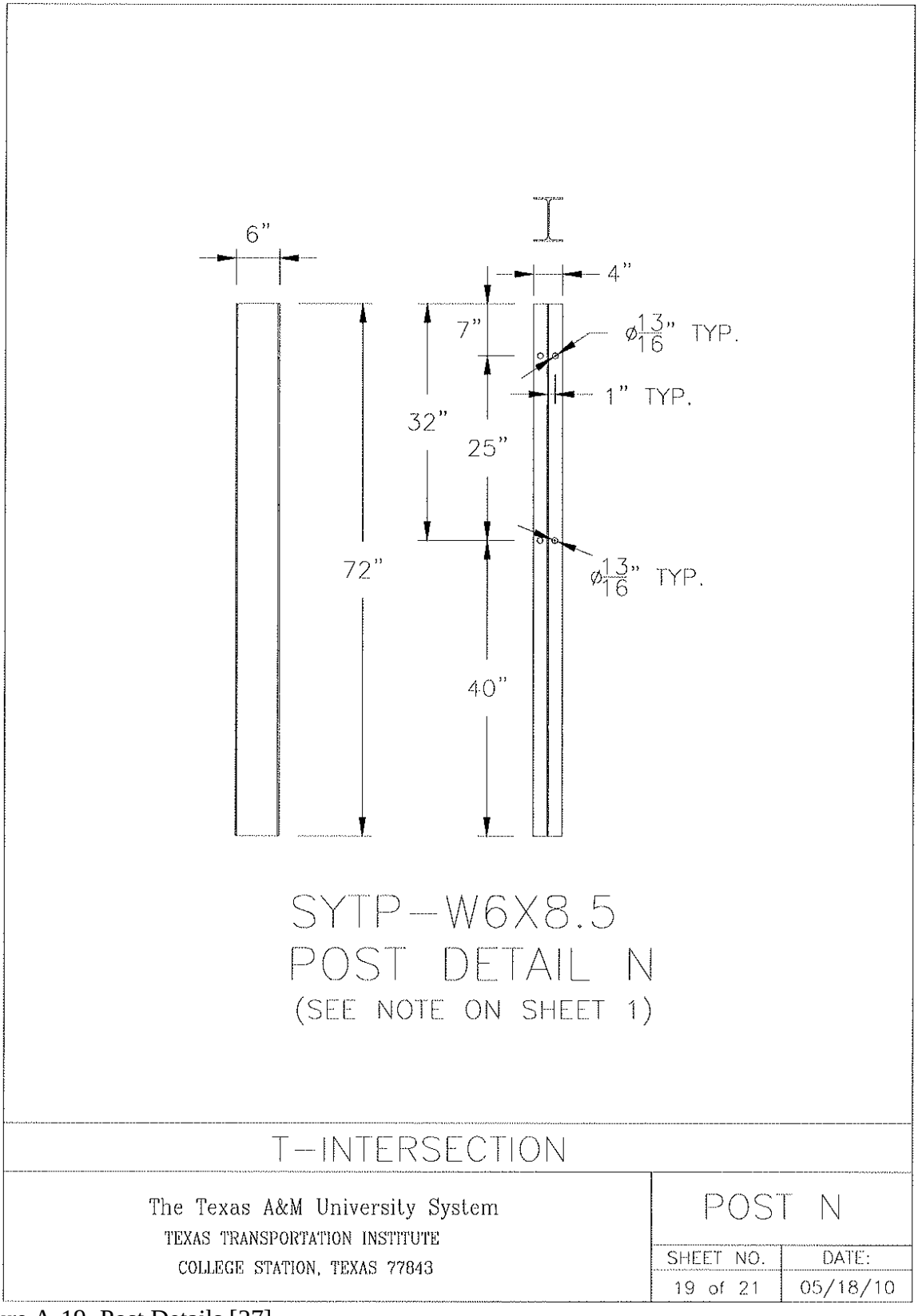

Figure A-19. Post Details [27]

END OF DOCUMENT